[redacted]

MARTIN MARIETTA ENERGY SYSTEMS LIBRARIES
3 4456 0285253 5

CENTRAL RESEARCH LIBRARY
DOCUMENT COLLECTION

ORNL-1674
Progress
5A

LABORATORY RECORDS
1954

AUG 25

CHEMISTRY DIVISION

SEMIANNUAL PROGRESS REPORT

FOR PERIOD ENDING DECEMBER 20, 1953

CENTRAL RESEARCH LIBRARY
DOCUMENT COLLECTION

LIBRARY LOAN COPY

DO NOT TRANSFER TO ANOTHER PERSON

If you wish someone else to see this document, send in name with document and the library will arrange a loan.

OAK RIDGE NATIONAL LABORATORY
OPERATED BY
CARBIDE AND CARBON CHEMICALS COMPANY
A DIVISION OF UNION CARBIDE AND CARBON CORPORATION
UCC
POST OFFICE BOX P
OAK RIDGE, TENNESSEE

[redacted]

[redacted]

[redacted]

CLASSIFICATION CHANGED TO: DECLASSIFIED
BY AUTHORITY OF: TID-1148
BY: G. Menzen 7/22/57

ORNL-1674

This document consists of 118 pages.
Copy 5 of 136 copies. Series A.

Contract No. W-7405-eng-26

CHEMISTRY DIVISION
SEMIANNUAL PROGRESS REPORT
for Period Ending December 20, 1953

S. C. Lind, Acting Director
G. E. Boyd, M. A. Bredig, Associate Directors

DATE ISSUED

MAR 25 1954

OAK RIDGE NATIONAL LABORATORY
operated by
CARBIDE AND CARBON CHEMICALS COMPANY
A Division of Union Carbide and Carbon Corporation
Post Office Box P
Oak Ridge, Tennessee

MARTIN MARIETTA ENERGY SYSTEMS LIBRARIES
3 4456 0285253 5

[redacted]

[redacted]

INTERNAL DISTRIBUTION

1. C. E. Center
2. Biology Library
3. Health Physics Library
4-5. Central Research Library
6-12. Laboratory Records Department
13. Laboratory Records, ORNL RC
14. Reactor Experimental Engineering Library
15. C. E. Larson
16. L. B. Emlet (K-25)
17. J. P. Murray (Y-12)
18. A. M. Weinberg
19. E. H. Taylor
20. E. J. Murphy
21. E. D. Shipley
22. S. C. Lind
23. F. C. VonderLage
24. R. C. Briant
25. J. A. Swartout
26. F. L. Culler
27. A. H. Snell
28. A. Hollaender
29. M. T. Kelley
30. G. H. Clewett
31. K. Z. Morgan
32. T. A. Lincoln
33. A. S. Householder
34. C. S. Harrill
35. C. E. Winters
36. D. W. Cardwell
37. E. M. King
38. J. A. Lane
39. G. E. Boyd
40. M. A. Bredig
41. R. W. Stoughton
42. R. B. Briggs
43. G. W. Parker
44. C. J. Borkowski
45. G. H. Jenks
46. K. A. Kraus
47. H. A. Levy
48. R. S. Livingston
49. T. E. Willmarth
50. C. H. Secoy
51. C. J. Hochanadel
52. W. H. Baldwin
53. A. R. Brosi
54. R. N. Lyon
55. S. A. Reynolds
56. P. F. Thomason
57. E. G. Bohlmann
58. C. P. Keim
59. C. D. Susano
60. D. D. Cowen
61. P. M. Reyling
62. R. Livingston
63. G. H. Cartledge
64. E. R. VanArtsdalen
65. G. C. Williams
66. R. W. Johnson
67. S. D. Schiffman (K-25)
68. E. P. Wigner (consultant)

EXTERNAL DISTRIBUTION

69-76. Argonne National Laboratory
77-84. Atomic Energy Commission, Washington
85-88. Brookhaven National Laboratory
89-92. Carbide and Carbon Chemicals Company (Y-12 Plant)
93-96. du Pont Compnay, Wilmington
97-98. Knolls Atomic Power Laboratory
99-104. General Electric Company, Richland
105. Phillips Petroleum Company
106-109. Los Alamos Scientific Laboratory
110. Mound Laboratory
111-113. New York Operations Office
114. Patent Branch, Washington
115. Savannah River Operations Office, Augusta
116-130. Technical Information Service, Oak Ridge
131-134. University of California Radiation Laboratory
135-136. Westinghouse Electric Corporation

[redacted]

Chemistry Division progress reports previously issued in this series are as follows:

ORNL-65	March, April, May, 1948
ORNL-176	June, July, August, 1948
ORNL-229	September, October, November, 1948
ORNL-336	December, 1948, January and February, 1949
ORNL-286	Period Ending June 30, 1949
ORNL-499	Period Ending September 30, 1949
ORNL-607	Period Ending December 31, 1949
ORNL-685	Period Ending March 31, 1950
ORNL-795	Period Ending June 30, 1950
ORNL-870	Period Ending September 30, 1950
ORNL-1036	Period Ending December 31, 1950
ORNL-1053	Period Ending March 31, 1951
ORNL-1116	Period Ending June 30, 1951
ORNL-1153	Period Ending September 30, 1951
ORNL-1260	Period Ending December 31, 1951
ORNL-1285	Period Ending March 31, 1952
ORNL-1344	Period Ending June 30, 1952
ORNL-1432	Period Ending September 30, 1952
ORNL-1482	Period Ending December 31, 1952
ORNL-1587	Period Ending June 20, 1953

[redacted]

CONTENTS

CHEMISTRY DIVISION PUBLICATIONS DURING 1953 vii

SUMMARY 1

INORGANIC AND PHYSICAL CHEMISTRY 5
- Anion-Exchange Studies 5
  - Separation of weak acids from strong acids with sulfate-form anion-exchange resin 5
  - Adsorption of osmium(IV) from chloride solutions 5
  - Uranium(VI) in nitrate solutions 5
  - Adsorption of lead(II) and bismuth(III) from nitrate solutions 5
  - Separation of alkaline earths and alkali metals by anion exchange 5
- Hydrolytic Polymerization of Zirconium(IV), Hafnium(IV), and Bismuth(III) 6
- Interaction of Thiocyanato Cations with Metal Cations in Aqueous Solution 7
- Chemistry of Corrosion 11
  - Studies on electrode potentials 11
  - Action of corrosion inhibitors 14
  - Hydrogen overvoltage on amalgams 17
- Chemistry of Fused Salts 21
  - Electrical conductivity and density 21
  - EMF measurements in fused salts 25
  - Cryoscopy 26
- Miscibility of Liquid Metals and Salts 27
  - Solubility measurements 27
  - Metal vapor pressure measurements 32

NUCLEAR CHEMISTRY 36
- Half-Life Measurements 36
- Characteristics of Pm^{145} 36
- Cross Section of Pa^{233} 36
- Radiochemical Decontamination Characteristics of Porcelain Enamel 36

ORGANIC CHEMISTRY 46
- Mechanism of the Wagner-Meerwein Rearrangement in the 1,2,2-Triphenylethyl System 46
- Comparative Rates of Radioactivity Redistribution and Acetoxyl Exchange During Isomerizations of Triply Labeled 1,2,2-Triphenylethyl Acetate 49
- Organic Chemistry of Solvents 53
  - Ester exchange between reagent tri-*n*-butyl phosphate and $H_3P^{32}O_4$ 53
  - Tri-*n*-octyl phosphine oxide-P^{32} 53

CHEMICAL PHYSICS 54
- Experiments in Chemical Kinetics with Molecular Beams 54
- Neutron-Diffraction Studies 54
  - Crystal structure of oxalic acid dihydrate 54
  - Crystal structure of iodic acid 55
- Radio-Frequency Spectroscopy 57
  - The iodine problem 57
  - Paramagnetic resonance 58
  - Pure quadrupole spectroscopy 59
- Low-Temperature Calorimetry 60

[redacted]

[redacted]

CHEMISTRY OF SEPARATION PROCESSES 62
Self-Diffusion of Cations in Linear Polystyrenesulfonate Solutions 62
Fundamental Studies on Ion-Exchange Selectivity 65

RADIATION CHEMISTRY 70
Gas-Phase Irradiation 70
Effect of Temperature on Decomposition of Aqueous Solutions by Gamma Radiation 70
Gas Yields in the Decomposition of Some Aqueous Solutions by Gamma Radiation 71
10^{-3} *M* KBr in 0.8 *N* H_2SO_4 (degassed) 71
10^{-3} *M* KBr in 0.8 *N* H_2SO_4 (+ oxygen) 72
0.8 *N* H_2SO_4 + oxygen, and pure water + oxygen 72
Ferrous sulfate solutions in 0.8 *N* H_2SO_4 with and without added oxygen 73
Ceric sulfate in 0.8 *N* H_2SO_4 solution 73
Molecular Yield of Hydrogen Peroxide in the Decomposition of Water by Cobalt Gamma Radiation 74
Effect of Fast Electrons on Corrosion of Type 347 Stainless Steel by Uranyl Sulfate Solutions 76
Oxidation of Uranium(IV) by Gamma Rays 78
Gamma Radiolysis of Aqueous Solutions of Organic Acids 79

INSTRUMENTATION 81
Method of Measuring an Electron Beam Deflection by Using Variation in the Secondary Emission of a Target 81
Multichannel Beam-Deflection Pulse-Amplitude Analyzer 81
Efficient Use of a Film Memory in Multichannel Pulse Analysis 82
Decoding Matrix for a Fast Binary Scaler 86
Linearity Improvement in Pulse Amplifiers 87
Linear Gate Circuit 87

REACTOR CHEMISTRY 90
Alkaline Chemistry for the Processing of Aluminum-Uranium Fuel Elements 90
Cathodic Protection of Type 309 SNb Stainless Steel Exposed to a Thorium Nitrate–Aluminum Nitrate–Nitric Acid–Hydrofluoric Acid Mixture 90
The System UO_3-NiO-SO_3-H_2O 90
The System UO_3-SO_3-H_2O Above 300°C 95
Preliminary Exploration of the $Th(NO_3)4$-HNO_3-H_2O System at Elevated Temperature 97
Estimation of Activity Coefficients of UO_2SO_4 Solutions from Vapor-Pressure Measurements . . . 98
Homogeneous Reactor Solutions Under Irradiation 100
Stainless steel 102
Titanium 104
Future work 104
Mechanism of the Hydrogen-Oxygen Recombination Reaction in Solutions 104
Dependence on copper concentration 104
Temperature coefficient of the reaction 105
Rate of reaction with deuterium 106
Plans for next quarter 106

[redacted]

[redacted]

CHEMISTRY DIVISION PUBLICATIONS DURING 1953

UNCLASSIFIED PUBLICATIONS

Inorganic and Physical Chemistry

K. A. Kraus and G. E. Moore, "Anion Exchange Studies. V. Adsorption of Hydrochloric Acid by a Strong Base Anion Exchanger," *J. Am. Chem. Soc.* **75**, 1457 (1953).

K. A. Kraus and G. E. Moore, "Anion Exchange Studies. VI. The Divalent Transition Elements Manganese to Zinc in Hydrochloric Acid," *J. Am. Chem. Soc.* **75**, 1460 (1953).

K. A. Kraus, F. Nelson, and J. F. Baxter, "Anion Exchange Studies. VII. Separation of Sulfuric Acid from Metal Sulfates by Anion Exchange," *J. Am. Chem. Soc.* **75**, 2768 (1953).

K. A. Kraus and F. Nelson, "Anion Exchange Studies. VIII. Separation of Iron and Aluminum in Sulfate Solutions," *J. Am. Chem. Soc.* **75**, 3273 (1953).

E. C. Campbell and F. Nelson, "Chemical Separation of 0.82-sec Pb^{207m} from Bi^{207}," *Phys. Rev.* **91**, 499 (1953).

J. S. Johnson and K. A. Kraus, "Density and Refractive Index of Uranyl Fluoride Solutions," *J. Am. Chem. Soc.* **75**, 4594 (1953).

K. A. Kraus and J. S. Johnson, "Hydrolytic Polymerization of Zirconium(IV)," *J. Am. Chem. Soc.* **75**, 5769 (1953).

K. A. Kraus, Book Review of *An Annotated Bibliography of Selected References on the Solid-State Reactions of the Uranium Oxides*, by S. M. Lang, in *J. Am. Chem. Soc.* **75**, 6354 (1953).

W. T. Smith, Jr., J. W. Cobble, and G. E. Boyd, "Thermodynamic Properties of Technetium and Rhenium Compounds. I. Vapor Pressures of Technetium Heptoxide, Pertechnic Acid and Aqueous Solutions of Pertechnic Acid," *J. Am. Chem. Soc.* **75**, 5773 (1953).

J. W. Cobble, W. T. Smith, Jr., and G. E. Boyd, "Thermodynamic Properties of Technetium and Rhenium Compounds. II. Heats of Formation of Technetium Heptoxide and Pertechnic Acid, Potential of the Technetium(IV)-Technetium(VII) Couple, and a Potential Diagram for Technetium," *J. Am. Chem. Soc.* **75**, 5777 (1953).

G. E. Boyd, J. W. Cobble, and W. T. Smith, Jr., "Thermodynamic Properties of Technetium and Rhenium Compounds. III. Heats of Formation of Rhenium Heptoxide and Trioxide and a Revised Potential Diagram for Rhenium," *J. Am. Chem. Soc.* **75**, 5783 (1953).

W. E. Clark, "The Half-Wave Potential of Lithium," *J. Am. Chem. Soc.* **75**, 6042 (1953).

J. C. Griess, Jr., "The Quantitative Electrodeposition of Radioruthenium," *J. Electrochem. Soc.* **100**, 429-433 (1953).

M. H. Lietzke and J. C. Griess, Jr., "A Study of the Electrodeposition of Ruthenium from Very Dilute Solutions," ORNL-1399 (Jan. 13, 1953) and *J. Electrochem. Soc.* **100**, 434-441 (1953).

M. H. Lietzke and R. W. Stoughton, "The Behavior of the Silver–Silver Sulfate and the Mercury–Mercurous Sulfate Electrodes at High Temperatures," *J. Am. Chem. Soc.* **75**, 5226 (1953).

Nuclear Chemistry

B. H. Ketelle, A. R. Brosi, and F. M. Porter, "Gallium 67," *Phys. Rev.* **90**, 567 (1953).

G. W. Parker and G. M. Hebert, "Radiochemical Decontamination Characteristics of Porcelain Enamel," Building Research Advisory Board, Conference Report No. 6, Nov. 12, 1953, National Research Council, National Academy of Sciences, Washington, D.C.

Organic Chemistry

C. J. Collins, D. N. Hess, R. H. Mayor, G. M. Toffel, and A. R. Jones, "Studies in the Wagner Rearrangement. III. Chrysene-5,6-C_1^{14}," *J. Am. Chem. Soc.* **75**, 397 (1953).

B. M. Benjamin and C. J. Collins, "Studies in the Wagner Rearrangement. IV. The Steric Effect of An Ortho Methyl Group," *J. Am. Chem. Soc.* **75**, 402 (1953).

[redacted]

[redacted]

C. J. Collins, L. S. Ciereszko, and J. G. Burr, Jr., "Studies in the Wagner Rearrangement. V. Further Evidence for a Steric Effect," *J. Am. Chem. Soc.* **75**, 405 (1953).

C. J. Collins and B. M. Benjamin, "Studies in the Wagner Rearrangement. VI. The Directive Effects of the Methyl and Methoxyl Groups," *J. Am. Chem. Soc.* **75**, 1644 (1953).

W. A. Bonner and C. J. Collins, "Studies in the Wagner Rearrangement. VII. The Dehydration of 2-Phenyl-1-acenaphthenol-1-C^{14}," *J. Am. Chem. Soc.* **75**, 3831 (1953).

W. A. Bonner and C. J. Collins, "An Isotope Effect in the Oxidation of a Secondary Carbinol," *J. Am. Chem. Soc.* **75**, 2308 (1953).

W. A. Bonner and C. J. Collins, "An Isotope Effect During Ozonization," *J. Am. Chem. Soc.* **75**, 3693 (1953).

W. A. Bonner and C. J. Collins, "Isotope Effects During Catalytic Hydrogenations," *J. Am. Chem. Soc.* **75**, 4516 (1953).

W. A. Bonner and C. J. Collins, "Molecular Rearrangements. I. The 1,2,2-Triphenylethyl System," *J. Am. Chem. Soc.* **75**, 5372 (1953).

C. J. Collins and W. A. Bonner, "Molecular Rearrangements. II. The 1,1,2-Triphenylethyl System," *J. Am. Chem. Soc.* **75**, 5379 (1953).

V. F. Raaen and G. A. Ropp, "Precision Obtained with Vibrating Reed Electrometer in Radioassaying Meta- and Para-Substituted Benzoic-Alpha-Carbon-14 Acids," *Anal. Chem.* **25**, 174 (1953).

G. A. Ropp, V. F. Raaen, and A. J. Weinberger, "Studies of Some Carbon-14 Isotope Effects in Organic Chemistry," *J. Am. Chem. Soc.* **75**, 3694 (1953).

V. F. Raaen and G. A. Ropp, "Intramolecular Isotope Effects in the Reactions of Benzoic-α-C^{14} Anhydride," *J. Chem. Phys.* **21**, 1902 (1953).

J. G. Burr, Jr., "The Addition of Water to Diphenylacetylene-1,2-$C_1{}^{14}$," *J. Am. Chem. Soc.* **75**, 1990 (1953).

P. S. Bailey and J. G. Burr, Jr., "Evidence for a Cyclic Intermediate in the Reaction of Diarylethylamines with Nitrous Acid," *J. Am. Chem. Soc.* **75**, 2951 (1953).

J. G. Burr, Jr., "The Rates and Migration Ratios Observed in the Unimolecular and Bimolecular Reactions of 2-Phenyl-2-(*p*-tolyl)-ethyl Tosylate and Related Compounds," *J. Am. Chem. Soc.* **75**, 5008 (1953).

E. C. Hendley and O. K. Neville, "C^{14} Tracer Studies in the Rearrangements of Unsymmetrical α-Diketones. III. *p*-Methoxybenzylideneacetophenone Oxide," *J. Am. Chem. Soc.* **75**, 1995 (1953).

H. W. Davis, E. Grovenstein, Jr., and O. K. Neville, "C-14 Tracer Studies in the Rearrangements of Unsymmetrical α-Diketones. IV. Ethyl α,β-Diketobutyrate to Methyltartronic Acid," *J. Am. Chem. Soc.* **75**, 3304 (1953).

A. R. Jones, E. J. Dowling, and W. J. Skraba, "Identification of Some Organic Compounds by Paper Chromatography," *Anal. Chem.* **25**, 394 (1953).

W. J. Skraba, J. G. Burr, Jr., and D. N. Hess, "The Decomposition of Methanol-C^{14} under the Influence of Its Own Radiation," *J. Chem. Phys.* **21**, 1296 (1953).

A. R. Jones and W. J. Skraba, "Syntheses of Methoplamine-C^{14} and Diozomethane C^{14}," *Science* **117**, 252 (1953).

A. R. Jones, "A Weighing Pipet to Hold Liquid Samples for Dry Combustion," *Rev. Sci. Instr.* **24**, 230 (1953).

Chemistry of Separation Processes

G. E. Boyd and B. A. Soldano, "Osmotic Free Energies of Ion Exchangers," *Z. Elektrochem.* **57**, 162 (1953).

F. S. Chance, Jr., G. E. Boyd, and H. J. Garber, "Sodium and Bromide Removal from Solvents by Nonaqueous Ion Exchange," *Ind. Eng. Chem.* **45**, 1671 (1953).

G. E. Boyd and B. A. Soldano, "Self-diffusion of Cations in and through Sulfonated Polystyrene Cation-exchange Polymers," *J. Am. Chem. Soc.* **75**, 6091 (1953).

[redacted]

[redacted]

B. A. Soldano and G. E. Boyd, "Self-diffusion of Cations in Hetero-ionic Cation Exchangers," *J. Am. Chem. Soc.* **75**, 6107 (1953).

G. E. Boyd and B. A. Soldano, "Self-diffusion of Water Molecules and Mobile Anions in Cation Exchangers," *J. Am. Chem. Soc.* **75**, 6105 (1953).

B. A. Soldano and G. E. Boyd, "Self-diffusion of Anions in Strong-base Anion Exchangers," *J. Am. Chem. Soc.* **75**, 6099 (1953).

B. A. Soldano, "The Kinetics of Ion Exchange Processes," *Ann. N. Y. Acad. Sci.* **57**, 116 (1953).

Chemical Physics

H. Zeldes and R. Livingston, "Pure Quadrupole Spectra: Alkyl Bromides and Iodides," *J. Chem. Phys.* **21**, 1418 (1953).

R. Livingston, "Pure Quadrupole Spectra in Solids," *Science* **118**, 61 (1953).

R. Livingston, "Pure Quadrupole Spectra of Solid Chlorine Compounds," *J. Phys. Chem.* **57**, 496 (1953).

R. Livingston and H. Zeldes, "The Quadrupole Moment Ratio of I^{129} and I^{127} from Pure Quadrupole Spectra," *Phys. Rev.* **90**, 609 (1953).

R. Livingston, B. M. Benjamin, J. T. Cox, and W. Gordy, "The Nuclear Spin and Quadrupole Moment of I^{131}," *Phys. Rev.* **92**, 1271 (1953).

H. A. Levy and S. W. Peterson, "Neutron Diffraction Study of the NaCl-type Modification of ND_4Br and ND_4I," *J. Chem. Phys.* **21**, 366 (1953).

H. A. Levy and S. W. Peterson, "Neutron Diffraction Determination of the Crystal Structure of Ammonium Bromide in Four Phases," *J. Am. Chem. Soc.* **75**, 1536 (1953).

J. Waser, H. A. Levy, and S. W. Peterson, "The Structure of PdO," *Acta Cryst.* **6**, 661 (1953).

W. O. Milligan, L. W. Vernon, H. A. Levy, and S. W. Peterson, "Neutron Diffraction Studies on Scandium Orthovanadate and Scandium Oxide," *J. Phys. Chem.* **57**, 535 (1953).

S. W. Peterson, H. A. Levy, and S. H. Simonsen, "Neutron Diffraction Study of Tetragonal Potassium Dihydrogen Phosphate," *J. Chem. Phys.* **21**, 2084 (1953).

A. S. Dworkin, D. J. Sasmor, and E. R. Van Artsdalen, "T^2 Dependence of the Low Temperature Specific Heat of Boron Nitride," *J. Chem. Phys.* **21**, 954 (1953).

Radiation Chemistry

C. J. Hochanadel and J. A. Ghormley, "A Calorimetric Calibration of Gamma-ray Actinometers," *J. Chem. Phys.* **21**, 880 (1953).

T. J. Sworski, "Hydrogen Peroxide Formation by Cobalt Gamma-Radiation," *J. Chem. Phys.* **21**, 375 (1953).

Instrumentation

C. J. Borkowski and R. L. Clark, "Gamma-Ray Energy Resolution with NaI-Tl Scintillation Spectrometers," *Rev. Sci. Instr.* **24**, 1046 (1953).

CLASSIFIED PAPERS

J. Halperin, C. V. Ellison, D. E. Ferguson, and R. W. Stoughton, *Capture Cross-Section of Pa^{233} for Thermal Pile Neutrons,*" ORNL-1462 (May 5, 1953).

J. Halperin, C. V. Ellison, D. E. Ferguson, and R. W. Stoughton, "Capture Cross Section of Pa^{233} for Thermal Reactor Neutrons," *Reactor. Sci. Technol.* 3, No. 3, 108 (1953).

J. Halperin and R. W. Stoughton, *Heavy Isotope Build-Up in Core of U^{233} Breeder*, ORNL-1567 (Oct. 6, 1953).

M. H. Lietzke, "Cathodic Protection of Type 347 Stainless Steel Exposed to Uranyl Sulfate Solutions," *Reactor Sci. Technol.* 3, No. 3, 101 (1953).

[redacted]

[redacted]

J. W. Boyle, J. A. Ghormley, C. J. Hochanadel, W. F. Kieffer and T. J. Sworski, "The Radiation Chemistry of Aqueous Reactor Solutions. Part 1. Radiation-Induced Decomposition," *Reactor Sci. Technol.* 3, No. 1, 32 (1953).

M. D. Silverman, G. M. Watson, and H. F. McDuffie, "The Radiation Chemistry of Aqueous Reactor Solutions. Part 2. The Decomposition of Peroxide in Aqueous Homogeneous-Reactor Systems," *Reactor Sci. Technol.* 3, No. 3, 43 (1953).

J. W. Boyle, *Slurry Systems*, ORNL CF-52-12-127 Rev. Chap. 4.5, from *Reactor Handbook* Sec. 2.4 (Feb. 3, 1953).

J. W. Boyle, H. O. Day, E. V. Jones, W. L. Marshall, H. F. McDuffie, C. H. Secoy, and K. S. Warren, *Properties of Aqueous Solution Systems*, ORNL CF-52-12-127 Rev. Chap. 4.5, from *Reactor Handbook* Sec. 2.4 (April 15, 1953).

W. E. Clark, *Chemical Aspects of the Elex Process*, ORNL 1524 (April 9, 1953).

W. E. Clark, *Elex Fundamental Studies; January 1, 1953 Through March 31, 1953*, ORNL 1544 (April 29, 1953).

W. E. Clark and B. Zemel, *Elex Fundamental Studies; October 1, 1952 Through December 31, 1952*, ORNL 1487 (Feb. 20, 1953).

W. E. Clark, *Elex and Colex Fundamental Studies Through November 1, 1953*, ORNL CF-53-11-207.

[redacted]

[redacted]

CHEMISTRY DIVISION SEMIANNUAL PROGRESS REPORT

SUMMARY

INORGANIC AND PHYSICAL CHEMISTRY

Tests with several weak acids such as phenol, which was found strongly adsorbed on the sulfate form of the anion exchange resin Dowex-1, indicate that considerable care is necessary in the application of a new separations technique which makes use of the observation that generally strong acids are much more strongly adsorbed on this adsorber than weak acids.

The possibility of processing uranium-aluminum nitrate solutions by anion exchange is indicated by the finding that uranium(VI) can be adsorbed at considerable resin loads from aluminum nitrate solutions in the range of 1.0 to 2.5 *M* $Al(NO_3)_3$.

Strong adsorbability of Os(IV), reminiscent of that of Pd(II) and Pt(IV), may be typical of the behavior of chloride complexes of charge minus 2 in the platinum group and indicates the probability of the separation from Ir(III). A difference found in the adsorbability of lead and bismuth from nitrate solutions permits their separation in such solution similar to that in chloride solution. It was demonstrated that the high adsorbability, on Dowex-1, of calcium and strontium, presumably as negatively charged citrate complexes, permits their separation from alkali metals.

The results of ultracentrifugation experiments indicate that Zr(IV) and Hf(IV) in strongly acidic solutions do not exhibit continuous polymerization with high molecular weight products but rather form only low molecular weight polymers with trimers apparently predominating at acidities near 1 *M*.

The stability and solubility of coordination complexes of Ag(I) and Hg(II) cations with complex cations of the mono- and dithiocyanatoammine and *cis*-dithiocyanatobis(ethylenediamine) cobalt(III) or chromium(III) type was studied applying the method of continuous variation to spectrophotometric measurements of the absorption spectra as a function of mole fraction. Interaction ratios of 1 to 1 and 2 to 1 for such complexes were found.

In a potentiometric study of the kinetics of the reaction of lithium amalgam with water, it is not presently possible to definitely assign a reaction order, although the data obtained thus far seem to indicate zero order.

The first phase of the studies of the effects upon the electrode potential of stainless steel of the addition of low concentrations of foreign ions has been completed. Among the additives studied since the last report, palladium(II), cobalt(III), periodiate, iodate, bromate, persulfate, vanadium(V) oxide and osmium(VIII) oxide have an ennobling effect. Only one, tin(II), was found to debase the potential. A list of additives which produced no potential changes is also given. The changes observed follow Nernst type equations. A multiplicity of processes, however, appears to be involved to which further study is being devoted.

In pursuing further the study of the extreme effect of pertechnetate ion as a corrosion inhibitor, it was demonstrated that this ion at, or above, 5 ppm inhibits the corrosion of carbon steel in distilled water at either 23, 100 or 250°C. The protection was observed for almost a year at the lower temperatures. Several specially designed experiments prove rather conclusively that the effect is dependent on the presence of soluble pertechnetate ion and is not due to the formation of an insoluble protective film. Of the elements V, Cr, Mn, Mo, Tc, Ru, W, Re, and Os in their highest oxidation states, only Cr, W, and Tc act as inhibitors, the W only at much higher concentrations than the Tc.

An apparatus for measuring the electrical equivalent conductivity and density of molten salt mixtures as a function of temperature and composition is described in detail. A significant minimum in the electrical conductance of molten LiCl-KCl mixtures at a concentration of 75 to 80 mole % KCl is, in the presence of proof from density measurements that there is no complex formation, interpreted to mean that the current is carried primarily by the cations, and that the movement of K^+ ions is made difficult by the shrinkage of the chloride ion semilattice accompanying the substitution of a few K^+ by Li^+ ions.

Preliminary emf measurements in fused $AgNO_3$-$NaNO_3$ mixtures indicate that the concentration cell employed may be used to determine transfer numbers (e.g. $t_{Na^+} = 0.45$ at an average $NaNO_3$ concentration of 87 mole %). Freezing point depressions in sodium nitrate were found to indicate

[redacted]

complete dissociation of a number of salts, and in some cases, like that of KNO_3 or $AgNO_3$, yield an approximate value for the distribution ratio of the solute between solid and liquid $NaNO_3$.

The discovery of a very high solubility of a typical salt, KF, in a typical metal, K, was followed by the determination of the minimum temperature of complete miscibility, 910 ± 5°C, and by an estimate of corresponding temperatures as low as 1000 to 1100°C in the sodium-sodium halide systems. One seems to be dealing with a rather general phenomenon at least for the alkali-metal systems. The changes in solubility observed with variation of either the anion of the salt or the cation and metal are discussed in terms of what are thought to be the principal effective variables, namely, the lattice, or cohesive, energy of the salt and the size of the metal atoms, or ions.

NUCLEAR CHEMISTRY

Statistical analysis of new half-life measurements yielded the following values: Ce^{144} 284.4 ± 1 d, Co^{60} 5.45 ± .1 y, Kr^{85} 10.7 ± .2 y, Pm^{145} 24 ± 2 y. Coincidence measurements of the two gamma rays, of energies 67.8 and 72.7 kev., found in Pm^{145}, and K and L x-rays indicate that there is electron capture to each of two excited levels in Nd^{145} which differ by only 5 kev in energy.

Porcelain enamel was found to show, in addition to its high chemical resistance, every indication of being an especially desirable material for radiochemical laboratory furniture.

ORGANIC CHEMISTRY

In a study of the mechanism of the Wagner-Meerwein rearrangement, a series of reactions of phenyl-labeled 1,2,2-triphenylethanol, its acetate and its tosylate has been carried out under identical reaction conditions used for the chain-labeled analogues, and the radiochemical consequences of these reactions in both systems have been compared. It has been shown by this novel double-labeling technique that the reactions studied fall into two categories: (1) Those in which a statistical redistribution of radioactivity has been achieved and (2) those in which a statistical redistribution has been approached, but not achieved. A simple kinetic relationship has been derived for the latter class of reactions, which allows a calculation of the radiochemical redistributions for various reactions in one series, knowing the results of the other.

The triply-labeled 1,2,2-triphenylethyl acetate system containing ring-labeled, chain-labeled and acetyl-labeled species has been studied kinetically with regard to rates of phenyl redistribution and rate of acetyl exchange under the influence of an acid catalyst. It is found that the rates of equilibration of the ring-labeled acetate and that of the chain-labeled acetate are equal, and that both are identical to the rate of acetyl exchange. These results are interpreted in terms of a mobile transition state mechanism.

Butyl groups were exchanged from reagent tertiary phosphate to labeled phosphoric acid yielding the three esters in labeled form.

Tri-*n*-octyl phosphine oxide-P^{32} when contacted in 0.2 M solution in decane with equal volumes of aqueous solutions lost no more than 5 mg of the phosphine oxide to the aqueous solution.

CHEMISTRY OF SEPARATION PROCESSES

In a study devoted to a comparison of the diffusion rate in ion-exchange resins and in polyelectrolyte solutions considerable lowering of the cation diffusion rate compared with that for NaCl, CsCl, and $CaCl_2$ solutions was observed in the presence of the linear polystyrene sulfonate ion. A very preliminary conclusion of this study is that diffusion rates in polymer solution and resin may approach each other, indicating that the diffusion process is essentially the same in the two systems.

Making use of a theoretical treatment involving the concept of the similarity of an ion exchange resin system with ordinary electrolyte mixtures, good agreement between theoretical and experimental ion exchange selectivities was observed. This makes it possible to estimate such selectivities for a given pair of ions for a wide range of crosslinkings and ionic compositions from two measurements of the selectivity for trace quantities of each ion, at a given crosslinking.

CHEMICAL PHYSICS

In the last and most precise experiment with molecular beams of K at 513°K and HBr at 458°K about two atoms of every 1000 measurably scattered by the HBr reacted to form KBr. The activation energy of the reaction must be assumed to be significantly greater than zero, the value that has been used in most theoretical considerations.

A very detailed and careful neutron-diffraction study of the structure of oxalic acid dihydrate using the single crystal method has led to the elimination of various uncertainties left after several x-ray diffraction studies. The planar configuration of the acid molecule includes the hydrogen atoms. H_3O^+ does not exist in this crystal. In a similar fashion the structure of iodic acid was determined. In refuting an assumption of bifurcated hydrogen bonds it is described in terms of hydrogen bonded molecules forming chains of pentagonal, almost plane rings, each ring involving parts of two molecules.

In cooperative microwave experiments with Duke University on the hyperfine structure of the $J = 2 \rightarrow 3$ rotational transition in CH_3I^{131}, the nuclear spin of eight-day half life I^{131} was found to be $7/2$, and the quadrupole moment to be -0.412×10^{-24} cm^2.

The most significant result of paramagnetic resonance measurements with substances such as H_2SO_4 and H_3PO_4 previously exposed at liquid-nitrogen temperature to ionizing radiation is the agreement within 1% of the observed hyperfine splitting with that expected for the pure 1S electron of a hydrogen atom indicating the presence of unbonded hydrogen atoms in the irradiated specimens.

Very accurate crystallographic information is being derived from studies of the Zeeman effect in pure quadrupole spectra, e.g. for the orientation of the ClO_3^- ion in the crystal of $KClO_3$.

Measurements of the low-temperature heat capacity of cadmium iodide, of interest because of its very typical layer structure, did not give a T^2 dependence as one might have expected, but, in the range from 15 to 20°K, C_p appeared to be varying as about the 1.4th power of T.

RADIATION CHEMISTRY

CO_2 was found not to enter the chemical reaction nor influence its rate when present during the alpha particle induced recombination of H_2 and O_2.

The effect of increased temperature, amounting to less than 15% in several gamma ray induced reactions such as the oxidation of ferrous sulfate, or the reduction of ceric sulfate, etc., in dilute sulfuric acid solution is interpreted in terms of increased yields of the primary decomposition products of water, H and OH, and of slightly decreased yields of H_2 and H_2O_2. Hydrogen and oxygen gas yields were measured using a special closed ampoule technique. The yield of H_2O_2 was found to be independent of pH while at pH > 2 the H_2 yield was greater and the H and OH yields lower than in 0.8 *N* acid solutions.

Potassium bromide in 10^{-3} *M* concentrations lowers the rate of hydrogen peroxide formation in oxygenated water but does not alter the influence of oxygen-concentration nor the influence of sulfuric acid. The hydrogen peroxide yield in an oxygenated bromide solution results from the dissociation of water in the regions of high ionization density. The rate of formation of hydrogen peroxide in pure oxygen-saturated water can be expressed by an equation based upon a back reaction which is first order in hydrogen peroxide concentration.

The oxidation of uranium(IV) by gamma-rays was studied as a function of dose for a wide range of concentrations of uranium(IV), and also with addition of either uranium(III), uranium(VI), hydrogen ion, hydrogen, hydrogen peroxide, or oxygen. In oxygen-free solutions, the decrease in oxidation yield with increased dose cannot be explained by build up of uranyl ion, hydrogen or hydrogen peroxide, but is presumably due to the intermediate formation of uranium(V).

The thermal oxidation of uranium(IV) by H_2O_2 was found to be first order in both uranium(IV) and H_2O_2, with specific rate constants (25°C) at pH 0.16 = 35 liters/mole/min and at pH 1.0 = 150 liters/mole/min.

By the technique of paper chromatography, the concentrations of non-volatile acidic products were measured qualitatively as a function of the gamma-ray dose received by various organic acids. Products usually showed an initial build-up with dose, followed by a decrease as they in turn underwent radiolysis. Some of the products have been identified by the x-ray diffraction patterns of the silver or barium salts.

In a study of the effect of fast electrons on the corrosion of stainless steel by uranyl sulfate solution at 250°C, the results of two 50 hr irradiations indicate that fast electrons, beam density 35 watts/g, had little effect on the formation and preservation of the protective film at the low flow rates used.

INSTRUMENTATION

A new electron beam deflection tube for use in the multichannel pulse amplitude analyzer has been tested. Measurements of channel width,

uniformity, and stability were made for various operating conditions.

It was found that by using the proper type of cathode ray tube display one may greatly extend the number of pulse heights which can be photographically recorded on a given area of film used as a memory in multichannel pulse analysis.

A method was devised for measuring the deflection of an electron beam by depositing narrow bands of nickel, a low secondary electron emitter, onto a target base of Be-Cu.

A germanium diode decoding matrix for a fast binary scaler was built to replace the relatively slow neon bulb matrix previously used.

In a conventional amplifier feedback group, by introducing additional feedback from the output cathode follower to the load resistor of the preceding stage in a bootstrap arrangement, it is possible to improve the linearity of the output signal by a factor of 10 and to double the available output voltage.

An improved circuit for gating the signal from a pulse amplifier has been devised. The new circuit neither affects the shape of the signal nor adds spurious pulses.

REACTOR CHEMISTRY

Results of experimental work on chemical processing of aluminum-uranium fuel elements is being reported in ORNL-1638.

The corrosion rate at 120°C of 309SNb stainless steel exposed to a solution similar in composition to that which results from the dissolution of aluminum jacketed thorium slugs in a HNO_3-HF mixture was found decreased with cathodic protection from 60 to 6 mills per year or by a factor of 10.

Continued study of certain regions of the four component system, UO_3-NiO-SO_3-H_2O has disclosed several new solid compounds some of which have been identified. The solubility of UO_3 in uranyl sulfate solutions of varying concentration at temperatures of 25, 100, 175, and 250°C respectively is reported. The 25°C isotherm for the system UO_2SO_4-$NiSO_4$-H_2O (stoichiometric compositions only) is presented with some of the solid compounds still to be identified.

An exploratory study of the effect of adding nitric acid to solutions of thorium nitrate on the hydrolysis of thorium nitrate and the resulting hydrolytic precipitation has been completed. The first mole of excess nitric acid markedly elevates the temperature at which precipitation occurs, further acid additions being decreasingly effective.

Measurements of the vapor pressures of uranyl sulfate solutions at various concentrations and from 25 to 100°C have been completed and the stoichiometric mean ionic molal activity coefficients have been calculated.

An extension of the kinetic studies of the effect of cupric ion catalysis on the hydrogen-oxygen recombination reaction have more firmly established the dependence on copper concentration and temperature. A few measurements, made with deuterium instead of hydrogen, indicate that the reaction is about 60% as fast with deuterium as with hydrogen.

A continuation of the static tests of the effects of pile radiation on corrosion has involved tests on type 347 stainless steel and on titanium. In addition several out-of-pile tests have been completed. A test on 347 stainless steel at a power density of 2.1 kw/liter show no significant departure from zero power tests and indicates no appreciable radiation effect. A test at 4 kw/liter showed behavior similar to previous tests at 6 kw/liter thus indicating a marked radiation effect.

INORGANIC AND PHYSICAL CHEMISTRY

ANION-EXCHANGE STUDIES

F. Nelson K. A. Kraus

Separation of Weak Acids from Strong Acids with Sulfate-Form Anion-Exchange Resin

As discussed earlier,[1] a strong-base anion-exchange resin in the sulfate form can be used to adsorb acids, particularly strong acids such as sulfuric acid or hydrochloric acid. This property provides a means of separating strong acids from salts as well as from other nonadsorbable materials. In this group fall, as shown some time ago, weak acids such as acetic acid which shows slight adsorption under conditions where a strong acid is strongly adsorbed. The separation of such weak acids from strong acids is readily achieved, the only limitation being that the amount of strong acid added cannot exceed the capacity of the resin. In attempts to demonstrate this principle further, a number of other weak acids as well as nonelectrolytes were investigated, and it was found that some of these materials show considerable adsorption by the resin (Dowex-1), particularly in the sulfate form. For example, the resin could adsorb all the phenol from ca. 5 column volumes of 0.5 *M* aqueous phenol solution when in the chloride form and over 6 column volumes when in the sulfate form. In such cases, of course, the separation from the strong acids will become ineffectual. Considerable care is thus indicated in the use of this technique for the separation of weak acids and nonelectrolytes from strong acids, and before the method can be applied each organic material will have to be tested individually.

Adsorption of Osmium(IV) from Chloride Solutions

The adsorbability of Os(IV) by Dowex-1 from chloride solutions has been studied in 1 to 12 *M* HCl solutions by the equilibrium method using Os^{191} tracer. Distribution coefficients at less than 1% loading of the resin with respect to osmium were ca. 20,000 in 1 *M* HCl and decreased to ca. 2300 in 12 *M* HCl. This behavior is reminiscent of the adsorbability of other platinum elements such as Pd(II) and Pt(IV)[2] and may be typical of the behavior of ions of charge −2 in the platinum group. As discussed earlier,[2] Ir(III) however is not adsorbed under these conditions, and hence separation of osmium from iridium should be readily feasible by this technique.

Uranium(VI) in Nitrate Solutions

It has been found earlier that U(VI) can be adsorbed by Dowex-1 from nitrate solutions. In a reinvestigation of the adsorbability of U(VI) from aluminum nitrate solutions containing 0.5 *M* HNO_3, it was found that excellent adsorption (distribution coefficients between 20 and 700) occurs in the aluminum nitrate concentration range 1.0 to 2.5 *M*. This implies that processing of uranium nitrate–aluminum nitrate solutions by anion exchange is feasible, particularly since these high distribution coefficients were observed when the resins were considerably loaded with uranium.

Adsorption of Lead(II) and Bismuth(III) from Nitrate Solutions

On the basis of earlier work, a number of conditions have been found under which the separation of lead and bismuth in chloride solutions can effectively be achieved. It has now also been shown that both lead and bismuth can be adsorbed from nitric acid solutions, Bi(III) showing an adsorption maximum near 4 *M* HNO_3 with a distribution coefficient $D = 26$, while Pb(II) shows maximum adsorption near 2 *M* HNO_3 with $D = 4$. The differences in adsorbability of lead and bismuth permit their separation in nitrate solutions. Although adsorption of lead is never high, it is sufficient to permit its separation from nonadsorbable elements.

Separation of Alkaline Earths and Alkali Metals by Anion Exchange

It has been found that strontium (as Sr^{89} tracer) can be strongly adsorbed by the strong-base anion-exchange resin Dowex-1 near pH 7.5 from 0.01 to 0.1 *M* ammonium citrate solutions. This adsorption is large even in the presence of appreciable amounts of lithium chloride. A similar behavior was found for calcium. It was demonstrated that this high adsorbability of calcium and strontium, presumably as negatively charged citrate complexes,

[1] K. A. Kraus, F. Nelson, and J. F. Baxter, *J. Am. Chem. Soc.* 75, 2768 (1953).

[2] F. Nelson and K. A. Kraus, *Chem. Semiann. Prog. Rep. June 20, 1953*, ORNL-1587, p. 12.

permits their separation from alkali metals. In the initial work some difficulties were encountered, since the alkaline earths tended to leak through when the columns were washed with citrate solutions of pH ca. 8. It was found that this leakage could be decreased considerably by the use of low cross-linked (nominal 4% DVB) resin and that it could be essentially completely eliminated if a wash with dilute ammonia solutions was substituted for the wash with citrate solutions.

HYDROLYTIC POLYMERIZATION OF ZIRCONIUM(IV), HAFNIUM(IV), AND BISMUTH(III)

J. S. Johnson R. W. Holmberg
K. A. Kraus

Granér and Sillén[3] suggested that in the hydrolysis of Bi(III) a continuous series of particles is formed, all in equilibrium with each other and ranging in size from monomers to "infinitely" large polymers, the exact distribution depending on acidity and concentration. Recently Connick and Reas,[4] in an attempt to interpret solvent extraction data on Zr(IV), advanced the same hypothesis of continuous polymerization and equilibrium between the species and postulated the existence of high molecular weight particles in acidic solutions of Zr(IV). Other workers[5,6,7] drew the conclusion that only low molecular weight polymers of zirconium are formed in strongly acidic media. High molecular weight polymers, not in equilibrium with the more "normal" species, are apparently formed under considerably more drastic conditions (e.g., lower acidity or after boiling).[8]

Since the assumption that high molecular weight polymers are in equilibrium with low molecular weight polymers and monomers appears rather improbable and since measurement of the acidity of $ZrCl_4$ solutions[9] made it unlikely that an infinite series of polymers exists at high acidities, equilibrium ultracentrifugations of Zr(IV) were carried out in chloride and perchlorate solutions.[10] The data were recently augmented and reanalyzed by a modification of the method of Lamm[11] which was suggested to us by Professor George Scatchard, details of which will be published separately. In this computation the charge of the polymer units was considered, and estimates of this charge were obtained by ultracentrifugations under a variety of conditions. Centrifugation of 0.05 *M* Zr(IV) solutions in 1 *M* HCl–1 *M* MCl (where M was Li, Na, and Cs) revealed the existence of only one principal species of Zr(IV) with an apparent degree of polymerization of 3 and charge $Z' < 1$ per monomer unit. At considerably higher and lower acidities (3 *M* HCl and 0.1 *M* HCl–1.9 *M* NaCl) mixtures were found with apparent degree of polymerization varying between ca. 2 to 2.6 (3 *M* HCl) and 4 to 5.4 (0.1 *M* HCl).

Similar low degrees of polymerization were found in ultracentrifugations in perchlorate solutions (1 *M* $HClO_4$–1 *M* $NaClO_4$). In this medium the zirconium particles appeared to carry a considerable charge, and hence preliminary estimation of the degree of polymerization is somewhat more uncertain than for the chloride solutions. The most probable degree of polymerization for 0.05 and 0.12 *M* Zr(IV) solutions in this medium was 3, with an outside possibility that it may be as high as 4.5. There was no indication of an increase in degree of polymerization with concentration. These results may be compared with the (weight average) degrees of polymerization (N_w) estimated by Connick and Reas.[4] These authors report $N_w = 18$ for a considerably more dilute solution [0.03 *M* Zr(IV)–1 *M* $HClO_4$–1 *M* $LiClO_4$] and a value of N_w between 10 and 300 at a higher acidity [0.17 Zr(IV)–2 *M* $HClO_4$].

The results of the ultracentrifugation experiments described here thus indicate that Zr(IV) in strongly acidic solutions (*M* $H^+ > 0.1$) does not show continuous polymerization with high molecular weight products but rather forms only low molecular weight polymers with trimers apparently predominating at acidities near 1 *M*.

[3] F. Granér and L. G. Sillén, *Acta Chem. Scand.* 1, 631 (1947).

[4] R. E. Connick and W. H. Reas, *J. Am. Chem. Soc.* 73, 1171 (1951).

[5] M. Adolph and W. Pauli, *Kolloid-Z* 29, 173 (1921).

[6] G. Jander and K. F. Jahr, *Kolloid-Beih.* 43, 295 (1936).

[7] B. A. J. Lister and L. A. McDonald, *J. Chem. Soc.*, p. 4315 (1952).

[8] See, e.g., R. Ruer, *Z. anorg. u. allgem. Chem.* 43, 282 (1905).

[9] S. Y. Tyree, Jr. and K. A. Kraus, *Chem. Quar. Prog. Rep. Sept. 30, 1949*, ORNL-499, p. 26.

[10] J. S. Johnson and K. A. Kraus, *Chem. Quar. Prog. Rep. Dec. 31, 1949*, ORNL-607, p. 32 and *Chem. Quar. Prog. Rep. March 31, 1951*, ORNL-1053, p. 18.

[11] O. Lamm, *Arkiv Kemi, Mineral. Geol.* 17A, Paper 25 (1944).

The results of ultracentrifugation of Hf(IV) solutions in similar media were almost identical with those of Zr(IV) solutions. Hence for this element also, high molecular weight products are not formed at moderate and high acidities.

A series of ultracentrifugations of Bi(III) perchlorate solutions was also carried out under conditions where Granér and Sillén[3] suggested degrees of polymerization in excess of 20. The results of these experiments are summarized in Table 1. The degrees of aggregation quoted in this table are preliminary estimates since the determination of the partial molar volume of bismuth perchlorate has not yet been completed and since it was furthermore assumed that the charge per monomer unit is +1.

It thus appears that the polymerization mechanism of Granér and Sillén does not apply to these elements. Instead there is now strong evidence that low molecular weight polymers of considerable stability are formed during the hydrolysis of these ions and that it is not necessary to postulate a continuous series of equilibria between monomers and high molecular weight polymers.

TABLE 1. PRELIMINARY DEGREES OF POLYMERIZATION OF Bi(III)

Bi(III) (M)	EXCESS MOLARITY OF H^+*	$NaClO_4$ (M)	N
0.05	0.080	3	4.2 to 4.7
0.05	0.007	3	3.2 to 4.8
0.05	–0.013**	3	4.9
0.05	0	1	5.8
0.025	0	2	4.0 to 5.5

*Excess molarity of $HClO_4$ beyond stoichiometric composition $Bi(ClO_4)_3$.

**Acid-deficient solution.

INTERACTION OF THIOCYANATO CATIONS WITH METAL CATIONS IN AQUEOUS SOLUTION

W. C. Waggener

The interesting addition of silver(I) ion to the thiocyanato radical of certain monothiocyanatoamminecobalt(III) cations in aqueous solution, first discovered by Werner and Mueller[12] in 1900, has been studied recently by spectrophotometric techniques.[13,14] The experiments show that these addition cations are much less stable species and more variable in composition than has been uniformly assumed from Werner's work.

In exploring this unique coordination property of the complex thiocyanato radical it was discovered that mercury(II) ion also interacts to form addition cations which are more stable than those formed by silver(I) ion. In addition, the silver-monothiocyanatoamminecobalt(III) type of interaction was expanded to include mercury(II) ion plus the isomeric *cis*- and *trans*-dithiocyanatoamminecobalt(III) ions and the series of analogous mono- and dithiocyanatoammine cations of tervalent chromium. The extension to the latter series is of special interest in connection with the question of the orientation of the NCS group in the chromium complexes. The nature of the reaction and the identity of type established between the cobalt and chromium series are used to infer that both series have the isothiocyanato structure.

Since becoming a member of ORNL the author has continued these studies, using a Beckman Model DU spectrophotometer to verify and improve results first obtained at the University of Buffalo with a Bausch and Lomb visual spectrophotometer. During the period covered by this report new experiments have been performed which give more insight into this type of cation-cation interaction.

The absorption, from 220 to 950 mμ, of a typical thiocyanato cation is shown in Fig. 1, together with the shift in absorption caused by the presence of an excess of mercury(II) ion.

The interaction ratios of the constituent cations and the stabilities of the species resulting have been investigated by applying the method of continuous variations to the light absorption of these solutions. Figures 2, 3, and 4 illustrate experiments performed with *cis*-dithiocyanatobis(ethylenediamine)cobalt(III)–mercury(II) systems. In each graph well-defined maxima in the plot of optical density difference (calculated, assuming

[12] A. Werner, H. Müller, R. Klien, and F. Bräunlich, *Z. anorg. Chem.* 22, 110 (1900).

[13] W. C. Waggener, *The Isosteric Cyanate Radicals as Coordinating Groups*, Ph.D. thesis, Univ. of Buffalo, 1949.

[14] W. C. Waggener, J. A. Mattern, and G. H. Cartledge, "The Isosteric Cyanate Radicals as Coordinating Groups, I.," paper presented at *122nd Meeting of the American Chemical Society, Atlantic City, N.J., September 1952.*

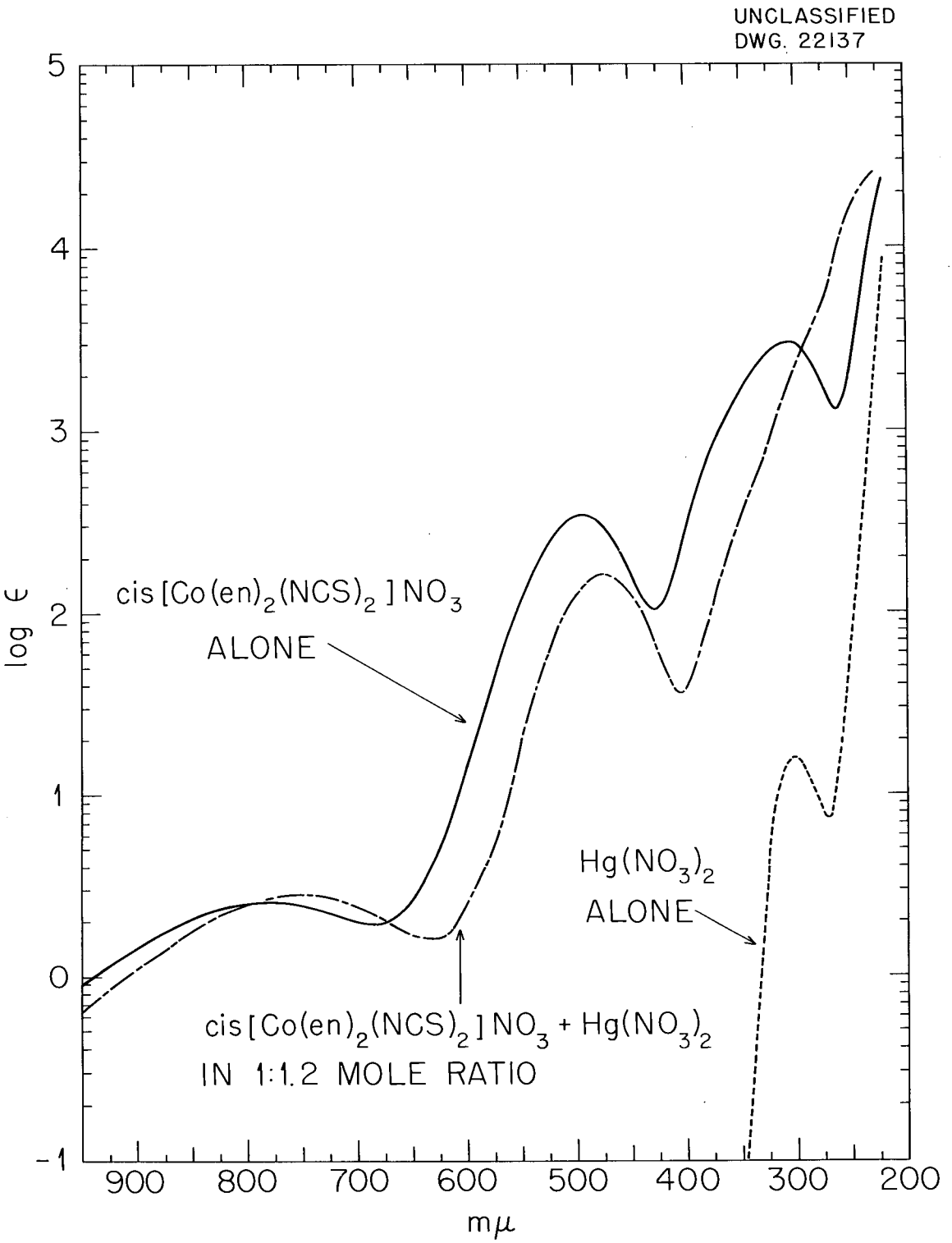

Fig. 1. Absorption Curves of *cis*[Co(en)$_2$(NCS)$_2$]NO$_3$ and Hg(NO$_3$)$_2$ in Aqueous 0.01 M HClO$_4$ as Solvent at 24°C.

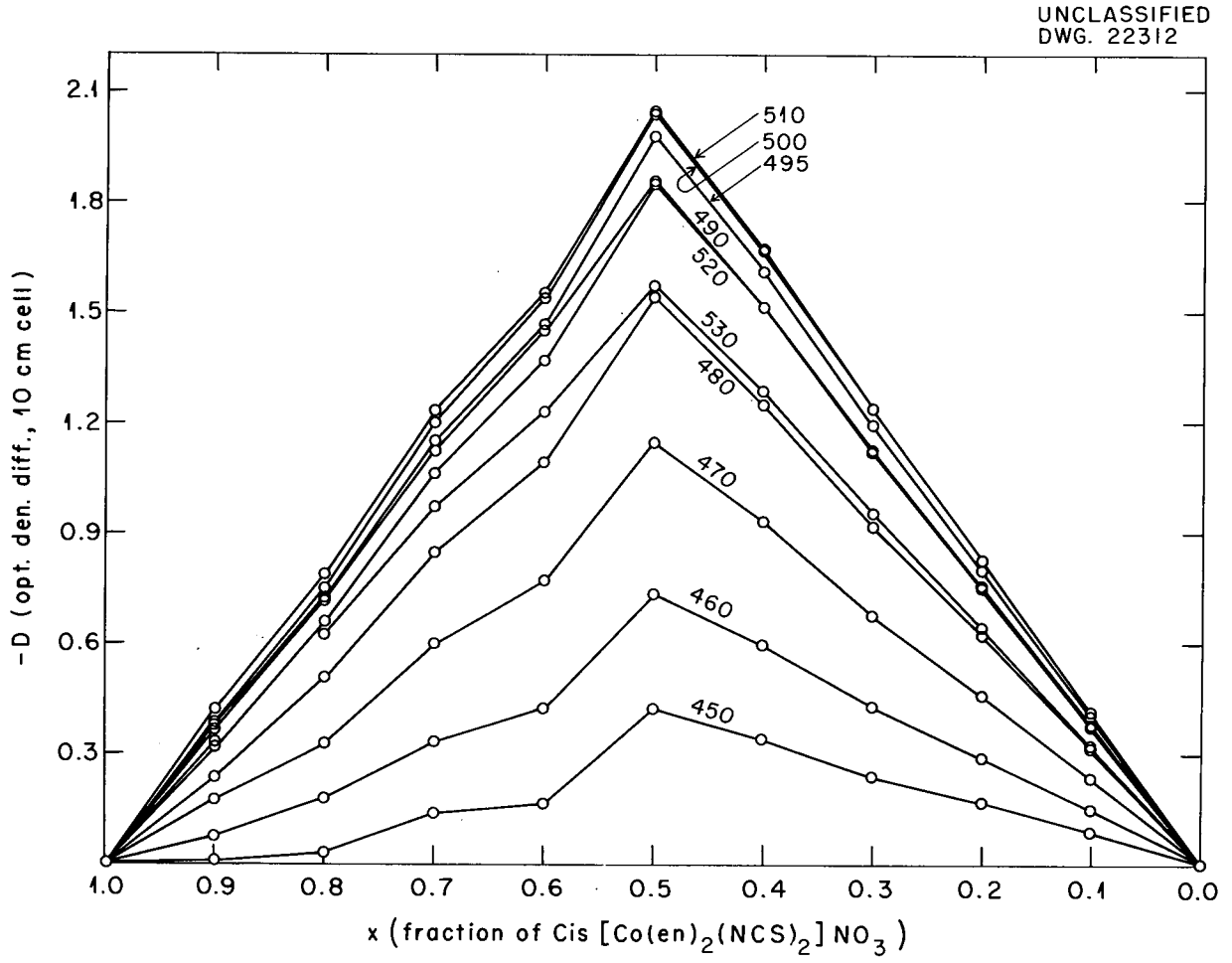

Fig. 2. Continuous Variations Experiment with the 0.002 *M* System *cis*[Co(en)$_2$(NCS)$_2$]NO$_3$–Hg(NO$_3$)$_2$ in Aqueous 0.001 *M* HClO$_4$ at 24°C. Points are from data at ten wavelengths between 450 and 530 mμ.

no complex formation, minus observed) vs. the fraction of *cis*-dithiocyanatobis(ethylenediamine)-cobalt(III) ion indicate a 1:1 interaction species.

The sharpness of the maxima in Figs. 2 and 3 indicates that dissociation of the species is slight at a concentration of 0.001 *M* and is virtually independent of acidity in the pH range from 1 to 3. Dissociation becomes measurable at a concentration of 0.0001 *f* of each parent cation. From the data of Fig. 4 the degree of dissociation was estimated to be approximately 16% for the 0.0002 *M* system.

The insolubility of the 0.002 *M* system, *cis*-dithiocyanatobis(ethylenediamine)cobalt(III) nitrate–mercury(II) nitrate, in 0.1 *M* perchloric acid in the range between $x = 0.5$ and $x = 0.9$ (Fig. 3) probably is due to the existence of complexes containing Co:Hg ratios greater than 1 which are both much more dissociated and much less soluble than the 1:1 species.

At least one insoluble species may be a 2:1 complex. The following experiment was performed with 0.005 *M* solutions of the parent *cis* complex and mercuric nitrate. Both solutions were also 0.5 *M* in perchloric acid. Addition of the solution of *cis* complex to the equilmolar solution of mercury(II) cation resulted in a clear yellow solution up to a 1:1 ratio of cations. The inception of precipitation was quite sharp as the 1:1 ratio was exceeded, and continued until a cation ratio of 2:1 was reached, at which point precipitation was sharply complete and the supernatant solution was virtually color-

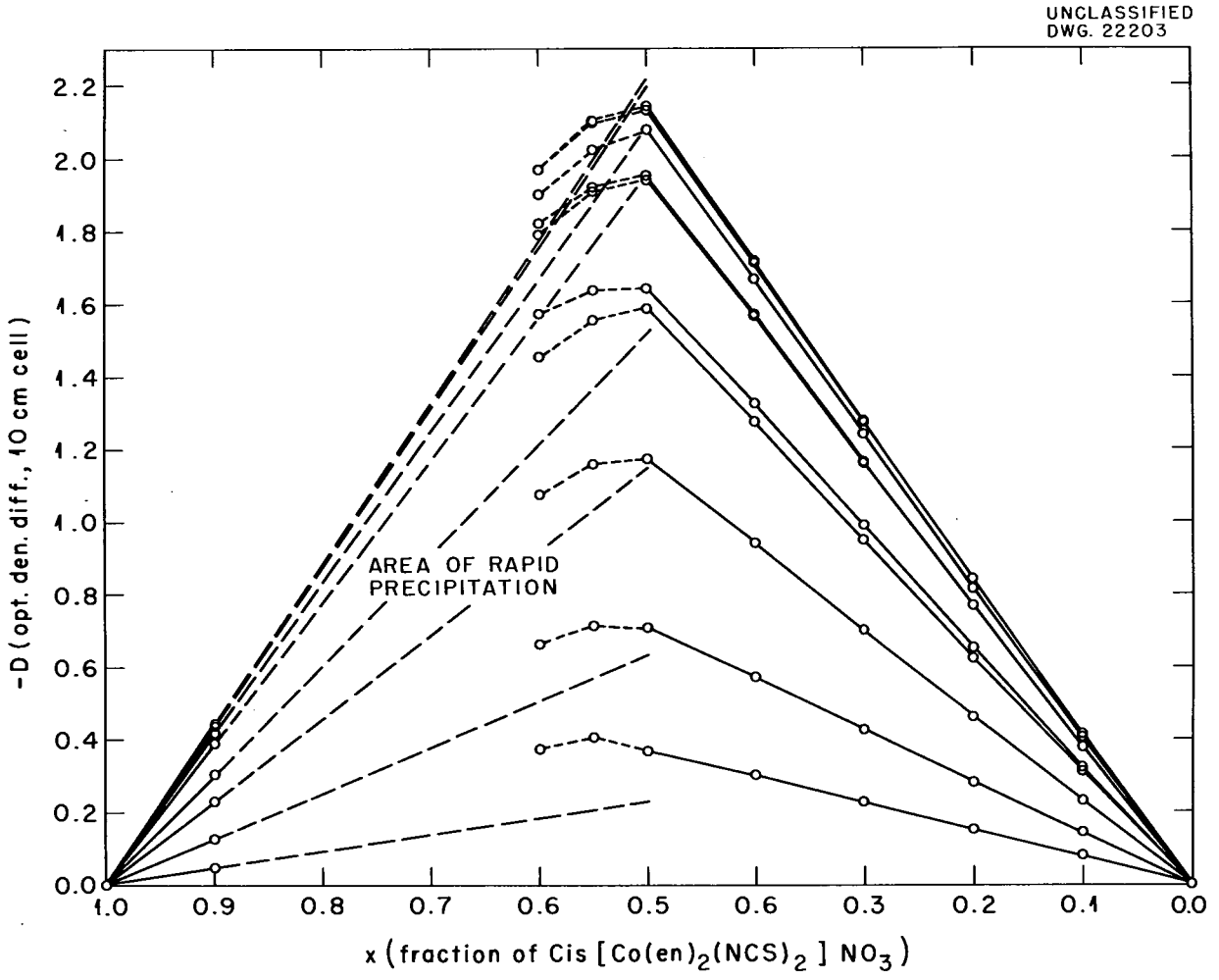

Fig. 3. Continuous Variations Experiment with the 0.002 M System *cis*[Co(en)$_2$(NCS)$_2$]NO$_3$–Hg(NO$_3$)$_2$ in 0.1 M Aqueous HClO$_4$ at 24°C. Points are from data at ten wavelengths between 450 and 530 mμ.

less. Further addition of the orange solution of the parent complex produced no additional visible action. The precipitation was readily reversed by adding more mercury(II) ion, the orange-yellow precipitate completely redissolving as soon as the cation ratio again reached 1:1.

Table 2 is a summary of the systems studied and the interaction ratios found for them. Several points regarding Table 2 should be mentioned.

First, the acid dependence of the interaction of monothiocyanato cations with mercury(II) cation may be due to either or both of the following: the formation of a 1:1 addition species with the monohydroxymercury(II) cation, or a competition between the thiocyanato cation and hydroxyl anion for mercury(II) cations.

Second, while most of the experiments appearing in Table 2 were conducted using the cobalt complexes because of their greater solution stabilities, it should be emphasized that the analogous thiocyanatochromium(III) ions exhibit no qualitative differences with respect to interaction with silver(I) or mercury(II) ions.

Finally, the absence of systems involving the *trans*-dithiocyanato cations is due to the fact that these isomers uniformly gave less soluble interaction products than the analogous *cis*-dithiocyanato complexes, and thus were not amenable to study

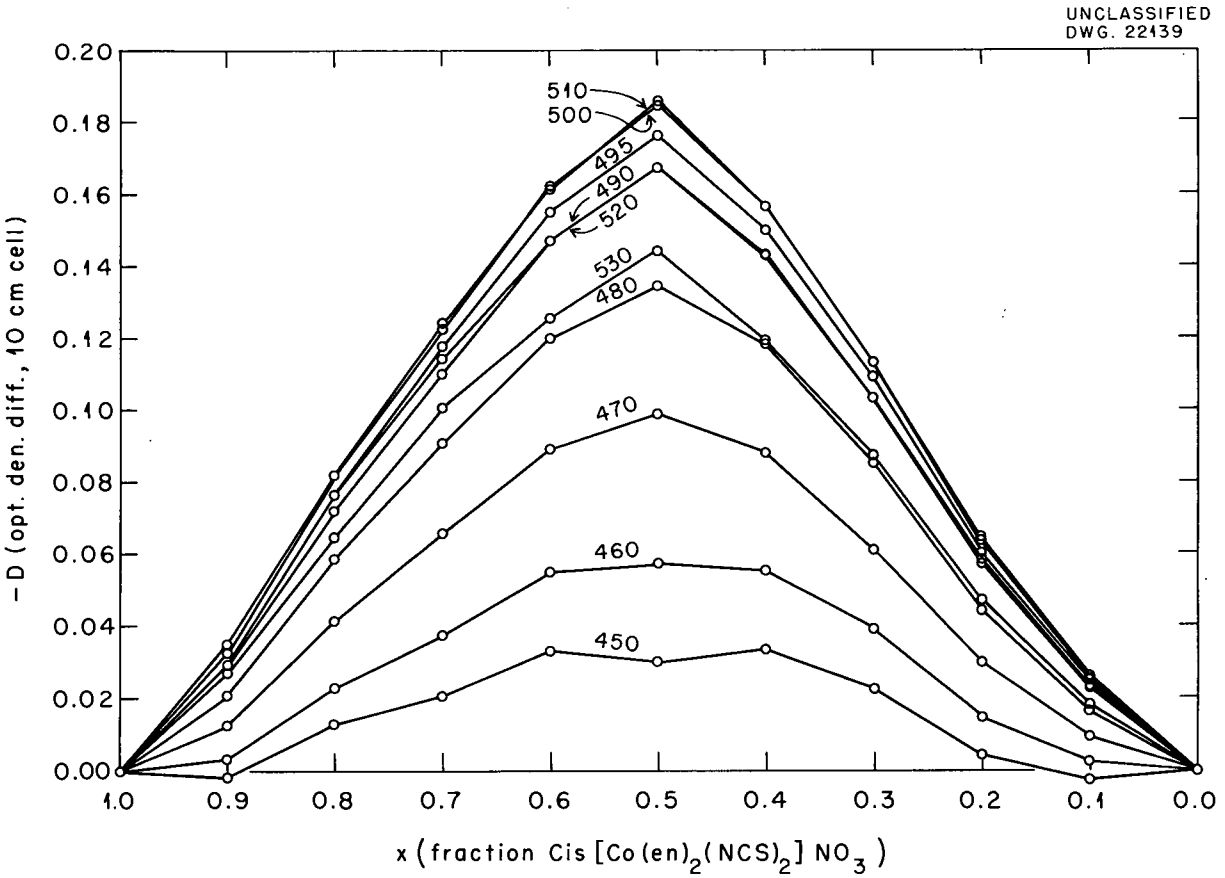

Fig. 4. Continuous Variations Experiment with the 0.0002 *M* System *cis*[Co(en)$_2$(NCS)$_2$]NO$_3$–Hg(NO$_3$)$_2$ in Aqueous 0.1 *M* HClO$_4$ at 24°C. Points are from data at ten wavelengths between 450 and 530 mμ.

in solution by the method here used. The lesser solubility might be attributed, at least in part, to a tendency of the *trans* structures to form polymeric chains involving alternate links of thiocyanato and metal cations.

CHEMISTRY OF CORROSION

G. H. Cartledge

Studies on Electrode Potentials

G. H. Cartledge R. P. Yaffe[15]

The first phase of the studies summarized in the last report[16] has been completed. This consisted of a broad survey of the effects upon the electrode potential of stainless steel, type 347, caused by the addition of low concentrations of foreign ions. As previously described, the measurements were made in 0.1 *N* sulfuric acid at 85°C, the solutions being adequately stirred with access to air. A vibrating-reed electrometer and a Brown recorder were used for the measurement of the emf of cells consisting of the steel electrodes bridged to a silver–silver sulfate reference electrode at room temperature.

The following additives, which have been investigated since the last report, have an ennobling effect: palladium(II), gold(III), periodate, iodate, bromate, persulfate, vanadium(V) oxide, and osmium(VIII) oxide. Gold(III) was reduced to colloidal metal which deposited on all exposed surfaces. Osmium(VIII) oxide began to give a

[15]Terminated Sept. 15, 1953.

[16]R. P. Yaffe, *Chem. Semiann. Prog. Rep. June 20, 1953*, ORNL-1587, p. 13.

TABLE 2. INTERACTION RATIOS IN AQUEOUS SOLUTION

COMPLEX SALT	METAL SALT	MOLARITY OF COMPLEX SALT PLUS METAL SALT	AQUEOUS SOLVENT	MOLE RATIO COMPLEX SALT / METAL SALT
$[Co(NH_3)_5NCS](NO_3)_2$	$AgNO_3$	0.004	0.005 *M* HNO_3	1.0
$[Co(NH_3)_5NCS](NO_3)_2$	$AgNO_3$	0.002	0.001 *M* $HClO_4$	1.0
$[Co(NH_3)_5NCS](NO_3)_2$	$Hg(NO_3)_2$	0.004	~0.004 *M* HNO_3	1.5
$[Co(NH_3)_5NCS](NO_3)_2$	$Hg(NO_3)_2$	0.002	0.001 *M* $HClO_4$	1.1
$[Co(NH_3)_5NCS](NO_3)_2$	$Hg(NO_3)_2$	0.002	0.100 *M* $HClO_4$	2.0
$[Cr(NH_3)_5NCS](NO_3)_2$	$Hg(NO_3)_2$	0.010	~0.01 *M* HNO_3	1.5
$[Cr(NH_3)_5NCS](NO_3)_2$	$Hg(NO_3)_2$	0.005	~0.005 *M* HNO_3	1.0
cis-$[Co(en)_2(NCS)_2]NO_3$	$AgNO_3$	0.002	H_2O	1.0
cis-$[Co(en)_2(NCS)_2]NO_3$	$Hg(NO_3)_2$	0.002	0.100 *M* $HClO_4$	1.0
cis-$[Co(en)_2(NCS)_2]NO_3$	$Hg(NO_3)_2$	0.002	0.001 *M* $HClO_4$	1.0
cis-$[Co(en)_2(NCS)_2]NO_3$	$Hg(NO_3)_2$	0.0002	0.100 *M* $HClO_4$	1.0
cis-$[Cr(en)_2(NCS)_2]NO_3$	$Hg(NO_3)_2$	0.01	~0.001 *M* HNO_3	1.0

black precipitate at concentrations above 6×10^{-5} *f*, but the ennobling followed the logarithmic equation up to that point. Palladium(II) ions were apparently reduced on the steel electrode initially to a sufficient extent to make it function essentially as a palladium–palladium(II) electrode, corresponding to a two-electron process. Again it was observed that, if no complicating reactions occurred, a graph of the electrode potential vs. the logarithm of the concentration of the added constituent was essentially linear.

Forty-seven foreign ions or compounds have been used as additives in the experiments. Of these, the only one which debased the potential was the tin(II) ion; even iodide ion was without effect at the concentration employed (up to 9×10^{-4} *f*). Table 3 shows all the ions which have been found to have no significant effect on the electrode potential under the conditions involved.

This rather wide survey of the field has demonstrated that the observed changes in potential follow an equation of the Nernst type so systematically that the regularities can hardly be fortuitous. There is apparently a multiplicity of processes involved, however. Thus, in certain cases, the rate of change of potential after addition of a foreign ion clearly indicates that there is first an almost instantaneous response like that of a platinum electrode in a redox system, which is then followed by a much slower ennobling that may take an hour or more for completion. Incomplete study of three such systems has shown that the logarithmic law describes the rapid changes in potential quite well, when correction is made for the slower process. The slopes obtained obviously depend upon the reliability with which such correction can be made, and details on these results will be reserved until further studies have been made.

Two studies have been made with radioactive tracers to determine the relation between the amount of the additive permanently deposited on the steel electrode and the concentration. These studies were made with cupric sulfate containing Cu^{64} and with chromate containing Cr^{51}. In each case, six electropolished and six hand-polished stainless steel electrodes were simultaneously

stabilized in 0.1 *N* sulfuric acid at 85°C. Then the cupric salt or chromate was added in six increments. After each increment, time was allowed for the potential to become steady. One electrode of each kind was then removed, carefully rinsed, and counted. Owing to the practical impossibility of hand-polishing the electrodes to exactly the same surface condition, it was hardly to be expected that the activity data would be precise. It was found, however, that the deposited activity increased with the concentration of the additive approximately linearly on a log activity–log

TABLE 3. IONS WHICH PRODUCED NO POTENTIAL CHANGES

ION	CONCENTRATION RANGE (moles/liter)	COMMENT
Na^+	3×10^{-5} to 2×10^{-3}	
K^+	1×10^{-5} to 1×10^{-3}	
Tl^+	3×10^{-5} to 2×10^{-3}	
Ca^{++}	3×10^{-5} to 2×10^{-3}	
Zn^{++}	3×10^{-5} to 2×10^{-3}	Very slight ennobling, possibly due to an impurity
Cd^{++}	3×10^{-5} to 2×10^{-3}	
Mn^{++}	3×10^{-5} to 2×10^{-3}	
Ni^{++}	3×10^{-5} to 2×10^{-3}	
Pb^{++}	1×10^{-8} to 9×10^{-7}	Concentration limited by solubility
UO_2^{++}	3×10^{-5} to 2×10^{-3}	Very slight ennobling, possibly due to an impurity
Cr^{+++}	3×10^{-5} to 2×10^{-3}	
Bi^{+++}	1×10^{-7} to 5×10^{-4}	Concentration limited by solubility
Ce^{+++}	3×10^{-5} to 2×10^{-3}	
La^{+++}	3×10^{-5} to 2×10^{-3}	Very slight ennobling, possibly due to an impurity
$Co(NH_3)_6^{+++}$	1×10^{-5} to 9×10^{-4}	
F^-	1×10^{-5} to 1×10^{-3}	
Cl^-	3×10^{-5} to 2×10^{-3}	Known to activate at higher concentrations
I^-	1×10^{-5} to 9×10^{-4}	
NO_3^-	1×10^{-5} to 1×10^{-3}	
ClO_3^-	1×10^{-5} to 1×10^{-3}	
ClO_4^-	2×10^{-5} to 3×10^{-3}	
ReO_4^-	1×10^{-5} to 1×10^{-3}	
TcO_4^-	7×10^{-6} to 1×10^{-3}*	
PO_4^{---}	1×10^{-5} to 1×10^{-3}	
AsO_4^{---}	1×10^{-5} to 1×10^{-3}	

*The beta activity of the electrodes from this experiment was determined after they were thoroughly rinsed with distilled water. The hand-polished electrode showed counts equivalent to about 1.3×10^{14} atoms/cm^2 (geometrical area) and the electropolished electrode about an eighth as many. A monatomic layer would require more than 10^{15} atoms per square centimeter of actual area. The counts demonstrate that the technetium deposited on the surface by reduction is adequate to cover only a very small fraction of the surface.

concentration plot. In both cases, the total amount of activity removed from solution at the highest concentration represented, at most, a monatomic layer, so that the concentration of the residual solution was not appreciably altered.

In order to obtain measurements over a wider range of concentrations, a second series of experiments was performed with active copper and chromium in the following manner. Hand-polished specimens 1 cm square were placed in test tubes containing 10 ml of the active additives at various concentrations in 0.1 *N* sulfuric acid. The tubes were heated in a boiling water bath for 30 min, then removed, rinsed thoroughly, and counted.

The resulting data are shown in Figs. 5 and 6, in which the percentage of the total activity deposited at each concentration, rather than the activity itself, is plotted against the concentration. It is to be observed that the activity retained on the specimens in these experiments at 100°C was greater than that found in the potential measurements at 85°C. In both cases, however, the log-log relationship gave the best correlation of the data. It may be shown that such a relationship and the quickly observed potential changes are consistent with the theory of the partial covering of an inert electrode with the reduced form of an oxidant in solution, as originally developed by Herzfeld.[17]

[17] K. F. Herzfeld, *Physik. Z.* 14, 29 (1913).

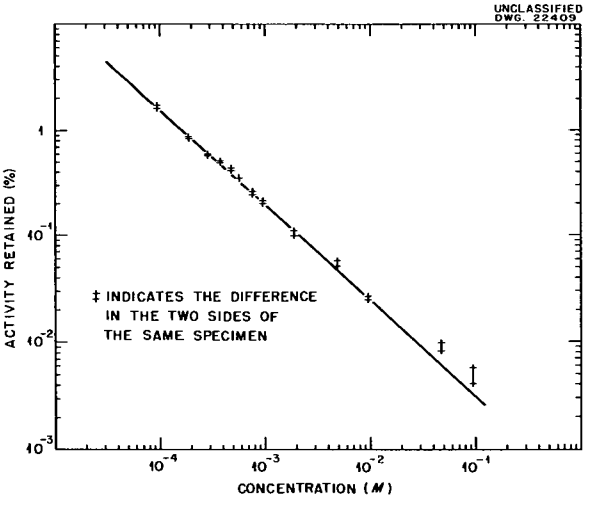

Fig. 5. Activity Deposited on Stainless Steel at 100°C From Cupric Sulfate Solutions of Varying Concentrations in 0.1 *N* H_2SO_4.

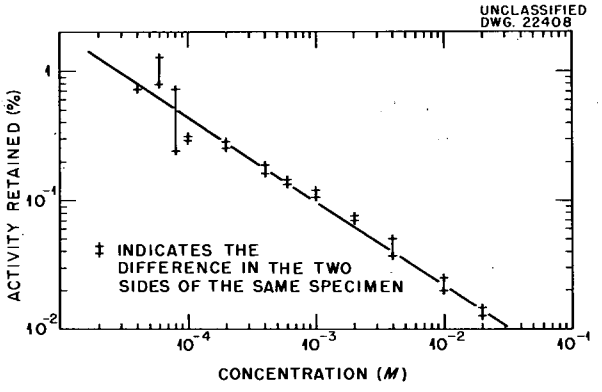

Fig. 6. Activity Deposited on Stainless Steel at 100°C From Potassium Chromate Solutions of Varying Concentrations in 0.1 *N* H_2SO_4.

Other assumptions are possible, however, and detailed discussion of the point will be postponed until completion of more thoroughgoing experiments now in progress.

Action of Corrosion Inhibitors

G. H. Cartledge

A few of the experiments on inhibition described in the last report[18] have continued throughout the past half-year. Two specimens of emeried carbon steel (SAE 1010) have been completely inhibited by 50 ppm of technetium for a total of 50 weeks. For the first 13 weeks, the solutions were maintained near 100°C during the days and at room temperature overnight. Since that time, the tubes have been at room temperature and loosely stoppered. The solutions have remained water-clear and the metal surfaces are unchanged. One of the solutions contains 10 ppm of chloride ion as potassium chloride. The beta activity of this specimen has remained essentially constant during the past eight months at a level corresponding to approximately 1.4×10^{-4} mg of technetium on the 4 cm^2 of geometrical area.

Likewise, the experiment with sodium tungstate as inhibitor for carbon steel has been extended to a total of 30 weeks. The solutions contained 20 ppm of chloride ion and sodium tungstate (Na_2WO_4) at concentrations of 0, 10^{-3}, 10^{-2}, and 10^{-1} *f*. The solutions were maintained near 100°C for a total

[18] G. H. Cartledge and R. P. Yaffe, *Chem. Semiann. Prog. Rep. June 20, 1953*, ORNL-1587, p. 17.

of 708 hr during the first 15 weeks and have been at room temperature subsequently. During this time the specimens in the 10^{-1} and 10^{-2} *f* solutions have not corroded, except for two or three small light-brown spots which formed at once and have not developed. The 10^{-3} *f* solution failed quickly, and the control specimen has lost more than 45 mg from 4 cm^2 of area.

In connection with this tungstate work, the solubility of tungstic acid (H_2WO_4) in uranyl sulfate solutions up to 290°C has been determined. For details of this work, reference is made to the last quarterly report of the HRP.[19]

A series of experiments was made to determine the minimum quantity of technetium required for inhibition of the corrosion of carbon steel (SAE 1010) in distilled water. The tests were run in tubes made from a water-cooled 19/38 standard-taper pyrex joint closed off at the bottom to make a 150-mm test tube and constricted at the top to provide a condenser with access of air. These tubes were held in a boiling water bath which was heated during the working hours and cooled at night. The specimens were hand-polished pieces of carbon steel 1 × 2 cm and were immersed in 10 ml of solution. Table 4 indicates the results obtained.

The apparently sharp break between 3 and 5 ppm under these conditions was confirmed in a duplicate test. Beta counts on the washed specimens at the conclusion of the tests showed the same sharp break between 3 and 5 ppm, the corroded specimens from the lower concentration being much more active.

The tests with 5 and 10 ppm of technetium in distilled water and carbon steel were repeated at 250°C. The 1-cm^2 specimens (hand polished) were mounted in a slot in a Teflon block within platinum-lined bombs. The bombs were held at temperature for 116 hours. At the end of this time the solutions were water-clear; each specimen showed a little tarnish where it was in contact with the Teflon. Elsewhere only a thin interference film was observed, and the weight remained unchanged within ±0.1 mg. In a previous similar test lasting only 92 hr, without technetium, the 0.27-g specimen lost 9 mg. The observations in the test with 5 ppm were indistinguishable from those obtained in the earlier test with 100 ppm.

Previous experiments indicated that the perrhenate ion, ReO_4^-, in spite of its close similarity to the pertechnetate ion, failed to inhibit the corrosion of carbon steel in concentrations at which technetium was effective. In order to determine whether inhibition could be found at any concentration, experiments were conducted with potassium perrhenate at the following concentrations: 5×10^{-5}, 1×10^{-4}, 5×10^{-4}, 1×10^{-3}, 3×10^{-3}, 3.5×10^{-2}, and 7×10^{-2} *f*, the last solution being saturated at about 30°C. In all cases, formation of a black smudge occurred at 100°C within a matter of minutes, and corrosion proceeded steadily.

[19] C. E. Coffee, W. L. Marshall, and G. H. Cartledge, *HRP Quar. Prog. Rep. Oct. 31, 1953*, ORNL-1658 (in press).

TABLE 4. INHIBITORY EFFECT OF POTASSIUM PERTECHNETATE AT DIFFERENT CONCENTRATIONS

Tc (ppm)	$KTcO_4$ CONCENTRATION (*f*)	OBSERVATIONS
1	1×10^{-5}	Spotting within 15 min; rusted overnight
3	3×10^{-5}	Spotting within 15 min; rust evident in 2 hours
5	5×10^{-5}	Complete inhibition; 10-week observation
7	7×10^{-5}	Complete inhibition
10	1×10^{-4}	Complete inhibition
15	1.5×10^{-4}	Complete inhibition
25	2.5×10^{-4}	Complete inhibition
36	3.6×10^{-4}	Complete inhibition
50	5×10^{-4}	Complete inhibition; 50-week observation

It is necessary to conclude that there is a fundamental difference between technetium and rhenium with respect to inhibition under the experimental conditions maintained in these tests. If the theoretical considerations underlying this study are valid, this difference most probably will be found to arise from a different distribution of charge within the two XO_4^- ions, since their dimensions are very much alike and the perrhenate ion has an even lower oxidation potential than the pertechnetate ion. If the perrhenate ion has a more nearly covalently bonded structure than the pertechnetate ion, it will then exert a smaller electrostatic polarization on the surface on which it is adsorbed, and hence will have less effect in tying up the electrons required for the cathodic half of the corrosion process. Unfortunately, no data are at present available to test this point, although it has been reported[20] that, in its 4^+ valence state, rhenium forms a hexachloro complex anion that is much more stable with respect to hydrolysis and thermal decomposition than the corresponding technetium complex. If this difference is generally true, it may be evidence for a higher degree of polarity in the technetium salts.

In one experiment, a mixture containing 3 ppm of technetium with 1×10^{-4} *f* potassium perrhenate was tested for inhibition. None was observed; so it seems unlikely that even part of the requisite technetium can be replaced by rhenium.

One of the objects of the technetium experiments has been to determine definitely whether the inhibition of corrosion in this case depends upon the presence of a protective film containing reduction products such as technetium dioxide. As previously indicated, the electrostatic polarization hypothesis considers the unreduced XO_4^- ion to be the effective inhibitor. Evidence that this is indeed the case was seen in the following observations which were referred to in the earlier report:

1. Whereas some technetium always remains on the metal in insoluble form, presumably as technetium dioxide, the amount of this deposit may vary over a very wide range, depending upon the surface activity of the metal. In no case, however, does such reduced material inhibit corrosion upon removal of the specimen from the solution. On the contrary, inhibition persists even with minimal quantities of deposited technetium, provided as much as 5 ppm of technetium remains in solution as the TcO_4^- ion.

2. In the experiments in which addition of technetium diminished the spontaneous current flowing between an iron cathode and a zinc anode,[18] the residual current caused a visible film of TcO_2 to deposit on the cathode. When the pertechnetate was flushed out of the cathode compartment by potassium sulfate, the current returned to its initial value in spite of the presence of the film. It was therefore the soluble technetium which diminished the current flow rather than the film. The film-covered electrode corroded readily when transferred to distilled water.

In order to make the argument stronger, an inhibition experiment was carried out under very corrosive conditions which were at the same time unfavorable to the existence of a film of TcO_2. This involved the use of hydrogen peroxide, which very rapidly oxidizes technetium dioxide to the pertechnetate ion in either ammoniacal or weakly acidic solution. In preliminary experiments, a 0.1 *f* potassium sulfate solution containing 8×10^{-4} *f* pertechnetate ion was electrolyzed between carbon steel electrodes until a blue cathodic deposit was obtained with a count corresponding to 0.01 to 0.03 mg of technetium as TcO_2. Simultaneously, the anode rusted and the deposit contained considerable technetium activity. Under the microscope the blue cathodic deposit was seen to contain a few microscopic brown areas, evidently indicating minute anodes from local-action cells persisting at the current density employed (*ca.* 0.4 ma/cm^2). Upon treatment of these electrodes with ammoniacal 3% hydrogen peroxide, the blue cathodic deposit disappeared almost instantaneously, whereas the brown anodes showed no visible change. Counting experiments demonstrated that 97% of the cathodic deposit could be removed by two treatments at room temperature but that only about 50% could be removed from the anodic product. After treatment of a cathode, the minute brown anodic deposits were still visible and probably accounted for much, if not all, of the residual activity.

In view of this ready solubility of TcO_2 in the peroxide treatment when it is not mixed (or combined) with iron oxides, inhibition tests were conducted with electropolished carbon steel specimens in potassium pertechnetate at 3.6×10^{-4} *f* (36 ppm of Tc) and containing 10 ppm of

[20] C. M. Nelson, *Magnetochemistry of Technetium and Rhenium*, p. 15, Ph.D. thesis, Univ. of Tennessee, 1952.

chloride. To this solution, 3% hydrogen peroxide was added dropwise at a sufficient rate to maintain a steady evolution of oxygen. Blanks (no technetium) showed that corrosion proceeded much more rapidly in these experiments at 85°C than in other tests at 100°C without the peroxide. Table 5 shows the results of one experiment in which the peroxide addition at 85°C was continued for 2 hours. These counts were made after the specimens were rinsed thoroughly. The specimens were counted on the top shelf of an open-end Geiger counter (2.46 mg/cm^2), and the last two specimens corresponded to 1.3×10^{-6} and 2.1×10^{-6} mg of technetium, respectively, on the 4-cm^2 area. These amounts are equivalent to the order of 10^{12} atoms per square centimeter of geometrical area, whereas about 10^{15} would make a monomolecular layer. Since the true area was doubtlessly considerably greater than 4 cm^2, it is evident that any film formed could cover only a minute fraction of the surface. All previous observations would make it probable that even these small amounts of activity are concentrated in microscopic areas that were initially anodic. Further experiments are to be made to determine, if possible, the precise origin of anodically deposited activity.

To summarize: of the elements V, Cr, Mn, Mo, Tc, Ru, W, Re, and Os in their highest valence state, only Cr, W, and Tc inhibit effectively at 100°C under the conditions of these experiments. Tungsten is inhibitive only at much higher concentrations than are required for Cr and Tc. Osmium is reduced to a film that is protective as long as it is intact, but the film is very sensitive and, once it is perforated, pitting attack proceeds, the attack being very rapid if electrolytes are present. Technetium at or above 5 ppm inhibits the corrosion of carbon steel (SAE 1010) in distilled water at either 23, 100, or 250°C. In two cases, the protection has persisted for almost a year at the lower temperatures.

TABLE 5. INHIBITION IN THE PRESENCE OF HYDROGEN PEROXIDE

SPECIMEN	WEIGHT CHANGE (mg)	COUNTS PER MINUTE
Control	−6.2	
Tc only	-0.0_5	232
Tc + H_2O_2	+0.1	13
Tc + H_2O_2 (dup.)	0.0	20

Hydrogen Overvoltage on Amalgams

W. E. Clark

The investigation referred to in the last report[21] was begun with a study of the kinetics of the decomposition of lithium amalgam. It is planned eventually to extend the study to include amalgams of potassium, barium, and perhaps other metals of the alkali and alkaline earth groups.

A metal amalgam in contact with an aqueous solution of the metal hydroxide decomposes according to the following equation:

$$M(Hg)_x + nH_2O \longrightarrow M^{n+} + nOH^- + n/2H_2 + xHg$$

The potential of the cell

$$M(Hg)_x \mid MOH \mid H_2(Pt)$$

can be represented by the classical Nernst equation

$$(1)\quad E = E^0_{M(Hg)} - \frac{RT}{F} \ln Kw - \frac{RT}{F} \ln \frac{[M^{n+}][OH^-]^n[Hg]^x[P_{H_2}]^{n/2}}{[M(Hg)_x][H_2O]^n}$$

in which E^0 is the potential of the amalgam of unit activity in equilibrium with its aqueous ion at unit activity, Kw is the ion product constant of water, and the bracketed symbols represent activities of the various components of the system. In the following development the activity of the mercury, [Hg], will be assumed to be unity.

Although the decomposition reaction is strongly exothermic for amalgams of active metals, particularly for those of the alkali and alkaline earth groups, amalgams of most of these metals decay at relatively slow rates provided the systems are kept sufficiently pure.

According to the published work on the subject of amalgam decomposition,[22,23,24] highly repro-

[21] W. E. Clark, *Chem. Semiann. Prog. Rep. June 20, 1953*, ORNL-1587, p. 19.

[22] J. N. Brönsted and N. L. R. Kane, *J. Am. Chem. Soc.* 53, 3624 (1931).

[23] F. A. Fletcher and M. Kilpatrick, *J. Phys. Chem.* 42, 113 (1938).

[24] O. L. Kaptsan and Z. A. Iofa, *Zhur. Fiz. Khim.* 26, 201 (1952).

ducible decay rates in alkaline media are difficult to obtain in the case of any given amalgam, but in any one experiment the kinetics follow approximately the relationship for a half-order reaction or

$$(2) \qquad -\frac{dM}{dt} = \frac{S}{V} kM^{1/2}$$

in which M is concentration of the metal in the amalgam, t is time, k is the rate constant, and S and V are the surface area and volume of the amalgam, respectively.

It appears probable that the rate controlling step in amalgam decomposition is one which involves the liberation of hydrogen on the mercury surface; if so, the Tafel overvoltage equation would be expected to apply.

$$(3) \qquad \eta = a + b \ln i ,$$

in which η is the overvoltage, a and b are constants, and i is the current density. Several investigators[24,25,26] have attempted to apply this relationship to the kinetics of amalgam decomposition. If this relationship is valid, the value of E in Eq. 1 is equal to η, the hydrogen overvoltage, and

$$(4) \quad a + b \ln i = E^0 - \frac{RT}{nF} \ln \frac{[M^{n+}][OH^-]^n[P_{H_2}]^{n/2}}{[M(Hg)][H_2O]^n}.$$

On a decomposing amalgam surface, the rate of hydrogen evolution is governed by the rate at which the amalgam reacts; so for a unit surface (assuming S/V is also unity) the current density $i = dx/dt\ F$, F being the faraday constant and dx/dt being the net rate at which metal atoms go from the amalgam into the aqueous phase. Then

$$(5) \quad a + b \ln \left(\frac{dx}{dt} F\right) = E^0 - \frac{RT}{nF} \ln \frac{[M^{n+}][OH]^n[P_{H_2}]^{n/2}}{[M][H_2O]^n}.$$

If the assumption is made that the Tafel constant, b, for this reaction has the often-reported value of $2RT/F$, then for the amalgam of a univalent metal, if Eq. 5 is solved for $\ln dx/dt$,

$$(6) \quad \ln \frac{dx}{dt} = \frac{F}{2RT}\left(E^0 - a + \frac{RT}{F} \ln Kw - \frac{2RT}{F} \ln F\right) - \frac{1}{2} \ln \frac{[M^+][OH^-][P_{H_2}]^{1/2}}{[H_2O][M(Hg)]}.$$

Since the terms in the parenthesis are all constant, they can be combined in one constant term. Then by substituting the average activity of the metal hydroxide for the individual ionic activities and by assuming $P_{H_2} = 1$ atm,

$$(7) \quad \ln \frac{dx}{dt} = \text{const.} - \ln [MOH] + \ln [H_2O]^{1/2} + [M(Hg)]^{1/2} .$$

This equation predicts the observed half-order relationship with respect to the amalgam concentration and also predicts that the rate will be directly proportional to the half power of the activity of the water and inversely proportional to the first power of the activity of the alkali, respectively. On the latter point the opinion of those in the field is rather sharply divided. It should be pointed out that the assumption of the unique value of $2RT/F$ for the Tafel constant, b, is unjustified. While this is perhaps the best average value of b for many systems and for a wide range of current densities, the experimental error in the determination of b is often on the order of 10 to 20%. Furthermore, Bockris[27] has shown that in lithium and sodium hydroxides the best value of b corresponds to 1.7 RT/F and in potassium hydroxide to 1.5 RT/F. These values predict reaction orders of about 0.6 and 0.7, respectively, with regard to amalgam concentration.

In order to allow the determination of amalgam concentration at any time during decomposition, a potentiometric method based on hydrogen electrode measurements and utilizing the relationships expressed in Eq. 1 was developed. This method has

[25] Z. A. Iofa and Z. B. Pechkovskaia, *Doklady Akad. Nauk S.S.S.R.* 59, 265 (1948).

[26] H. H. Garretson, ORNL CF-53-10-207 (limited access report).

[27] J. O'M. Bockris and R. G. H. Watson, *J. chim. phys.* 49, C70 (1952).

the advantage of giving the amalgam concentration at any instant without the necessity of sampling. It should be more accurate, particularly during the first and last stages of a decomposition experiment, than the hydrogen evolution methods which have been employed by most of the previous workers in this field. Details of this method have been published elsewhere.[28]

From the data of Lewis and Keyes[29] and of Harned and Swindells,[30] Garretson[26] calculated $E^0_{Li(Hg)}$ to be approximately 2.079 volts. This value, as will be seen later, is in error by about 3 mv. From his own work, Garretson[26] established the following expressions for the variation of activity with concentration in the amalgam and aqueous phases, respectively:

$$\log[Li(Hg)] = \log M + 0.1428M ,$$

$$\log \frac{[LiOH]^2}{[H_2O]} = 0.1183 \log m - \frac{0.06\sqrt{m}}{1 + 1.1\sqrt{m}} .$$

Therefore at 25°C,

$$(8)\quad E = E^0_{Li(Hg)} - 0.8280 - \left(0.1183 \log m - \frac{0.06\sqrt{m}}{1 + 1.1\sqrt{m}}\right) - 0.02958 \log\left(\frac{P - 23.7}{760}\right) + 0.05916 (\log M + 0.1428M) ,$$

where P is the total pressure in millimeters of mercury, 23.7 is the vapor pressure of water at 25°C, and M and m are the molalities of lithium in amalgam and aqueous phases, respectively.

The pyrex cell in which the decomposition studies were made is shown in Fig. 7. Water at 25°C was circulated through the jacket during the course of each run. Purified hydrogen was constantly bubbled through the aqueous phase, and both phases were gently agitated by the double-bladed pyrex stirrer driven by a 100-rpm synchronous motor. With the very small stirrer blade used it was found that the difference in the potential of the amalgam when stirred and when quiet was less than 0.1 mv. Three hydrogen electrodes were employed, and readings of all three vs. the amalgam pool were taken periodically by use of a Rubicon type B potentiometer. The readings of the three electrodes usually agreed within 0.02 mv except during the very first part of a run when occasional variations on the order of 0.1 mv were observed. During the first few runs amalgam samples were taken periodically and analyzed by means of the electrometric zinc-amalgam method.[31] After the accuracy of Eq. 8 was established, this was discontinued and the amalgam concentration was determined directly from the hydrogen-electrode measurements and Eq. 8. Since the volume of the aqueous phase used (350 to 400 ml) was several times that of the amalgam (40 to 60 ml) and the aqueous was relatively concentrated (1.5 to 2.5 m), the relative change in concentration of the hydroxide was small, amounting to about 0.05 molal in the usual case. In 1.5 molal hydroxide this amounts to a correction of about 1.8 mv. By titrating the hydroxide at the end of the run and by assuming that the hydroxide concentration increased linearly with time during the run, a close approximation of m at any given time was obtained. In these experiments it was not found possible to calculate the change in concentration of the aqueous phase from the change in concentration of the amalgam, since a very appreciable part of the lithium leaving the amalgam did not enter the aqueous phase but remained out of solution, apparently as solid $LiOH{\cdot}H_2O$, on the walls of the reaction cell. It is possible that the formation of this solid is at least partly responsible for the unexplained irregularities observed in the kinetic studies as described below.

A comparison of experimental potentials with those calculated from amalgam analysis during the first three runs revealed that the calculated values were consistently low by an average of 3.3 mv.

[28] W. E. Clark, ORNL CF-53-11-207 (limited access report).

[29] G. N. Lewis and F. G. Keyes, *J. Am. Chem. Soc.* 35, 341 (1913).

[30] H. S. Harned and F. E. Swindells, *J. Am. Chem. Soc.* 48, 126 (1926).

[31] H. H. Garretson, ORNL-1272 (limited acess report).

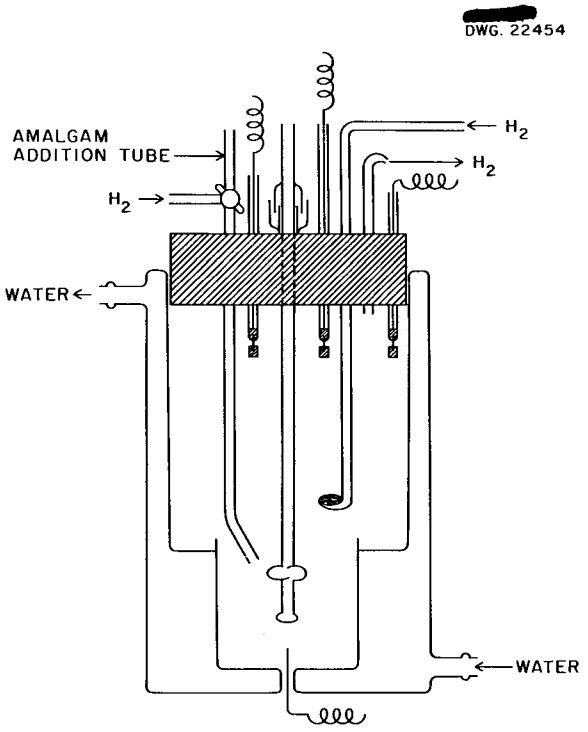

Fig. 7. Amalgam Decomposition Cell.

This indicated that $E^0_{Li(Hg)}$ should be about 2.0816. Consequently, a redetermination of $E^0_{Li(Hg)}$ was made by using dropping and flowing amalgams, and the average values obtained from four runs using two different concentrations of amalgam and two of aqueous lithium hydroxide was 2.0814. It was observed that the results obtained from the dropping and flowing electrodes were less consistent than those obtained from the stirred amalgam pool, the experimental scatter of potential readings from the former being on the order of several tenths of a millivolt. This behavior of flowing lithium-amalgam electrodes has been remarked upon by Harned and Swindells.[30]

The value of 2.0814 volts for $E^0_{Li(Hg)}$ is believed to be accurate to ± 0.5 mv. An error of this magnitude results in errors of 1.5 to 2.0% in the determination of M at concentrations of 0.85 and 0.10, respectively.

Consideration of the data thus far obtained from the study of amalgam decomposition fails to confirm the relationships expressed in Eq. 7. Within the limits of experimental error, no effect has been observed when the concentration of the aqueous phase was changed from 1.5 to 2.5 m. As far as reaction order is concerned, the results seem to indicate that the rate of decomposition tends to be independent of the amalgam concentration (i.e., zero order), although complicating factors are present which thus far have made a definite determination of reaction order impossible.

Assuming the S/V ratio to be constant and including it in the value of k, the rate constant, the equations for half-order and zero-order reactions are as follows:

For half order,

$$-\frac{dM}{dt} = kM^{1/2} .$$

Integrating between limits,

$$2(\sqrt{M_1} - \sqrt{M_2}) = k(t_2 - t_1) .$$

For zero order,

$$-\frac{dM}{dt} = k .$$

Integrating between limits,

$$(M_1 - M_2) = k(t_2 - t_1) .$$

Plots of M and $M^{1/2}$ vs. time are rather inconclusive as to which order is more nearly correct. The differential plot of log $(-dM/dt)$ vs. log M shows that in every experiment run thus far the initial reaction is or approaches zero order and that in most cases appreciable portions of the plot are linear with a slope of zero. Unfortunately, in every instance there are marked changes in the slope of the M vs. t plot which must correspond to changes in k or in the active surface, S. There is a possibility that this effect can be minimized by altering the geometry of the cell and also that further purification of the system will eliminate traces of impurities which by their presence may increase the active surface during an experiment. While it is not presently possible definitely to assign an order to the reaction under study, the data obtained thus far seem to indicate zero-order kinetics.

Plots of M vs. time and of log $(-dM/dt)$ vs. log M for a rather typical experiment are shown in Figs. 8 and 9.

Plans for future work include further investigation of lithium amalgam kinetics, specifically with

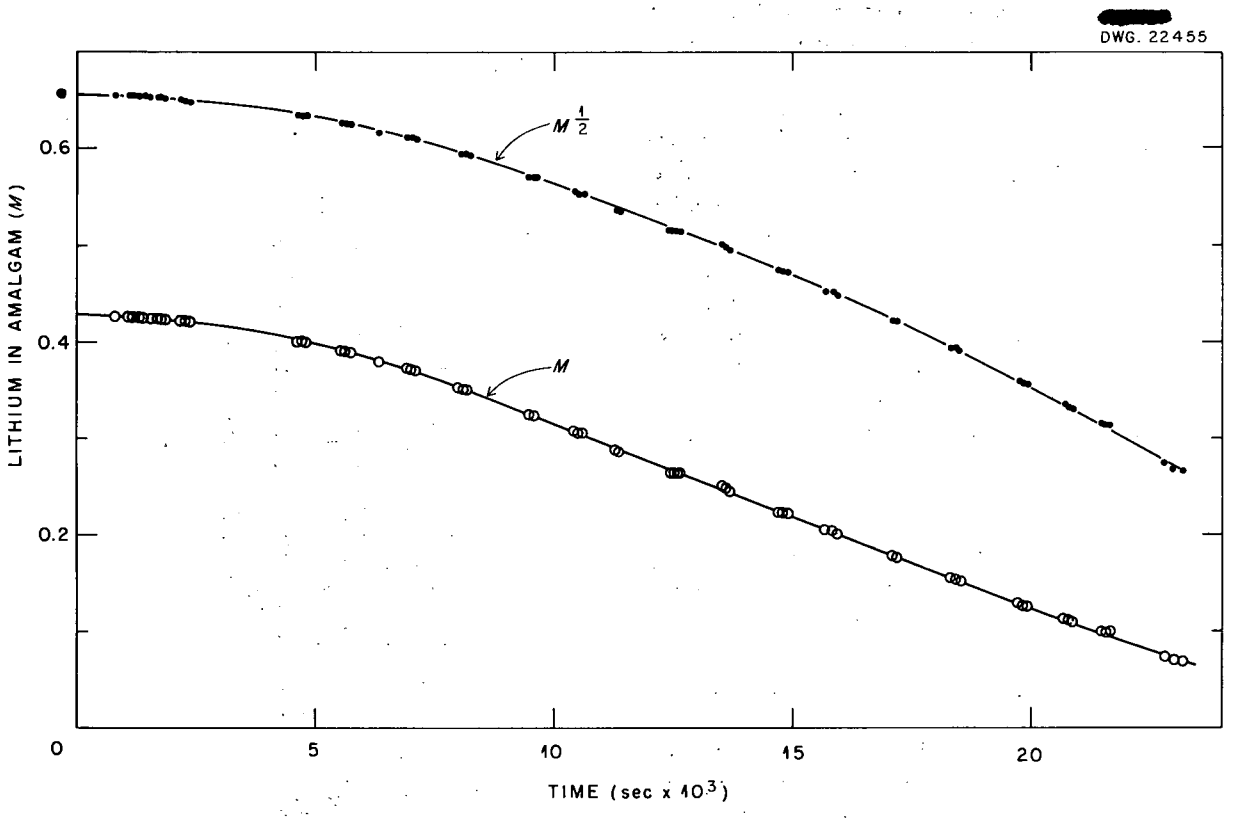

Fig. 8. Decomposition of Lithium Amalgam; Comparison of Intergral Plots for Half-Order and Zero-Order Kinetics.

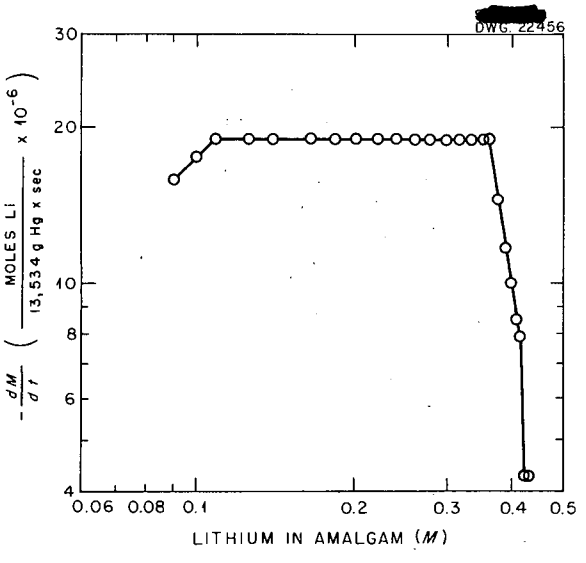

Fig. 9. Decomposition of Lithium Amalgam – Differential Plot.

respect to changing aqueous concentrations and the S/V ratio, determination of the reaction order, and runs at several different temperatures to allow determination of activation energy. Extension of the study to other alkali and alkaline earth metals is also planned.

CHEMISTRY OF FUSED SALTS

A. S. Dworkin D. J. Sasmor
F. J. Miller[32] I. S. Yaffe
E. R. Van Artsdalen

Electrical Conductivity and Density

Many studies have been made in the past of electrical conductivity of pure fused salts, but relatively few investigations of fused-salt mixtures have been attempted. The present investigations were undertaken in the hope that they would help to

[32]Analytical Chemistry Division.

elucidate the fundamental nature of the fused-salt state and give indications of transport phenomena for both simple and complex ions.

The high-temperature part of the apparatus is shown in Fig. 10. Temperature control was maintained within the melt in the platinum crucible (*A*) to ±0.05°C by means of a Speedomax-DAT controller unit which employs a Chromel-Alumel thermocouple as the temperature sensing element in thermal contact with the base of the crucible. The actual temperature within the melt was determined with a carefully calibrated auxiliary thermocouple and a precision potentiometer. Uniformity of temperature was enhanced by a heavy-wall nickel tube (*E*) and heat baffles (*L*) within a Marshall furnace with shunt-taps (*H*). The platinum crucible containing the melt was placed in an Alundum crucible (*B*) to insulate it electrically from its surroundings. Purified and dried argon gas was passed through the apparatus during use. The conductivity cells used were of the capillary dip type (Fig. 11) fabricated from fused silica. Platinum electrodes rested on the shelves formed by the juncture of the approximately 1.5-mm-bore capillary tubing (*C*) with the 6-mm-bore tubing (*B*). Jiggling the electrodes inside the cell did not affect the resistance readings which were of the order of 100 ohms for the salt melts. As long as the cell was not within ¼ in. of the walls of the platinum container and provided the electrodes were immersed to a minimum of ¼ in. within the melt, there was no change of resistance with change of position of the cell. The cell constants were of the order of 300 to 500 cm^{-1}. Platinum leads from the electrodes, encased in Alundum tubes, extended outside the furnace.

The cells were calibrated both before and after use in a melt. In general the cell constants did not change by more than about 0.1% during use. The calibration was made against 1.000 demal[33] KCl solution at 25.00°C.[34] No correction was made for thermal expansion of the fused-silica cells because such correction would amount to appreciably less than 0.1% at 1000°C. The electrodes were platinized before calibration, but the "platinum black" was converted to "platinum grey" by the high-temperature molten salts. Measured resistance

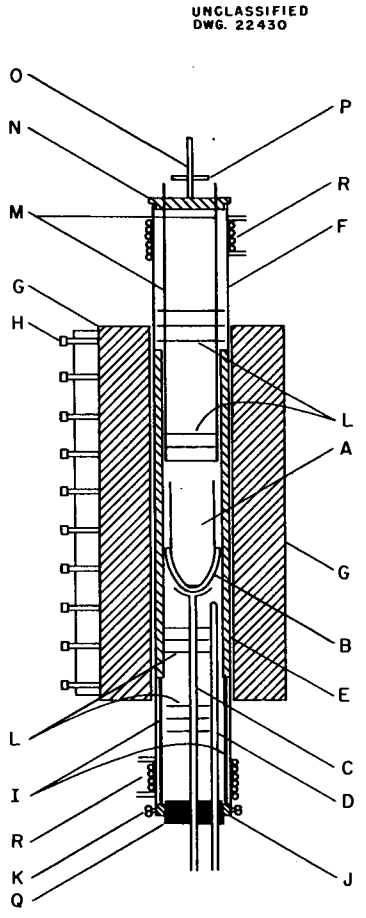

A - Pt CRUCIBLE
B - ALUNDUM CRUCIBLE
C - Ni SUPPORT TUBE
D - QUARTZ THERMOCOUPLE SHEATH
E - HEAVY-WALLED Ni TUBE
F - INCONEL TUBE
G - FURNACE
H - EXTERNAL TAPS FOR SHUNTS
I - STAINLESS STEEL SUPPORT RODS
J - BOTTOM RING
K - WING NUTS
L - RADIATION SHIELDS
M - RADIATION SHIELD SUPPORT
N - BRASS TOP PLATE
O - CELL SUPPORT
P - CELL YOKE
Q - NO. 14 RUBBER STOPPER
R - COOLING COILS

Fig. 10. Furnace Assembly for Conductance and Density Measurements in Molten Salts.

[33] A 1-demal solution contains 1 g mole of solute per cubic decimeter of solution at 0°C.

[34] G. Jones and B. C. Bradshaw, *J. Am. Chem. Soc.* 55, 1780 (1933).

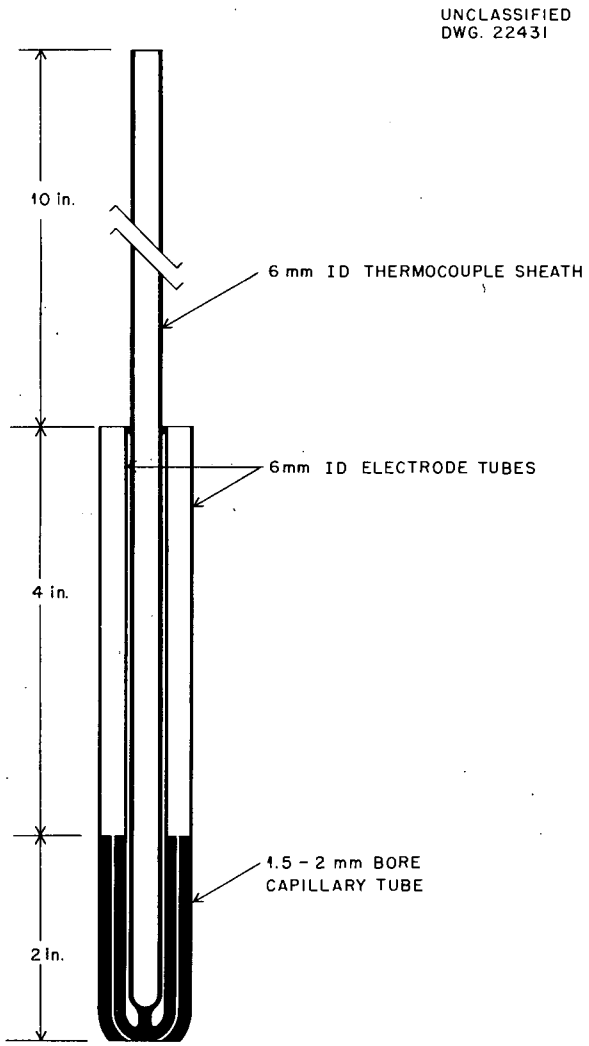

Fig. 11. "Fused"-Silica Conductivity Cell.

varied with frequency; consequently, readings were taken at various frequencies between 2000 and 20,000 cps. The resistance at infinite frequency was obtained by linear extrapolation of a plot of resistance against the reciprocal of frequency squared. Conductance measurements were made with a Jones conductance bridge and auxiliary apparatus.

Density measurements were made by the displacement method employing a thick-walled, hollow, platinum bob suspended by No. 36 gage platinum wire from one arm of a magnetically damped Chain-o-matic balance. The bob, of about 6-cc volume, was calibrated against pure water at room temperature, and the known thermal expansion of platinum was used to determine its volume at elevated temperatures.

The molten system KCl-LiCl was chosen for study because its phase diagram is well established and there appears to be no complexing.

The specific conductance of this system can be expressed by the relation

(1) $$\kappa = a + bt + ct^2 ,$$

where a, b, and c are adjustable parameters and t is centigrade temperature, while the density is given by

(2) $$\rho = a + bt ,$$

with a and b having different values from the parameters in the specific-conductance equation. Conductance and density data obtained for seven different compositions in the KCl-LiCl molten system are recorded in Table 6.

The molar volumes of the molten system KCl-LiCl have been calculated at 600, 700, 800, and 900°C from the data of Table 6, and these volumes are plotted in Fig. 12. It will be observed that a very exact linear relationship exists at any given temperature between molar volume and composition.

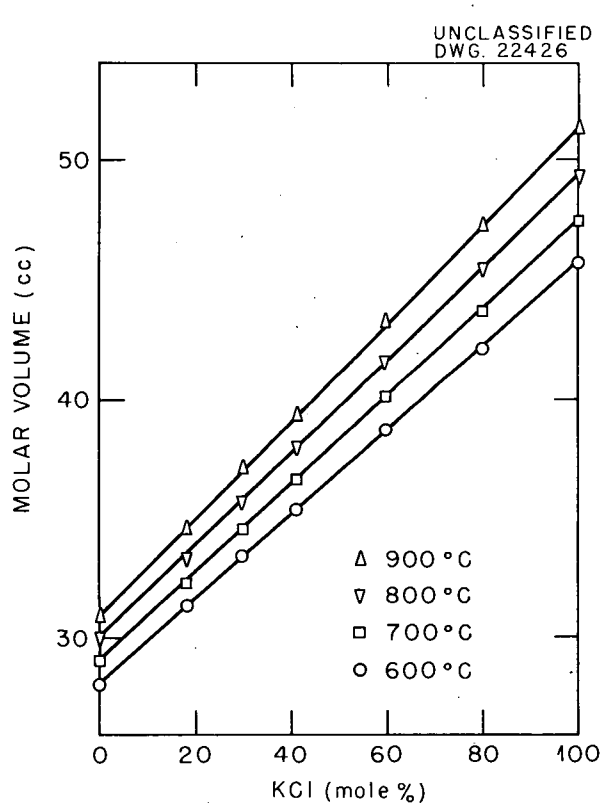

Fig. 12. Molar Volume of Molten System KCl-LiCl.

TABLE 6. CONDUCTANCE AND DENSITY RELATIONSHIPS OF THE MOLTEN SYSTEM KCl-LiCl

KCl (mole %)	SPECIFIC CONDUCTANCE, $\Lambda = a + bt + ct^2$			TEMPERATURE RANGE (°C)	DENSITY, $\rho = a + bt$	
	a	b ($\times 10^2$)	c ($\times 10^6$)		a	b ($\times 10^3$)
100.0	−1.750	0.738_3	-3.00_0	800 to 930	1.976_7	-0.583_1
80.0_4	−3.160	1.11_5	-5.31_0	700 to 860	1.959_8	-0.578_1
59.5_5	−4.138	1.48_8	-8.00_9	580 to 740	1.923_4	-0.561_0
41.2_0	−2.275	1.08_4	-5.10_0	380 to 600	1.885_1	-0.527_5
29.6_4	−2.969	1.45_0	-7.91_7	460 to 620	1.855_9	-0.507_4
18.2_3	−2.185	1.38_3	-7.22_2	530 to 680	1.835_4	-0.489_3
0.00	+0.528	1.12_5	-4.55_4	630 to 790	1.766_0	-0.432_8

This is interpreted to mean that complexing does not occur in this system which may be looked upon as "ideal" with respect to molar volume.

The equivalent conductance, Λ, of the molten system KCl-LiCl has been calculated from the data of Table 6 by the relation

$$\Lambda = \frac{\kappa W}{\rho}, \tag{3}$$

in which W is the equivalent weight of the melt. In Fig. 13 Λ has been plotted as a function of composition at 600, 700, 800, and 900°C. The significant observation is made that the substitution of some of the better conducting LiCl for the poorer conducting KCl actually lowers the equivalent conductance, i.e., the Λ curves pass through minima at about 75 to 80 mole % KCl.

The minima in these curves may be caused by the contraction of the chloride semilattice as Li^+ ion replaces K^+ ion. It is well known that the chloride lattice is smaller in crystalline LiCl than in crystalline KCl. Assuming no change in coordination number on melting (or, alternatively, the same relative change in both LiCl and KCl), this same relationship of the chloride lattices should be expected to hold in the molten state. If electrical conductance is primarily by the cations, then some shrinkage of the chloride semilattice on substituting a few mole per cent of Li^+ ion for K^+ ion should make conduction by the K^+ ion considerably more difficult, thereby reducing electrical conductivity. Gradually, as more and more Li^+ ion is substituted, the conductance must again rise to the final value in pure LiCl.

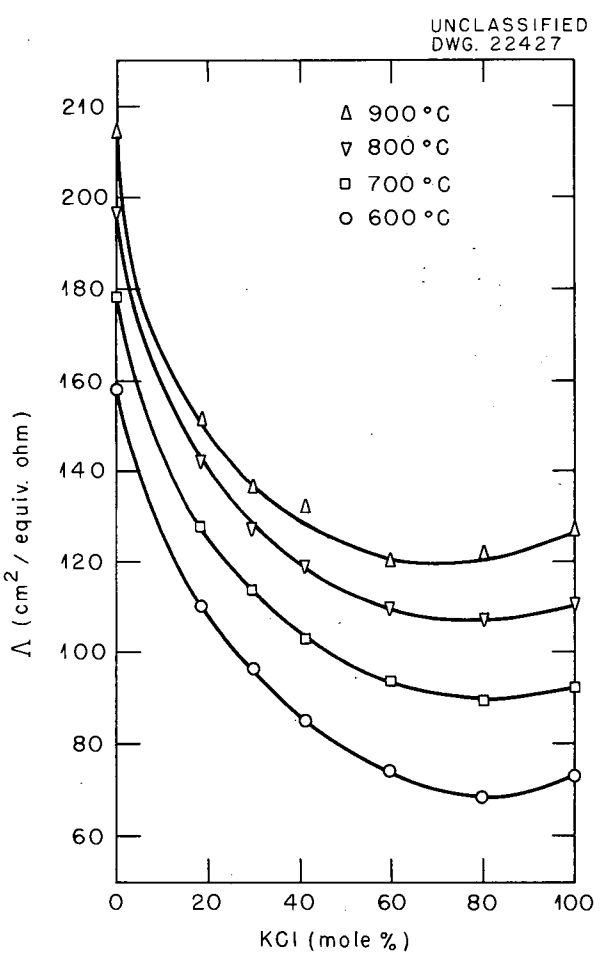

Fig. 13. Equivalent Conductance of Molten System KCl-LiCl.

The temperature dependence of electrical conductivity for the pure salts can be expressed quite well by the relation

$$\Lambda = A\, e^{-\Delta E^*/RT} \tag{4}$$

from about 15 or 20°C above the melting point to the highest temperatures measured. However, the conductivity decreases, close to the melting point, much more rapidly than predicted by Eq. 4, and this indicates that considerable structural ordering occurs in this range. This same relation (Eq. 4) can be used for the temperature dependence of the equivalent conductance of the molten mixtures of LiCl and KCl, but ΔE^* is temperature dependent over a larger temperature interval and becomes constant only at temperatures of the order of 100 to 150°C above the melting point. A plot of the experimental activation energies ΔE^* against composition in the constant ΔE^* range (high temperature) is shown in Fig. 14. The significance of the maximum at 50 mole % KCl is not entirely clear. However, the minimum at about 75 to 80 mole %, corresponding with a minimum in conductivity, has important implications concerning the correlation of liquid structure and conductivity. This problem is being investigated further with other molten systems.

The pre-exponential factor A in Eq. 4 is usually looked upon as involving entropy of activation with

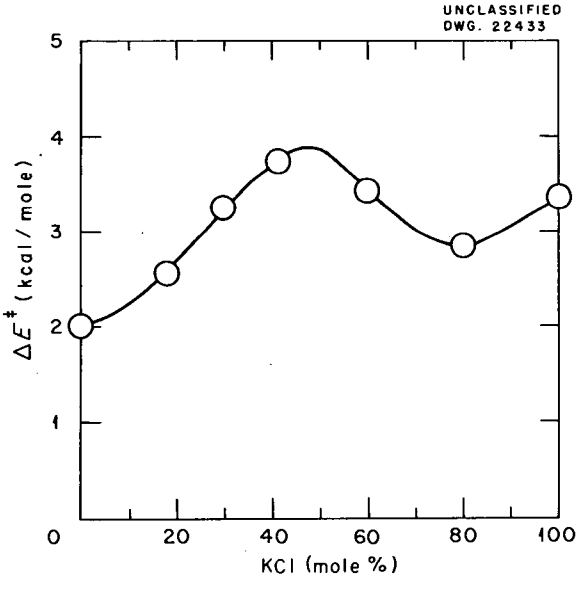

Fig. 14. Activation Energy for Conductance by Molten System KCl-LiCl.

$$A = \chi\, e^{\Delta S^*/R}, \tag{5}$$

where χ is a "transmission coefficient" and ΔS^* is the entropy of activation. Figure 15 is a plot of this apparent entropy of activation against composition for the temperatures 600, 700, and 800°C. Apparently, ΔS^* shows a maximum at the same concentration where the electrical conductivity is a minimum, and this is correlated with the structural ordering discussed above.

Electrical conductivity and density measurements of molten NaCl over a wide temperature range have been completed. Work is progressing with molten mixtures of NaCl and KCl.

EMF Measurements in Fused Salts

A simple concentration cell of the type

1	2	3	4
Ag	MY $({}^2X_2)$ | M'Y $({}^2X_1)$	MY $({}^3X_2)$ | M'Y $({}^3X_1)$	Ag

has been designed.

The equation

$$E = t_M \frac{RT}{\mathfrak{F}} \ln \frac{{}^3X_1\ {}^2X_2}{{}^3X_2\ {}^2X_1} \tag{6}$$

has been derived for this cell on the assumption that the cations only transport the electric current. In Eq. 6, E is the potential, t_M is the transport number of the M^+ ion, R is the gas constant, T the absolute temperature, $\mathfrak{F}$ the faraday, and X is the mole fraction of the species of the designated subscript contained in the cell compartment indicated by the superscript. This concentration cell may be used to measure transference numbers, or alternatively, if transference numbers are known, to obtain information concerning the activities of the ions.

A few preliminary experiments have been made using $AgNO_3$-$NaNO_3$ mixtures. A 90 mole % $NaNO_3$ mixture was placed in one compartment and an 80 mole % $NaNO_3$ in the other. The two compartments are connected through a capillary with a glass rod serving to separate the mixtures until they are melted, at which time the rod is raised and a junction is formed.

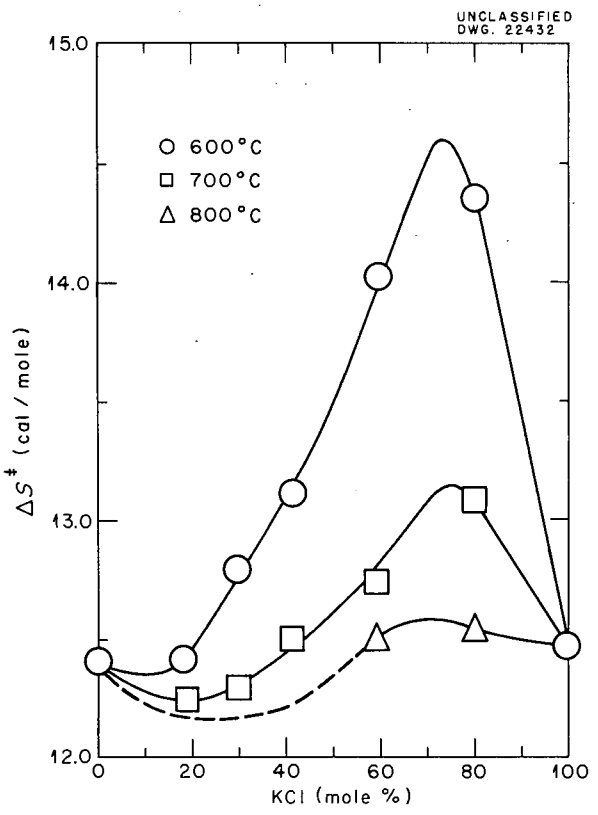

Fig. 15. Apparent Entropy of Activation for Conductance by Molten System KCl-LiCl.

The cell appears to be workable, although a number of difficulties were encountered. Such things as better temperature control and an improved method of separating the two compartments to prevent diffusion may be accomplished easily. More serious is the apparent dissolution of the Ag electrodes in the melt. Experiments are being performed to determine the nature of the dissolution and it may be necessary to go to other systems.

However, the measurements were reproducible over a period of a day. The quantity E/T remained essentially constant as the temperature was raised and lowered a number of times between 300 and 350°C. Assuming ideal mixtures, an approximate value of 0.45 was obtained for the transference of the Na^+ ion at the average $NaNO_3$ concentration of 87 mole %. This confirms some previous work on transport numbers[35,36] which indicates that the Ag^+ ion is a better conductor than Na^+.

[35] P. M. Aziz and F. E. W. Wetmore, *Can. J. Chem.* **30**, 779 (1952).

Cryoscopy

Freezing-point depressions in sodium nitrate have been determined with a considerable number of salts. The average depression per molal concentration unit for the chloride, sulfate, carbonate, bromate, and tungstate of sodium with repeated determinations of the chloride and sulfate is 15.1 ± 0.2°C when computed by the equation

$$\Delta T_i = \frac{RT_0^2}{1000\, l_0}\, m_i \,, \tag{7}$$

where ΔT_i is the freezing-point depression, R is the gas constant, T_0 is the freezing point of pure solvent in degrees absolute, l_0 is the latent heat of fusion per gram of solvent, and m_i is the molality of the solute. Using this depression of 15.1°C one calculates that l_0 is 44.1 ± 0.7 cal/g for $NaNO_3$. A direct calorimetric determination of 43.4 cal/g has been reported in the literature.[37] Thus it is clear that these freezing-point measurements fit theory, for the Na^+, from sodium salts, should not depress the freezing point of $NaNO_3$ since it is not a "foreign" ion.[36]

Potassium salts should be expected to show depression for the K^+ ion, and indeed this is the case. However, it is known that KNO_3 and $NaNO_3$ form solid solutions,[38] and under these circumstances freezing-point lowering is less than expected. Equation 7 can be rewritten in this case as

$$\Delta T_i = \frac{RT_0^2}{1000\, l_0}\, (m_i - m_i') \,, \tag{8}$$

where m_i is the molality in the liquid solution and m_i' that in the solid solution. Using the value 15.1°C for the anions, the series of potassium salts, nitrate, chloride, bromate, metaperiodate (decomposes to iodate), carbonate, sulfate, chromate, and dichromate, showed an average depression from K^+ of 13.4 ± 0.4°C. This datum can be used to estimate the distribution of K^+ between solid and liquid solutions of KNO_3 and $NaNO_3$ in the low KNO_3 region where phase diagrams are difficult to

[36] A. S. Dworkin, D. J. Sasmor, I. S. Yaffe, and E. R. Van Artsdalen, *Chem. Semiann. Prog. Rep. June 20, 1953*, ORNL-1587, p. 26.

[37] H. M. Goodwin and H. T. Kalmus, *Phys. Rev.* **28**, 1 (1909).

[38] *International Critical Tables*, Vol. 4, p. 69, McGraw-Hill, New York, 1928.

determine. Thus, the distribution ratio 13.4/15.1 = 0.89 ± 0.04 is the proportion of K^+ remaining in the liquid phase. In other words, 11% of KNO_3 goes into solid solution and 89% remains in the liquid phase for equal weights of liquid and solid phases. The phase diagram of KNO_3-$NaNO_3$ is not inconsistent with this value, though it has not been studied below 4 mole %.

Silver salts were found to give very low depressions in $NaNO_3$, but it is known that $AgNO_3$ and $NaNO_3$ form solid solutions,[39] and so a study of the type indicated in the preceding paragraph was made. Using $AgNO_3$, Ag_2SO_4, and Ag_2CrO_4, the average depression for Ag^+ was found to be 7.2 ± 0.8°C. This yields a distribution ratio of Ag^+ between liquid and solid of 0.48 ± 0.07, corresponding to 48% of the Ag^+ remaining in the liquid phase for equal weights of liquid and solid phases. This value appears entirely reasonable from Hissink's[39] data; but here again, this value refers to concentrations well below 1 mole %, while the phase diagram studies do not extend below 6 mole %.

It is evident from the above examples that the freezing-point-depression method is useful in phase-diagram studies in the quite low concentration range.

Investigations completed so far indicate that the following salts are essentially completely dissociated into their corresponding ions in molten sodium nitrate: sodium and potassium fluorides; chlorides of Li, K, Rb, Ca, Sr, Ba, Zn, Cd, Cu, Pb, and La; sulfates of K and Ag; nitrates of Na, K, Ag, and Pb; carbonates and bromates of K; chromates of K and Ag; and potassium dichromate.

Preliminary evidence seems to indicate that $NaZrF_5$ and Na_2ZrF_6 dissociate to give Na^+ and ZrF_5^- and ZrF_6^{--} ions, respectively, which are moderately stable in molten $NaNO_3$. However, further work remains to be done with these and similar salts.

Ferric chloride, $FeCl_3$, appears to give two ions per formal mole. This would indicate ionic dissociation into $FeCl_2^+$ and Cl^- ions, which is interesting in that the concentration is quite low and evidently $FeCl_2^+$ is fairly stable.

Bromides and iodides are oxidized by molten sodium nitrate, and studies with them are inconclusive.

[39] D. J. Hissink, *Z. physik. Chem.* 32, 543 (1900).

MISCIBILITY OF LIQUID METALS AND SALTS

M. A. Bredig H. R. Bronstein
J. W. Johnson W. T. Smith[40]

In the last report, ORNL-1587 of June 1953, the discovery of an unexpectedly high solubility of a typical salt, potassium fluoride, in the liquid phase of a typical metal, potassium, was described. Evidence obtained during the past period confirms this result and suggests that this behavior is not an isolated case restricted to the KF-K system but in contrary appears to be quite general at least for the alkali metal systems and is inclusive of complete miscibility at slightly higher temperatures.

Experimental methods were developed (1) for more accurately ascertaining the composition of the solution of the fused salt in the liquid metal and (2) for determining the partial vapor pressure of the metal in the solution. On the basis of these data a calculation, or estimation, of thermodynamic functions such as the activities of both components at various temperatures, heats and entropies of mixing will be possible.

Solubility Measurements

While, at least below 950°C, the sampling of the salt-rich phase was successful with the ball check valve type capsule (ORNL-1432, page 16, and Figs. 16a and 16b, this report) the analysis of the metal-rich phase, found above the check valve, was subject to some doubt because of possible segregation and settling-out of the salt component. The

[40] Consultant from the University of Tennessee.

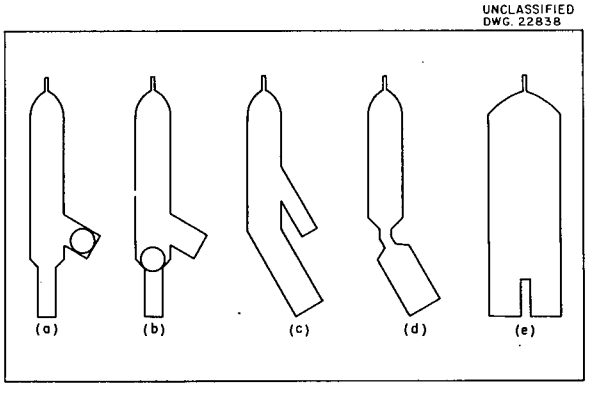

Fig. 16. Types of Containers for Solubility Measurements.

simple principle of an improved method of sampling the liquid metal-rich equilibrium phase consists of decanting into a side arm of the sealed stainless steel equilibrating tube (Fig. 16c) a portion of the less dense liquid metal-rich phase which collects after equilibration on top of the heavier salt-rich phase. The results obtained in this manner together with additional tests with the ball check type capsule for analysis of the salt-rich phase are summarized in Figs. 17, 18, 19, 20, 21, 22, and 23 for one potassium and three sodium systems, namely, Na-NaCl, Na-NaBr, Na-NaI and K-KF. The solubilities of KF in K given are those determined with the older method. A few data from a study of the Na-NaF system now underway, but as yet incomplete, are also included in Figs. 21, 22, and 24.

The most significant result of these measurements is the finding that complete miscibility exists in

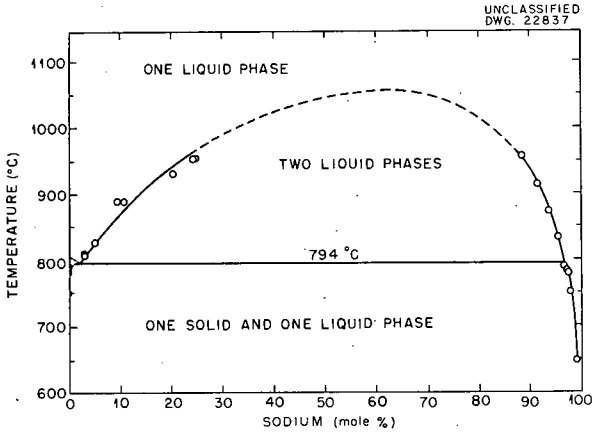

Fig. 17. Sodium-Sodium Chloride System.

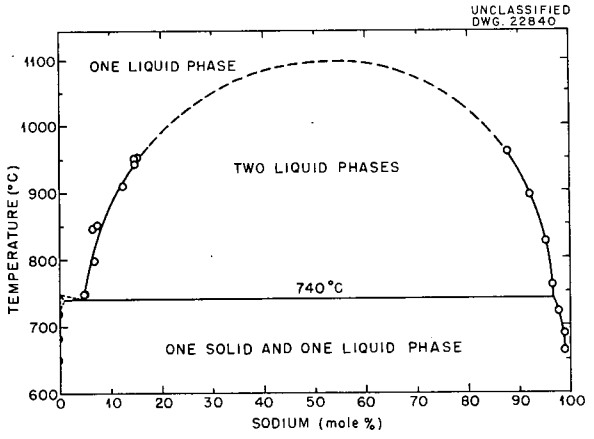

Fig. 18. Sodium-Sodium Bromide System.

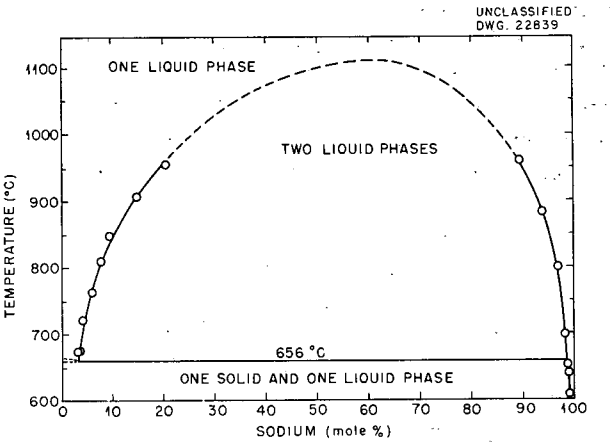

Fig. 19. Sodium-Sodium Iodide System.

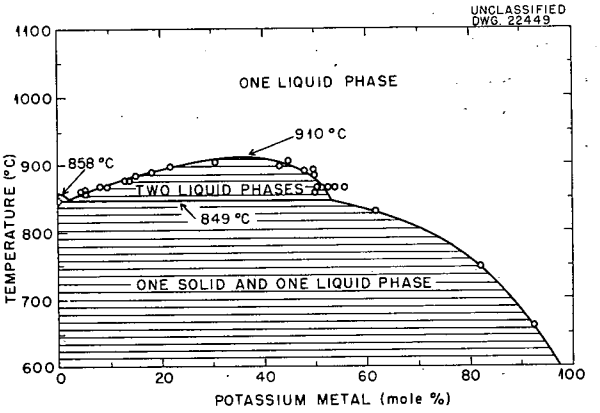

Fig. 20. Potassium Fluoride–Potassium Metal System.

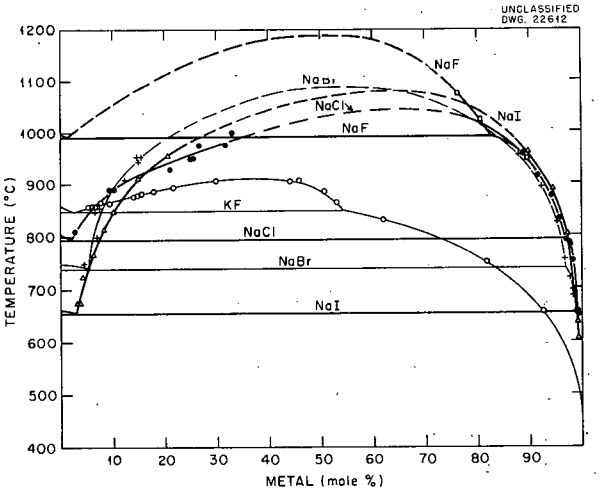

Fig. 21. Metal-Metal Halide Systems.

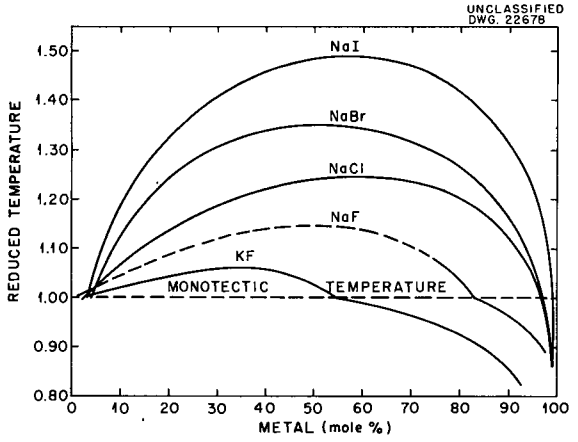

Fig. 22. Comparison of Alkali Metal–Alkali Halide Systems.

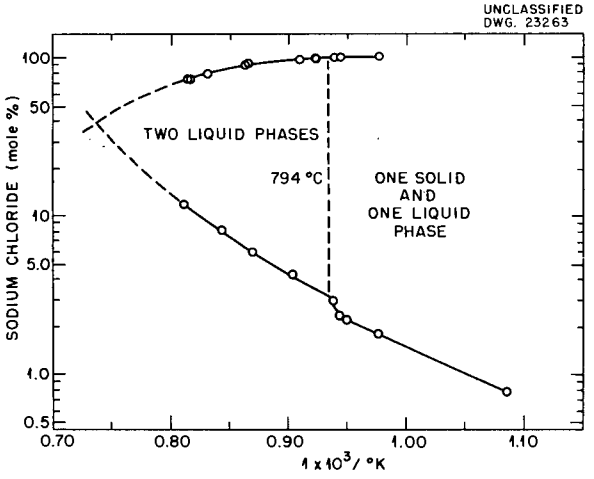

Fig. 23. Sodium-Sodium Chloride System.

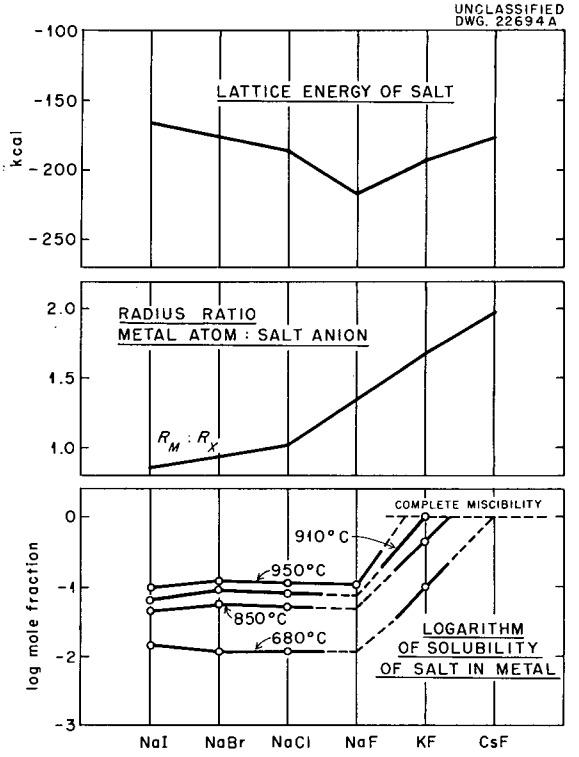

Fig. 24. Effect of Salt Lattice Energy and Metal-Atom: Anion Radius Ratio on Solubility of Salt in Metal.

these systems above a certain temperature, as definitely demonstrated in the KF-K system and clearly indicated, even though by extrapolation only, in the others. The extrapolation was performed by plotting the logarithm of the solubility against the reciprocal of the absolute temperature (Fig. 23). In the temperature range where the salt is solid and does not dissolve more than 0.15 mole % of sodium metal, this procedure appears to lead to a straight line in the Na-NaCl system and consequently to a reasonable value, of ΔH = 16000 ± 1000 cal, for the differential heat of solution at saturation of solid NaCl in liquid Na. A deviation from the straight line, a few degrees below the monotectic temperature, apparent in the sodium systems is considered as a special "pre-melting" effect that may deserve further attention. Values very similar to the 16000 cal of the chloride system were calculated for both the bromide and iodide systems, but call for further refinement in view of the scarcity of the present data. On the other hand, a value of 20000 ± 500 cal for the saturated solutions of solid KF in K is considered reliable within the limits given. (These tests were carried out with single crystals of the salts, approx. $\frac{3}{8}$ in. in size, held above the constriction in capsule *d*, Fig. 16.)

For the liquid-liquid equilibria curved lines are obtained in the logarithmic plot (Fig. 23) indicating that the relationship between the logarithm of the concentration and the reciprocal of the absolute temperature is not a simple one. Fitting parabolic functions (as suggested for non-electrolytes, e.g. in J. Hildebrand's book) to the curves in plots of the absolute temperature against mole fraction

seems impossible, as does a correlation of solubilities with "solubility parameters" or "internal pressures". The salt (electrolyte) character of one of the components of these systems is thought to be responsible. However the derivation, by extrapolation, of consolute temperatures, i.e. of the temperatures above which salt and metal are completely miscible (Table 7), is believed to be valid within better than ±50°C for the sodium systems, and within better than ±5°C for the KF-K system.

In the last previous report (ORNL-1587, page 80), after a discussion of the first results with the Na-NaCl and Na-NaBr systems, it has been stated that "a larger solubility of sodium in sodium iodide, possibly even with a negative temperature coefficient, and a smaller solubility of sodium in sodium fluoride near its melting point, but with a large temperature dependence and possibly with a rather low temperature of complete miscibility, is anticipated."[41] Actually, in the experiments on the sodium-sodium iodide system as reflected in the table and in Fig. 19, the thermal coefficient of the solubility of sodium in molten sodium iodide was not found to be negative. However, in at least qualitative agreement with the notion expressed above, the area of the liquid immiscibility is by far the greatest of the systems studied thus far (Fig. 22). Similarly, the corresponding area for the Na-NaF system, as indicated by the few data obtained thus far, appears to be the smallest of the four sodium systems. The fact that the solubility of sodium in sodium iodide at the monotectic temperature as well as the temperature coefficient of this solubility is intermediate between those in NaCl and NaBr (Fig. 21 and Table 7) may be interpreted to demonstrate the effect of the larger size and polarizability of the iodide ion. This must lead to a more effective screening of the field of the Na^+ ion even with a lower number of coordinated anions and thus make interaction between Na^+ and Na more difficult than in the case of the bromide. However, the mere effect of the lower monotectic temperature with accompanying decrease in the fugacity of pure sodium must not be overlooked even though its effect is, at least qualitatively, not observed in going from the chloride to the bromide where the solubility increases. It is clear and not surprising that various factors have to be considered for a correlation, even if limited to the alkali metal systems, of solubility with the nature of the ions and atoms involved. However, the relative sizes and the numbers of the three constituents of the solutions, namely the cations

[41] The quotation above is the correct version of the statement appearing in a distorted form in the previous report.

TABLE 7. SOME CRITICAL DATA OF SODIUM METAL-SODIUM HALIDE SYSTEMS, AND OF THE POTASSIUM-POTASSIUM FLUORIDE SYSTEM

METAL	SALT		MONOTECTIC TEMPERATURE °C	MONOTECTIC COMPOSITIONS		NEAR-MONOTECTIC COMPOSITION SOLID SALT PHASE		CONSOLUTE TEMPERATURE DATA (By Extrapolation)	
M	Formula MX	M.Pt., °C*		Liquid Metal Phase Mole % Salt	Liquid Salt Phase Mole % Metal	Mole % Metal	Temperature °C	Temperature °C	Mole % Na
		(±0.5)	(±0.5)	(±0.1)	(±0.2)	(±0.03)	(±0.5)	(±50)	(±5)
Na	NaF	995	990	17.0**	(1?)			(1100?)	
Na	NaCl	803	794	3.0	2.4	0.15	790	1030	65
Na	NaBr	747	740	3.1	4.2	0.15	720	1090	50
Na	NaI	661	656	1.2	2.9			1110	60
K	KF	858	849	45.0**	2.5			910***	37

*As indicated by Chromel-Alumel thermocouples used with capsules (e), Fig. 16.

**±1.0.

***±5.

the anions, and the metal atoms which might also be considered as cations and electrons, appear at present as the most important parameters. Thus, the much greater solubility of KF compared with that of NaF in the corresponding metals (Fig. 21) might at first glance simply be attributed to the larger spaces, available to anions on "substitution" for electrons, in liquid potassium, in connection with the larger size of, and greater distances between, K atoms, evident also in the lower heat of vaporization (18.9 for K, as compared with 23.1 kcal for Na). However, it would be reasonable to expect that the *ratio* of the size of these spaces to that of the anions would be the decisive parameter, rather than their absolute size. Yet, Fig. 21 demonstrates the rather remarkable observation that at a given temperature, at least below 1000°C, the solubilities of the four sodium salts are quite similar, even though the relative change in the size of the anion is much greater (R_{F^-} = 1.35 Å, R_{I^-} = 2.15 Å, change:60%) than the above change in the size of the metal (R_{Na} = 1.86 Å, R_K = 2.29 Å, change: 23%). The solubility of sodium metal in the four salts does not vary very greatly either.

These observations may be given the following tentative explanation which, at least in a qualitative way, is expected to hold more or less for all of the alkali metal–alkali halide systems and possibly for others. The solubility of the salt in the metal is thought here to be largely determined by two major factors connected with the two steps into which the process of transferring ions, or molecules, from the salt into the metal phase may be thought to be divided. One, already mentioned and connected with entering the metal phase, is the effect of the ratio of the sizes of metal atom and anion: e.g. the *smaller* the anion the *less* energy is thought to be required when it enters a space of a size given by the nature of the liquid metal. The second influence affects the removal of the ions from the salt: its lattice energy (e.g. –164 kcal for NaI, –216 kcal for NaF) like its heat of vaporization (e.g. 38 kcal for NaI, 53 kcal for NaF) is greatly changed, e.g. its magnitude is *increased* by a *decrease* in the size of the anion. In the case of variation of the anion, then, this effect is opposite to the first one. In the sodium series (Fig. 24) the constancy of solubility is taken to indicate that the two effects just cancel each other. There are indications that in other alkali metal systems this is not the case to the same extent, with LiF expected to be less soluble than LiCl in Li metal, but CsF more soluble than CsCl in Cs metal.

The large change in solubility on variation of the metal (and cation), as in going from the NaF-Na to the KF-K system, may be attributable to the same two effects. In this case, however, they do not oppose, but reinforce, each other, because both the salt and the metal contain the component that is being varied and thus suffer parallel changes (Fig. 24). E.g. an *increase* in the size of the metal (and cation) widens the spaces in the liquid metal and thus, like the decrease in the size of the anion, above, *decreases* the energy necessary to "replace" an electron by an anion. As to the second effect, operative in the salt, the lattice energy of the salt with the larger cation is considerably *smaller*, namely 193 kcal for KF as against 216 kcal for NaF, and so is the heat of vaporization, namely 41 as against 53 kcal respectively, thus also requiring *less* energy for transfer of ions, or molecules, from the salt.

On the basis of these relationships one may tentatively predict for the Cs-CsF system complete or almost complete miscibility of salt and metal in the liquid phase at or slightly above 680°C, melting point of the salt. For the lithium salts the extrapolation leads to rather small solubilities of the salts in lithium metal. These like a possibly high solubility of the metal in its molten salts, evidence for which found in the literature is contradictory, remain to be determined experimentally.

The question of the solubility of salts of one metal in the liquid phase of another, e.g. LiF in Cs, is naturally of great interest, and on the program of future experimentation.

The general, though somewhat preliminary, conclusion here arrived at that the solubility of the salt of a metal in the liquid phase of the metal increases rapidly with the atomic number (size) of the metal, while it changes little with variation in the anion, is reflected, though it does not seem to have been recognized, in the measurements at Berkeley[42] on alkaline earth metal systems. The solubilities, e.g. at 850°C, of these salts, appear to increase from 1 mole % of $CaCl_2$ in Ca to 2 mole % $SrBr_2$ or SrI_2 in Sr to 10 ± 2 mole % $BaCl_2$ or $BaBr_2$ in Ba, the solubility in barium metal found particularly enhanced probably in connection with

[42] D. D. Cubiciotti and C. C. Thurmond, *J. Am. Chem. Soc.* 71, 2149 (1949).

its less close packed (body-centered cubic crystal lattice) structure.

Metal Vapor Pressure Measurements

Determination of the metal vapor pressure was originally planned as a single, more or less qualitative experiment to demonstrate that mixtures of K and KF obtained above 910°C with approximately equal mole fractions of metal and salt (ORNL-1587, page 81 to 82) represented true solutions, characterized by a greatly lowered partial vapor pressure of the dissolved metal. It appears, however, that the measurements are accurate enough to reflect at least semi-quantitative features of the equilibrium diagram and even to permit calculation of approximate activities of both components which may be compared with activity values calculated from the solubility measurements.

An apparatus was built and designed as shown in Fig. 25. In the measurements that temperature is determined which at a given pressure of an inert gas, such as argon, remains constant with time and increasing heat input from the furnace thus indicating a large heat absorption due to violent boiling. With varied compositions this procedure yields the vapor pressure as a function of temperature and mole fraction.

Plotting the logarithm of the pressure against the reciprocal of the absolute temperature leads to practically straight lines (Figs. 26 and 27). For pure sodium metal (Fig. 26) our data, representable in the temperature range from 905 to 1023°C by the formula,

$$\log P_{mm} = -\frac{5423}{T} + 7.5485 ,$$

lie between those given by K. K. Kelley's formula,[43]

$$\log P_{atm} = -\frac{5775}{T} - 1.274 \log T + 8.86 ,$$

[43] U. S. Bur. Mines Bull. No. 383 (1935).

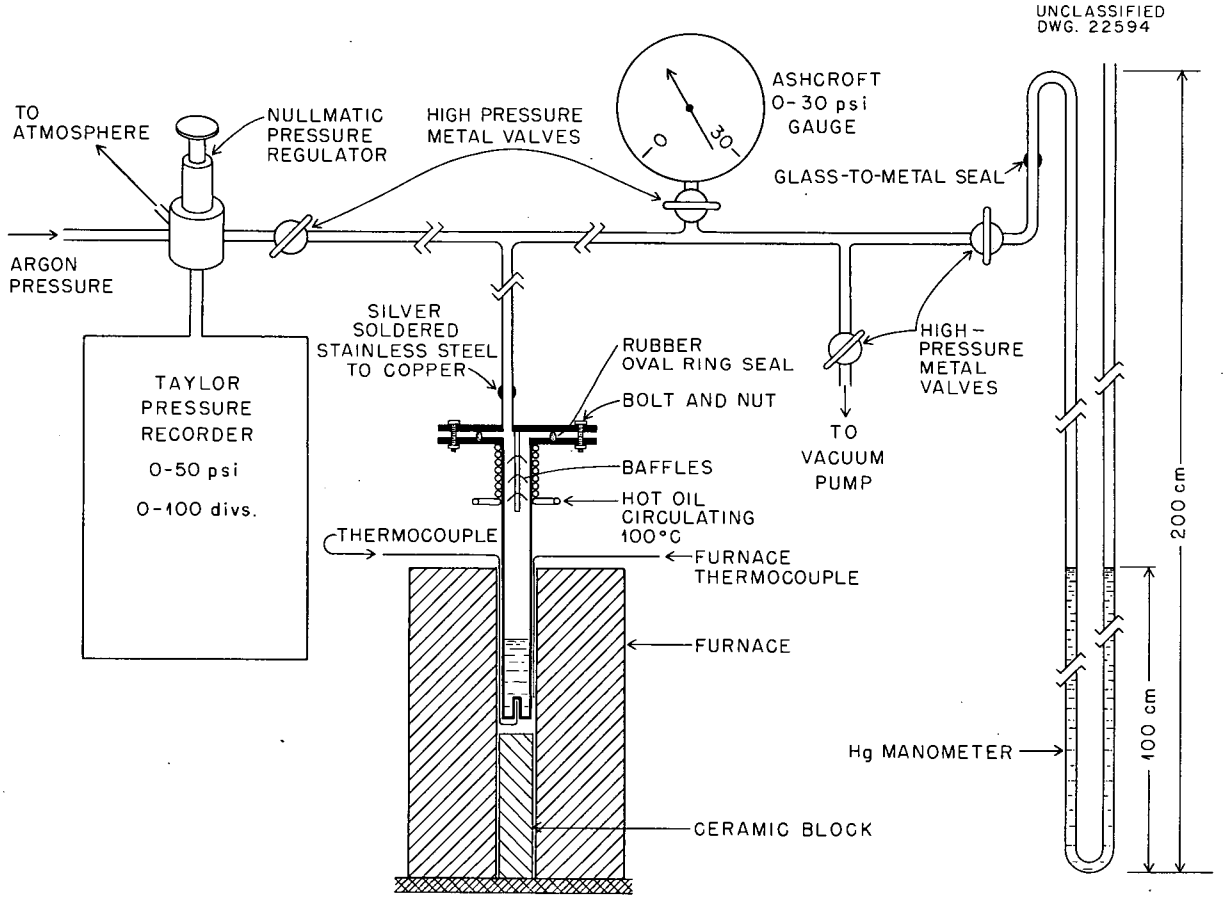

Fig. 25. Apparatus for Measuring Vapor Pressure.

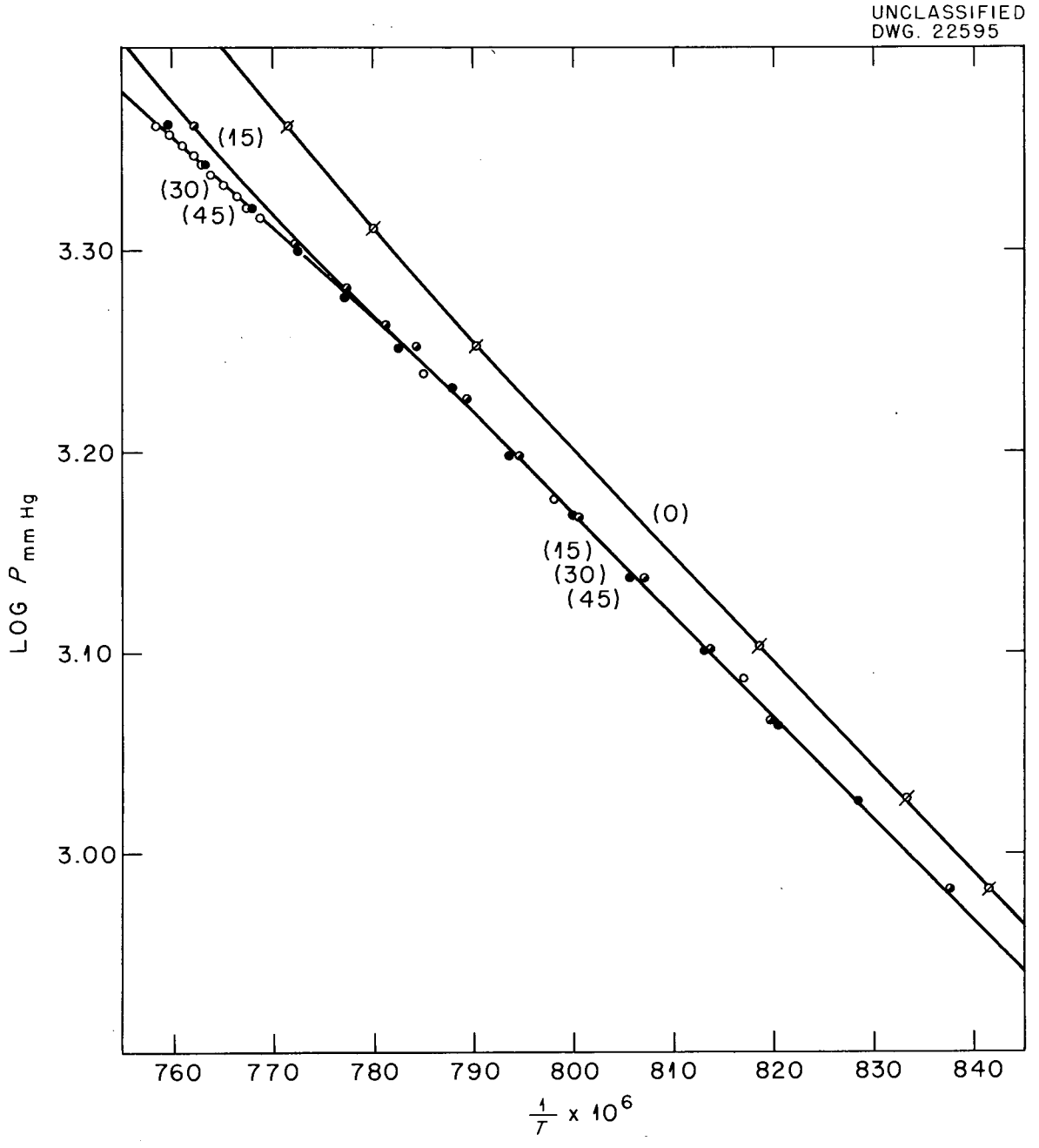

Fig. 26. Vapor Pressure of Sodium-Sodium Chloride Mixtures. Numbers designate mole per cent NaCl.

and that by Ditchburn and Gilmour,[44]

$$\log P_{mm} = -\frac{5567}{T} - 0.5 \log T + 9.235 .$$

[44] *Revs. Modern Physics* 13, 310 (1941).

The boiling point 883°C as determined by us compares with 892°C (Kelley) and 881.5°C (D. and G.)

Mixtures with 15, 30 and 45 mole % NaCl gave identical metal vapor pressure curves up to 1020°C, in agreement with the phase equilibrium diagram

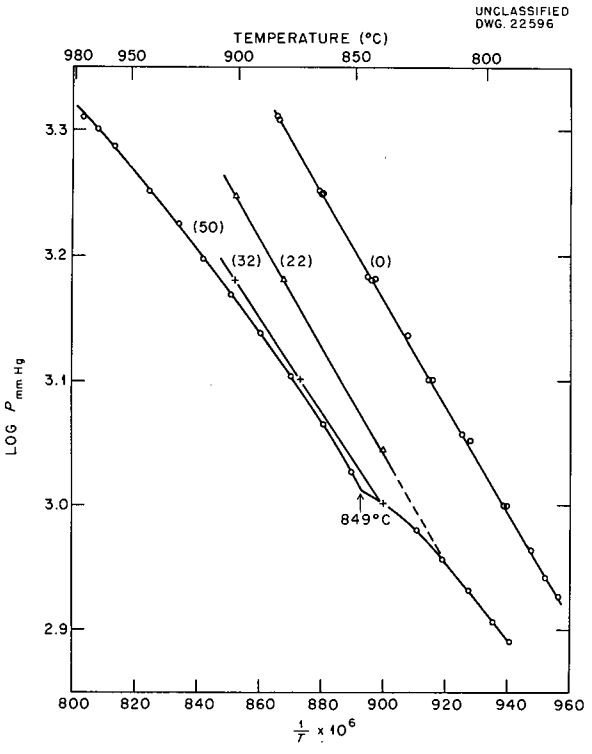

Fig. 27. Vapor Pressure of Potassium-Potassium Fluoride Mixtures. Numbers designate mole per cent KF.

(Fig. 17). All three compositions lie within the two-liquid-phase area in which the partial pressures are independent of the overall mole fraction. Above 1020°C, the deviation of the 15 mole % curve from the 30 and 45 mole % curves becomes clearly noticeable. This again is in essential, if only qualitative, agreement with the equilibrium diagram as derived from chemical phase analysis which at this temperature shows 18 rather than 15 mole % NaCl dissolved in the metal. It seems possible that the difference is due to the hold-up of a certain amount of condensed metal in the colder parts of the apparatus, and/or to some oxidation by impurities in the argon. Both these factors may well have caused the mole fraction of the metal to have dropped from .85 to .82.

For pure potassium metal in the range from 772 to 882°C (Fig. 12) the formula,

$$\log P_{mm} = -\frac{4191}{T} + 6.938 ,$$

gives an agreement with our measurements as satisfactory as, or slightly better than, the formula,

$$\log P_{mm} = -\frac{4552}{T} - 0.5 \log T + 8.793 ,$$

given by Ditchburn and Gilmour.[44] Our data yielding 758 ± 1°C for the boiling point of potassium are also in good agreement with several older experimental determinations[45] and in considerable disagreement with a boiling point of 774°C and a formula,

$$\log P_{atm} = -\frac{4769}{T} - 1.375 \log T + 8.708 ,$$

proposed by Kelley[43] on a partially theoretical basis.

In the KF-K system there is strikingly good agreement between the temperature of a distinct break at 850°C in the vapor pressure curve of the run with 50 mole % K and the monotectic temperature as derived from both thermal analysis (carried out in capsules of type *e*, Fig. 16) and chemical analysis of the salt-saturated metal-rich phase (Fig. 20). In this concentration range, i.e. above the salt concentration of 45 mole % KF of the saturated metal-rich phase at 850°C, or with other words, in the concentration range of the two-liquid-phase region, the temperature of the break is independent of concentration and therefore not influenced by faults of the method that make the actual concentration uncertain. The break is so distinct because the concentration of the salt in the saturated metal solution rises with increasing temperature so rapidly immediately below, and so slowly immediately above the monotectic temperature. On the other hand, the agreement for the other two compositions is far less satisfactory. The temperatures for the intersections of the runs with 22 and 32 mole % KF with the 50 mole % curve should, according to the analytical phase diagram, be 770 and 815°C, respectively, but the intersections actually were found at 814 and 838°C, respectively, where concentrations of 32 and 41 mole % are expected. The cause of this discrepancy may be the same as in the Na-NaCl case,

[45] C. T. Heycock and F. E. E. Lamplough, *Proc. Chem. Soc. London* 28:3 (1912), O. Ruff and Johannsen, *Ber. deut. chem. Ges.* t XIV 3601 (1905), Fiock and Rodebush, *J. Am. Chem. Soc.* 48, 2522 (1926).

namely a lowering of the effective mole fractions of the metal from 0.78 to 0.68, and 0.68 to 0.59 during the experiments.

It seems, then, that the method has served well to further demonstrate qualitatively the existence of true solutions of salts in metals but that as a quantitative tool it would not be very useful with these concentrated solutions unless a modification permitting a more precise knowledge of the concentration can be worked out.

NUCLEAR CHEMISTRY

HALF-LIFE MEASUREMENTS

A. R. Brosi B. H. Ketelle

Tentative half-lives for Ce^{144}, Co^{60}, and Kr^{85} were given in the last progress report of the Chemistry Division.[1] The values reported were obtained from statistical analyses of precision activity measurements made over a period of time which was short relative to the half-lives. Since the half-lives found for Co^{60} and Kr^{85} were considerably longer than previously reported values, supporting data obtained from coincidence measurements and constant deflection ion chamber measurements were reported.[1] It has been found that these supporting data were subject to nonrandom errors and, therefore, the uncertainties in the half-lives obtained from these data are much greater than were indicated.[1] In addition, in the rate of drift measurements the variance in mean values of measurements made on different days was several times as large as would be expected from the variance in single measurements made on a given day.

Two components of the instrument which were sources of fluctuations were replaced, and a new series of measurements extending over a period of six months has been made. In this series the discrepancy in variance between measurements made on a single day and in the variance in mean values of measurements made on different days has been reduced by a factor of 3.

Statistical analyses of the new data give the following half-lives: Ce^{144} 284.4 ± 1 d, Co^{60} 5.45 ± 0.1 y, and Kr^{85} 10.7 ± 0.2 years. The errors are twice the standard deviations obtained in the statistical analyses and therefore represent the 95% confidence level if the attempt to remove all sources of constant error was successful.

CHARACTERISTICS OF Pm^{145}

B. H. Ketelle A. R. Brosi

The radiations of a sample of Pm^{145}, prepared by Parker and Martin as previously described,[2] have been studied with various spectrometers. Although only one gamma ray peak is found in the scintillation counter spectrum, this is resolved into two gamma ray peaks in the proportional counter spectrum. A study of the conversion electron spectrum shows the presence of two gamma rays which have energies of 67.8 and 72.7 kev.

Coincidence measurements show that each of the gamma rays is in "prompt" coincidence with both K and L x rays. However, the two gamma rays are not in coincidence with each other. This indicates that there is electron capture to each of two excited levels in Nd^{145} which differ in energy by only 5 kev.

Precision measurements of the activity in a sample of Pm^{145} have been made over a period of five months. A statistical analysis of these data gives a half-life of 24 ± 2 years.

A considerable effort is being made to determine the relative intensities of the gamma ray peaks in the K x-ray coincident spectrum. If these relative intensities should be different from the relative gamma ray intensities, a difference in the K/L electron capture ratio could be determined and used to compute the total decay energy. Measurements are also in progress to determine conversion coefficients and branching ratios.

CROSS SECTION OF Pa^{233}

J. Halperin R. W. Stoughton

The capture cross section of Pa^{233} for pile neutrons has been reported[3] as 152 ± 15 barns. This value differs from that reported in ORNL-1462[4] in that a correction for resonance absorption in thorium has been applied.

RADIOCHEMICAL DECONTAMINATION CHARACTERISTICS OF PORCELAIN ENAMEL

G. W. Parker G. M. Hebert

The radiochemical decontamination characteristics of porcelain enamel were investigated in a program

[1] A. R. Brosi and B. H. Ketelle, *Chem. Semiann. Prog. Rep. June 20, 1953*, ORNL-1587, Table 10.

[2] G. W. Parker and W. J. Martin, *Chem. Quar. Prog. Rep. Dec. 31, 1952*, ORNL-1482, p. 9.

[3] J. Halperin, C. V. Ellison, D. E. Ferguson, and R. W. Stoughton, *Reactor Sci. Technol.* 3, No. 3, 108 (1953), TID-2010.

[4] J. Halperin, C. V. Ellison, R. W. Stoughton, and D. E. Ferguson, *Capture Cross-Section of Pa^{233} for Thermal Pile Neutrons*, ORNL-1462 (May 5, 1953).

intended to prove the suitability of porcelain for the construction of radiochemical laboratory furniture. A limited number of porcelain enamels have been compared with conventional materials of construction generally rated superior in decontamination characteristics.

The requirements of a good material for radiochemical decontamination have been summarized by Terrill,[5] who also reviewed the available test results and procedures including those developed by Tompkins and Bizzell,[6] and by Watson, Handley, and West.[7] These criteria parallel the general properties of glass – versatile chemical resistance, low absorption and chemical exchange characteristics, and freedom from surface defects and porosity. These characteristics are found to a varying degree in all porcelain enamels.

The tests applied to commercial porcelain were intended to simulate those of Watson, Tompkins, and others and to include some of the various reference materials used by them. For this reason it was felt that the results could be correlated with the previous work and with some specialized research on porcelain conducted by the U. S. Army Corps of Engineers,[8] the National Bureau of Standards,[9] and the Naval Radiological Defense Laboratory.[10]

Materials Tested

Porcelain-Enameled Steel. The porcelain-enamel coatings were of one principal type – commercial acid-resisting porcelain that generally consisted of a blue-black, nickel-cobalt ground coat and an opacified enamel cover coat which was sometimes replaced or supplemented by a glaze.

In some instances, only one side of the specimen had received the cover coat; in others, both sides were assumed to be identical. The thickness of the steel was generally found to be 20 gage, and the thickness of the enamel was about 0.005 in. of ground coat and about 0.015 in. of cover coat (Fig. 28). In only one instance was an extra thickness of cover coat noted; this was apparently a double coat and is indicated as such in Table 8.

Visually, these enameled surfaces are quite different. The better enamels are smooth, glossy, and highly reflecting. On examination with a 150X microscope, most white enamels seem to be transparent, with small bubbles throughout their depth. The bubbles do not produce surface pits but are contained in the enamel and result from the outgassing of hydrogen dissolved in the base metal. Uniformly small gas bubbles are characteristic of a good enamel (Figs. 28 and 29, code Nos. D-1 and D-2). Figure 30 (code No. B-3) shows a poor enamel structure.

The white enamels are opacified by the addition of a few per cent of an oxide of either antimony, titanium, or zirconium during preparation of the frit, a modified low-fusing glass containing some clay together with the usual glass formers.[11] Chemical resistance seems to be limited by the opacifier, with the order of decreasing resistance being from antimony to zirconium.

Glass Coatings. The glass coatings (described as true borosilicate glasses) differ from the enamels in that they are generally a single homogeneous layer (without suspended particles) applied more heavily to a heavier gage steel. Only one manufacturer (A. O. Smith Co.) supplied flat glass-coated specimens. Because of the higher firing temperature required, the glass coatings are limited in practice to massive curved structures.

Uncoated Reference Materials. The uncoated reference materials were:

1. Saran, $\frac{1}{16}$-in. rolled sheet;
2. Teflon, $\frac{1}{8}$-in. sheet;
3. sheet glass, type B;
4. Polythene, $\frac{1}{8}$-in. rolled sheet (smooth);
5. plate glass, $\frac{1}{4}$-in., glazing quality;

[5] J. G. Terrill, "Surfaces and Finishes for Radioactive Laboratories," *Laboratory Design for Handling Radioactive Materials*, Building Research Advisory Board, Research Correlation Conference No. 3, Nov. 1951, Division of National Research Council, National Academy of Sciences, Washington, D. C.

[6] P. C. Tompkins and O. M. Bizzell, *Radioactive Decontamination Properties of Laboratory Surfaces. I. Glass, Stainless Steel and Lead*, ORNL-381 (Sept. 21, 1949); P. C. Tompkins, O. M. Bizzell, and C. D. Watson, *Radioactive Decontamination Properties of Laboratory Surfaces. II. Paints, Plastics and Floor Materials*, ORNL-382 (Sept. 26, 1949).

[7] C. D. Watson, T. H. Handley, and G. A. West, *Decontamination and Corrosion Resistance Properties of Selected Laboratory Surfaces*, AECD-2996, Rev. (Aug. 29, 1950).

[8] E. H. Dhein, Department of the Army, Office of the Chief of Engineers, private communication.

[9] J. C. Richmond, J. R. Crandall, A. G. Eubanks, and W. N. Harrison, *Porcelain Enamels as a Surfacing Material for Protection Against Special Effects*, NBS No. 7A-101.

[10] W. W. Hawes, B. Singer, E. C. Arbuckle, and A. M. Branch, *Survey of Decontamination. XII. Decontaminability of Vitreous Enamels*, Naval Radiological Defense Laboratory, AD-162(C) (Aug. 1949).

[11] A. I. Andrews, *Enamels*, Twin City Printing Co., Champaign, Ill., 1935.

TABLE 8. SURFACE CHANGES AS A MEASURE OF RELATIVE ACID RESISTANCE*

NAME OR CODE LETTER OF PORCELAIN ENAMEL OR GLASS	COLOR	ROUGHNESS (μ-in.-rms)	
		Average Profilometer Reading Before Acid Treatment	Average Change in Profilometer Reading After Treatment
Sheet glass	Type B	1–2	0
A. O. Smith Co.	Blue-glass coating	10–15	0
A. O. Smith Co.	Black-glass coating	11–15	0
B-1	White (double thick)	20–30	0
B-2	Black (double thick)	10–20	0
I-1	White (TiO_2)	15–20	0
D-1	Gray	10–15	0
D-2	Antimony opacified white	8–12	0
Tile	Glazed-sanitary	18–22	0
Tile	Glazed-building	35–45	0
D-3	Black	12–15	+2
C-1	White	10–15	+2
G-1	White	20–25	+5
E-1	White (TiO_2)	20–25	+5
D-4	Titanium opacified white	9–15	+5
I-2	Black	20–25	+5
G-2	White	13–20	+6
D-5	Black (pitted)	9–16	+7
E-2	Blue-black clear glaze	15–25	+10
F-1	White	13–30	+18
F-2	Black	10–30	+20

*Acid treatment: 10% citric, 10% hydrochloric for 1 hr at room temperature.

6. Fluorothene, ⅛-in. pressed sheet (smooth);
7. No. 7 stainless steel, mirror finish;
8. No. 2B stainless steel, mill finish (normal laboratory grade).

The samples of the above materials and of the enameled surfaces were not screened for flaws but were taken as they were cut from larger pieces. This may explain variations in duplicate or similar samples; however, in spite of the variations, overall agreement between samples was good.

Acid Resistance

Since porcelain enamels vary considerably, even within the acid-resisting grades,[12] in resistance to attack by strong chemical reagents, a limited test was designed to represent a normal condition, within practicability, that would assist in establishing relative acid resistance among the various commercial products solicited.

The test was carried out by means of the inverted-watch-glass method, and a mixture of 10% each of hydrochloric and citric acids was used. A 1-in. watch glass was half-filled (about ½ cc) with reagent and then covered with an enamel specimen before both were inverted. One hour was allowed as sufficient time to etch or otherwise change the surface of an average specimen.

As a measure of the degree of attack, the increase in surface roughness, recorded in Table 8, was gaged on a surface profilometer (Physics Research Corp.). The reading is given in microinches-root-mean-square. A change of 2 μin. was barely visible. The titanium- and zirconium-

[12] R. L. Stedfield, "A Designers Guide to Vitreous Coatings," *Machine Design* 24, No. 12, 165 (Dec. 1952); 25, No. 1, 141 (Jan. 1953); 25, No. 2, 166 (Feb. 1953).

UNCLASSIFIED
M-1474

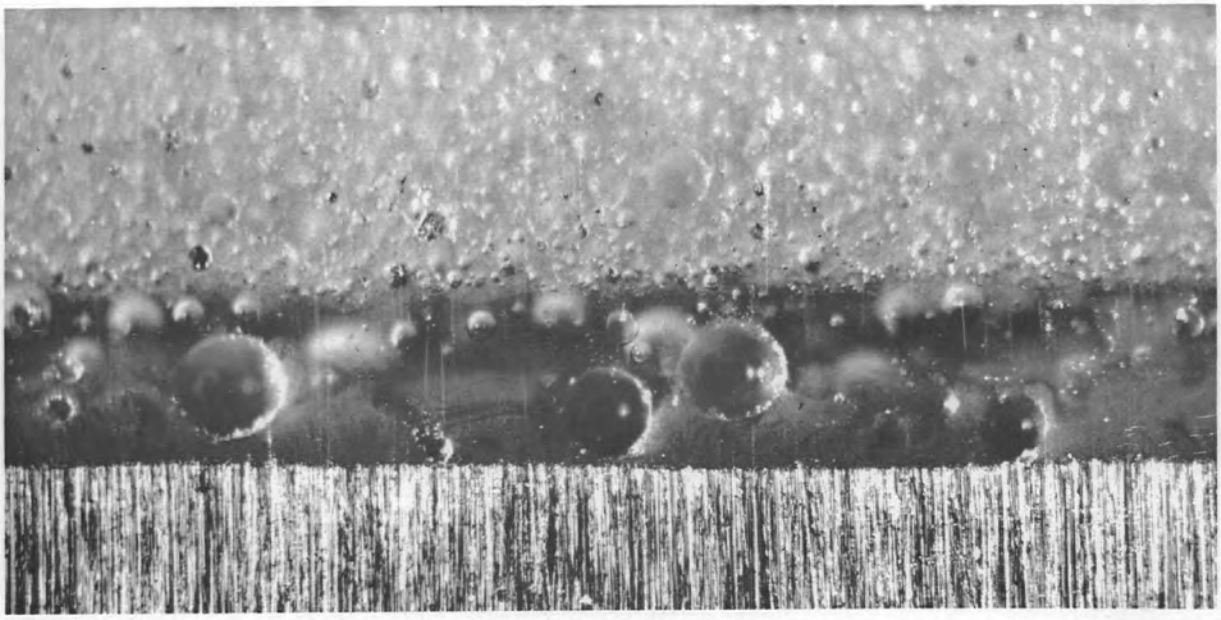

Fig. 28. Structure of a Good Enamel. Sample D-1, gray. 250X. Reduced 28%.

UNCLASSIFIED
M-1473

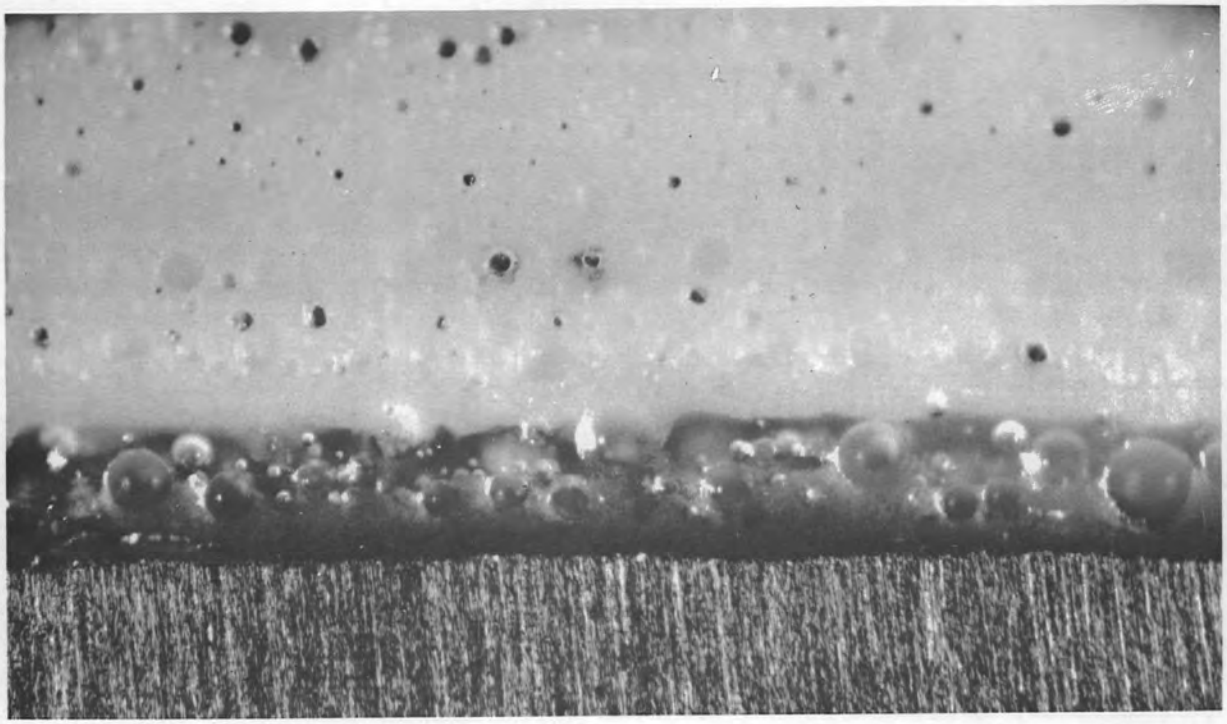

Fig. 29. Structure of a Good Enamel. Sample D-2, white. 250X. Reduced 28%.

UNCLASSIFIED
M-1499

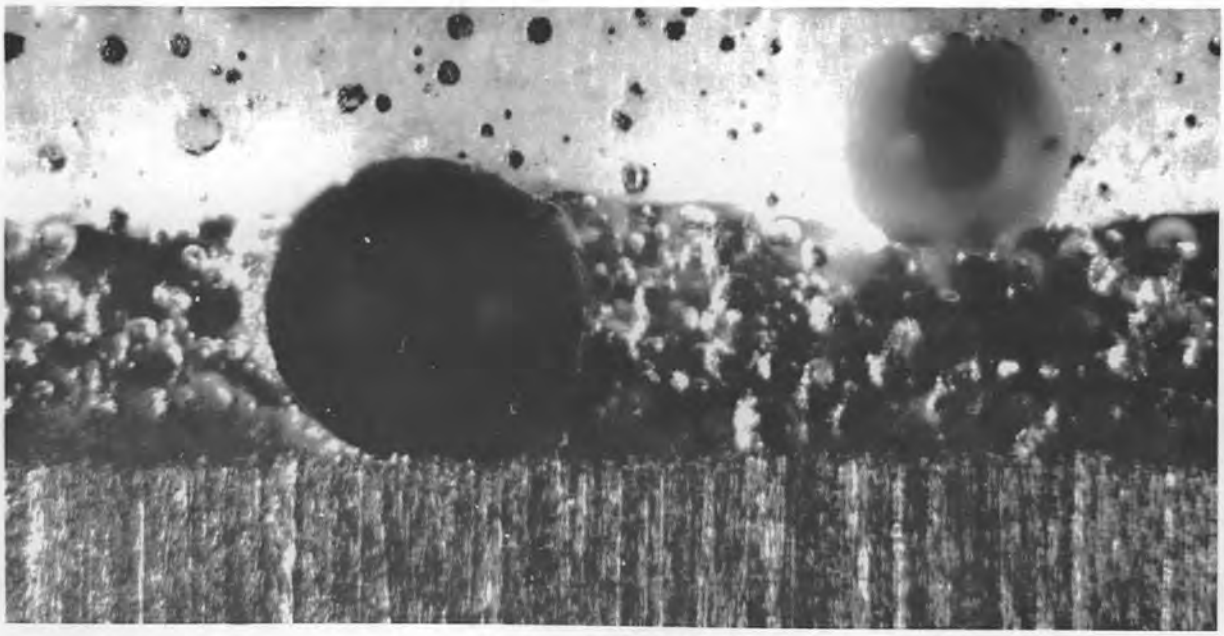

Fig. 30. Structure of a Poor Porcelain Enamel. Sample B-3. 250X. Reduced 28%.

opacified enamels were consistently less resistant than those opacified with antimony.

Contaminating Reagents

The contaminating activity applied to the samples was selected from two distinctly different radiochemical process wastes containing three-year-old fission products:

Mild Contaminant. This was a Redox type of aluminum nitrate extraction-column waste that was slightly acid deficient (basic aluminum nitrate) and contained a high salt content (500 mg/ml). Besides aluminum nitrate, the salts present were those of the metals that make up stainless steel. This material, because of the effect of the massive salt content, gave low retention of activity (Tables 9 and 10).

Severe Contaminant. This was a Purex type, nitric acid extraction-column waste of three-year-old cooled fission products that was 1.7 *N* in free acid and contained less than 25 mg of solids per milliliter. The salt content was principally salts of sodium and iron. The effect of the lower salt content and higher acid strength was to produce a much higher retention of, or susceptibility to, contamination that was roughly inversely proportional to the weight of inert salts (Table 11).

The radiochemical analysis of the two contaminating reagents differed slightly, but is not considered sufficient to alter the results materially. The predominant radioelements involved were cerium, promethium, ruthenium, strontium, zirconium and niobium, and cesium.

Besides a number of reference materials, only those porcelains already rated superior in acid resistance and in retention of the mild contaminant were further exposed to the higher degree of contamination. At this level of contamination, the poorer enamels fail to compare favorably with standard reference materials (Table 9). Only the best porcelains and glass coatings are sufficiently resistant.

Decontaminating Reagents

No significant portion of the investigation was devoted to the selection of an ideal reagent, with the exception of a brief study of the effect of pH on the most commonly used reagent, 5% citric acid. In the case of citric acid it was concluded that a mixture of 5% citric acid, 0.5 *N* in HCl and containing 0.5% aerosol, was more effective than a basic or neutral 5% sodium citrate solution.

TABLE 9. EFFECT OF VARIOUS REAGENTS ON DECONTAMINATION OF PORCELAIN ENAMELS (MILD CONTAMINANT)

CODE	COLOR	ACTIVITY REMAINING AFTER WATER WASH	CONTAMINABILITY RELATIVE TO SHEET GLASS	5% HNO_3	5% $(NH_4)_2SiF_6$	5% HNO_3	5% $(NH_4)_2SiF_6$	5% HNO_3	PER CENT ACTIVITY REMAINING AFTER 3RD WASH	5% HNO_3–5% $(NH_4)_2SiF_6$	PER CENT ACTIVITY REMAINING (Final)
D-6	White*	20,587	5.64		4500		2000	7	0.04	7	0.04
		11,113	3.04	113		19	15		0.09	2	0.01
D-2	Antimony opacified white	5,943	1.63	400		93	48		1.5	1	0.03
		4,009	1.10		183		65	9	0.28	3	0.09
		3,070	0.84	34		3	3		0.09	2	0.09
D-1	Gray	5,386	1.5	117		49	18		0.33	2	0.04
B-3	Black	4,714	1.3	85		53	58		1.2	10	0.21
D-4	Titanium opacified white	5,308	1.45	97		27	15		0.28	3	0.06
F-2	Black	14,900	4.1	750		677	677		4.55	1	0.005
G-2	White	8,747	2.4		26		26	12	0.13	6	0.06
F-1	White	9,996	2.7	27		3	23		0.23	4	0.04
G-1	White	4,419	1.21		89		28	13	0.28	6	0.14
		3,823	1.05	36		8	11		0.24	4	0.09
		6,996	1.92	352	95	51			1.12	7	0.15
Average			2.08						0.74		0.075

*Not acid resisting.

TABLE 10. DECONTAMINABILITY OF PORCELAIN ENAMELS (MILD CONTAMINANT)

MATERIAL	CONTAMINATION SUSCEPTIBILITY			DECONTAMINATION					
	Activity Not Removed by Water Wash (10^8 counts added)	Contaminability		Activity Remaining After					Per Cent of True Contamination Remaining
		Per cent retained	Relative to glass	1st wash	2nd wash	3rd wash	4th wash		
							5% $(NH_4)_2SiF_6$	5% HNO_3–5% $(NH_4)_2SiF_6$	
Glasses									
Sheet glass	3,650	0.00365	1	36	21	17	15		0.42
A. O. Smith Co. Blue*	3,066	0.00306	0.8	218	129	89	71		2.3
A. O. Smith Co. Black	5,066	0.00506	1.4	163	95	68	35		0.7
Acid-Resisting Porcelains									
I-1 White	3,775	0.00377	1.03	145	85	72	58		1.54
D-1 Gray	5,386	0.00538	1.5	222	57	26		6	0.1
D-2 Antimony opacified white	3,892	0.00389	1.06	110	39	19		3	0.08
D-3 Black	4,714	0.00471	1.3	1,881	1462	1450		23	0.49
C-1 White	2,384	0.00238	0.6	15	15	14	11		0.44
G-1 White	4,560	0.00456	1.3	74	39	32	15		0.33
E-1 White	10,920	0.01092	3.0	2,458	1233	1027		92	0.09
D-4 Titanium opacified white	5,308	0.0053	1.45	877	355	248		26	0.49
I-2 Black	4,928	0.00492	1.4	85	51	41		9	0.2
G-2 White	8,747	0.00874	2.4	332	171	141		12	0.1
D-5 Black	6,660	0.00666	1.7	864	288	138		2	0.03
E-2 Clear glaze blue-black	11,160	0.01116	3.2	1	898	643		62	0.5
F-1 White	9,996	0.00999	2.7	1,202	529	353		33	0.3
F-2 Black	14,900	0.0149	4.1	4,057	1749	1423		217	1.45
D-6**	15,850	0.0158	4.3	13,600				37	0.2

*Only one side coated.
**Not acid resisting.

TABLE 11. DECONTAMINABILITY OF PORCELAIN ENAMELS (SEVERE CONTAMINATION)

MATERIAL	CONTAMINATION SUSCEPTIBILITY			DECONTAMINATION						
	True Contamination Activity Not Removed By Water Wash (10^8 counts added, $\times 10^5$ counts)	Contaminability		Activity Remaining After						Per cent of True Contamination Remaining
				1st wash		2nd wash		3rd wash	4th wash	
		Per cent retained	Relative to sheet glass	5% HNO_3	0.5 *N* citric	5% oxalic	0.5 *N* citric	5% HNO_3 1% $(NH_4)_2SiF_6$	Enamel polish	
Reference Materials										
A. O. Smith Co. black-glass coating	4.2	0.42	2.4		5,159	3,117		216	126	0.03
Sheet glass	1.73	0.173	1		2,516	1,280		381	15	0.009
Plate glass	2.3	0.23	1.33		3,571	1,622		457	0	
Polythene	1.67	0.167	0.96		6,580	3,419		2,140	195	0.1
No. 7 stainless steel	1.44	0.144	0.83		1,431	484		342	137	0.095
No. 2B stainless steel	8.49	0.849	4.9		26,676	17,204		11,798	196	0.49
Porcelain Enamels										
D-2 Antimony opacified white	3.46	0.346	2.0		9,994	5,258		1,763	88	0.025
D-1	3.32	0.332	1.92	4,963			3,755	472	244	0.073
I-1	3.46	0.346	2.0	18,910			15,872	7,033	6223	1.8
G-1	6.78	0.678	3.92	52,666			44,752	15,029	3004	0.44
C-1a	4.06	0.406	2.34		56,324	41,762		20,854	7050	1.7
C-1b	6.78	0.678	3.92	163,000			134,000	14,516	4449	0.65
B-1	2.3	0.23	1.33	10,332			8,192	320	192	0.08
B-3	31.7	3.17	18.32	970,000			634,000	388,000	3200	0.10

The tendency to favor a reagent containing a low fluoride ion activity compatible with preservation of the original surface gloss of the porcelain is indicated in the tables. The reagents used most commonly are as follows:

Reagent	Composition
Acidic citrate	0.3 M citric acid, 0.5 M HCl, 0.5% aerosol O.T.
Nitric acid	5% HNO_3
Ammonium silicofluoride	5% $(NH_4)_2SiF_6$
Ammonium silicofluoride–nitric acid mixture	2.5% $(NH_4)_2SiF_6$, 2.5% HNO_3 0.5% $(NH_4)_2SiF_6$, 0.5% HNO_3
Enamel polish	One of several fine-grain pumice-type commercial preparations

Method of Testing

Contamination Susceptibility Test. The materials to be tested were cut into plaques about 2 × 2 in. square and were contaminated with fission products by pipetting a 0.1-ml portion of the contaminant, containing 10^8 beta counts per minute at the counter geometry used, onto each plaque. The contaminant was then allowed to dry without heating for approximately 6 hr in an open hood before proceeding with decontamination. The contaminating solution covered about 1 sq cm and presented a field of about 1 r/hr at 1 cm or about 50 mr/hr at 1 foot.

The samples were then flushed with water flowing at a rate of 2 to 3 gpm for 1 minute. The water flowed across the spot of maximum contamination instead of impinging upon it. Plaques were then air dried and counted on a mica-end-window G-M counter at approximately 10% geometry or 18 mm below the window. Little difficulty was experienced in counting samples exposed to the mild contaminant; however, when severely contaminated specimens beyond the capacity of the G-M counter were counted, an average equivalent counting rate was deduced from the counting rate through an aluminum absorber and a thin-window sodium-iodide crystal count-rate meter.

The first count obtained, known as the "susceptibility" or "true contamination" of the plaques, is an expression of the per cent of the total activity remaining after hosing or flushing. This activity is assumed to be vaguely absorbed on or combined with the surface. The following expression of susceptibility factor is only relative, since it depends not so much upon the specimen as upon the mass per unit area contaminated.

$$\frac{\text{Counts remaining after flushing}}{\text{Original counts applied}} \times 100 = \text{SF} .$$

Attempts to report absolute values on susceptibility factor are believed to be without basis; therefore for the purpose of this report the factors are given only as a ratio relative to sheet glass. These values are given as part of Tables 9 and 10.

Reagent Decontamination Scrub. In a preliminary experiment in which the mild Redox type of contaminant was used, the plaques for decontamination were first divided into three groups for conventional treatments with either acid-citrate, 5% HNO_3, or 5% ammonium silicofluoride. Each plaque was scrubbed with the proper reagent by hand with two paper-tissue swabs for a period of 1 min and then rinsed with water for 1 minute. The plaques were again air dried, mounted, and counted as before. The remaining activity has been expressed as a ratio or reagent decontamination factor (DF):

$$\frac{\text{Counts remaining from the susceptibility test}}{\text{Counts remaining after reagent scrubbing}} = \text{reagent DF}$$

An over-all decontamination factor has been expressed as follows:

$$\frac{\text{Initial counts applied}}{\text{Counts remaining after reagent scrubbing}} = \text{over-all DF} .$$

Obviously, this figure is dependent largely upon the amount of activity added and upon the mass and contact of the activity with the area involved. Since some specimens were decontaminated to zero counting rate, DF's as high as 10^8 could be proposed with little or no meaning.

Second and Third Reagent Scrub. Two additional scrubbings with the acid reagent were made on the duplicate porcelain plaques only. Part of the group being treated with nitric acid or ammonium silicofluoride was exposed alternately to each reagent (Table 10).

Ammonium Silicofluoride–HNO_3 Scrub. After the reagent decontamination scrubs, the number of

residual counts on the mildly contaminated porcelain-enameled plaques was quite low, but in spite of this, it was decided to determine the effectiveness of a mixture of ammonium silicofluoride–nitric acid in removing the residual activity which had resisted the previous treatments.

Alternate samples were then scrubbed with the 5% ammonium silicofluoride–5% HNO_3 solution in the same manner as the previous scrubbings. They were then rinsed, air dried, and counted. The corrosive effect of this mixture caused prohibitive frosting of the porcelain; however, no surface change was noted in the case of glass. A similar mixture that was only 1% in silicofluoride seemed to be adequate and was used subsequently.

Enamel Polish. One commercial fine-abrasive polish (Sun-Glo, Household Helps Co., Columbus, Ohio) was used finally in an effort to completely decontaminate some of the specimens used in the severe-contamination test. In some cases a further reagent DF of 20 or more was obtained after several previous reagent scrubs.

Trisodium Phosphate Scrub. One group of reference materials was decontaminating so poorly that a 5% trisodium phosphate solution was used as a final scrub. This was also ineffective. No further surface-removing methods were employed although specific methods, which are sometimes mildly destructive in effect, are available for decontaminating almost any material.

Conclusions

The susceptibility of porcelain-enameled steel to decontamination was found to be of about the same order as that of reference materials. Commercial porcelain enamels were found to vary widely in susceptibility and decontaminability, with both properties being proportional to acid resistance and to surface quality. The very best porcelains were equal to the true glass coatings and to mirror-finish stainless steel and were therefore superior to all other nonglass materials tested. (In the event of chloride attack, mirror-finish stainless steel can be expected to perform no better than the mill-finish grades.)

The best porcelains seem to withstand, without visible damage, effective decontamination with reagents containing low fluoride concentrations. However, in most cases the same net result may be had with other milder reagents.

ORGANIC CHEMISTRY

MECHANISM OF THE WAGNER-MEERWEIN REARRANGEMENT IN THE 1,2,2-TRIPHENYLETHYL SYSTEM

C. J. Collins W. A. Bonner

A series of reactions of phenyl-labeled 1,2,2-triphenylethanol (IIc), its acetate (IIIc), and its tosylate (IVc) has been carried out under reaction conditions identical with those used for the chain-labeled analogues, and the radiochemical consequences of these reactions in both systems have been compared. It has been shown by this novel double-labeling technique that the reactions studied fall into two categories: those in which a statistical redistribution of radioactivity has been achieved and those in which a statistical redistribution has been approached but not achieved. A simple kinetic relationship has been derived for the latter class of reactions, which allows a calculation of the radiochemical redistributions for various reactions in one series if the results of the other are known. These calculated values agree with the observed values within experimental error.

The syntheses of the ring-labeled ketone (I), carbinol (IIc), acetate (IIIc), and tosylate (IVc) were carried out in a manner similar to that employed for the preparation of their chain-labeled analogues, with the exception, of course, that non-radioactive diphenylacetyl chloride and carbon-labeled diphenylcadmium were used for the preparation of I. The bromobenzene-C^{14} used in the preparation of di(phenyl-C^{14})cadmium was obtained from benzene-C^{14} by a modification of the method of Derbyshire and Waters.[1] The labeled benzene was prepared by a standard method[2] starting with sodium cyanide-C^{14} and pentamethylene dibromide. The radiochemical structures of I, IIc, and IIIc were demonstrated by oxidation of these compounds with potassium permanganate, followed by carbon-14 assay of the ensuing benzophenone and benzoic acid fractions.[3]

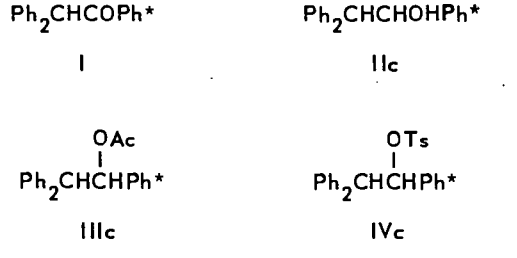

Various reactions were next conducted on the ring-labeled compounds IIc, IIIc, and IVc. The products arising from these reactions were analyzed for their distribution of radioactivity by degradation of each product to benzophenone and benzoic acid by procedures previously discussed.[4] Radiochemical assay of the benzophenone fraction from such degradations gave a measure of the net phenyl migration attending the reaction in question. The radiochemical consequences of the reactions studied were compared with corresponding data from the previous chain-labeled series, and the reactions were found to fall into two categories: those in which a statistical distribution of radioactivity was found in the product and those in which a statistical distribution was not found. The data pertaining to each category are presented separately in Charts 1 and 2.

The formolysis of tosylate IVa has been shown[4] to proceed with elimination to yield triphenylethylene (Vab) in which a net 50% phenyl migration had taken place. It was pointed out[4] that this phenyl migration could have arisen through the equilibration of 1,2,2-triphenylethyl formate under the conditions of formolysis. It has now been shown, by a study of the reactions indicated in Chart 1, that such an equilibration may, in fact, occur. Thus, when either acetate IIIa (Chart 1, Reaction 1) or acetate IIIc (Chart 1, Reaction 2) was dissolved in warm formic acid, the addition of *p*-toluenesulfonic acid caused the instantaneous formation of the olefin. Subsequent oxidation and radioactivity assay of the products indicated that in both cases the statistical radioactivity distribution had been obtained. Similarly, when a formic acid solution of the ring-labeled acetate IIIc (Chart 1, Reaction 3) was allowed to stand on the steam bath, the olefin gradually precipitated during a period of 20 minutes. From the solution the formate VI could be isolated. The statistical radioactivity distribution was again observed in the

[1] D. H. Derbyshire and W. A. Waters, *J. Chem. Soc.*, p. 575-6 (1950).

[2] R. J. Speer, M. L. Humphries, and A. Roberts, *J. Am. Chem. Soc.* 74, 2443 (1952).

[3] C. J. Collins and W. A. Bonner, *J. Am. Chem. Soc.* 75, 5379 (1953).

[4] W. A. Bonner and C. J. Collins, *J. Am. Chem. Soc.* 75, 5372 (1953).

CHART 1

Irreversible Reactions Proceeding with Statistical Redistribution of Radioactivity

(1)	Ph_2CHC^*HPh (OAc)	$\xrightarrow[p\text{-TSA}^a]{HCOOH}$	$Ph_2C^*{=}C^*HPh$	$\xrightarrow{KMnO_4}$	$Ph_2C^*{=}O$	+ PhC^*OOH
	IIIa (1.000)[b]		Vab		(0.500)	(0.492)
(2)	$Ph_2CHCHPh^*$ (OAc)	$\xrightarrow[p\text{-TSA}]{HCOOH}$	$Ph_2^*C{=}CHPh^*$	$\xrightarrow{KMnO_4}$	$Ph_2^*C{=}O$	+ Ph^*COOH
	IIIc (1.000)		Vcd		(0.663)	(0.332)
(3)	$Ph_2CHCHPh^*$ (OAc)	$\xrightarrow{HCOOH}$	$Ph_2^*C{=}CHPh^*$	$\xrightarrow{KMnO_4}$	$Ph_2^*C{=}O$	+ Ph^*COOH
	IIIc (1.000)		Vcd		(0.658)	(0.335)
			+			
			$Ph_2^*CH(OC{=}O)CHPh^*$	$\xrightarrow[(2)\ KMnO_4]{(1)\ LiAlH_4}$	$Ph_2^*C{=}O$	
			VI			
(4)	$Ph_2CH(OH)CHPh^*$	$\xrightarrow{HCOOH}$	$Ph_2^*C{=}CHPh^*$	$\xrightarrow{KMnO_4}$	$Ph_2^*C{=}O$	+ Ph^*COOH
	IIc (1.000)		Vcd		(0.653)	(0.337)
(5)	$Ph_2^*C{=}CHPh$	$\xrightarrow[p\text{-TSA}]{HCOOH}$	$Ph_2^*C{=}CHPh^*$	$\xrightarrow{KMnO_4}$	$Ph_2^*C{=}O$	+ Ph^*COOH
	Vd (1.000)		Vcd		(0.935)	(0.048)

[a] *p*-TSA = *p*-toluenesulfonic acid.

[b] Radioactivity assay reactant expressed as unity and degradation product assays reported as fractions thereof.

CHART 2

Irreversible Reactions Proceeding Without a Statistical Distribution of Radioactivity

(1)	$Ph_2CHC^*H(OTs)Ph$	$\xrightarrow[NaOAc]{HOAc}$	$Ph_2C^*HC^*H(OAc)Ph$	$\longrightarrow$	Ph_2C^*O +	PhC^*OOH
	IVa (1.000)[a]		IIIab		(0.387)	(0.593)
(2)	$Ph_2CHCH(OTs)Ph^*$	$\xrightarrow[NaOAc]{HOAc}$	$Ph_2^*CHCH(OAc)Ph^*$	$\longrightarrow$	Ph_2^*CO +	Ph^*COOH
	IVc (1.000)		IVcd		(0.468)	(0.517)
(3)	$Ph_2CHC^*H(OTs)Ph$	$\xrightarrow[Me_2CO]{H_2O}$	$Ph_2C^*HC^*H(OH)Ph$	$\longrightarrow$	Ph_2C^*O +	PhC^*OOH
	IVa (1.000)		IIab		(0.222)	(0.744)
(4)	$Ph_2CHCH(OTs)Ph^*$	$\xrightarrow[Me_2CO]{H_2O}$	$Ph_2^*CHCH(OH)Ph^*$	$\longrightarrow$	Ph_2^*CO +	Ph^*COOH
	IVc (1.000)		IIcd		(0.236)	(0.738)
(5)	$Ph_2CHC^*H(OH)Ph$	$\xrightarrow[Xylene]{p\text{-TSA}^b}$	$Ph_2C^*{=}C^*HPh$	$\longrightarrow$	Ph_2C^*O +	PhC^*OOH
	IIa (1.000)		Vab		(0.486)	(0.524)
(6)	$Ph_2CHCH(OH)Ph^*$	$\xrightarrow[Xylene]{p\text{-TSA}}$	$Ph_2^*C{=}CHPh^*$	$\longrightarrow$	Ph_2^*CO +	Ph^*COOH
	IIc (1.000)		Vcd		(0.602)	

[a]Actual radioactivity assay taken as unity and degradation product assays reported as fractions thereof.

[b]*p*-TSA = *p*-toluenesulfonic acid.

degradation products, and this indicated a complete equilibration at some stage during their formation. When the ring-labeled carbinol IIc was heated in formic acid (Chart 1, Reaction 4), statistically equilibrated triphenylethylene again resulted. It was shown independently that these equilibrations could not be accounted for by the isomerization of the olefin product itself in the presence of *p*-toluenesulfonic acid, because although this acid will, in time, effect a statistical equilibration of the olefin,[5] under the conditions of the reactions outlined in Chart 1, this isomerization is relatively slow. This fact is indicated by the results of Reaction 5, Chart 1 where the olefin, warmed for 15 min in formic acid containing one equivalent of *p*-toluenesulfonic acid, was found to be rearranged only to the extent of 4.8%.

[5]S. F. Clark and C. J. Collins, unpublished work.

Irreversible reactions not proceeding to statistical redistribution of radioactivity are given in Chart 2 for both the chain-labeled and ring-labeled triphenylethyl systems. It has already been shown that 1,2,2-triphenylethyl-1-C^{14} acetate is not rearranged under the acetolyzing conditions of Reactions 1 and 2 of Chart 2, so long as at least one molar equivalent of sodium acetate is present. 1,2,2-Triphenylethanol-1-C^{14} is likewise not rearranged when treated with acetone-water and *p*-toluenesulfonic acid when the hydrolysis conditions of Reactions 3 and 4 of Chart 2 are employed. It was further found[5] that the statistical radiochemical equilibration of 1,1,2-triphenylethylene-1-C^{14} with *p*-toluenesulfonic acid in xylene requires several weeks under experimental conditions similar to Reactions 5 and 6 of Chart 2. It thus can be said with assurance that the distributions of radioactivity found in the products of Reactions 1 to 6 of Chart 1 are uncomplicated by subsequent equilibration of the products, once these products have been formed.

Using the general kinetic relationship[6]

$$\frac{1}{2t}\ln\frac{x_e}{x_e - x} = \frac{2}{3t}\ln\frac{y_e}{y_e - y},$$

where x is the fraction of rearrangement for the chain-labeled products of Chart 2, y is the fraction of rearrangement for the ring-labeled products of Chart 2, and x_e and y_e are the equilibrium values 0.500 and 0.667, respectively, the experimental values of y have been used to calculate x, and these calculated x values are compared with those actually observed. The results of this comparison are listed in Table 12.

[6]K. J. Laidler, *Chemical Kinetics*, p. 20, McGraw-Hill, New York, 1950.

COMPARATIVE RATES OF RADIOACTIVITY REDISTRIBUTION AND ACETOXYL EXCHANGE DURING ISOMERIZATIONS OF TRIPLY LABELED 1,2,2-TRIPHENYLETHYL ACETATE

W. A. Bonner C. J. Collins

The triply labeled 1,2,2-triphenylethyl acetate system containing ring-labeled, chain-labeled, and acetyl-labeled species has been studied kinetically with regard to rates of phenyl redistribution and to the rate of acetyl exchange under the influence of an acid catalyst. It was found that the rate of equilibration of the ring-labeled acetate and that of the chain-labeled acetate are equal and that both are identical with the rate of acetoxyl exchange. These results are best interpreted in terms of a mechanism involving ion-pairs in which the classical cation undergoes radiochemical equilibration while in the ion-pair state.

The kinetic studies were conducted by placing the appropriate 1,2,2-triphenylethyl acetate in

TABLE 12. COMPARISON OF OBSERVED DISTRIBUTION OF RADIOACTIVITY IN PRODUCTS FROM REACTIONS IN THE CHAIN-LABELED TRIPHENYLETHYL SYSTEM WITH DISTRIBUTION CALCULATED FROM DATA OBTAINED IN THE RING-LABELED TRIPHENYLETHYL SYSTEM

REACTION IN CHART 2	MOLE FRACTION OF ISOMERIZED STRUCTURE IN REACTION PRODUCT		
	Ring-Labeled	Chain-Labeled	
		Calculated	Found
Tosylate hydrolysis (4)	0.236 ± 0.0005		
Tosylate hydrolysis (3)		0.222 ± 0.001	0.222 ± 0.002
Tosylate acetolysis (2)	0.468 ± 0.004		
Tosylate acetolysis (1)		0.399 ± 0.008	0.387 ± 0.0002
Carbinol dehydration (6)	0.602 ± 0.0005		
Carbinol dehydration (5)		0.477 ± 0.001	0.479 ± 0.002

acetic acid solution containing an equivalent of *p*-toluenesulfonic acid in a thermostat at 54.6 ± 0.4°C and quenching aliquots of the reaction mixture in water after various time intervals. The acetate from each aliquot was recovered and purified. The extent of phenyl migration in the chain- and ring-labeled acetates was acertained by deacetylating the recovered acetate, oxidizing the resulting carbinol, and assaying the benzophenone oxidation product for radioactivity. The extent of acetoxyl exchange of the acetyl-labeled acetate with its nonradioactive environment was ascertained by merely assaying the acetate recovered from each aliquot for total radioactivity. Both isomerization reactions, as well as the acetoxyl exchange reaction, were found to obey strict first-order kinetic expressions quite closely. First-order rate constants for formation of radiochemically equilibrated product and for acetoxyl loss at the time of each aliquot removal are presented in Tables 13, 14, and 15.

Examination of Tables 13, 14, and 15 indicates that the first-order rates of equilibration of the chain-labeled acetate and the ring-labeled acetate are essentially equal and that each is essentially the same as the first-order rate of acetyl exchange for the acetyl-labeled acetate. These results indicate that during the *p*-toluenesulfonic acid catalyzed isomerization of labeled 1,2,2-triphenylethyl acetates, *statistical redistribution of all phenyl groups occurs each time an acetyl group is removed from the discretely labeled starting material.*

Although the possibility was considered unlikely, there was a chance that a consistent external error was operative in the data of Tables 13 and 14 which would make it seem that the rates of equilibration of the chain-labeled and the ring-labeled acetates were equal when in reality they should bear the 4:3 ratio predicted on the basis of the previously derived kinetic relation (see ref. 6). This possibility has now been completely excluded by the results of an experiment in which the two acetates, differently labeled, have been mixed and isomerized in the same reaction vessel. The results of this experiment are outlined in Chart 3. The reaction conditions were identical to those employed in gathering the data of Tables 13 and 14 except that only one aliquot was removed (after 72 hours). From these data k_I (chain) is calculated to be $2.03 \pm 0.12 \times 10^{-2}$/hr, while k_{II} (ring) is calculated to be $2.11 \pm 0.08 \times 10^{-2}$/hr. The errors in the values of the two constants are calculated from the average deviations of the radioactivity determinations shown in Chart 3. In Tables 16, 17, and 18 are given the data which have been summarized in Tables 13, 14, and 15.

TABLE 13. FIRST-ORDER RATE CONSTANTS FOR THE EQUILIBRATION OF 1,2,2-TRIPHENYLETHYL-1-C^{14} ACETATE

RUN NUMBER	$k_I \times 10^2$/hr
1	2.22 ± 0.06
2	2.22 ± 0.02
	Avg. 2.22 ± 0.04

TABLE 14. FIRST-ORDER RATE CONSTANTS FOR THE EQUILIBRATION OF 1-PHENYL-C^{14}-2,2-TRIPHENYLETHYL ACETATE

RUN NUMBER	$k_{II} \times 10^2$/hr
1	2.17 ± 0.09
2	2.04 ± 0.07
	Avg. 2.10 ± 0.08

TABLE 15. FIRST-ORDER RATE CONSTANTS FOR ACETYL EXCHANGE OF 1,2,2-TRIPHENYLETHYL ACETATE-2-C^{14}

RUN NUMBER	$k_{III} \times 10^2$/hr
1*	2.39 ± 0.08
2**	2.56 ± 0.03
3	1.97 ± 0.06
	Avg. 2.31 ± 0.06

*One-half of the value obtained using 2 eq of *p*-toluenesulfonic acid.

**Value obtained running the ring-labeled and acetyl-labeled 1,2,2-triphenylethyl acetates in the same reaction vessel.

CHART 3

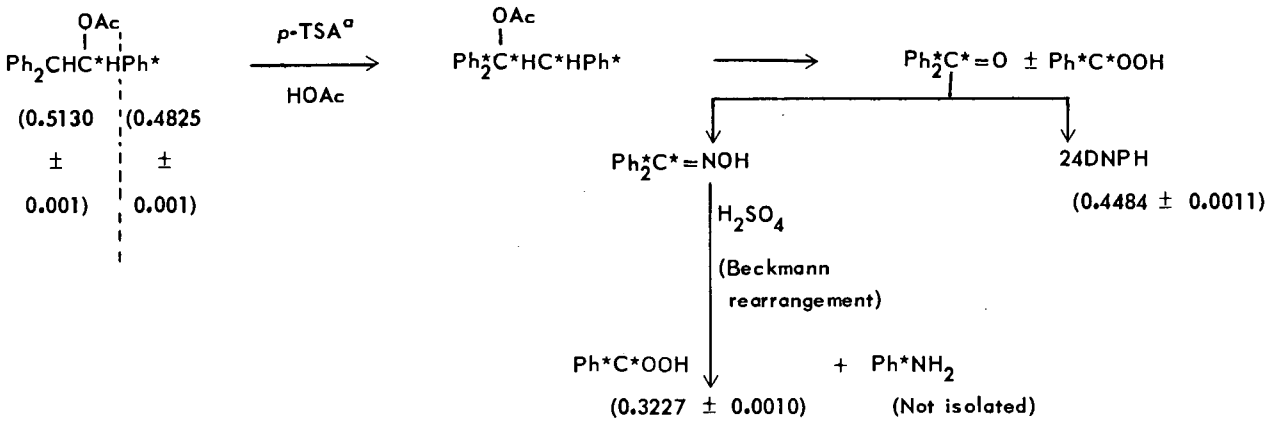

[a]p-TSA = p-toluenesulfonic acid.

TABLE 16. EQUILIBRATION CONSTANTS FOR 1,2,2-TRIPHENYLETHYL-1-C^{14} ACETATE

RUN NUMBER	ASSAY OF STARTING ACETATE (mc/mole)	TIME (hr)	Ph_2C^*O ASSAY (mc/mole)	$k_1 \times 10^2$/hr
1	2.161*	6	0.172	(2.900)
		22	0.419	2.229
		30	0.529	2.243
		46	0.689	2.207
		70	0.848	2.192
				Avg. 2.218 ± 0.018
2	1.000**	9	0.0996	(2.460)
		21	0.191	2.296
		44	0.314	2.250
		48	0.317	2.130
		52	0.347	2.280
		57.5	0.365	2.272
		70	0.398	2.268
		76	0.402	2.130
		95	0.435	2.164
				Avg. 2.224 ± 0.062

*Equilibrium value = 1.081.
**Equilibrium value = 0.500.

TABLE 17. EQUILIBRATION CONSTANTS FOR 1-PHENYL-C^{14}-2,2-DIPHENYLETHYL ACETATE

RUN NUMBER	ASSAY OF STARTING ACETATE (mc/mole)	TIME (hr)	$1.009 \times Ph_2^*CO$ ASSAY (mc/mole)	$k_{II} \times 10^2$/hr
1	0.991*	6	0.107	(2.914)
		22	0.270	2.356
		30	0.318	2.162
		46	0.419	2.150
		71.5	0.510	2.023
				Avg. 2.173 ± 0.092
2	0.991*	9	0.119	2.205
		21	0.241	2.138
		44	0.399	2.075
		48	0.414	2.025
		52	0.435	2.040
		57.5	0.457	1.938
		70	0.501	2.000
		76	0.518	1.978
		95	0.560	1.930
				Avg. 2.037 ± 0.069

*Equilibrium value = 0.667.

TABLE 18. ACETOXYL EXCHANGE CONSTANTS FOR 1,2,2-TRIPHENYLETHYL ACETATE-2-C^{14}

RUN NUMBER	ASSAY OF STARTING ACETATE (mc/mole)	TIME (hr)	ASSAY OF RECOVERED ACETATE (mc/mole)	$k_{III} \times 10^2$/hr
1	0.549	6.5	0.483	1.982
		23	0.344	2.035
		30.75	0.293	2.042
		47	0.224	1.905
		54	0.198	1.890
				Avg. 1.971 ± 0.059
2	0.495	6	0.382	(4.318)
		22	0.278	2.621
		30	0.230	2.560
		46	0.153	2.553
		71.5	0.083	2.500
				Avg. 2.558 ± 0.032
3	0.549 (p-Toluenesulfonic acid concentration doubled)	4.5	0.438	5.00
		23	0.178	4.90
		27	0.151	4.77
		30.75	0.137	4.51
				Avg. 4.79 ± 0.15
				Avg./2 2.39 ± 0.07

ORGANIC CHEMISTRY OF SOLVENTS

W. H. Baldwin C. E. Higgins

Ester Exchange Between Reagent Tri-*n*-butyl Phosphate and $H_3P^{32}O_4$

Organic phosphorus derivatives, labeled with radioactive phosphorus, have been used to study the distribution of these compounds between immiscible solvents. Radioactive phosphorus is readily available as o-phosphoric acid. Direct utilization of the labeled acid for ester exchange with tertiary esters would be useful for preparing labeled esters; thus,

$$(RO)_3PO + H_3P^{32}O_4 \longrightarrow (RO)_3P^{32}O_4 + (RO)_2P^{32}(O)OH + ROP^{32}(O)(OH)_2 + H_3P^{32}O_4$$

Tri-*n*-butyl phosphate exchanged at 170°C, and radioactive phosphorus was found in all four fractions. Distribution of the reaction products between carbon tetrachloride and aqueous alkali removed the neutral ester in the organic phase. The aqueous solution containing the salts of the acids was passed over Dowex-1 where the anions were adsorbed. Elution with 0.1 *N* HCl removed phosphoric acid with the peak of the radioactivity at 0.9 to 1.1 column volumes. Butyl dihydrogen phosphate appeared with the peak of activity at 5 to 5.4 column volumes and the dibutyl hydrogen phosphate peak was at 32 column volumes.

The results of heating the reaction mixture for 1, 4, and 24 hr at 170°C are shown in Table 19. The selection of the time of heating can be used to direct the radioactivity toward the product desired. The reaction is complicated by the following factors:

1. Butyl groups are lost during the reaction, as is evidenced by the increased titratable acidity. Theoretically, the maximum acidity is three equivalents, whereas at 24-hr heating, five equivalents were found.
2. Other forms of radioactive phosphorus have been found in the tracer after heating at 100°C and in the products of the exchange reaction at the same temperature.
3. Reaction between the pyrex reaction vessels and phosphoric acid is evident when the tracer is used without carrier.

Identification tests are being made on the unknown fractions. Ultimately the exchange reaction will be applied to the octyl esters that are of more interest to processing.

Tri-*n*-octyl Phosphine Oxide-P^{32}

$P^{32}OCl_3$ (from the action of PCl_5 on anhydrous $H_3P^{32}O_4$) was added to an excess of *n*-octyl magnesium bromide. The phosphine oxide was obtained from the reaction products, m.p., 53.2°C. A 0.2 *M* solution in decane was equilibrated with equal volumes of aqueous solutions. The equilibrium concentrations in milligrams per liter were:

Distilled water	1.8
1 *M* HCl	0.2
2% Na_2CO_3	3.6
5% Na_2CO_3	3.0
MVL	5.1

MVL is a source of uranium that contains iron, aluminum, sulfate, phosphate ions, and 1.3 g of uranium per liter.

The solubility of the phosphine oxide is sufficiently low to make the reagent attractive for process applications.

TABLE 19. DISTRIBUTION OF P^{32} FOLLOWING THE EXCHANGE OF BUTYL GROUPS BETWEEN TRI-*n*-BUTYL PHOSPHATE AND $H_3P^{32}O_4$*

FRACTION	REACTION TIME		
	1 hr	4 hr	24 hr
Phosphoric acid	46.5**	0.7	1.0
Butyl dihydrogen phosphate	41.7	10.0	16.2
Dibutyl hydrogen phosphate	14.6	46.0	56.3
Tributyl phosphate	2.7	40.0	24.7

*One mmole H_3PO_4 carrier and 0.5 mc tracer dehydrated at 105°C for 16 hr, then heated at 170°C with 4.4 mmoles tri-*n*-butyl phosphate for the times indicated.

**Numbers are the per cent of the starting phosphorus activity found in the fraction indicated.

CHEMICAL PHYSICS

EXPERIMENTS IN CHEMICAL KINETICS WITH MOLECULAR BEAMS

S. Datz E. H. Taylor

During this period further experiments have been made in which the angular distribution of the products of the reaction between molecular beams of HBr and K has been studied. In the previous report, it was indicated that out to an angle of about 15 deg from the K beam all the scattered material was unreacted K. A new detector mount, capable of scanning out to about 90 deg from the K beam, has been used in the current work. The first experiments performed with the new detector mount indicated little or no reaction, but further work of improved precision has revealed a very small amount of KBr.

In the latest and most precise experiment, with K at 513°K and HBr at 458°K, about 2 of every 1000 atoms measurably scattered by the HBr reacted to form KBr. This is clearly a very small amount of reaction, even considering that the total cross section is largely accounted for by the van der Waals attractive potential, and is hence in qualitative agreement with the earlier results showing no reaction. It will be necessary to measure the yield as a function of temperature to arrive at an unambiguous value for the activation energy, but it is clear that it is significantly greater than zero, the value derived from earlier work[1] and used in most subsequent theoretical considerations.

The distribution in angle of the KBr is of interest in that it depends on such things as the presence or absence of steric effects. The present experiments show that the distribution is rather sharply peaked, and it is almost certain that the peak is asymmetric. A detailed comparison will be made with the shapes to be expected from various assumptions about steric factor, lifetime of the activated state, activation energy, etc.

NEUTRON-DIFFRACTION STUDIES

H. A. Levy S. W. Peterson
B. S. Garrett

Crystal Structure of Oxalic Acid Dihydrate

Although the crystal structure of oxalic acid dihydrate has been the subject of several x-ray investigations,[2,3,4] some of the important features of the structure have remained in question. Previous investigators have agreed that the C_2O_4 group of the acid molecule is accurately planar and that the water oxygen makes a close (2.5 Å) approach to one of the carboxyl oxygens. The principal points on which they have disagreed are the carbon-carbon bond length, the equality of the two carbon-oxygen bond lengths in the carboxyl group, and the existence of OH_3^+ in the crystal. The objective of this neutron-diffraction investigation was to delineate the hydrogen-bond network and to answer as many of these questions as possible, particularly the one pertaining to the existence of OH_3^+.

Conclusions. It was found that the acid molecule is planar, including the hydrogen atoms. The carbon-carbon bond length is 1.53 Å, essentially a single bond (compare 1.54 Å in diamond). The two carbon-oxygen bonds are nearly equal in length, indicating considerable resonance within a carboxyl group but little or none across the carbon-carbon link. An anisotropic thermal motion was found which is interpreted as libration of the carboxyl groups about the carbon-carbon bond.

The nonexistence of OH_3^+ was conclusively established by the observation that the dimensions of the water molecule in the crystal (and also the O-H stretching frequency[5]) are nearly identical with those of a gaseous water molecule.[6]

The hydrogen-bond network can be described in terms of four chains: two helical chains parallel to the *b* axis and one parallel to each diagonal of the monoclinic cell face. The carboxyl hydrogen atom is situated colinearly with hydroxyl and water oxygen atoms and 1.05 Å from the former. The water hydrogen atoms, on the contrary, are not colinear with the oxygen atoms they bridge.

Experimental Procedure and Analysis. Single-crystal diffraction data were taken on a neutron

[1] H. v. Hartel, *Z. physik. Chem.* **B11**, 316 (1931).

[2] W. H. Zachariasen, *Z. Krist.* **A89**, 442-7 (1934).

[3] J. M. Robertson and I. Woodward, *J. Chem. Soc.*, p. 1817-24 (1936).

[4] R. Brill, C. Hermann, and C. Peters, *Ann. Physik.* 42, 357-77 (1942).

[5] R. Marignan, *Bull. soc. chim. France* 75, 352 (1948).

[6] D. M. Dennison, *Revs. Mod. Phys.* 12, 175 (1940).

spectrometer similar to that described by Wollan and Shull.[7] Data were obtained with a minimum amount of attention from an operator by use of an automatic programmer for scanning 20 reflections in sequence. The techniques for single-crystal work described by Peterson and Levy[8] were employed for taking data and calculating structure factors from observed intensities. Cylindrical specimens were used to facilitate making absorption corrections. A comparison of single-crystal data with data from a powdered sample indicated secondary extinction in the single-crystal specimen to be negligible.

Data were taken from crystal specimens of two sizes in both the ($h0l$) and ($0kl$) zones. Ninety-eight reflections were measured in the former and 58 in the latter zone at a wavelength of 1.142 Å. An empirical normalization factor was required to bring the data from the two ($h0l$) specimens into agreement. Agreement between ($0kl$) specimens was satisfactory without normalization.

The data were analyzed by the Fourier series synthesis method. In order to determine signs of the structure factors for the ($h0l$) zone, a procedure involving no assumptions regarding hydrogen positions was used. Statistical methods[9] were used to estimate an average temperature-factor coefficient for carbon and oxygen. The calculated structure-factor contributions of carbon and oxygen from this temperature-factor coefficient and x-ray parameters determined the signs of two thirds of the experimental structure factors. Signs of most of the remaining structure factors were determined by application of Harker-Kasper[10] inequalities to the residual hydrogen contribution. A preliminary Fourier map was then prepared and approximate atomic coordinates were determined. The remaining signs were determined and a final Fourier map was prepared. Artificial convergence was introduced into the series by means of a modification function.[11] Parameters were read by Gaussian interpolation of the peaks, temperature factors were refined by peak-shaped analysis, and a backshift correction was applied to all atoms except the two water hydrogen atoms. Final refinement of the parameters of these atoms was carried out by the method of least squares.

The problem of sign determination in the ($0kl$) zone was attacked by assuming the hydrogen atoms to be located on the lines connecting the water oxygen with the three nearest oxygen atoms and to have the z parameters determined in the analysis of the ($h0l$) zone. The Fourier map prepared with this set of signs did not have peak heights or shapes in close agreement with expectation; two additional starts from different assumptions were therefore made, each converging on the original set of signs. The initial agreement between calculated and observed structure factors was poor, especially for large values of the k index. Severely anisotropic temperature factors were deduced for several atoms including the carboxyl oxygens and the water molecule. This temperature factor greatly improved the structure-factor agreement and provided an interpretation of the unusual features of the Fourier map. Because of poor resolution it was necessary to refine the structure by alternate least-squares treatments of the water molecule and the carbonyl group. A backshift correction was applied to the two resolved atoms, the hydroxyl group of the acid molecule. Only y parameters were estimated in this zone.

Results. The final set of parameters and the estimates of their standard errors[12] are given in Table 20, interatomic distances in Table 21, and bond angles in Table 22.

Comparison of these results with the best previous treatment of x-ray data[4] showed satisfactory agreement on atomic positions but general nonconcordance in the analyses of the thermal motion of the atoms. It was concluded that errors in the determination of the photographic intensity scale for the x-ray data were probably responsible for the discrepancies.

Crystal Structure of Iodic Acid

The crystal structure of alpha iodic acid was determined by Rogers and Helmholz[13] by x-ray diffraction. They deduced iodine and oxygen parameters and found the iodic acid molecule to

[7] E. O. Wollan and C. G. Shull, *Phys. Rev.* 73, 830-41 (1948).

[8] S. W. Peterson and H. A. Levy, *J. Chem. Phys.* 19 1416-8 (1951).

[9] A. J. C. Wilson, *Acta Cryst.* 2, 318-21 (1949).

[10] E. Grison, *Acta Cryst.* 4, 489-90 (1951).

[11] J. Waser and V. Schomaker, *Revs. Mod. Phys.* 25, 671-90 (1953).

[12] D. W. J. Cruickshank, *Acta Cryst.* 2, 154-7 (1949).

[13] M. T. Rogers and L. Helmholz, *J. Am. Chem. Soc.* 63, 278-84 (1941).

TABLE 20. ATOMIC PARAMETERS AND ESTIMATES OF PRECISION FOR OXALIC ACID DIHYDRATE

ATOM	x	y	z
C	−0.0450 ± 0.0013	0.054 ± 0.003	0.0501 ± 0.0003
O_1	0.0817 ± 0.0009	−0.057 ± 0.002	0.1467 ± 0.0004
O_2	−0.2235 ± 0.0010	0.227 ± 0.005	0.0375 ± 0.0005
O_3	−0.0452 ± 0.0013	0.114 ± 0.006	0.3222 ± 0.0003
H_1	−0.1361 ± 0.0032	−0.062 ± 0.009	0.3506 ± 0.0016
H_2	0.0729 ± 0.0032	0.118 ± 0.005	0.3870 ± 0.0016
H_3	0.0227 ± 0.0020	0.015 ± 0.004	0.2180 ± 0.0013

TABLE 21. INTERATOMIC DISTANCES AND ESTIMATED PRECISION FOR OXALIC ACID DIHYDRATE

ATOMS	DISTANCE (Å)	STANDARD ERROR (Å)
C-C	1.533	0.011
$C-O_1$	1.254	0.008
$C-O_2$	1.229	0.014
O_1-O_3	2.518	0.008
O_1-H_3	1.057	0.016
O_3-H_1	0.968	0.029
O_3-H_2	0.945	0.021
O_3-O_2'	2.840	0.008
O_3-O_2''	2.856	0.008

consist of irregular pyramids of IO_3. An irregular coordination octahedron about each iodine was found to be formed by the three oxygen atoms within the molecule and three more from molecules which approach iodine more closely than in a normal van der Waals contact. They also proposed the existence of a bifurcated hydrogen bond. Wells[14] suggested an alternative hydrogen-bond arrangement, in which the bond is not bifurcated but forms strings of molecules parallel to the b axis. The purpose of this neutron-diffraction study was to determine the actual hydrogen-bond arrangement and to refine the oxygen parameters in order to confirm the unusually short intermolecular contacts.

Conclusions. It was confirmed that the IO_3 group is an irregular pyramid and that there are three short intermolecular iodine-oxygen approaches, described by Rogers and Helmholz as completing a coordination octahedron around iodine. The suggestion of Wells that the hydrogen bonds form strings along the b axis was confirmed.

An alternative description of the crystal is suggested. Hydrogen-bonded molecules form chains of pentagonal rings, each ring involving parts of two molecules:

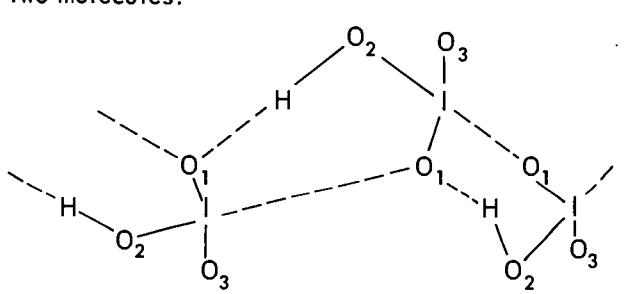

These rings, which are closely planar throughout a chain, involve the hydrogen bond and the shortest of the three short intermolecular I-O contacts described by Rogers and Helmholz. Neighboring chains are tilted 64 deg toward each other.

The iodine-oxygen bonds in the molecule vary in length from 0.04 Å less than a single bond ($I-O_2$) to that of a double bond ($I-O_3$). Rogers and Helmholz have interpreted these lengths as evidence of large amounts of double-bond character in $I-O_1$ and $I-O_3$ and suggest the bonds to be sp hybrids in accordance with the observed angles, which are near 100 degrees.

[14] A. F. Wells, *Acta Cryst.* 2, 128-9 (1949).

TABLE 22. BOND ANGLES AND ESTIMATED PRECISIONS FOR OXALIC ACID DIHYDRATE

BONDS	ANGLE	σ
$C\text{-}C\text{-}O_1$	112° 22′	0° 41′
$C\text{-}C\text{-}O_2$	120° 54′	0° 50′
$O_1\text{-}C\text{-}O_2$	126° 43′	0° 57′
$O_1\text{-}H_3\text{-}O_3$	175° 21′	2° 0′
$C\text{-}O_1\text{-}H_3$	112° 56′	1° 40′
$H_1\text{-}O_3\text{-}H_2$	105° 41′	3° 0′
$O_3\text{-}H_2\text{-}O_2'$	167° 2′	2° 30′
$O_3\text{-}H_1\text{-}O_2''$	156° 6′	3° 0′

An attempt was made to correlate information from nuclear quadrupole spectroscopy[15,16] with structural information in order to describe the iodine-bonding orbitals more completely. It was found that hybridizations consistent with the experimental observations could be obtained, but not unambiguously.

The hydrogen atom is situated 0.99 Å from an oxygen atom and nearly colinearly with the hydrogen-bonded oxygen atoms. The length of the hydrogen bond is 2.68 Å.

Experimental Procedure and Analysis. With the exception of the necessity for making a correction for secondary extinction of the $(0kl)$ zonal data, the analysis of the diffraction data was straightforward. Data were collected on 75 reflections in the $(0kl)$ zone and 72 in the $(h0l)$ zone at a wavelength of 1.062 Å. Signs were determined in both zones by calculation of iodine and oxygen contributions from the x-ray parameters. Hydrogen was assigned approximate parameters on the basis of its contribution to reflections for which the iodine and oxygen contributions were small or canceled.

After estimation of parameters from a preliminary Fourier map of the $(0kl)$ zone, comparison of calculated and observed structure factors indicated the necessity of making a correction for secondary extinction. The extinction effect was treated as an isotropic absorption coefficient which was proportional to intensity. After choosing the extinction corrections which gave the best agreement between specimens and between corrected observed and calculated structure factors, a final experimental Fourier map was prepared. Parameters were read and corrected by the backshift method for termination-of-series errors.

A preliminary Fourier map of the $(h0l)$ zone was prepared and parameters were estimated. The iodine and hydrogen peaks were unresolved; a graphical analysis of the compound peak was made in order to obtain an approximate x parameter for hydrogen. The x parameters for the oxygen atoms were read directly; the iodine x-ray x parameter and the z parameters from the $(0kl)$ zone were used to calculate a set of structure factors from which a final set of signs was obtained. A final Fourier map was prepared and x parameters for two oxygen atoms were read and backshifted. The x parameters of the hydrogen, iodine, and remaining oxygen atom and the temperature factor of hydrogen were refined by the method of least squares.

The final sets of atomic parameters, interatomic distances, and bond angles are given in Tables 23, 24, and 25.

RADIO-FREQUENCY SPECTROSCOPY

The Iodine Problem

R. Livingston B. Benjamin

Cooperative microwave experiments with Duke University on the hyperfine structure of the $J = 2 \rightarrow 3$ rotational transition of CH_3I^{131} have been completed. The nuclear spin of 8-day half-life I^{131} was found to be 7/2 and its quadrupole coupling in CH_3I, -973 ± 9 megacycles. This coupling gives -0.412×10^{-24} cm^2 for the quadrupole moment of I^{131}.

Two successful experiments were carried out. In the first experiment eight hyperfine lines of CH_3I^{131} were measured. A number of CH_3I^{129} lines were also seen. In the second experiment these lines were confirmed and two additional, weaker lines were measured. The observations indicated that the iodine obtained from slugs irradiated at Hanford contained roughly comparable amounts of I^{129} and I^{131} (atom basis) and a

[15] C. H. Townes and B. P. Dailey, *J. Chem. Phys.* 20, 35-40 (1952).

[16] R. Livingston and H. Zeldes, *Chem. Semiann. Prog. Rep. June 20, 1953*, ORNL-1587, p. 63.

TABLE 23. FINAL PARAMETERS OF ATOMS IN ALPHA IODIC ACID

ATOM	x	y	z
H	0.2340 ± 0.0043	0.3220 ± 0.0015	0.1350 ± 0.0020
I	0.2036 ± 0.0011	0.0861 ± 0.0015	0.1580 ± 0.0010
O_1	0.0712 ± 0.0016	0.5225 ± 0.0011	0.2429 ± 0.0010
O_2	0.3340 ± 0.0014	0.1978 ± 0.0012	0.0864 ± 0.0010
O_3	0.4043 ± 0.0010	0.1566 ± 0.0014	0.4481 ± 0.0010

TABLE 24. INTERATOMIC DISTANCES IN ALPHA IODIC ACID

ATOMS	DISTANCE (Å)
$H\text{-}O_2$	0.990 ± 0.017
$H\text{-}O_1'$	1.700 ± 0.018
H-I	2.407 ± 0.013
$I\text{-}O_1$	1.816 ± 0.010
$I\text{-}O_2$	1.899 ± 0.011
$I\text{-}O_3$	1.780 ± 0.010
$O_1\text{-}O_2$	2.800 ± 0.010
$O_1\text{-}O_3$	2.769 ± 0.009
$O_2\text{-}O_3$	2.686 ± 0.010
$O_2\text{-}O_1'$	2.685 ± 0.010
$I\text{-}O_1'$	2.503 ± 0.011
$I\text{-}O_3''$	2.879 ± 0.010
$I\text{-}O_3'''$	2.767 ± 0.009

TABLE 25. BOND ANGLES IN ALPHA IODIC ACID

ATOMS	ANGLES
$O_1\text{-}I\text{-}O_2$	$97^0\ 45' \pm 0^0\ 35'$
$O_1\text{-}I\text{-}O_3$	$100^0\ 38' \pm 0^0\ 36'$
$O_2\text{-}I\text{-}O_3$	$93^0\ 45' \pm 0^0\ 37'$
$I\text{-}O_2\text{-}H$	$108^0\ 15' \pm 1^0\ 33'$
$O_1'\text{-}H\text{-}O_2$	$172^0\ 56' \pm 3^0\ 0'$

negligible amount, at least for this work, of I^{127}. This is in contrast to iodine prepared from ORNL irradiated slugs in which the I^{127} content in one experiment proved to be the main constituent (atom basis). The carrier iodine presumably is introduced as an impurity in process reagents, and the higher isotopic content of the product from Hanford slugs results from its much higher specific activity.

The above results are being published elsewhere in greater detail.[17] Consideration is now being given to measuring the I^{131} magnetic moment.

[17] R. Livingston, B. M. Benjamin, J. T. Cox, and W. Gordy, *Phys. Rev.* 92, 1271 (1953).

Paramagnetic Resonance

R. Livingston H. Zeldes
E. H. Taylor

Simple, paramagnetic resonance equipment has been assembled. The apparatus operates in the *K*-band region (23,500 megacycles), which requires a magnetic field for the free electron spin of roughly 8300 gauss. The magnetic field is sinusoidally modulated at 60 cps, and the resonance absorption lines are viewed directly on an oscilloscope. Separations of observed lines are measured with a proton resonance apparatus.

A variety of preliminary observations has been made mostly on samples in which the paramagnetism has been produced by ionizing radiation. In most cases, samples have been cooled to liquid-nitrogen temperature, irradiated in a high-intensity cobalt gamma source, and then examined for resonances while still cold. One main limitation has been the inhomogeneity of the field in the present magnet. A new magnet has been designed and is under construction.

The most significant observation in the present work has been that a pair of the four resonance lines seen in irradiated H_2SO_4 corresponds in

separation to the atomic hydrogen hyperfine splitting. A similar pair of lines appears in a four-line spectrum for H_3PO_4. The observed atomic beam hyperfine splitting for hydrogen, 1420.410 megacycles,[18] gives a computed hyperfine separation of 504 gauss in the experimental configuration used by the authors. This same separation, to within 1%, was observed for H_2SO_4 and H_3PO_4. In view of the preliminary nature of these observations, the agreement may be fortuitous. These measurements imply that the unpaired electron must be a pure 1*S* electron and that there is no chemical bonding to the hydrogen atom. Experiments are now under way with deuterium-substituted acids. Much more accurate measurements should be possible with the new magnet.

[18] J. E. Nafe and E. B. Nelson, *Phys. Rev.* 73, 718 (1948).

Pure Quadrupole Spectroscopy

H. Zeldes R. Livingston

Zeeman studies of the pure quadrupole spectra of Cl^{35} in $NaClO_3$ and $KClO_3$ have been completed. Measurements of the absorption line splittings where the magnetic field was oriented along the twofold, the threefold, and the fourfold axes of $NaClO_3$ agreed with the theory and gave no new crystallographic information. It was found that these symmetry axis directions could be located to within about 0.2 deg at a field of 100 gauss by observing the nature of the absorption line splittings. In the case of $KClO_3$, unlike that of $NaClO_3$, the known crystal structure does not give the direction of the main component, ϕ_{zz}, of the field gradient tensor. Also, unlike $NaClO_3$, $KClO_3$ is expected to have asymmetry in its field gradient tensor, since there is not a threefold axial symmetry about the Cl. Since the *a*-*c* plane is a mirror plane,

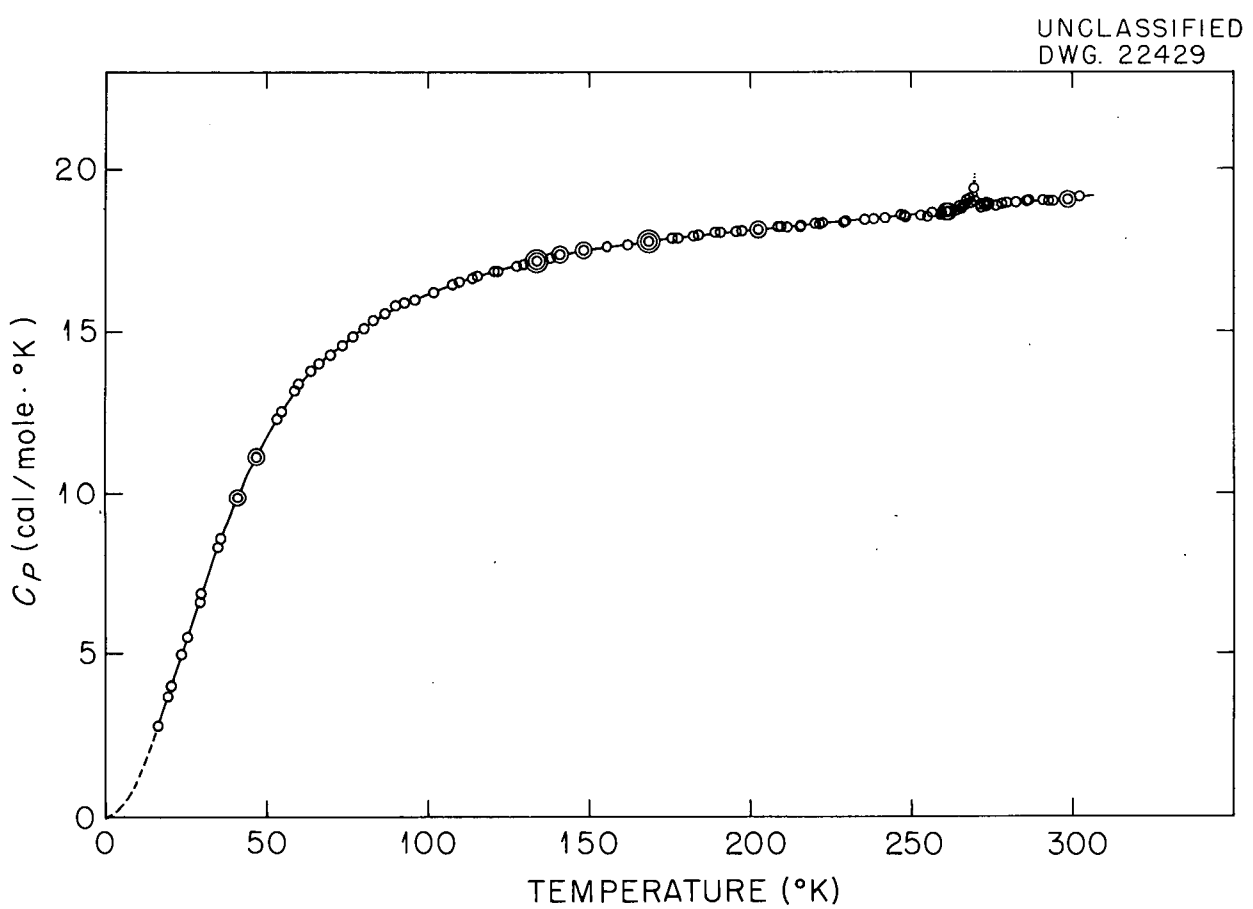

Fig. 31. Heat Capacity of Cadmium Iodide.

two of the principal axis components of the field gradient tensor are in this plane and the third is normal to it. The experimental measurements showed that the asymmetry, i.e., $|(\phi_{xx} - \phi_{yy})/\phi_{zz}|$, is in the order of 0.01. This amount was small enough to be near the limit that could be detected experimentally. Only the main principal axis direction, ϕ_{zz}, could be determined. This turned out to be in the a-c plane (experimentally ±0.2 deg) inclined 52.1 ± 0.2 deg from the a axis. Since the asymmetry is so slight, the ϕ_{zz} direction is expected to be the direction of the normal to the plane of the three O atoms nearest to a chlorine. The direction of this normal, computed from the known[19] crystal structure parameters, is in the a-c plane inclined 55.7 deg from the a axis. It is expected that the presently reported determination is much more accurate. In the foregoing discussion, the crystal axis directions a, b, and c were chosen so that b is the unique direction, and the ratio of axial lengths, a:b:c, is 0.8331:1:1.2673.

LOW-TEMPERATURE CALORIMETRY

A. S. Dworkin D. J. Sasmor
E. R. Van Artsdalen

The heat capacity of crystalline cadmium iodide, CdI_2, has been determined in the temperature range 15 to 300°K by using the adiabatic calorimeter described previously.[20] The weight of the empty calorimeter can, including heater, thermometer, and accessories, was 56.3980 g, and the can was charged with 124.2934 g of cadmium iodide (J. T. Baker Chemical Company "CP Analyzed"). The experimental data are shown in Fig. 31. Smoothed values of C_p and the derived quantities S^0, $-(F^0 - H_0^0)/T$, and $(H^0 - H_0^0)/T$ are given in Table 26 at 10-deg intervals.

The heat capacity of cadmium iodide rises very rapidly in the low-temperature range although a fairly common curve shape is obtained. Figure 31 shows that the heat capacity is nearly 3 cal/mole·deg at the lowest temperature reached. At about 269°K a very small hump was observed in the heat-capacity curve. The exact explanation of this is not known, although it is probable that traces of moisture are responsible. In any case, the presence of this small hump exerts a rather negligible effect upon the derived thermodynamic values.

Cadmium iodide was selected because it has a so-called "layer structure," and it was of interest to determine the temperature dependence of heat capacity in the low-temperature range to see whether it would show the same type of T^2 dependence observed with boron nitride.[20] The temperature dependence can be shown in a log-log plot. In Fig. 32, log C_p is plotted against log T, and it is seen that down to 15°K no simple power relationship exists between T and C_p; indeed, the dependence increases as the temperature is lowered. In the range 15 to 20°K, C_p appears to be varying as about the 1.4 power of T. Therefore, the extrapolation to 0°K cannot be made by either the T^2 method or the customary Debye T^3 law and is somewhat uncertain. Hence all derived values of Table 26 must be looked upon as subject to slight future revision at such time as the authors are able to measure the heat capacity in the very low temperature range (helium range).

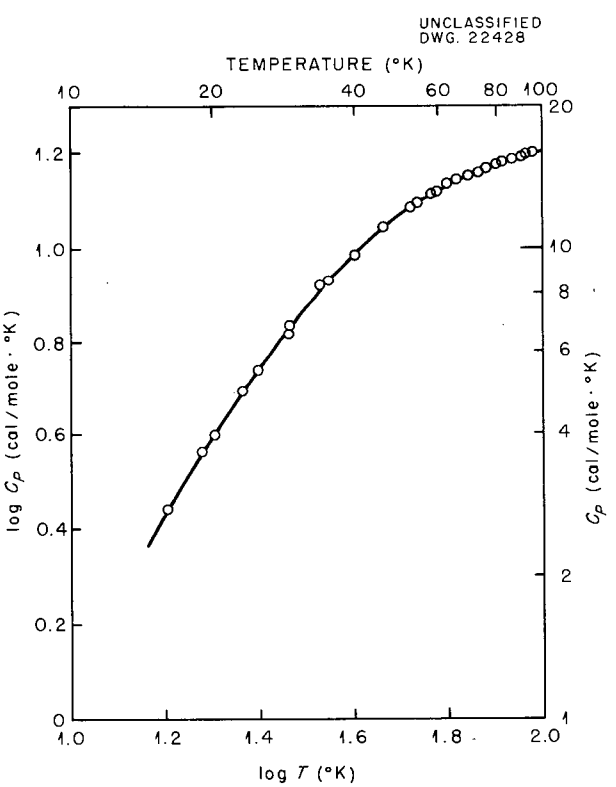

Fig. 32. Log-Log Plot of Low-Temperature Heat Capacity of Cadmium Iodide.

[19] W. H. Zachariasen, *Z. Krist.* 71, 501 (1929).

[20] A. S. Dworkin, D. J. Sasmor, and E. R. Van Artsdalen, *Chem. Semiann. Prog. Rep. June 20, 1953*, ORNL-1587, p. 19.

TABLE 26. SMOOTHED MOLAR THERMODYNAMIC FUNCTIONS OF CdI_2

TEMPERATURE (°K)	C_p (cal/mole·deg)	S^0 (cal/mole)	$-\frac{(F^0 - H_0^0)}{T}$ (cal/mole·deg)	$\frac{(H^0 - H_0^0)}{T}$ (cal/mole·deg)
10	1.35	0.60	0.26	0.34
20	3.93	2.22	0.83	1.39
30	6.99	4.39	1.66	2.73
40	9.74	6.79	2.64	4.15
50	11.84	9.19	3.70	5.49
60	13.33	11.51	4.82	6.69
70	14.33	13.65	5.93	7.72
80	15.10	15.61	7.02	8.59
90	15.72	17.43	8.08	9.35
100	16.17	19.11	9.10	10.01
110	16.53	20.67	10.08	10.59
120	16.82	22.12	11.03	11.09
130	17.07	23.48	11.93	11.55
140	17.29	24.75	12.81	11.94
150	17.48	25.95	13.64	12.31
160	17.65	27.09	14.45	12.64
170	17.80	28.16	15.23	12.93
180	17.92	29.18	15.98	13.20
190	18.05	30.15	16.70	13.45
200	18.14	31.08	17.39	13.69
210	18.22	31.97	18.07	13.90
220	18.30	32.82	18.72	14.10
230	18.39	33.64	19.35	14.29
240	18.49	34.42	19.96	14.46
250	18.56	35.18	20.55	14.63
260	18.65	35.91	21.13	14.78
270	18.86	36.62	21.69	14.93
273.16	18.89	36.84	21.86	14.98
280	18.94	37.31	22.24	15.07
290	19.03	37.98	22.77	15.21
298.16	19.11	38.50	23.19	15.31
300	19.12	38.62	23.29	15.33

CHEMISTRY OF SEPARATION PROCESSES

SELF-DIFFUSION OF CATIONS IN LINEAR POLYSTYRENESULFONATE SOLUTIONS

G. E. Myers B. A. Soldano

Introduction

An intensive investigation into the problem of the self-diffusion of small ions in sulfonated polystyrene ion-exchange resins has previously been made by Boyd and Soldano.[1] They observed a strong dependence of the "apparent" self-diffusion coefficient upon ionic size, ionic charge, and resin cross-linking and further inferred that the diffusion process in the resin should be considered as similar to that occurring in normal aqueous or alcoholic media.

The present study, which continues earlier work[2] on the self-diffusion of cations in the presence of a linear polystyrenesulfonate ion, is a logical outgrowth of the previous studies upon the resins and represents an extension into analogous systems of zero cross-linking. If the resin diffusion process is essentially that in an aqueous medium, similar effects of ion size and charge should be observed in the linear polyelectrolyte systems. Further, the effects of cross-linking should be primarily those of concentration; so self-diffusion data for ion exchangers should extrapolate into analogous data for polyelectrolyte solutions. It was also felt that self-diffusion measurements would be of considerable interest in themselves with reference to the problem of the effects of strong ionic interaction with linear polyelectrolytes.

Experimental

Measurements were performed with the use of radioactive tracers and a porous diaphragm-type cell thermostatted at 25°C.

Self-diffusion was allowed to occur until approximately one-third of the activity had passed into the side of the cell initially inactive. Depending upon the intensity of the activity, 50- to 500-μl aliquots were pipetted for counting. The gamma activities were placed in small tubes and counted in the 4π geometry scintillation counter, while beta activities were evaporated to dryness on small watch glasses and counted by means of a Geiger counter.

Self-diffusion coefficients D were calculated by the usual formula

$$D = \frac{1}{Kt} \log \frac{C_u + \frac{V_L}{V_u} C_L}{C_u - C_L} , \tag{1}$$

where t is the diffusion time, C_u and C_L are the final concentrations, i.e., counts/cc·min, of the upper initially active compartment and the lower initially inactive compartment, V_L and V_u are the corresponding compartment volumes, and K is the cell constant,

$$K = \frac{A}{l} \frac{V_u + V_L}{2.3\, V_u V_L} .$$

The polymer employed was a sulfonated linear polystyrene (uncross-linked) obtained from the Dow Chemical Company. This material, received as the sodium salt, was dissolved in distilled water and passed slowly through a column containing cation-exchange resin in the hydrogen form to remove all cations save hydrogen. The resulting solution was then passed through another column containing freshly prepared anion resin in the hydroxyl form. Neutron activation analysis of this final solution showed that fewer than 0.1% of the sulfonate groups contained sodium. This was taken as sufficient evidence of purity of the hydrogen polymer. The equivalent weight of the polymer in the hydrogen form was determined as 192.3 g/eq by means of dry-weight measurements and potentiometric acid-base titrations.

The various salt forms of the polyanion were prepared by addition of measured amounts of standardized base solutions to the acid form. These were added in a calculated deficiency of 1% of the total acid groups to avoid the presence of any excess of the base; it was felt that the 1% of sulfonate groups remaining as hydrogen form would have no appreciable effect upon the self-diffusion of the various cations. Above approximately 10^{-3} N the radioactively tagged solutions were prepared by simply adding the appropriate tracer, as the dried chloride, to the necessary volume of poly-

[1] G. E. Boyd and B. A. Soldano, *J. Am. Chem. Soc.* 75, 6105 (1953).

[2] B. A. Soldano, G. E. Boyd, and J. W. Cobble, *Chem. Quar. Prog. Rep. Sept. 30, 1952*, ORNL-1432, p. 38.

anion salt solution. The final concentration resulting from tracer and its "carrier" never was greater than about 10^{-5} *N*. However, at the lowest polymer concentrations, to reduce the possibility of the radiotracer concentration being of comparable magnitude to that of the polyanion salt, the "tagged" solutions were prepared by including the tracer as the hydroxide in the standardized base solution with which the acid polyanion was to be titrated. The tracers were "converted" from the chloride to the hydroxide by passage through freshly prepared hydroxide anion exchanger until no test for chloride was obtained. The corresponding inactive polyelectrolyte solutions were made up to as nearly as possible the same concentration as the active solutions, and then these two solutions were equilibrated isopiestically under vacuum for several days.

Results and Discussion

Self-diffusion coefficients calculated by Eq. 1 are shown in Fig. 33 for Na^+ and Cs^+ as a function of concentration. Coefficients for Ca^{++} at one concentration are given in Table 27. The experimental error indicated in the figure for the polystyrenesulfonate data amounts to approximately ±2% and was calculated from an over-generous estimate of a 1% maximum counting error. The points marked as crosses on the curve for sodium chloride were taken from the data of Adamson and co-workers for the self-diffusion of sodium in NaCl;[3] the circle points are from similar data of Wang and Miller.[4] No self-diffusion data appear to be available as yet for the other ions reported herein, save for the calcium ion in chloride solutions.[5] The dotted lines in Fig. 33 and the fourth column in Table 27 represent self-diffusion coefficients calculated from Onsager's limiting law.[6] It is recognized, of course, that the limiting law is dependent upon the Debye-Hückel treatment of ionic atmospheres and thus cannot be obeyed by the polyelectrolyte systems described in this report. The calculations are included only to demonstrate the extent of the deviation from the more normal aqueous systems. Onsager's equation, for the self-diffusion of microcomponents, reduces to

$$(2)\quad D_j^* = \frac{0.023\lambda_j^0}{|Z_j|} - 0.01266\lambda_j^0\,|F_j|\left[1 - \sqrt{d(w_j)}\right]\sqrt{\Gamma}\,,$$

where λ_j^0 and Z_j are the equivalent conductance at infinite dilution and the valence of the diffusing ion, respectively, and Γ is the ionic strength. The term $d(w_j)$ is defined by

$$(3)\quad d(w_j) = \frac{|Z_j|}{|Z_j| + |Z_p|}\left(\frac{1}{2} + \frac{\lambda_p^0\,|Z_p|}{\lambda_j^0\,|Z_p| + \lambda_p^0\,|Z_j|}\right),$$

where λ_p^0 and Z_p are, respectively, the equivalent conductance at infinite dilution and the valence of the *polyion*. Sufficient evidence is available to indicate that λ_p^0 is considerably smaller than λ_j^0; then also $\lambda_p^0|Z_j|$ must be very much smaller than $\lambda_j^0|Z_p|$.[7] With these assumptions, Eq. 2 reduces to

[3] J. M. Nielsen, A. W. Adamson, and J. W. Cobble, *J. Am. Chem. Soc.* 74, 446 (1952).

[4] J. H. Wang and S. Miller, *J. Am. Chem. Soc.* 74, 1611 (1952).

[5] J. H. Wang, *J. Am. Chem. Soc.* 75, 1769 (1953).

[6] L. J. Gosting and H. S. Harned, *J. Am. Chem. Soc.* 73, 159 (1951).

[7] J. R. Huizenga, P. F. Grieger, and F. T. Wall, *J. Am. Chem. Soc.* 72, 2636 (1950).

TABLE 27. SELF-DIFFUSION COEFFICIENTS OF Ca^{++} AND La^{+++} IN POLYSULFONATE SALT

ION	CONCENTRATION (eq/liter)	*D* (cm^2/day)		
		OBSERVED IN POLYSTYRENE-SULFONATE	CALCULATED: "LIMITING LAW"	OBSERVED* IN $CaCl_2$
Ca^{++}	0.0095	0.207	0.477	0.662
La^{+++}	2.82×10^{-4}	1.07	0.456	

*J. H. Wang, *J. Am. Chem. Soc.* 75, 1769 (1953).

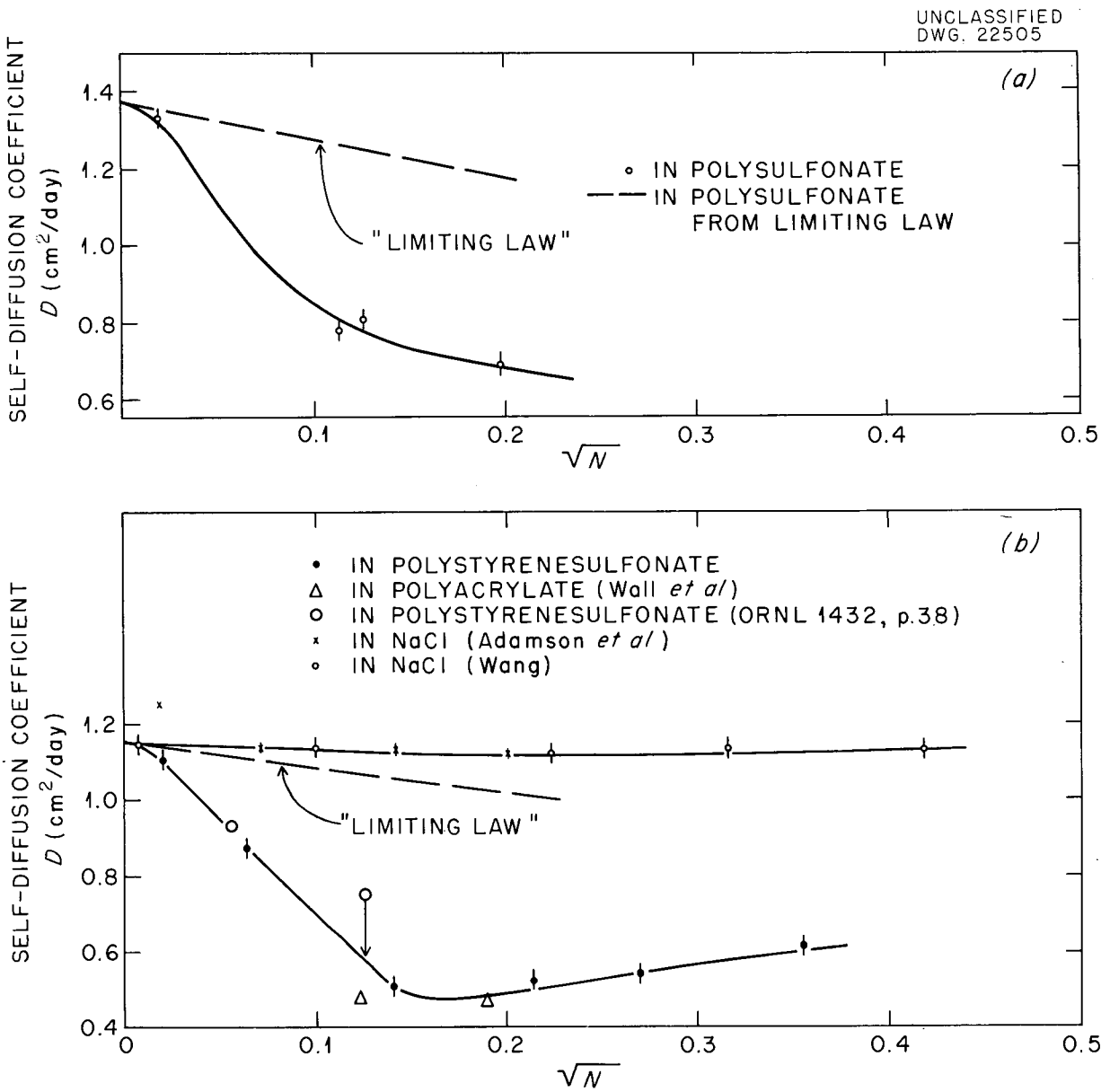

Fig. 33. Self-Diffusion of (*a*) Cs^+ Ion and (*b*) Na^+ Ion.

the following equations for Na^+, Cs^+, Ca^{++}, and La^{+++} ions:

$$(4)\quad D^*_{Na} = 1.154 - 0.635\left[1 - \sqrt{\frac{1}{2(1+Z_p)}}\right]\sqrt{N},$$

$$(5)\quad D^*_{Cs} = 1.370 - 0.979\left[1 - \sqrt{\frac{1}{2(1+Z_p)}}\right]\sqrt{N},$$

$$(6)\quad D^*_{Ca} = 0.685 - 2.13\left[1 - \sqrt{\frac{1}{(2+Z_p)}}\right]\sqrt{N},$$

$$(7)\quad D^*_{La} = 0.533 - 4.58\left[1 - \sqrt{\frac{3}{2}\,\frac{1}{(1+Z_p)}}\right]\sqrt{N}.$$

The quantity Z_p is unknown and undoubtedly varies with concentration; since it must be considerably larger than 1 at these concentrations, the

further simplification was made that the expression under the square root could be neglected with respect to unity. All assumptions made in obtaining the calculated values will tend to make those values smaller.

Considerable lowering of the cation diffusion rate compared with that for NaCl, CsCl, and $CaCl_2$ solutions may be seen to have occurred in the presence of the polysulfonate ion. The decrease actually may be even more pronounced than is apparent from the observed values, for there is much evidence that diffusion coefficients measured with porous diaphragm cells at very low concentrations may be high owing to surface conductance effects. For example, the value of Nielsen *et al.*[3] for Na^+ in their most dilute NaCl solution may be seen (Fig. 33) to be too high by approximately 10%. It is possible, therefore, that the first two or three values for Na^+ ion in the polystyrenesulfonate solution may be too high by several per cent, the deviation increasing with dilution. As a consequence of this uncertainty, the exact manner in which the Na^+ and Cs^+ curves approach zero concentration, or even how closely they may approach the theoretical limiting values of the cations at practicable concentrations, remains in doubt. It does seem reasonable, nevertheless, to conclude that the curves eventually would approach the limiting values.

Similar reductions in cation diffusion rates have been observed for other polyanion systems by Brady and Salley[8] and by Huizenga and co-workers.[7] These authors have interpreted the phenomenon as resulting from "cation binding" (i.e., ionic association) and have exploited such measurements to calculate the extents of such "binding," obtaining reasonable agreement with values from other procedures. The observed diffusion rate is considered to be an average of the rates of the "free" cations and those bound more tightly to the polyanion. The fraction, f, of cation "unbound" is defined by D_{obs}/D^0, where D_{obs} is the observed coefficient and D^0 is the "true" coefficient of the free Na^+ ion. Required values of D^0 were obtained from diffusion or conductance data for ordinary strong electrolytes at the estimated concentration of "free" cations in the polyelectrolyte solution. Such an assumption obviously cannot be entirely correct, since even the relatively "free" cations must be moving in a different field in the presence of polystyrenesulfonate ions than exists in ordinary 1:1 electrolyte solutions. The concept of "bound ions" is rather an elastic one, in any event, and f values should not be accepted too literally.

Further indication that the assumption of D^0 values from electrolyte self-diffusion measurements may be erroneous is given by the increase in the diffusion coefficients for Na^+ ion observed at higher concentrations (Fig. 33). (The variation in the cesium points is not significant.) If this behavior is a true reflection of the Na^+ ion diffusion, it suggests the existence of quite specific effects in this polyelectrolyte system.

Maxima in the self-diffusion-concentration curves for Na^+ in NaCl, for K^+ in KCl, and for Ca^{++} in $CaCl_2$ have been observed by Wang[4,5,9] and in the curve for K^+ in KI by Mills and Kennedy.[10] It is to be expected that the curve for the self-diffusion of sodium ion in sodium polystyrenesulfonate will also exhibit a maximum; if so, this would be the first instance of a maximum in data obtained with a diaphragm cell.

The original problem regarding the possible correlation of cation diffusion in polystyrenesulfonate solutions with that in the cross-linked resins is not definitively answered by the present data. In Fig. 34, diffusion data for the Na^+ and Cs^+ polystyrenesulfonates are compared with self-diffusion data for the same cations in cross-linked ion exchangers. The general trend appears to be for the diffusion rates in polymer and in resin to approach one another, indicating that the diffusion process is essentially the same in the two systems. However, more data in the intermediate region would be necessary before a valid extrapolation of either the Na^+ or Cs^+ ion self-diffusion rates could be made from the polymer to the resin system.

FUNDAMENTAL STUDIES ON ION-EXCHANGE SELECTIVITY

B. A. Soldano G. E. Myers

During this period, considerable effort was devoted to the interpretation of experimental results on ion-exchange selectivity previously reported[11]

[8] A. P. Brady and D. J. Salley, *J. Am. Chem. Soc.* 70, 914 (1948).

[9] J. H. Wang, *J. Am. Chem. Soc.* 74, 1182 (1952).

[10] R. Mills and J. W. Kennedy, *J. Am. Chem. Soc.* 75, 5696 (1953).

[11] B. A. Soldano, G. E. Myers, and Q. V. Larson, *Chem. Semiann. Prog. Rep. June 20, 1953*, ORNL-1587, p. 53.

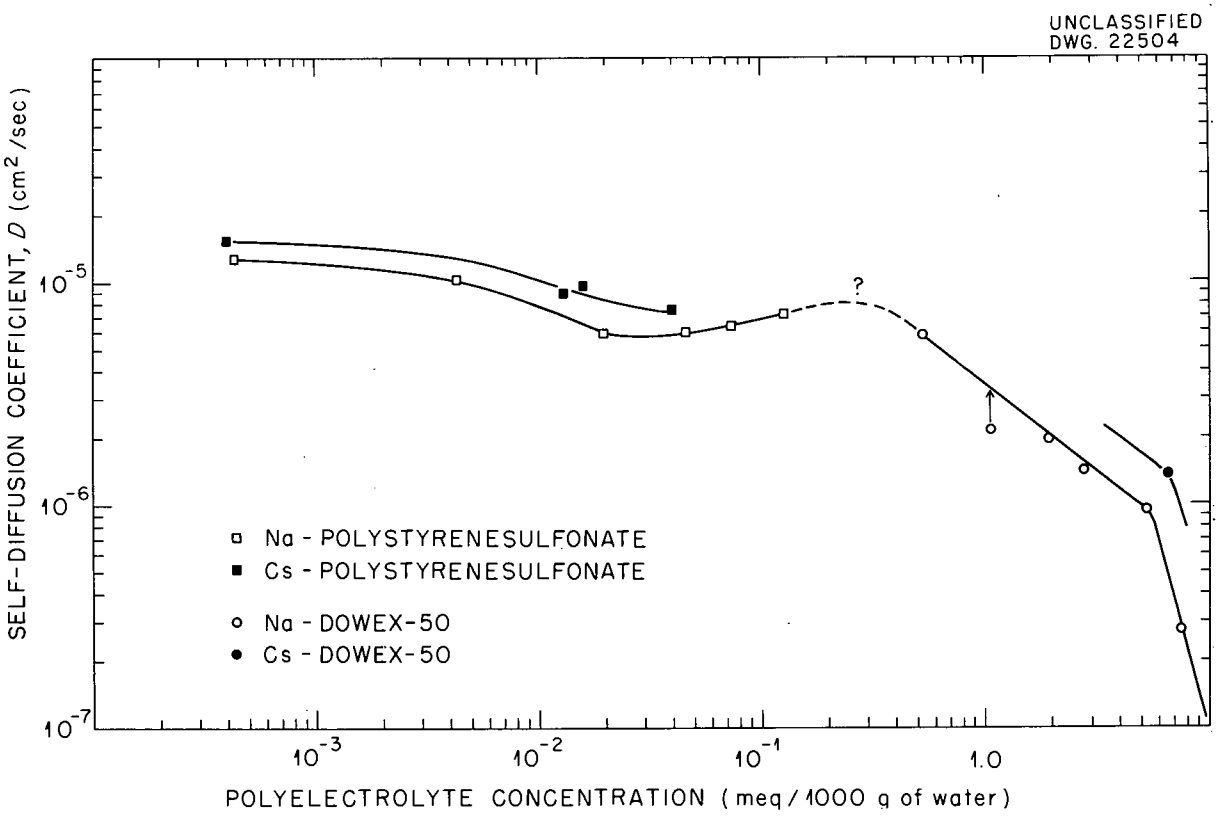

Fig. 34. Comparison of Self-Diffusion Coefficients for Na^+ and Cs^+ Ions in Linear and Cross-linked Exchanger.

and to the measurements of anionic selectivity with Dowex-2, a strong-base anion exchanger. A summary is given here, since a detailed presentation of the data and their treatment will appear in two papers now being prepared for publication.

An exact thermodynamic treatment of ion-exchange equilibria may be based on several alternative approaches. The equation of Donnan[12] may be applied if, for example, it is assumed that the system comprised of an ion exchanger in equilibrium at constant temperature with a 1:1 electrolyte solution may be taken as analogous to a membrane equilibrium:

$$\text{(1a)}\quad \log D = \frac{P(\bar{V}_1^0 - \bar{V}_2^0)}{RT} + \log(\gamma_1/\gamma_2)_r - \log(\gamma_1/\gamma_2)_w .$$

[12]F. G. Donnan, *Z. physik. Chem.* *168A*, 369 (1934).

Here the experimentally observed selectivity coefficient, D, for the exchange of like-charged, univalent ions, 1 and 2, is defined by:

$$D \equiv \frac{(m_2/m_1)_r}{(m_2/m_1)_w} ,$$

where m_1 and m_2 are the stoichiometric concentrations (i.e., molalities) of the ions in the exchanger, r, and in the mixed aqueous electrolyte solution, w, respectively. Further, P is the swelling pressure and $\bar{V}_1^0$ and $\bar{V}_2^0$ are the partial molal volumes of the ions in the ion-exchanger at infinite dilution. The γ's are the respective ionic activity coefficients for the ions in the exchanger and electrolyte, the former, however, referring to an exchanger in which $P = 1$ atm (i.e., weakly cross-linked) but in which the molality is the same as in the exchanger being studied. The activity coefficient ratios appearing in Eq. 1a are defined and may be replaced by the corresponding mean molal activity coefficient

ratios. The last term of the right member of Eq. 1a may be neglected for exchange equilibria with dilute (i.e., <0.1 m) electrolyte solutions so that

$$\text{(1b)} \quad \log D = P\Delta\bar{V}^0/RT + \log (\gamma_1/\gamma_2)_r \ .$$

When stoichiometric concentrations and volumes are used, it may be demonstrated[13] that the swelling pressure-volume term of Eq. 1b is small, sometimes negligible, compared with the contribution of the activity coefficient ratio term to log D. In any case, it may be evaluated by using moisture absorption measurements[14] and need not be considered further here.

The problem of the ionic selectivity shown by resinous exchangers in equilibrium with binary 1:1 electrolyte mixtures therefore reduces to that of evaluating the ratio of the activity coefficients of the ions in the exchanger. It is necessary to use certain nonthermodynamic assumptions to proceed further; one hypothesis which has seemed promising is the suggestion[15] that the exchanger may be considered as a type of electrolyte mixture to which Harned's relation[16] for activity coefficients in ordinary electrolyte mixtures applies. Thus (dropping the symbol r, since the subsequent discussion is for the exchanger),

$$\text{(2a)} \quad \log \gamma_1 = \log \gamma_{1(0)} - a_{12}m_2$$

and

$$\text{(2b)} \quad \log \gamma_2 = \log \gamma_{2(0)} - a_{21}m_1 \ ,$$

where $\gamma_{1(0)}$ and $\gamma_{2(0)}$ are the activity coefficients for ions 1 and 2, respectively, when present alone in the exchanger (i.e., pure salt-forms). The quantities a_{12} and a_{21} are coefficients which may vary with the total molality $m = m_1 + m_2$ but which are independent of the ratio m_1/m_2 when m is constant. Harned's relations, as applied here, will be regarded simply as empirical equations which may represent certain observations on ion-exchangers within limits of experimental error. A check on these assumptions will be afforded by reason of the "cross-differentiation" relation:

$$\text{(3)} \quad (\partial \ln \gamma_1/\partial m_2)_{m_1} = (\partial \ln \gamma_2/\partial m_1)_{m_2}$$

which requires that $(a_{12} + a_{21})$ be a constant independent of the molality.

Substitution of Eqs. 2 in Eq. 1b gives at constant m:

$$\text{(4)} \log D = \frac{P\Delta\bar{V}^0}{2.303RT} + \log \frac{\gamma_{1(0)}}{\gamma_{2(0)}} - a_{12}m_2 + a_{21}m_1 \ .$$

The term log $(\gamma_{1(0)}/\gamma_{2(0)})$ may be evaluated by using osmotic coefficients $\phi_{1(0)}$ and $\phi_{2(0)}$ derived from isopiestic measurements on pure salt-forms of weakly cross-linked (i.e., exchangers for which $P = 0$ effectively) exchangers. Glueckauf[14] has proposed a linear dependence of the osmotic coefficients on concentration:

$$\text{(5a)} \quad (\phi - 1) = -f(m) + Am \ ,$$

from which, by application of the Gibbs-Duhem equation, the activity coefficient ratio term of Eq. 4 is given by

$$\text{(5b)} \quad \log \frac{\gamma_{1(0)}}{\gamma_{2(0)}} = 2\left[\phi_{1(0)} - \phi_{2(0)}\right] \ .$$

It has been found, however, that the osmotic coefficients determined in this Laboratory[17] (Fig. 35) are more accurately described by

$$\text{(6a)} \quad \phi = f(m) + \left(\frac{am}{1 + bm}\right) \ ,$$

where a and b are characteristic constants for each ion and where $f(m)$ is some unknown function of m, identical for all univalent cationic or anionic salts which describes the variation of ϕ for concentrations below 1 M. Equation 6a was found to hold within experimental error in the range 1 to 10 M for the alkali metal salt forms of weakly cross-linked (i.e., nominal 0.5% DVB) Dowex-50, and for the halide salts of Dowex-1 and Dowex-2 to concentrations sometimes exceeding 30 M. Application of the Gibbs-Duhem relation to Eq. 6a gives

$$\text{(6b)} \log \gamma = g(m) + \frac{a}{b} \log (1 + bm) + \frac{(a/2.3)m}{1 + bm} \ ,$$

[13] G. E. Boyd and B. A. Soldano, *Z. Elektrochem.* 57, 162 (1953).

[14] E. Glueckauf, *Proc. Roy. Soc. (London)* 214A, 207 (1952).

[15] S. W. Mayer, *J. Am. Chem. Soc.* 72, 2292 (1950).

[16] H. S. Harned and B. B. Owen, *The Physical Chemistry of Electrolytic Solutions*, p. 461, 2d. ed., Reinhold, New York, 1950.

[17] G. E. Boyd and B. A. Soldano, *Z. Elektrochem.* 57, 166 (Fig. 5) (1953).

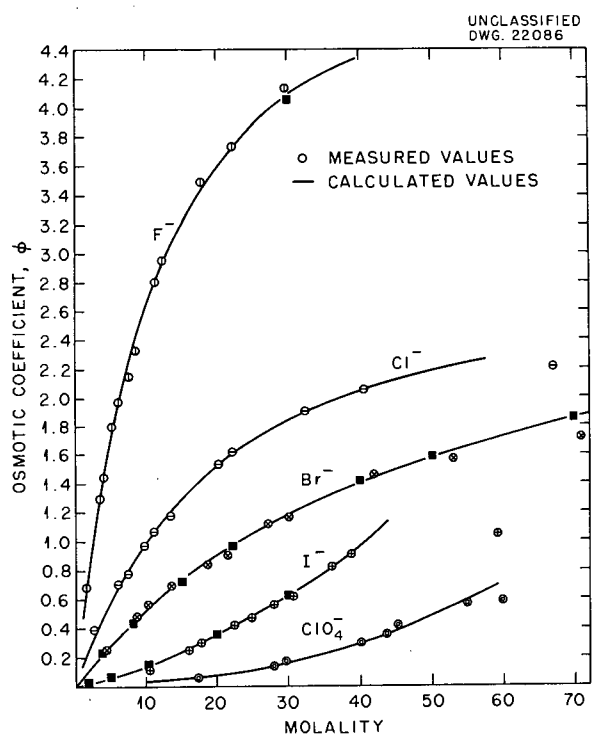

Fig. 35. Comparison of Calculated With Measured Osmotic Coefficients for Dowex-2.

from which log $[\gamma_{1(0)}/\gamma_{2(0)}]$ may be found, assuming $g_1(m) = g_2(m)$.

The coefficients α_{12} and α_{21} may be estimated from selectivity determinations made for trace amounts of ions 1 and 2 (i.e., $m_1 = 0$, or $m_2 = 0$, respectively) by using radioactive isotopes. Their variations with the molality of the exchanger are shown in Fig. 36 for the cesium-sodium exchange in Dowex-50 and in Fig. 37 for the bromide-fluoride exchange in Dowex-2. Interestingly, expressions of the type

(7a) $$\alpha_{12} = K_{12}/R_1$$

and

(7b) $$\alpha_{21} = K_{21}/R_2 ,$$

where

$$R_1 = \frac{a_1}{2.3b_1}\left[\log(1 + b_1 m) + \frac{b_1 m}{1 + b_1 m}\right],$$

and

$$R_2 = \frac{a_2}{2.3b_2}\left[\log(1 + b_2 m) + \frac{b_2 m}{1 + b_2 m}\right],$$

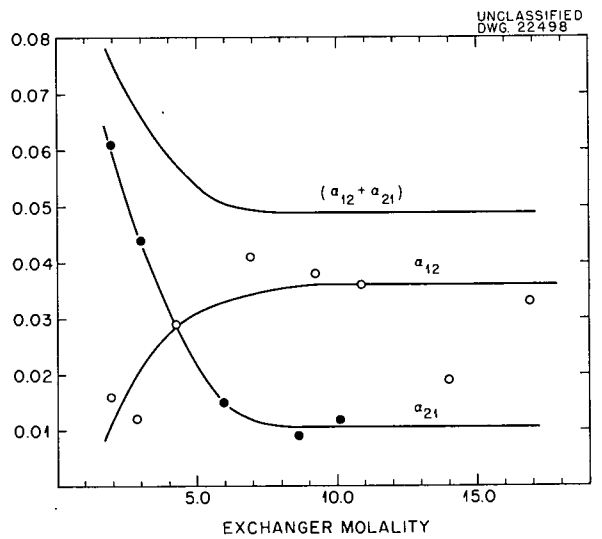

Fig. 36. Harned's Coefficients, α_{12} and α_{21}, for the Cesium-Sodium Ion Exchange in Variously Cross-linked Dowex-50.

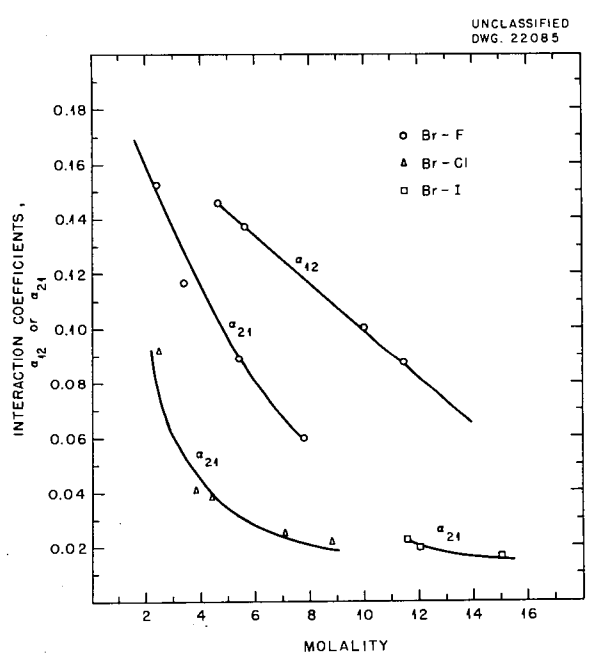

Fig. 37. Dependence of Interaction Coefficients on Molality.

in general, described the concentration dependences of α_{12} and α_{21} for the anion exchangers. These coefficients were independent of the molality, however, for most of the cation exchanges examined.

By making use of Eqs. 7 and 4, it becomes possible to estimate ion-exchange selectivities

for a given pair of ions for a wide range of cross-linkings and ionic compositions (i.e., "loadings") from two measurements of the selectivity for trace quantities of each ion at a given cross-linking. A comparison of selectivities so estimated with experimentally measured values is afforded by Figs. 38, 39, and 40 for the bromide-fluoride, bromide-chloride, and sodium-lithium ion-exchange reactions, respectively. The agreement has appeared to be quite satisfactory for these, as well as for a number of other pairs of ions, thus demonstrating empirically, at least, the value of the foregoing treatment.

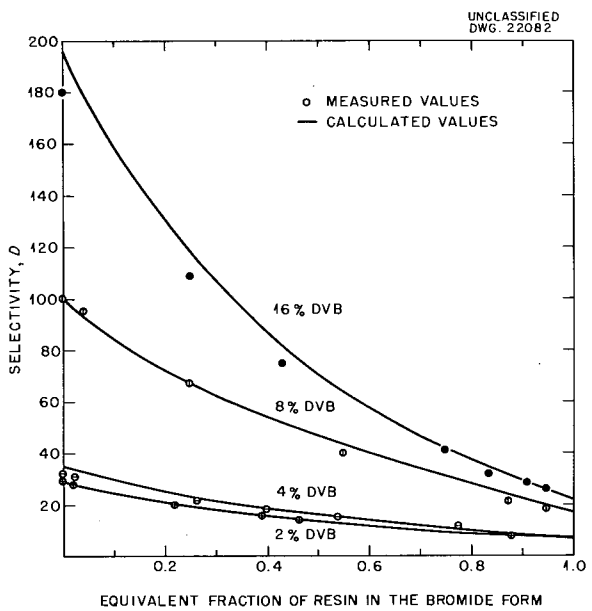

Fig. 38. The Br-F System – Comparison of Calculated and Measured Selectivities as a Function of Cross-Linking and Resin Composition.

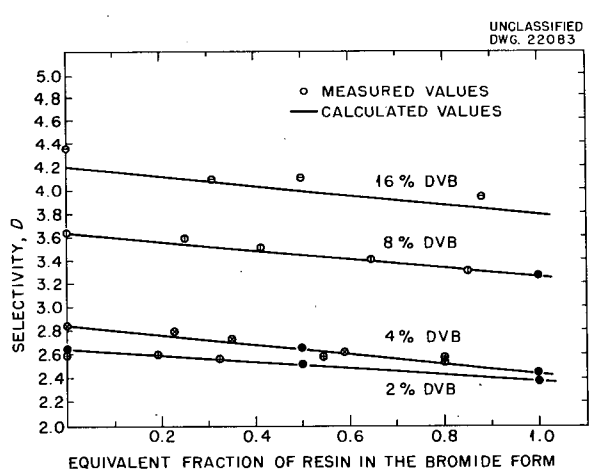

Fig. 39. Selectivity Coefficients for Bromide-Chloride Exchange.

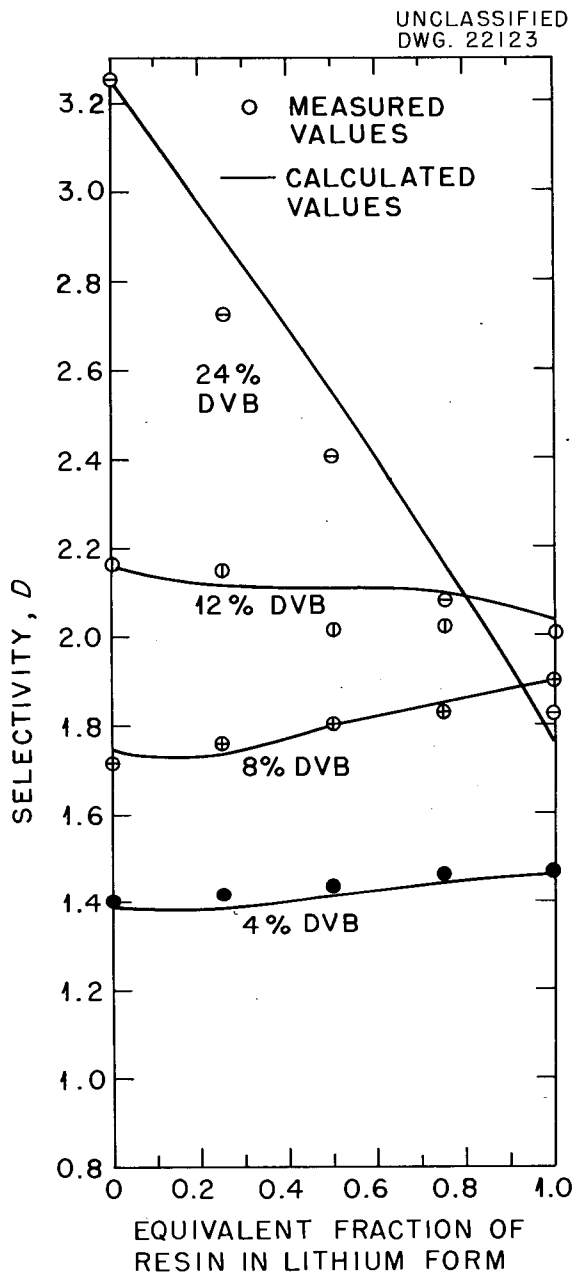

Fig. 40. Calculated and Observed Selectivities of Na-Li System.

RADIATION CHEMISTRY

GAS-PHASE IRRADIATION

S. C. Lind P. S. Rudolph

The radon collecting station previously reported[1] has now been in operation for seven months, and 14 charges of radon have been extracted. The average minimum efficiency of the system for the last ten extractions is 83.8% and the maximum pressure increase over the $RaCl_2$ solution has been 2.1 cm for a growth period of 31 days.

Two separate experiments on alpha-particle-induced recombination of H_2 and O_2 in the presence of CO_2 have been completed. These experiments show that CO_2 does not enter into the chemical reaction nor does the ionization of the CO_2 contribute to the reaction rate. No solid polymer is formed, as in the $H_2 + CO_2$ reaction,[2] and there is no depletion of the CO_2.

In the first experiment a reaction vessel of 7.533 cc was filled with 591.8 mm of $2H_2 + O_2$ and 290.8 mm of CO_2 together with 141.7 mc of radon. The rate constant $(k\mu/\lambda)'$ was 22.6 ± 1.4 based on the pressure change of the $H_2 + O_2$ only. No other kinetic treatment resulted in a constant value. For example, $(k\mu/\lambda)'$ based[3] on

$$P_{(H_2+O_2)} + P_{EqCO_2}$$

varied from 18.4 to 6.3 progressively. In the second experiment the rate constant was 19.6 ± 1.0. These values are in good agreement when correction is made for the difference in diameters of the reaction vessels.

The $H_2 + CO_2$ reaction previously studied[2] was duplicated. The current experiment is in complete accord with the previous findings. That is, a considerable white, crystalline appearing solid was deposited on the walls of the vessel, and the rate constants agree well within the average error when corrected for difference in diameters of the reaction vessel. A value of 2.1 was calculated for $(k\mu/\lambda)'$ in the current experiment.

The gas phase alpha irradiation of $H_2O + CO_2$ is the next reaction whose study is planned.

EFFECT OF TEMPERATURE ON DECOMPOSITION OF AQUEOUS SOLUTIONS BY GAMMA RADIATION

C. J. Hochanadel J. A. Ghormley

Initial yields for several gamma-ray-induced reactions in 0.8 *N* sulfuric acid solution have been measured at 2, 23, and 65°C. The oxidation of ferrous sulfate both in the presence and absence of oxygen showed a small positive coefficient, while the reduction of ceric sulfate, the formation of hydrogen peroxide in air-saturated acid solution, and the formation of peroxide in potassium bromide solutions both in the presence and absence of oxygen showed negative temperature coefficients. The yields listed in Table 28 show that in all cases the effect of temperature was small, amounting to less than 15% over the entire range. The results were interpreted in terms of an effect of temperature on the yields of H, OH, H_2O_2, and H_2 produced in the primary reactions in the radiation-induced decomposition of water.

This decomposition reaction can be written

$$G^P_{H_2O}H_2O \rightsquigarrow G^P_{H_2}H_2 + G^P_{H_2O_2}H_2O_2 + G^P_{H}H + G^P_{OH}OH ,$$

where G^P indicates primary yield (molecules per 100 ev). Dainton and Sutton showed that $G^P_{H_2}$ and $G^P_{H_2O_2}$ are not equal; stoichiometry requires only that

$$G^P_{-H_2O} = 2G^P_{H_2O_2} + G^P_{OH} = 2G^P_{H_2} + G^P_{H} .$$

Values for these primary yields G^P, at 2, 23, and 65°C, as deduced from measured yields in several of the reactions mentioned above, are listed in Table 29 and illustrated in Fig. 41. Details of proposed mechanisms and the calculation of primary yields are presented in a paper to be submitted for publication. Values for $G^P_{H_2}$ and $G^P_{H_2O_2}$ were based on measured peroxide yields in KBr solutions in the presence and absence of oxygen.

[1] P. S. Rudolph and S. C. Lind, *Chem. Semiann. Prog. Rep. June 20, 1953*, ORNL-1587, p. 68.

[2] S. C. Lind and D. C. Bardwell, *J. Am. Chem. Soc.* 47, 2691 (1925).

[3] S. C. Lind, *The Chemical Effects of Alpha Particles and Electrons*, p. 186, 2d. ed., Chemical Catalogue Co., New York, 1928.

TABLE 28. YIELDS FOR GAMMA-RAY-INDUCED REACTIONS IN 0.8 *N* H_2SO_4 SOLUTION AT SEVERAL TEMPERATURES

SOLUTION IRRADIATED	PRODUCT MEASURED	YIELD, *G*		
		2°C	23°C	65°C
Ferrous ammonium sulfate + oxygen	Fe^{3+}	15.2	15.6	16.3
Ferrous ammonium sulfate, oxygen free	Fe^{3+}	7.80	8.02	8.19
Ceric sulfate	$-Ce^{4+}$	2.53	2.44	2.26
0.8 *N* H_2SO_4 + oxygen	H_2O_2	1.22	1.18	1.09
10^{-3} *M* KBr + oxygen	H_2O_2	1.04	1.01	0.94
10^{-3} *M* KBr, oxygen free	H_2O_2	0.40	0.39	0.37

TABLE 29. CALCULATED YIELDS OF PRIMARY PRODUCTS IN THE DECOMPOSITION OF 0.8 *N* H_2SO_4 SOLUTIONS AT SEVERAL TEMPERATURES

PRODUCT	YIELD, G^P		
	2°C	23°C	65°C
$-H_2O$	4.40	4.48	4.64
H_2	0.40	0.39	0.37
H	3.60	3.70	3.90
H_2O_2	0.72	0.70	0.66
OH	2.96	3.08	3.33

Values for G^P_H and G^P_{OH} were based upon the yield for ferrous oxidation in the presence of oxygen. Independent checks of $G^P_{H_2}$ at 23°C were obtained from H_2 gas yields in various solutions, as discussed in the section "Gas Yields in the Decomposition of Some Aqueous Solutions by Gamma Radiation." Independent checks of $G^P_{H_2O_2}$, G^P_H, and G^P_{OH} were obtained from H_2O_2 yields in ferrous sulfate solutions both in the presence and absence of oxygen. These yields were obtained from the kinetics of the post-irridiation reaction of H_2O_2 with Fe^{++}.

GAS YIELDS IN THE DECOMPOSITION OF SOME AQUEOUS SOLUTIONS BY GAMMA RADIATION

J. A. Ghormley C. J. Hochanadel

Sealed, pyrex or quartz ampoules that incorporated a capillary tube for determining total gas pressure in the ampoule by measurement of the boiling temperature of the solution, a platinum filament for igniting hydrogen and oxygen gas mixtures, and, in some cases, thin windows for spectrophotometric analysis of the solute have been used to study gas yields in the decomposition of aqueous solutions by gamma radiation. Changes in pressure and in solute concentration could be measured as a function of radiation dose by using a single sample, and, at any time during an experiment, the gases could be ignited, thereby giving a partial analysis. Yields were determined at 23°C for hydrogen formation and oxygen depletion in oxygen-saturated 0.8 *N* sulfuric acid with and without added KBr, hydrogen formation in degassed KBr solutions, hydrogen and oxygen formation in ceric sulfate solutions, hydrogen formation and oxygen depletion in ferrous sulfate solutions containing oxygen, and hydrogen formation in oxygen-free ferrous sulfate solutions. These values supplement those reported in the preceding section in establishing yields of H, OH, H_2, and H_2O_2 produced in the decomposition of the acid solution by gamma radiation.

10^{-3} *M* KBr in 0.8 *N* H_2SO_4 (Degassed)

Pressure buildup in a typical ampoule containing degassed 10^{-3} *M* KBr is shown in Fig. 42. Initially, H_2O_2 and H_2 are found in equivalent amounts, but as the H_2O_2 concentration builds up, some decomposition to oxygen occurs. The average hydrogen yield in six determinations was 0.39 ± 0.01, in exact agreement with the initial H_2O_2 yield, and is taken as a measure of $G^P_{H_2}$ in Eq. 1.

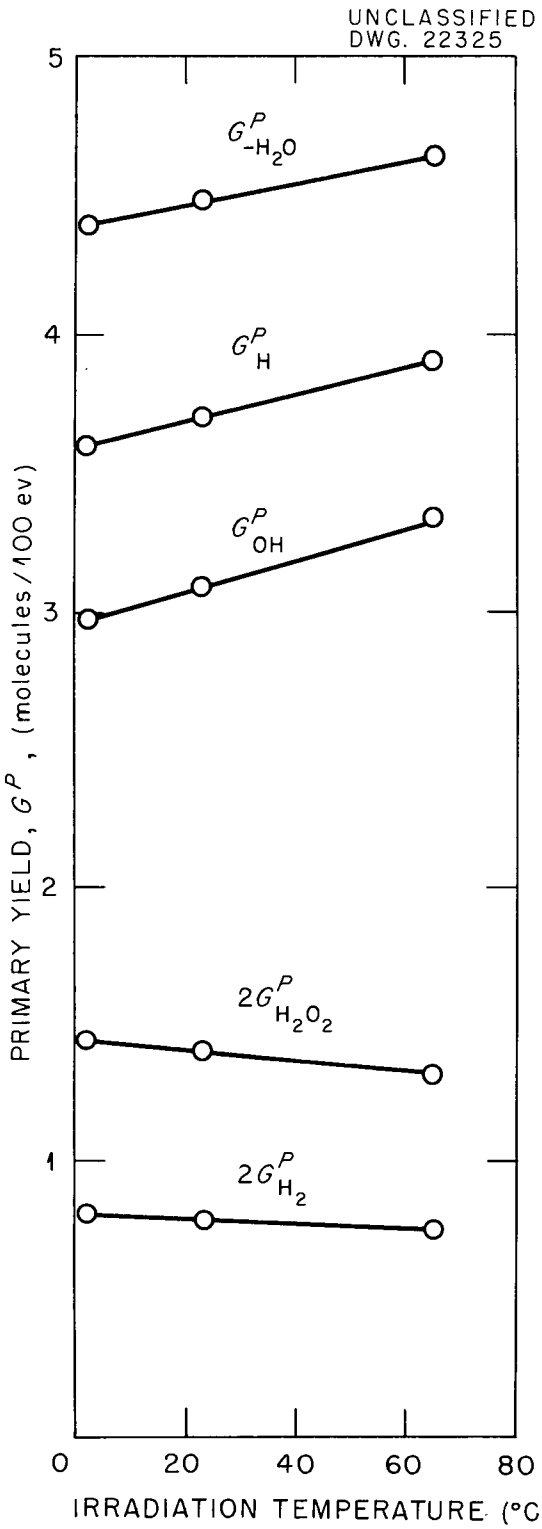

Fig. 41. Effect of Temperature on Primary Yields of H, OH, H_2, and H_2O_2 in Decomposition of 0.8 *N* H_2SO_4 Solutions by Gamma Rays.

10^{-3} M KBr in 0.8 *N* H_2SO_4 (+ Oxygen)

As discussed in the previous section, the initial yield of 1.01 H_2O_2 for 100 ev is believed to be the sum of that produced in the primary decomposition of water, $G^P_{H_2O_2} = 0.70$, and that produced from the oxygen, $G_{-O_2} = 0.31$. A typical experiment is shown in Fig. 43. Unfortunately, it was not possible to measure gas yields accurately at low doses, and as the peroxide concentration increased with increased dose, some decomposition to oxygen occurred and the yields for oxygen depletion were low, the maximum being 0.27. The other product, H_2, was produced with an average yield of 0.38, which is again a measure of $G^P_{H_2}$.

0.8 *N* H_2SO_4 + Oxygen, and Pure Water + Oxygen

On irradiating 0.8 *N* H_2SO_4 in an ampoule containing initially 30 cm pressure of oxygen, the pressure remained nearly constant over the dose range from 0 to 7×10^{22} ev/liter, and gas yields

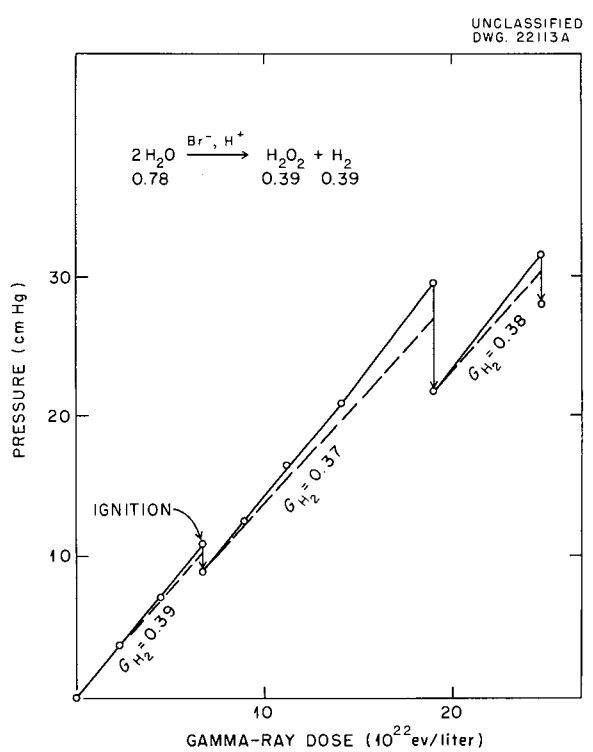

Fig. 42. Pressure Changes on Irradiating an Ampoule Containing 10^{-3} M KBr in 0.4 M H_2SO_4 (degassed). Dose rate: 7.46×10^{20} ev/liter·min.

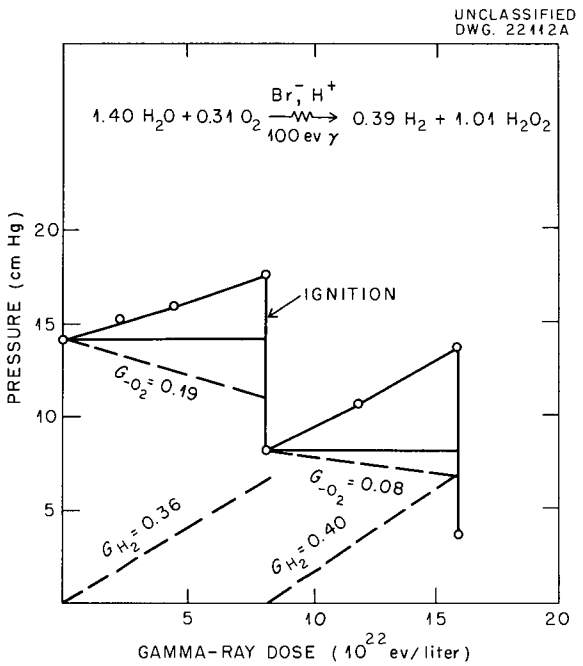

Fig. 43. Irradiation of 10^{-3} M KBr in 0.4 M H_2SO_4 ($+O_2$). Dose rate: 7.46×10^{20} ev/liter·min.

were $G_{H_2} = 0.31$ and $G_{-O_2} = 0.41$. On reirradiating with a dose of 4.5×10^{22} ev/liter, the yields were 0.20 and 0.09, indicating decomposition of H_2O_2 and perhaps some reaction of the hydrogen, although the role of H_2 in solutions at this high acidity is not clear.

At higher pH (>2) it is known that the reaction $H_2 + OH \rightarrow H_2O + H$ occurs readily in the absence of Br. On irradiating pure water in an ampoule containing initially 25 cm pressure of oxygen, the pressure remained nearly constant over the same dose range, and very little pressure change occurred on ignition. The hydrogen yield at a dose of 7×10^{22} ev/liter was only 0.03, indicating that most of the hydrogen had reacted with O_2 to form H_2O_2.

Ferrous Sulfate Solutions in 0.8 *N* H_2SO_4 with and without Added Oxygen

In the oxidation of ferrous sulfate in the presence of oxygen, according to the generally accepted mechanism, the yield of hydrogen is equivalent to $G^P_{H_2}$ and the yield for oxygen depletion is equivalent to G^P_H. Pressure changes in two typical ampoules are shown in Fig. 44. In six ampoules the average yield for oxygen depletion was 3.6, which is in good agreement with the value reported in the previous section for $G_H = 3.7$. The average hydrogen yield was 0.49 and is believed to be too high. In this system the hydrogen measurement is less accurate than in KBr or ceric sulfate solutions which were initially degassed and therefore allowed more accurate measurement of small pressure changes.

Ampoule 2 was irradiated until all the oxygen had been consumed and then the hydrogen yield was measured during ferrous oxidation in the absence of oxygen. The hydrogen yield of 4.0 was equivalent to the yield for ferrous oxidation of 8.02.

Ceric Sulfate in 0.8 *N* H_2SO_4 Solution

The linear pressure buildup in a typical ampoule containing 3×10^{-3} *M* ceric sulfate is shown in Fig. 45. The average yields in six ampoules were $G_{H_2} = 0.40$ and $G_{O_2} = 0.80$. The hydrogen yield is again equivalent to $G^P_{H_2}$, and the oxygen yield

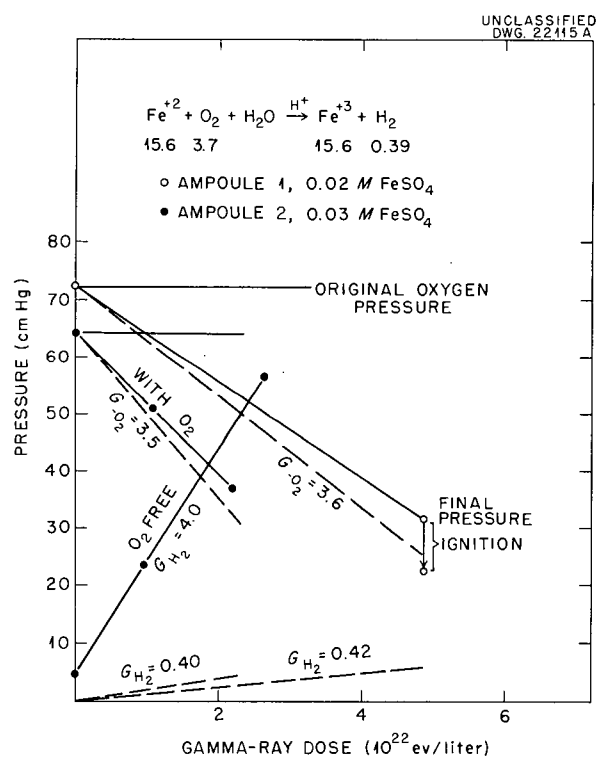

Fig. 44. Irradiation of $FeSO_4$ in 0.4 M H_2SO_4 ($+O_2$). Dose rate: $1.8 + 10^{20}$ ev/liter·min.

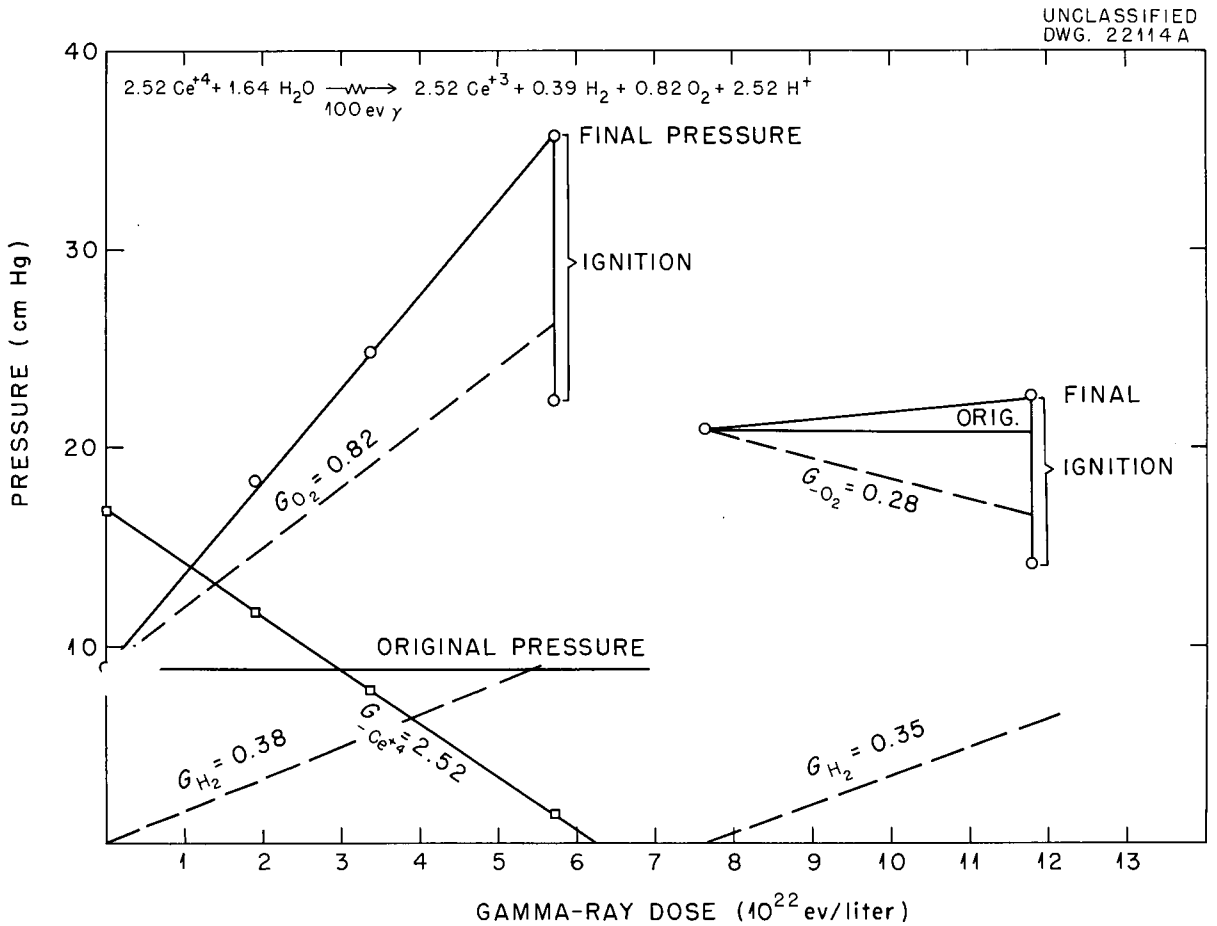

Fig. 45. Irradiation of 3×10^{-3} M $Ce(SO_4)_2$ in 0.4 M H_2SO_4. Dose rate: 6.36×10^{20} ev/liter·min.

is as predicted on the basis of stoichiometry.

MOLECULAR YIELD OF HYDROGEN PEROXIDE IN THE DECOMPOSITION OF WATER BY COBALT GAMMA RADIATION

T. J. Sworski

Water, when subjected to ionizing radiation, has been considered to behave as though two reactions were occurring simultaneously:[4]

$$(F) \qquad 2H_2O \longrightarrow H_2 + H_2O_2$$

$$(R) \qquad H_2O \longrightarrow H + OH$$

Dainton and Sutton[5] have recently presented experimental evidence showing that hydrogen peroxide is formed in excess of hydrogen in reaction F in 0.8 N sulfuric acid solutions. If this is so, Allen[6] has suggested that a third reaction should be added to reactions F and R:

$$(E) \qquad 2H_2O \longrightarrow 2H + H_2O_2$$

Allen[6] has suggested that the yield of hydrogen peroxide in water containing oxygen is equal to $F + 2E$. This mechanism shows that reaction R makes no contribution and that the molecular H_2 does not compete initially with H_2O_2 or HO_2 for the OH radical.

The effect of 10^{-3} M potassium bromide upon the formation of hydrogen peroxide in air-saturated

[4] A. O. Allen, C. J. Hochanadel, J. A. Ghormley, and T. W. Davis, *J. Phys. Chem.* **56**, 575 (1952).

[5] F. S. Dainton and H. C. Sutton, *Discussions Faraday Soc.* No. 12, 121 (1952).

[6] A. O. Allen, *The Yields of Free H and OH in the Irradiation of Water*, BNL-1498 (1953).

and oxygen-saturated water and sulfuric acid solutions is shown in Fig. 46. The presence of bromide ion does not remove the previously reported[7] effects of oxygen concentration and sulfuric acid but does result in a lower concentration of hydrogen peroxide at any particular dose in all solutions (compare Fig. 46 with Fig. 33, p. 75, ORNL-1587). The bromide-ion effect indicates that, in the absence of bromide ion, the molecular hydrogen formed in reaction F enhances the rate of hydrogen peroxide formation.

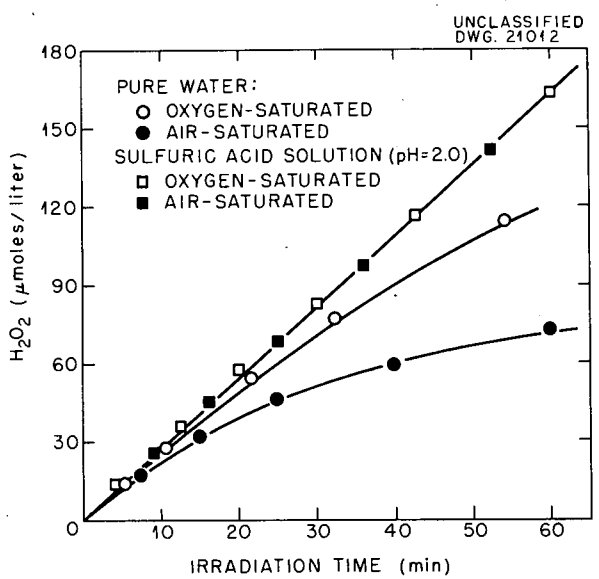

Fig. 46. Effect of 10^{-3} M KBr on H_2O_2 Formation by Cobalt Gamma Radiation. Dose rate: 1.86 $\times 10^{20}$ ev/liter·min.

Figure 47 shows that the rate of formation of hydrogen peroxide in oxygen-saturated water can be expressed by the following equation:

$$0.324 \frac{d(H_2O_2)}{dt} = G_{H_2O_2} = 1.35 - \frac{1.35}{506}(H_2O_2)$$

Integration of this differential equation leads to the simple exponential function employed by Ebert and Boag[8] which provided a reasonable fit to their experimental data. Figure 47 also shows that the rate of formation of hydrogen peroxide in oxygen-saturated water containing 10^{-3} M potassium bromide can be expressed by a similar equation:

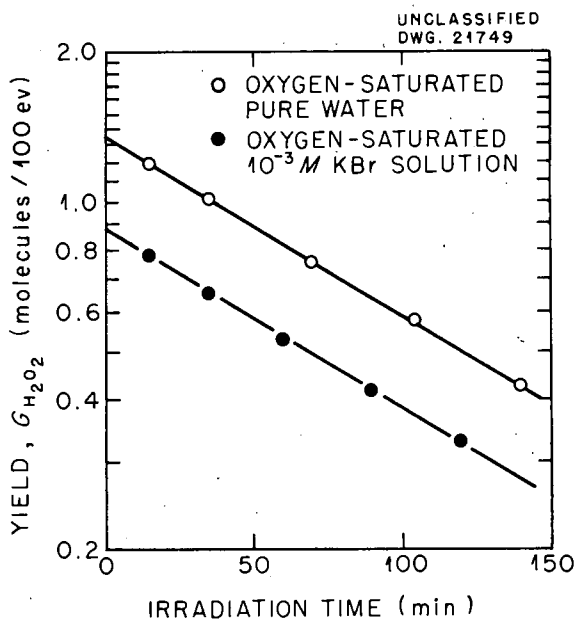

Fig. 47. Hydrogen Peroxide Formation by Cobalt Gamma Radiation. Dose rate: 1.86 $\times 10^{20}$ ev/liter·min.

$$0.324 \frac{d(H_2O_2)}{dt} = G_{H_2O_2} = 0.88 - \frac{1.35}{506}(H_2O_2)$$

It is concluded that in oxygen-saturated pure water a low steady-state concentration of hydrogen is reached and that the enhancement by hydrogen of the hydrogen peroxide yield becomes equivalent to the hydrogen yield[9] in reaction F of 0.46. This is in excellent agreement with the observed enhancement of 1.35 − 0.88 = 0.47. The yield of hydrogen peroxide in oxygenated solutions containing 10^{-3} M potassium bromide is interpreted as having a yield equal to $F + 2E$.

The yield of hydrogen peroxide in 0.8 N sulfuric acid[10] is lowered by 10^{-3} M potassium bromide from 1.26 to 0.96 molecules per 100 ev. In oxygen-free bromide solutions a yield of 0.38 molecules of hydrogen peroxide per 100 ev is observed.

The molecular yield of hydrogen peroxide ($F + E$) can be calculated if the conclusions that the yield in oxygen-free bromide solutions is equal to F and

[7] T. J. Sworski, *Chem. Semiann. Prog. Rep. June 20, 1953*, ORNL-1587, p. 74.

[8] M. Ebert and J. W. Boag, *Discussions Faraday Soc.* No. 12, 189 (1952).

[9] C. J. Hochanadel, *J. Phys. Chem.* 56, 587 (1952).

[10] T. J. Sworski, *J. Chem. Phys.* 21, 375 (1953).

that the yield in oxygenated bromide solutions is equal to $F + 2E$ are accepted. The results of such a calculation are shown in Table 30. The molecular yield of hydrogen peroxide is 0.67 molecules per 100 ev and is independent of acid concentration in the range studies. The ratio of yields of molecular hydrogen peroxide and ferrous oxidation in aerated solution is 0.67:15.6 which is equal to 0.043. This is in very good agreement with the experiments of Dainton and Sutton[11] who observe as their best value a ratio of 0.82:20 which is equal to 0.041.

TABLE 30. YIELDS OF HYDROGEN PEROXIDE BY COBALT GAMMA RADIATION

	PURE WATER	0.8 *N* SULFURIC ACID
Reaction F	0.46	0.38
Reaction E	0.21	0.29
Molecular H_2O_2	0.67	0.67

EFFECT OF FAST ELECTRONS ON CORROSION OF TYPE 347 STAINLESS STEEL BY URANYL SULFATE SOLUTIONS

J. A. Ghormley C. J. Hochanadel

The effect of fast electrons on the corrosion of type 347 stainless steel by uranyl sulfate solution at 250°C was studied to determine whether the corrosion mechanism was affected by chemical action of the irradiated solution and by displacement and trapping of electrons in the protective oxide film on the metal. For this purpose a small thermal circulation loop, shown schematically in Fig. 48, was used to maintain the specimen at the desired temperature during irradiation with 2-Mev electrons from a Van de Graaff generator. With a 5-μa collimated beam of 0.2 cm^2 area (neglecting scattering), the beam power density in solution was about 35 watts/cc.

It was difficult to make a reliable estimate of the specimen temperature on the basis of heat transfer coefficients and the nature of the flow as determined from Reynolds number; therefore, the temperature difference between solution and specimen under irradiation was measured at room temperature with the use of a glass mockup in which water

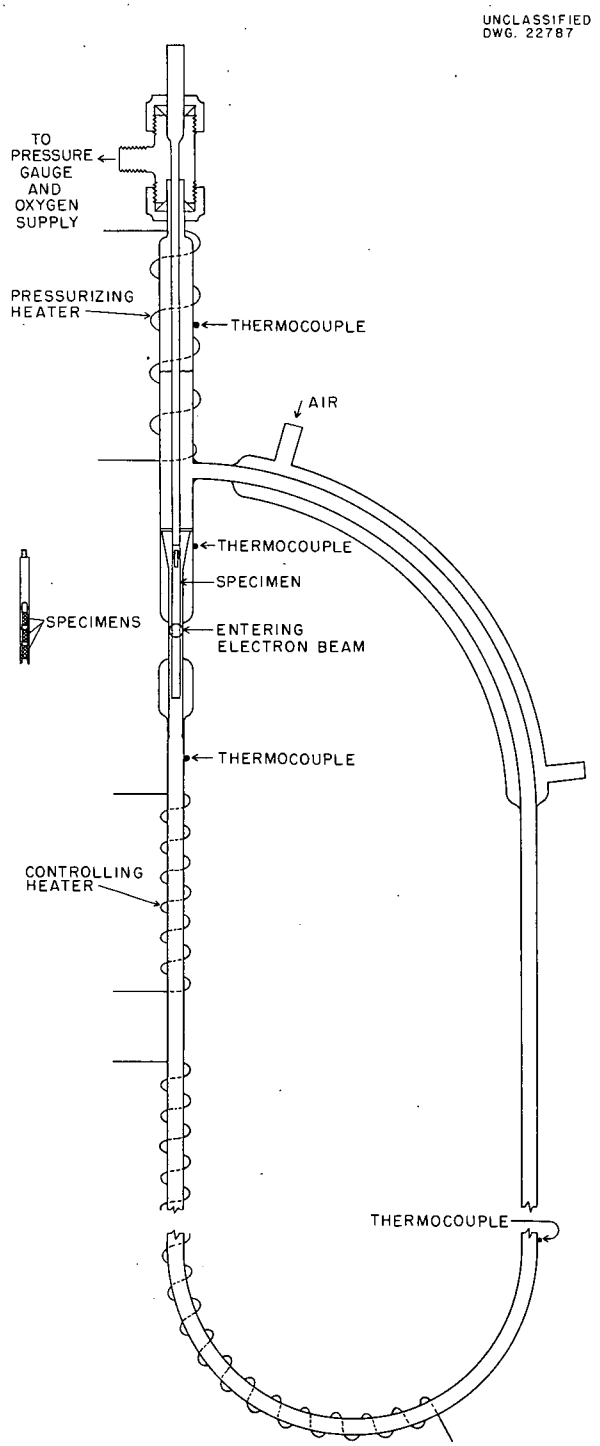

Fig. 48. Small Thermal Circulation Loop.

[11] F. S. Dainton and H. C. Sutton, *Trans. Faraday Soc.* 49, 1011 (1953).

flowed past an irradiated foil at a controlled rate. Two No. 40 copper wires soldered to a 4-mil-thick strip of stainless steel served as a differential thermocouple to give the temperature difference between irradiated and unirradiated positions on the specimen. The flow rate in the loop was estimated from observations on a glass mockup operated at lower temperatures and also from power input and temperature differentials in the steel loop. The observed flow rate of about 10 cm/sec was adequate to maintain the temperature of irradiated specimens within 5 deg of the bulk solution temperature, thereby ensuring that any observed effect was caused by radiation rather than by localized heating by the electron beam.

Uranyl sulfate at a concentration of 44 g of uranium per liter was used in all experiments, and oxygen at a pressure of 100 to 200 psi (25°C) was added to keep the uranium in solution. In one of the earlier experiments depletion of the oxygen occurred and resulted in loss of the uranium from solution, deposition of U_3O_8 on the specimen and loop, a drop in pH, greatly enhanced corrosion with formation of thick flaking films, and production of hydrogen. In ensuing runs more oxygen was added initially and pressures were carefully checked each day.

To ensure uniformity, the original specimens ($6 \times 2 \times 0.1$ mm) were first polished with No. 600 emery paper, then annealed at 1100°C (wrapped in stainless steel foil and contained in an evacuated silica tube), and finally electropolished. The same three specimens (A, B, and C) were used in both of the 50-hr runs listed in Table 31, but in different positions in the two runs. Only the center specimen was irradiated, and the upper and lower specimens served as blanks. The upper specimen (downstream) also allowed observation of possible effects of longer-lived reactive species produced in solution by the radiation.

After 50 hr of irradiation, specimens were removed from the loop, weighed, and defilmed by making each specimen the cathode, with the lead anode in an inhibited 5% H_2SO_4 solution with a current of about 0.2 amp/cm^2. Corrosion was measured as the weight of the oxide film, and as total weight of metal lost. Specimens were electropolished between runs.

In the results shown in Table 31 there appears to be no correlation between the amount of corrosion observed and the position of the specimen in the sample holder. Instead, the observed corrosion appears to be characteristic of the individual specimens. In both runs specimen A showed the greatest metal loss and specimen B the least. It is concluded from these data that this type of radiation has little if any effect on the formation and preservation of the protective film at these very low flow rates. There remains the question of what effect this type of radiation may have on corrosion at higher flow rates, but this question can be answered only with a considerably larger engineering effort.

TABLE 31. EFFECT OF FAST ELECTRONS ON CORROSION OF TYPE 347 STAINLESS STEEL BY URANYL SULFATE SOLUTION

	WEIGHTS (mg)					
	Top Specimen (Downstream)		Center Specimen (Irradiated)		Bottom Specimen (Upstream)	
	Run 1 Sample A	Run 2 Sample B	Run 1 Sample B	Run 2 Sample C	Run 1 Sample C	Run 2 Sample A
Original specimen	9.911	8.021	10.383	7.319	9.908	7.180
Corroded specimen	9.869	8.023	10.431	7.302	9.921	7.134
Defilmed specimen	9.779	7.963	10.361	7.191	9.825	7.041
Corrosion film	0.090	0.060	0.070	0.111	0.096	0.093
Metal loss	0.132	0.058	0.022	0.128	0.083	0.139

OXIDATION OF URANIUM(IV) BY GAMMA RAYS

W. F. Kieffer[12] C. J. Hochanadel

A more thorough study[13] of the oxidation of uranium(IV) by gamma radiation has been made. Reactions were followed by measuring changes in absorption spectra brought about by irradiation of the solutions. Spectra of the (III), (IV), and (VI) valence states in sulfuric acid solutions are shown in Fig. 49. Solutions were irradiated in a silica cell of the type shown in Fig. 50, and the absorption spectrum was then measured in the same cell by using a Cary recording spectrophotometer. Since thin windows were used, the coloring of the silica by the radiation did not interfere appreciably with measurements of absorption spectra of the solutions. The cells were filled under controlled conditions (e.g., oxygen free) by the method previously described.[9] A typical experiment is shown in Fig. 51, which indicates depletion of uranium(IV) by a decrease in absorption at 6520 Å and a corresponding buildup of uranium(VI) by absorption at 4200 Å and also at wave lengths below 3500 Å. In a few experiments uranium(III) was observed by its very strong absorption at 3550 Å. Unfortunately, it was not possible to measure uranium(V) by its absorption spectrum.

[12]Summer employee on leave from Wooster College, Wooster, Ohio.

[13]C. J. Hochanadel, *Chem. Quar. Prog. Rep. Sept. 30, 1952*, ORNL-1432, p. 46-47.

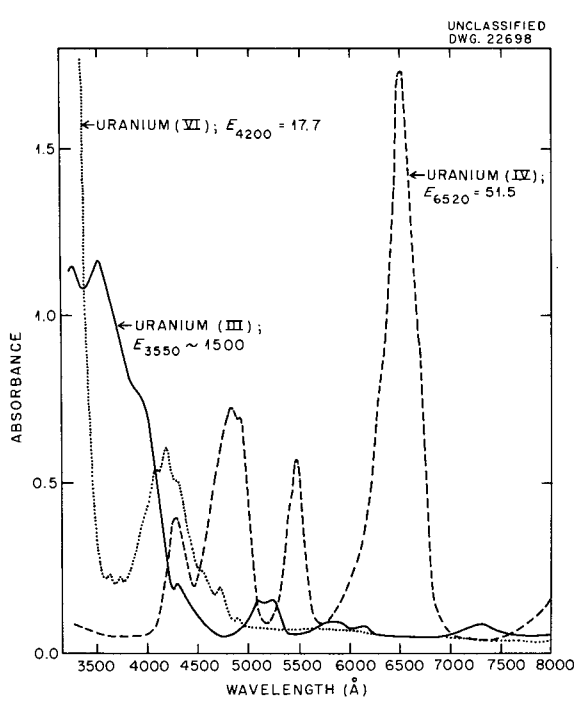

Fig. 49. Absorption Spectra of Uranium(III), Uranium(IV), and Uranium(VI) in Sulfate Solution.

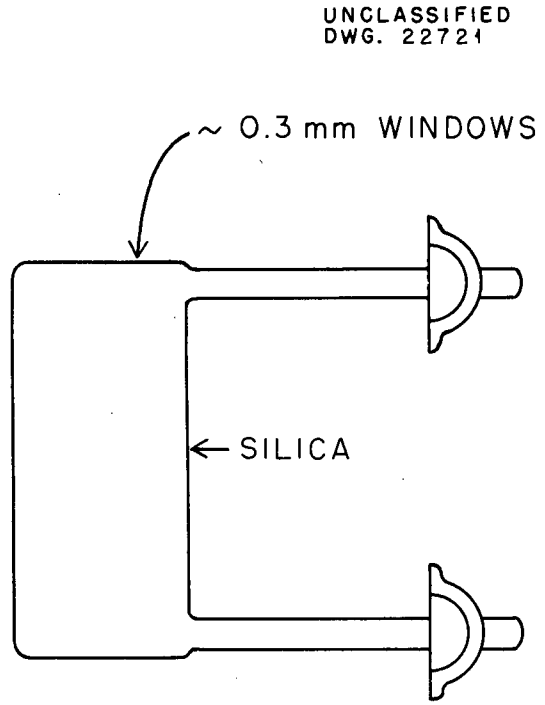

Fig. 50. Typical Cell Used for Both Irradiation of Solutions and Measurements of Absorption Spectra.

The net reaction was the complete oxidation of uranium(IV) to uranium(VI) with the production of an equivalent amount of hydrogen. The gas was measured in an ampoule of the type described in the previous section on gas yields. In oxygen-free solutions, the reaction is characterized by a constant decrease in yield with increased radiation dose. The initial yield in oxygen-free solutions (~2 ions oxidized per 100 ev) is slightly dependent upon the concentrations of uranium(IV), uranium(VI), and H_2; however, the continuous drop in yield with dose cannot be explained by the decrease in uranium(IV), the increase in uranium(VI), or H_2, but is presumably due to the intermediate formation of uranium(V). The yield was independent of pH as measured with the Beckman pH meter over the range from 0.1 to 2.0. In solutions containing oxygen, the yield of 7 to 8 ions oxidized per 100

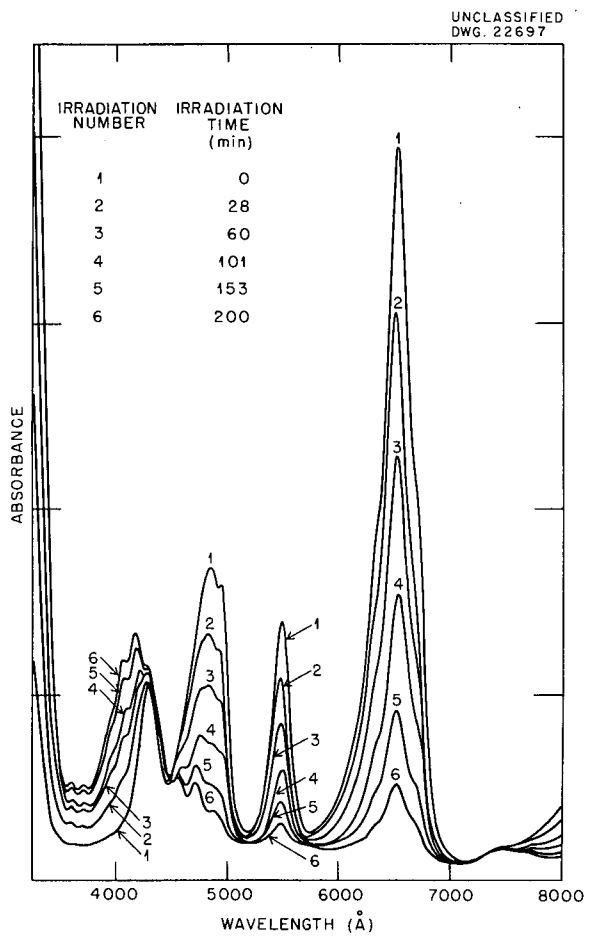

Fig. 51. Changes in Absorption Spectra on Irradiating Uranium(IV) Solution With Gamma Rays.

ev is equivalent to the yield for ferrous oxidation under these conditions. The presence of H_2O_2 in solution during irradiation caused an increase in yield as expected. To determine this effect, it was first necessary to study the thermal oxidation of uranium(IV) by H_2O_2. The reaction was found to be first order in both uranium(IV) and H_2O_2, with specific rate constants (25°C) at pH 0.16 = 35 liters/mole·min and at pH 1.0 = 150 liters/mole·min.

Several miscellaneous observations were the following:

1. A small amount of uranium(III) initially present in solution at pH 2 persisted while the uranium(IV) was being oxidized; production of uranium(III) was not observed in solutions initially free of uranium(III).

2. No oxidation of uranium(IV) or reduction of uranium(VI) was observed on photolyzing solutions at pH 1.0 with light at 2537 Å.

3. After allowing a previously irradiated solution of uranium(IV) to stand overnight, on reirradiating, the initial yield was always greater than the previous final yield, indicating the disappearance of some intermediate on standing.

4. On irradiating an oxygen-free solution and then exposing it to air, an enhanced rate of air oxidation of uranium(IV) was observed. This could be an impurity transformed by radiation to an oxidation state such that it could oxidize uranium(IV) and then be reoxidized by the air, or it could be an intermediate characteristic of the system.

GAMMA RADIOLYSIS OF AQUEOUS SOLUTIONS OF ORGANIC ACIDS

A. R. Jones

Aqueous solutions of some aliphatic acids at a concentration of 20 mg/liter were irradiated in 50-ml aliquots at an energy input rate of 3.5×10^{19} ev/min for total doses of from 3.5 to 112×10^{19} ev. The number and relative amounts of the acidic products that were nonvolatile with steam were determined for each dose for each acid by paper chromatography. It was found that corresponding to the disappearance of the starting material, the concentration of the individual nonvolatile acids that were produced rose and subsequently fell as they, in turn, underwent radiolysis.

For each starting material such a set of observations of its radiolysis products showed an optimum dose at which identifiable amounts of each of its products were present. A set of observations was then made to determine the optimum concentration for that optimum energy input per molecule. Sufficient aqueous solution of the starting material was then prepared at the optimum concentration and irradiated at the optimum dose to provide 40 to 80 mg of non-steam-volatile product.

This mixture was partitioned between 0.5 *N* sulfuric acid and mixtures of chloroform and *n*-butanol of gradually increasing butanol content on a Celite-545 column. The effluent of the column was collected in small fractions and these were titrated with a standard base.

By evaporation of the combined fractions which contained a single acidic component, the salts of the constituent acids were isolated. They were contaminated with neutral organic material and with a sulfate salt.

The impure acids were obtained in a semicrystalline form by treatment of the salt with a sulfonic acid resin, Norit, and Filter-aid, but the melting range of even the more crystalline substances was too great to be of help in identification. A comparison of the R_f values in several pairs of solvents for the product constituents and for various aliphatic acids gave a tentative characterization.

Unequivocal identification by comparison of the x-ray diffraction patterns of the silver or barium salts is in progress. The acids irradiated included: acetic, succinic, tricarballylic, 1,2,3,4-butanetetracarboxyllic, malic, malonic, tartaric, citric, maleic, and fumaric.

INSTRUMENTATION

METHOD OF MEASURING AN ELECTRON BEAM DEFLECTION BY USING VARIATION IN THE SECONDARY EMISSION OF A TARGET

C. J. Borkowski J. K. East

In ORNL-1587 an electron-beam pulse-amplitude analyzer was described which used a "picket fence" type of grid as a means of sorting pulses into many discrete channels. Instead of using a grid structure of this type to define the position of the electron beam, a different type of target was devised and investigated.

The target was made from a strip of commercial Be–Cu that was 0.5 in. wide, 2.0 in. long, and 0.020 in. thick. After cleaning and polishing, the Be–Cu strip was activated at 600°C in a vacuum at a pressure of 10^{-6} mm. The secondary emission yield of such an activated surface is usually about 3.0 at an incident electron energy of 2 kv. At this energy the unactivated Be–Cu surface has a secondary emission yield of about 1.3.

After activation, a metal grid mask was placed over the Be–Cu target and a thin layer of nickel was deposited through the openings in the grid by vacuum evaporation. Thus a series of uniformly spaced bands of nickel, each separated by a band of Be–Cu, was produced. Since the secondary emission yield difference between a nickel surface and activated Be–Cu is about 2.0, a series of pulses will be observed when an electron beam is deflected across such a target. The number of pulses obtained will define the position of the deflected beam into discrete channels.

A target of this type was tested in a 5CP1 cathode-ray tube. The pulses obtained from this target were quite uniform and flat topped.

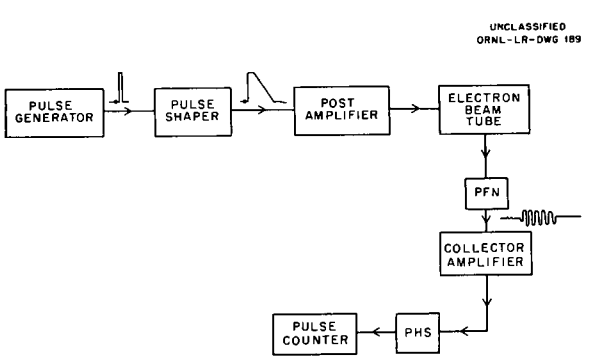

Fig. 52. Electron-Beam Tube-Test Circuit.

Advantages of this type of target over the metal grid type are:

1. The use of only a single strip of solid metal as a target provides a means of obtaining a 50- to 100-channel pulse-amplitude analyzer.
2. Once a master grid is obtained, duplicates are readily made by vacuum evaporation.

The principal disadvantage of a target grid of this type is the possible change of secondary emission of the surface if material evaporated from the cathode deposits on it.

MULTICHANNEL BEAM-DEFLECTION PULSE-AMPLITUDE ANALYZER

F. M. Porter H. J. Hurst
C. J. Borkowski

The electron-beam deflection tube reported in ORNL-1587 has been incorporated in the system shown in Fig. 52. It will be recalled that the electron-beam tube consists of a conventional electron gun, in front of which has been placed a target grid with equal open and closed spaces; directly behind the grid is placed a collector plate which has a secondary emission ratio of approximately 6 for 2-kv electrons. From the arrangement shown in Fig. 52 information has been obtained concerning the uniformity and stability of channel widths of the electron-beam deflection tube as a pulse-amplitude analyzer. The circuitry is essentially a portion of the multichannel pulse-amplitude analyzer in which the electron-beam tube will be used.

The electron-beam tube input signal circuit consists of a pulse-shaping circuit and a post-amplifier having a push-pull output for driving the deflection plates. The output signal is obtained from a differentiating circuit that is directly coupled to the collector plate. The differentiated signal is fed through an amplifier to a pulse-height selector and counter.

The pulse-shaping circuit referred to above accepts pulses from a linear amplifier or a pulse generator which simulates the amplifier pulse and converts the amplifier pulse into a pulse of the same peak amplitude and rise time, but which has a flat top lasting a few microseconds and a constant rate of fall which is independent of pulse amplitude. In response to the shaped pulse, the electron beam is deflected across the grid structure and remains

for the duration of the flat top, then returns to the initial position with constant velocity. The pulses generated on the return of the beam are alternately positive and negative, uniform in shape, and, with the exception of the first pulse, are of uniform amplitude. A photograph of these pulses is shown in Fig. 53. The amplitude of the first pulse will depend upon how far over the edge of a grid bar the beam is when it returns to the initial position.

Both polarity pulses may be counted to determine the deflection within one bar or space width. There are 60 such increments or channels in the present electron-beam tube. Alternately, only one polarity pulse may be counted, thus fixing a channel width as the sum of one bar and one space; in this case there are 30 channels.

Measurements of relative channel width were made for both 60- and 30-channel systems as defined above. The input to the shaping circuit was varied and the number of output pulses counted to determine the channel corresponding to the input-pulse amplitude. The channel width was determined by taking the difference between an input pulse which deflects the beam over one edge 0.2% of a channel width and a second pulse which deflects the beam over the next edge 0.2% of a channel width. The results of relative channel width measurements are shown in Table 32.

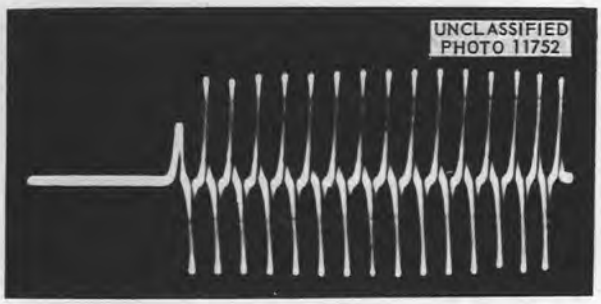

Fig. 53. Differentiated Pulses from Collector of Beam-Deflection Tube.

The variations may be attributed to physical variations in the grid spacing which result from the relatively rough edge of the bars. A second effect that is present in the 60-channel case is the dissimilarity of the electrostatic field near alternate channel edges. The effect of secondary emission variation is not believed to affect appreciably the channel widths, since a temporary increase in emission was induced at one edge without changing the channel width. The channel widths were observed to change only slightly with beam current or pulse-height selector setting. The variation in channel width due to defocusing of the electron beam is inconsequential at 2 kv.

EFFICIENT USE OF A FILM MEMORY IN MULTICHANNEL PULSE ANALYSIS

E. Fairstein R. S. Stone

It has been shown in previous work[1] that the use of photographic film as a multichannel memory offers certain definite advantages in energy analysis at very fast or very slow counting rates. In general, the procedure is to photograph pulses as they appear on the screen of a cathode-ray oscilloscope and then to scan the film, sorting pulses of various heights into appropriate channels.

Until recently, the entire trace was photographed, and the resulting tangle of rising and falling

[1]R. S. Stone and C. J. Borkowski, *Chem. Quar. Prog. Rep. June 30, 1950*, ORNL-795, p. 148.

TABLE 32. RELATIVE CHANNEL WIDTH MEASUREMENTS

NUMBER OF CHANNELS USED	TYPE OF ELECTRON COLLECTION	REMARKS CONCERNING CHANNEL WIDTH DEVIATIONS FROM THE MEAN CHANNEL WIDTH
60	Primary	53 channels within ±3.5% 7 channels with deviations from 4 to 8%
60	Secondary	60 channels within ±3.5%
30	Primary	1st channel deviation +5% 29 channels within ±1.8%
30	Secondary	1st channel deviation +3.5% 29 channels within ±1.4%

edges made it very hard to read a film with more than 10 or 20 pulses per inch. A multichannel pulse-height analysis system such as that described in other reports[2] has been built here and will be used for obtaining coincidence spectra of various beta-gamma emitters.

A block diagram of the system, which has been nicknamed "the dot analyzer," appears in Fig. 54. Input signals are converted to flat-topped pulses proportional to the original signal heights by a stretcher circuit. The duration of the flat top is two or more microseconds. These pulses are then passed through a biased cathode follower to the vertical amplifier of an oscilloscope. Only those pulses which exceed the bias level will cause a beam deflection. A gating pulse, initiated by the incoming signal, is generated and applied to the *A* input of a coincidence circuit. This gating pulse is shorter than the stretched signal, and its position is adjusted to fall entirely within the time interval determined by it. If a coincident pulse appears at input *B*, the gating signal turns the oscilloscope beam on.

The film moves continuously in the *x* direction at a low speed. If no sweep, or a very slow saw-tooth sweep not synchronized with the input pulses, is applied to the *x* input, a series of dots is recorded on the film, corresponding to those pulses which were transmitted by the circuit. The displacement of the dots in the *y* direction is proportional to their amplitude.

The biased cathode follower permits the expansion of a portion of the spectrum to give the system greater resolution. The oscilloscope amplifier acts as a postamplifier in this case.

In this application it is desirable to limit scope deflection to 1 in. at the center of the tube in order to obtain good linearity and to avoid defocusing of the beam. This meant adding a lens-extension tube to the moving film camera to permit filling the whole 35 mm negative with one square inch of scope picture. It was found that the finest spot on the phosphor was obtained with as low a beam intensity as could be used. However, poor resolution of the lens when used wide open at f/1.5 made it necessary to increase the intensity to a level which permits work at f/2.8 or f/4. (All apertures mentioned are nominal; since a 1:1 object-to-image ratio is being used, the effective f values are twice those marked on the lens.)

Since no mechanical sorter is available, the film is read by projecting it onto a ruled screen and visually tabulating the number in each channel. For accurate reading a dependable zero is required. The baseline is composed of pulses too small to trigger the scope but capable of intensifying the

[2]D. J. Zaffarano, F. I. Boley, and W. A. Hunt, *A Multichannel Pulse Height Analysis System Utilizing Photographic Recording on 35 mm Film*, ISC-253 (Aug. 4, 1952); also W. A. Hunt, W. Rhinehart, J. Weber, and D. J. Zaffarano, *A Multichannel Pulse Height Analysis System Utilizing a 35 mm Film Record*, ISC-359 (June 22, 1953).

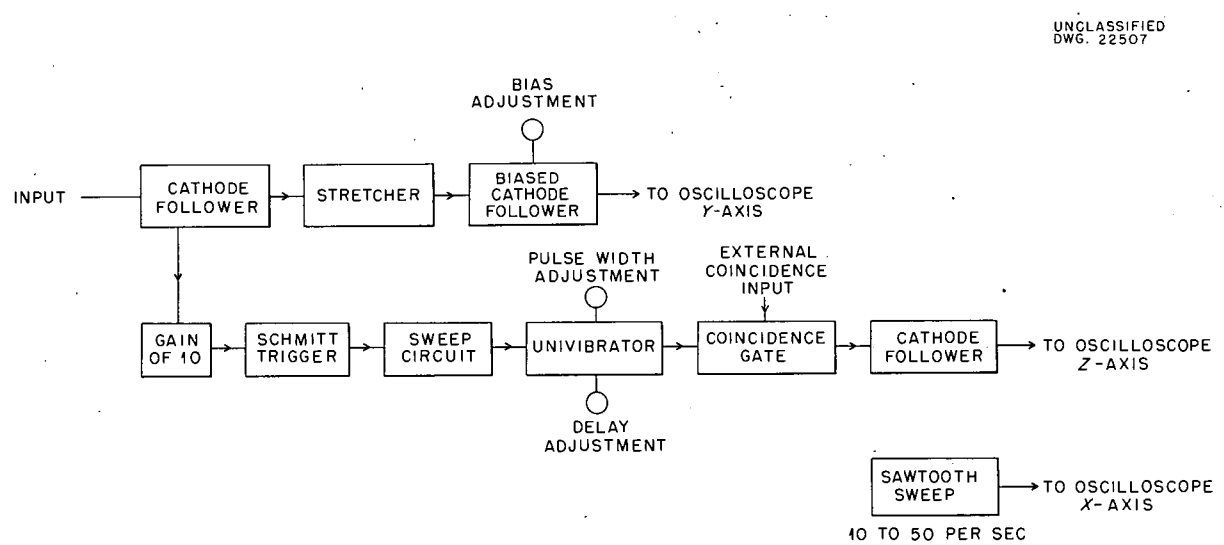

Fig. 54. Dot Analyzer.

beam and is subject to various deviations; among these are d-c fluctuations in the oscilloscope, lateral film play in the camera, and failure to precisely align the camera with the x-y scope axes. Such fluctuations in the baseline are unimportant if their presence is recognized and a suitable correction is made by measuring pulses only from those baseline dots which were made almost simultaneously. This presumably means from baseline pulses which lie directly below the pulse to be measured. Unfortunately, there is no way of distinguishing on the film between a pair of dots which appeared one above the other on the scope face at almost the same instant and another pair which also appeared one above the other, but laterally displaced by a distance x, and separated in time by a period $t = x/\text{film speed}$. In both cases two dots are obtained, one above the other, although in one case the lower dot was not made at the same time as the one above and does not constitute a reliable base point for it. A solution for this possible ambiguity is to eliminate all lateral displacements by disconnecting the x-axis sweep. The reason for the x sweep in the Ames setup was to spread the dots over a wider area of tube face, and in this manner minimize fatigue and charge buildup resulting from hitting the same bit of phosphor too frequently. Moderate counting rates will be used, and consequently these considerations should not present a problem. Should future high counting rates necessitate using a slow sawtooth sweep to spread the pulses on the scope, greater care must be taken to obtain a stable baseline.

Results obtained are shown in Figs. 55 through 58. Figure 55 is a 6X enlargement of the film record obtained from a mercury-relay pulse generator. Here the film did not move, and six short exposures were taken of the generator output at 1-volt intervals. Fluctuations in each level are due to jitter in the relay.

Figure 56 shows a record obtained with the use of a Cs^{137} source and a scintillation counter. Here the x sweep was connected, and the area to the left shows the result when the film remained motionless for a few seconds. The film then started to move, and the area to the right shows the type of record that is taken for analysis. Note the heavy concentration in the peak at the top.

Figure 57 shows a record obtained with the use of a Co^{60} source on a scintillation counter. The x sweep is disconnected here, and the vertical line at the left shows the result when the film is motionless. The area to the right illustrates the type of record that is taken for counting. The dot diameter on the film is about 0.010 inch. If it is assumed that a 50% or more overlap of two dots results in reading them as one, a "dead space" of $0.010^2\pi = 0.000314$ in.^{2} surrounds each pulse seen

Fig. 55. Pulse-Generator Linearity Check.

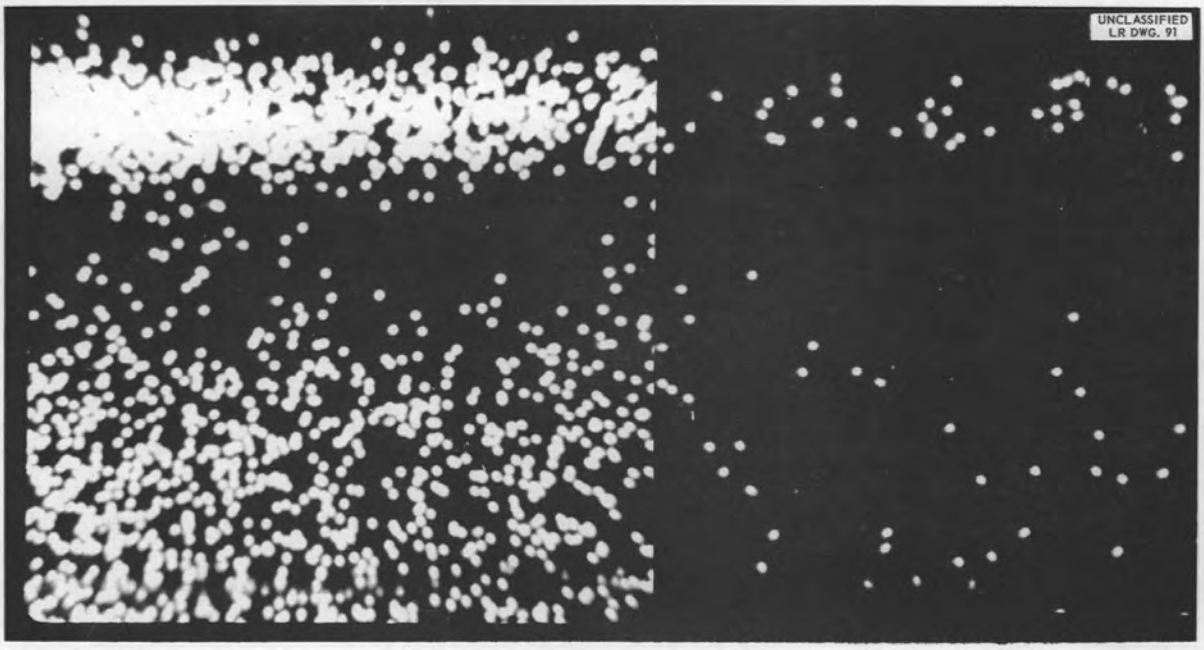

Fig. 56. Dot Display from Cs^{137} Source.

Fig. 57. Dot Display from Co^{60} Source.

on the film. The coincidence loss for 200 pulses per square inch is then

$$\frac{N\sigma}{1+N\sigma} = \frac{200 \times 0.000314}{1 + 200 \times 0.000314} = \frac{0.0628}{1.0628} = 5.9\%.$$

This is not an unreasonable value, although the film speed must be set for the most densely populated area that is to be read. Considerable improvement is obtained by counting as two all dots much brighter than their fellows (see Fig. 57).

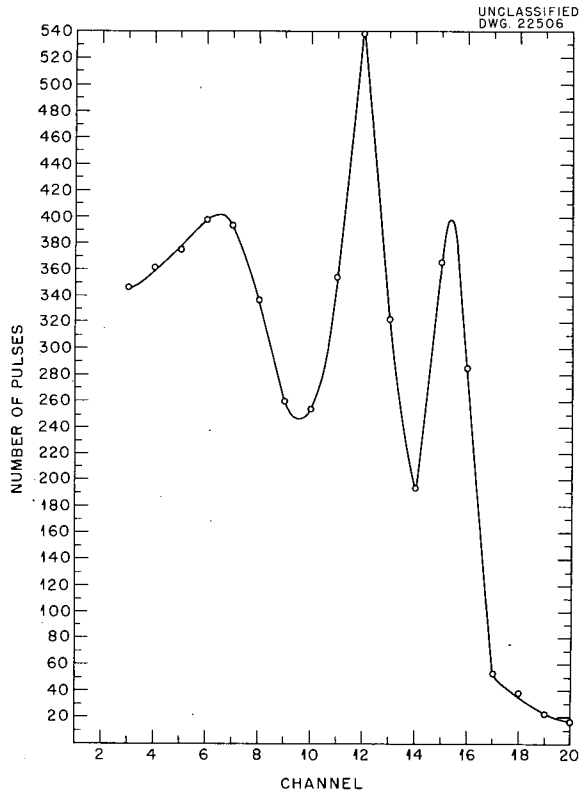

Fig. 58. Distribution of 4917 Pulses from Co^{60} Source as Read from a Film Record.

Multiple pulses are well indicated in this fashion, and the chances for three or more spatially coincident pulses are negligible.

Figure 58 shows the results of analyzing about 4900 pulses from the Co^{60} film illustrated in Fig. 57. This involved about 3 ft of film, far less than would have been required with the previous whole-pulse method. Note that the peaks are well resolved.

DECODING MATRIX FOR A FAST BINARY SCALER

J. D. Eddlemon C. J. Borkowski

A decoding matrix for a fast binary scaler utilizing neon bulbs as gates was described in ORNL-1587. Since the dead time of this matrix was 35 μsec, crystal diodes were used to replace the neon bulbs in order to increase the matrix speed.

The Raytheon 1N67 diode appears to be the one best suited for this application, since it has good stability and a high back resistance – 1 megohm or greater at 50 volts back voltage. The diodes presently in use were selected from stock 1N67 diodes by testing each at 50 volts back voltage with the criteria of less than 50 μa current and no drift in this current with time. The number of diodes rejected by this test was less than 10% of the total number tested.

One element of the matrix consists of two diodes and two 220 K isolating resistors. The diodes are coupled back-to-back through these resistors to the plates of a scaling stage; the conducting state of this scaling stage determines which diode is biased off. Thus, each element of the matrix provides one of two signal paths depending upon the state of scaling stage (Fig. 59).

For a given element, the magnitude of bias on a diode depends upon the potential difference of the scaler plates, the value of the isolating resistors, and the back resistance of the diode. With the diodes directly coupled in the matrix, however, the bias is changed by interstage currents. Because of bias changes due to interstage currents, a pulse amplitude of about 25 volts is required to drive the

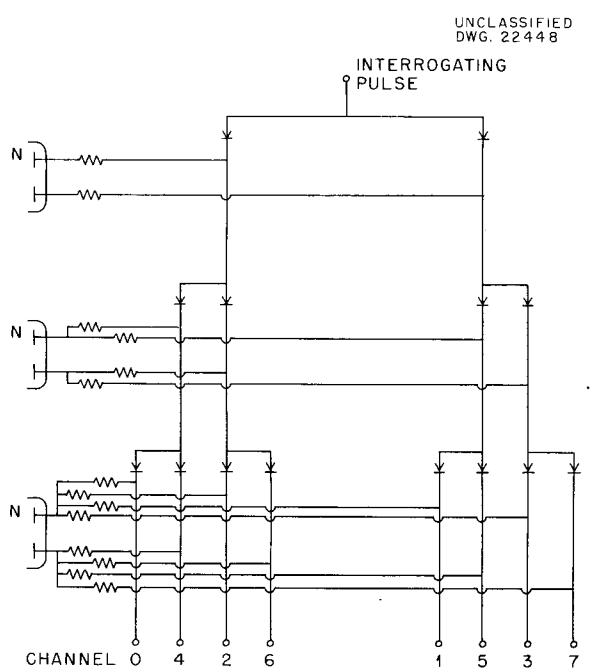

NOTE: N SHOWS CONDUCTING HALF OF SCALING STAGE. WITH CONDITION AS INDICATED, INTERROGATING PULSE APPEARS AT CHANNEL ZERO OUTPUT.

Fig. 59. A Decoding Matrix for a Fast Binary Scaler.

matrix satisfactorily. A channel-selector matrix for use with a scale of 32 delivers an output pulse from the selected channel with an amplitude that is 10 volts greater than that of the other channels.

LINEARITY IMPROVEMENT IN PULSE AMPLIFIERS

E. Fairstein

In pulse-amplitude spectrometry, it is necessary that the gain of the associated amplifier be independent of the output-pulse height to prevent distortion of the measured spectrum. No amplifier is perfect, of course, and the degree of permissible deviation from constant gain is a compromise between a number of factors which will not be discussed here.

In general, most of the gain change in a conventional amplifier arises in the last amplifier tube, since this tube must handle the greatest current swing. In the A-1 amplifier, for instance, the voltage drop across the plate-load resistor of the last stage changes from 150 volts at no signal to about 40 volts when the output signal is 100 volts. Under these conditions, the tube current changes over a range of 3.8 to 1, with a corresponding gain change of about 2.5 to 1. A feedback factor of 20 reduces the gain change to 1.12 to 1, which still leaves an appreciable variation.

The gain change can be greatly reduced by keeping the voltage drop across the plate-load resistor – and therefore the current through the output tube – more nearly constant throughout the signal range. This can be accomplished by the method shown in Fig. 60. (Only those components which have been changed from the original A-1 circuit have been labeled.)

Note that a choke coil has been placed in series with the plate-load resistor. This coil passes direct current but acts as an open circuit to pulses. Also, the output of the cathode follower has been fed back to the top of the plate resistor. The circuit is essentially the same as the conventional bootstrap circuit used for obtaining linear sweeps in oscilloscopes, and its function here is exactly the same: it keeps the voltage drop across the plate resistor nearly independent of the output signal and therefore keeps the gain constant.

The diode is used to keep the output signal limited to a maximum of about 120 volts to prevent

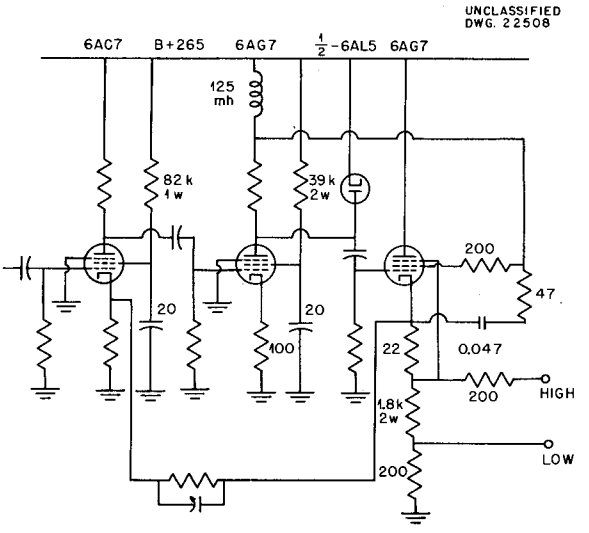

Fig. 60. Improved Version of A-1 Amplifier Output Section.

overloading the circuits into which the amplifier is connected. The low-valued resistors in the screen and cathode circuits of the cathode follower are to prevent parasitic oscillations.

The resulting improvement is shown in Fig. 61. The curves were taken with the limiting diode disconnected.

LINEAR GATE CIRCUIT

E. Fairstein

In most multichannel pulse-height analyzers, a gate circuit that can prevent unwanted pulses from

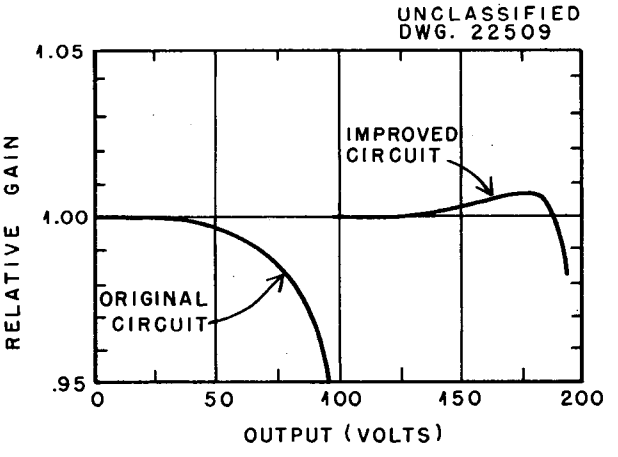

Fig. 61. Gain vs. Output of A-1 Amplifier.

being recorded is necessary. This is certainly the case if coincidence measurements are to be made. The gate circuits are usually placed in that part of the circuit where standardized pulses only are encountered, so that only a yes-no response is required from it. The main reason for this is that none of the circuits which operate on the amplifier signal have given satisfactory results thus far. Since a gate circuit placed far along the analyzer chain often entails undesirable circuit complexity, a good linear gate circuit which could be placed ahead of the pulse-height selector circuits would simplify spectrometer design.

Such a circuit has been devised and appears in Fig. 62. It must be used with an amplifier whose output polarity is positive.

In this version, the gate is placed between the pulse amplifier and the biased postamplifier usually used with a multichannel discriminator. It is important that the input grid of the postamplifier be directly connected to the output of the gate. Furthermore, the first tube in the postamplifier must not conduct until the input signal level exceeds the voltage to which the bias control is set.

Examination of the diagram will show that it is very similar to a conventional coincidence circuit. It differs only in that precautions were taken to ensure linearity.

For the moment, assume that $D_2 \ldots D_n$ and $CF_2 \ldots CF_n$ have been disconnected, leaving only D_1 and CF_1. The bias voltage on CF_1 is set so that point B is about 2 volts beyond cutoff of the postamplifier. Under these conditions, a high-amplitude pulse will not be transmitted to the postamplifier because point A will be clamped to point B by D_1. For a signal to be transmitted through the gate, it is necessary that a positive pulse be applied to input 1 in coincidence with the amplifier signal. If the input signal is to pass through the gate without distortion, the gating signal must be greater in both duration and amplitude than the input signal.

To ensure linearity, a bootstrap circuit is used to keep the voltage drop across T_2 and R_1 independent of the signal, and a constant current load is provided for T_2.

The gate signal for CF_1 is normally provided by a trigger circuit connected to the output of the amplifier.

The rate at which point A can rise is determined by the current through R_1 and the capacity to ground of point A. If the input signal is not to be distorted, point A must be able to rise faster than the input signal does. In practice, it is usually possible to make the rise time less than 0.1 μsec and the delay in the CF_1 gate signal also less

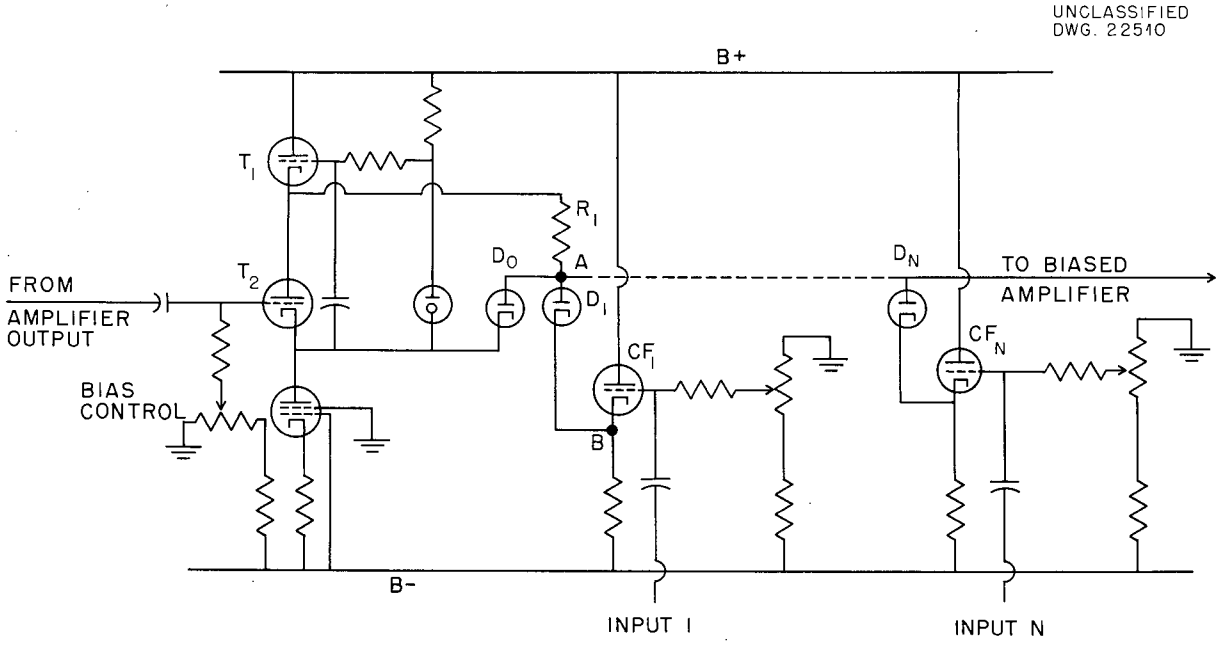

Fig. 62. Linear Gate Circuit.

than this, making it unnecessary to delay the signal to T_2.

In principle, as many additional gate inputs can be added to the circuit as desired, but there is a practical limit determined by the capacitive loading added to point A. There is nothing to prevent these additional circuits from being connected into the trigger circuit for CF_1, however, which gives the same result without adding capacitance to the signal circuit.

By limiting the height of the gate signal into CF_1, it is also possible to limit the height of the transmitted amplifier pulse to prevent overloading the postamplifier and the circuits that follow it.

ORNL-1674
12/53

REACTOR CHEMISTRY

J. Halperin R. W. Stoughton

ALKALINE CHEMISTRY FOR THE PROCESSING OF ALUMINUM-URANIUM FUEL ELEMENTS

As part of the program prompted by E. P. Wigner's re-examination of the costs of chemical processing (Project Hope), the alkaline chemistry for the processing of aluminum-uranium fuel elements was examined and the results will be published in ORNL-1638.

CATHODIC PROTECTION OF TYPE 309 SNb STAINLESS STEEL EXPOSED TO A THORIUM NITRATE–ALUMINUM NITRATE–NITRIC ACID–HYDROFLUORIC ACID MIXTURE

M. H. Lietzke

An experiment was performed in conjunction with the Chemical Technology Division to determine whether cathodic protection would decrease the corrosion rate of type 309 SNb stainless steel exposed to a solution containing 3 *M* $Th(NO_3)_4$, 6 *M* HNO_3, 1.2 *M* $Al(NO_3)_3$, 0.15 *M* F^-, and 0.01 *M* Hg^{++}. The composition of this mixture represents approximately the composition causing maximum corrosion to a stainless steel dissolver during the boiling off of excess acid after the dissolution of aluminum-jacketed thorium slugs in an HNO_3-HF mixture.

The solutions were refluxed in a stainless steel reaction vessel fitted with a stainless steel reflux condenser. The vessel itself served as the corrosion specimen. The experiment was performed under two different conditions: (1) the solution was refluxed at 120°C for 200 hr with no cathodic protection; (2) the solution was refluxed at 120°C for 225 hr with a cathode current density of 15 ma/ft^2. The current was supplied by means of a d-c rectifier.

It was found that under the conditions of the experiment the corrosion rate of the steel was decreased from 60 mpy without cathodic protection to 6 mpy with cathodic protection, or by a factor of 10. The corrosion rates were determined on the basis of nickel analyses performed on the solution before and after each run.

THE SYSTEM UO_3-NiO-SO_3-H_2O

C. H. Secoy E. V. Jones
J. S. Gill D. M. Richardson

Certain portions of the phase diagram for the four-component system, UO_3-NiO-SO_3-H_2O, are of interest in understanding the behavior of uranyl sulfate fuel solutions contained in stainless steel. Much exploratory work has been reported earlier concerning these regions of importance in which approximate boundary or limiting data rather than definitive data were obtained. No attention was given to the identification of solid phases, and frequently compositions were expressed on a volumetric basis and, therefore, were not useful for the graphic representation of the phase relationships.

During the last few months, a longer-range and more systematic approach has been adopted. The immediate objectives were to describe completely the UO_3-rich portion of the UO_3-SO_3-H_2O system, the NiO-rich portion of the NiO-SO_3-H_2O system, and the UO_2SO_4-$NiSO_4$-H_2O system at 25, 100, 175, and 250°C. This work was to be followed by a thorough study of the UO_3-NiO-SO_3-H_2O system at uranium concentrations of less than 15 g of uranium per liter. Completion of this program and completion of the studies of the two-liquid-phase region of the UO_3-SO_3-H_2O system (300 to 400°C) described elsewhere in this report should provide an adequate picture of the phase relationships in proposed reactor fuel systems and should provide a basis for further studies of the effect of additional components.

Experimental methods have involved saturating a solution with an excess of a solid, stirring for a period of time (usually about two weeks), and sampling and chemically analyzing the liquid phase and the wet solid residue. In many cases the solid phases have been examined by the x-ray diffractometer.[1] The data are summarized in Tables 33 to 37. Careful plotting of the data indicates considerably more scatter to the points than can be attributed to analytical error. This may be because of one or more factors. First, the UO_3-rich solutions give some indications of the presence of colloidal material. If this is the case, error would be introduced by failure to effect complete phase

[1] Preparation and interpretation of the x-ray diffraction patterns have been the work of R. D. Ellison of the Chemistry Division, whose help is gratefully acknowledged.

TABLE 33. THE SYSTEM UO_3-SO_3-H_2O AT 25°C

SAMPLE NUMBER	LIQUID PHASE			WET SOLID		X-RAY IDENTIFICATION OF SOLID
	UO_3 (wt %)	SO_3 (wt %)	Mole Ratio UO_3/SO_3	UO_3 (wt %)	SO_3 (wt %)	
K - 1	0.119	0.021	1.59			
K - 2	0.225	0.041	1.54			
K - 3b	0.853	0.163	1.46			
K - 3a	0.865	0.161	1.50			
K - 4a	2.43	0.465	1.46			
K - 4b	3.07	0.464	1.25			
K - 5b	3.77	0.537	1.96			
K - 5a	3.79	0.779	1.36			
G -18	5.10	0.94	1.52			
G -17	5.12	0.93	1.54			
J - 1	5.23	0.93	1.57			
K - 6	7.72	1.77	1.22			
G -12	9.32	1.96	1.33			
G -13	9.36	1.83	1.43			α-$UO_3 \cdot H_2O$
O - 1	10.03	1.73	1.62	88.99	0.42	α-$UO_3 \cdot H_2O$
K - 7	15.16	3.08	1.38			
G -15	16.34	3.14	1.46			
G -16	16.46	3.16	1.46			
J - 2	16.68	2.98	1.57			
M - 2	17.39	3.06	1.59	78.59	1.17	α-$UO_3 \cdot H_2O$
G -14	22.94	4.19	1.53			
K - 7a	23.10	4.74	1.36			
G -10	23.19	4.48	1.45			
O - 2	24.84	4.34	1.60	79.79	1.25	α-$UO_3 \cdot H_2O$ + K basic salt
K_2- 7b	30.67	5.95	1.44	54.25	3.90	K basic salt
G - 5	33.04	6.43	1.44			
O - 3	33.16	6.33	1.47	67.17	4.00	K basic salt
G -11	33.76	6.45	1.46			α-$UO_3 \cdot H_2O$
M - 3	34.35	6.19	1.55	79.07	2.25	α-$UO_3 \cdot H_2O$
K_2- 8	34.41	6.85	1.41	58.88	7.92	
J - 3	34.75	6.22	1.56			
K - 7b	35.06	6.48	1.51			G basic salt

-1674
12/53

TABLE 33. (continued)

SAMPLE NUMBER	LIQUID PHASE			WET SOLID		X-RAY IDENTIFICATION OF SOLID
	UO_3 (wt %)	SO_3 (wt %)	Mole Ratio UO_3/SO_3	UO_3 (wt %)	SO_3 (wt %)	
K_2- 9	37.49	9.23	1.14	59.60	8.79	
K -13	40.88	9.01	1.27			G basic salt
K_2-13	41.64	8.79	1.33	55.86	8.66	G basic salt
G - 4a	42.37	8.76	1.35			
G - 3a	42.90	8.92	1.35			
K_2-10	44.11	11.11	1.11	58.40	9.92	
O - 4	44.71	8.78	1.43	75.58	8.83	G basic salt
O - 5a	45.16	9.38	1.35	64.17	8.08	G basic salt
M - 4	45.40	9.49	1.34	62.36	8.92	Unknown
G - 6	45.54	9.58	1.33			
G - 8	45.54	9.58	1.33			G basic salt
K -12	45.65	10.35	1.23			G basic salt
J - 4	46.54	9.64	1.35	76.23	10.04	
O - 5	47.04	9.90	1.33	76.06	9.67	G basic salt
K_2-12	47.51	10.38	1.28	58.13	9.73	
G - 7	50.35	11.00	1.28			G basic salt
G - 9	50.35	11.08	1.27	76.42	9.92	G basic salt
M - 5	50.79	11.47	1.24	62.60	9.92	Unknown
J - 5	50.91	10.81	1.32	75.66	10.48	
K -11	51.61	11.43	1.26			
O - 6a	52.74	11.74	1.26	65.13	9.17	G basic salt
K_2-11	53.27	12.49	1.19	61.70	11.28	
U - 1	55.81	12.68	1.23	63.80	11.25	G + unknown lines
U - X	56.91	12.95	1.23	65.97	13.08	G + K + unknown
U - Y	57.30	12.90	1.24	64.89	11.08	G + unknown
U - Z	57.76	13.38	1.21	66.93	15.67	G + unknown

separations. Second, the solid material used in saturating the solutions was frequently not the true equilibrium solid phase. Thus a solid-solid transition was necessary and the time allowed for the establishment of equilibrium was probably insufficient for the completion of such a transition. The x-ray diffraction patterns were not indicative of pure solid phases in many cases. It is expected that the quantitative character of the data can be improved by proper changes in technique designed to eliminate these uncertainties.

In spite of these factors, a schematic representation of the phase diagram is possible. Such diagrams for the different isotherms are shown in Figs. 63, 64, 65, 66, 67, and 68. As indicated on the figures, the identity of several of the solid

TABLE 34. THE SYSTEM UO_3-SO_3-H_2O AT 100°C

SAMPLE NUMBER	LIQUID PHASE			WET SOLID		X-RAY IDENTIFICATION OF SOLID
	UO_3 (wt %)	SO_3 (wt %)	Mole Ratio UO_3/SO_3	UO_3 (wt %)	SO_3 (wt %)	
H-1	2.19	0.50	1.23			
H-2	4.28	0.94	1.27			
H-3	8.12	1.76	1.29			
L-1	8.40	1.70	1.38			
I-1	8.43	1.57	1.50			
H-4	15.56	3.11	1.40			
I-2	21.47	4.45	1.35			
L-2	21.90	4.29	1.43	88.20	2.17	α-$UO_3 \cdot H_2O$
H-5	22.01	4.61	1.34			
H-6	31.55	6.60	1.34			
L-3	31.65	6.27	1.41	81.83	3.08	α-$UO_3 \cdot H_2O$
I-3	33.78	6.39	1.48			
I-4a	43.18	8.78	1.38			
H-7b	43.23	9.06	1.34			
L-4	43.23	8.64	1.40	89.04	3.25	
L-5	45.58	9.24	1.38	86.58	3.17	
N-1	46.46	9.07	1.43	80.99	2.17	α-$UO_3 \cdot H_2O$ + G basic salt
I-8a	46.96	9.61	1.37			
H-8b	47.01	9.94	1.32			
L-6	47.51	9.30	1.43	85.07	4.08	
I-5a	47.64	9.74	1.37			
N-2	50.98	9.63	1.48	77.50	4.67	α-$UO_3 \cdot H_2O$ + G basic salt
H-9c	52.30	10.65	1.37			
H-9b	52.83	10.64	1.39	67.17	10.25	
I-6a	53.03	11.06	1.34			
L-7	53.19	11.05	1.35	66.81	11.92	
I-6	53.47	11.11	1.35			

phases remains uncertain. In particular, the exact compositions of the K and G basic salts in the tables are not certain, and at least three undefined solid phases appear in the UO_2SO_4-$NiSO_4$-H_2O system. The evidence to date indicates that none of the latter are double salts, acidic salts, or basic salts. They are all, therefore, most likely lower hydrates of uranyl sulfate and nickel sulfate, respectively.

The 250°C isotherm (Fig. 66) is of special interest in view of the fact that the solubility curve crosses the stoichiometric line. The cross-over occurs at very nearly 0.6 wt % UO_3, which corresponds almost exactly to 5 g of uranium per liter.

-1674
12/53

TABLE 35. THE SYSTEM UO_3-SO_3-H_2O AT 175°C

SAMPLE NUMBER	LIQUID PHASE			WET RESIDUE		X-RAY IDENTIFICATION OF SOLID
	UO_3 (wt %)	SO_3 (wt %)	Mole Ratio UO_3/SO_3	UO_3 (wt %)	SO_3 (wt %)	
U-30	0.13	0.031	1.17	94.93	<0.1	
U-36	0.81	0.21	1.08	86.40	<0.1	
U-51a	1.34	0.34	1.10	87.12	<0.1	
U-79a	1.93	0.45	1.20	86.03	0.93	
U-88a	2.11	0.49	1.21	87.24	<0.1	
U-80a	4.43	0.98	1.27	85.43	0.83	α-$UO_3 \cdot H_2O$
U-81a	9.61	2.02	1.33	86.15	0.42	α-$UO_3 \cdot H_2O$
U-82a	14.63	3.15	1.30	84.23	1.08	
U-83a	20.38	4.50	1.27	85.91	1.20	α-$UO_3 \cdot H_2O$
U-84a	29.74	6.25	1.33	91.20	1.42	α-$UO_3 \cdot H_2O$ + β-$UO_3 \cdot H_2O$
U-85a	39.17	8.71	1.26	87.36	1.50	
U-40	45.11	9.66	1.31	74.14	3.33	
U-86a	46.45	9.92	1.31	86.27	2.25	α-$UO_3 \cdot H_2O$ + G basic salt
U-39a	49.23	10.87	1.27	84.35	4.83	
U-87a	54.41	11.15	1.37	81.11	5.08	α-$UO_3 \cdot H_2O$ + G basic salt

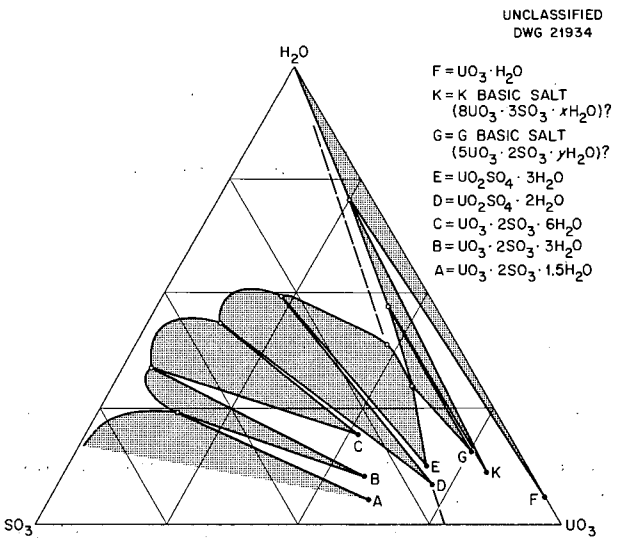

Fig. 63. The System UO_3-SO_3-H_2O at 25°C.

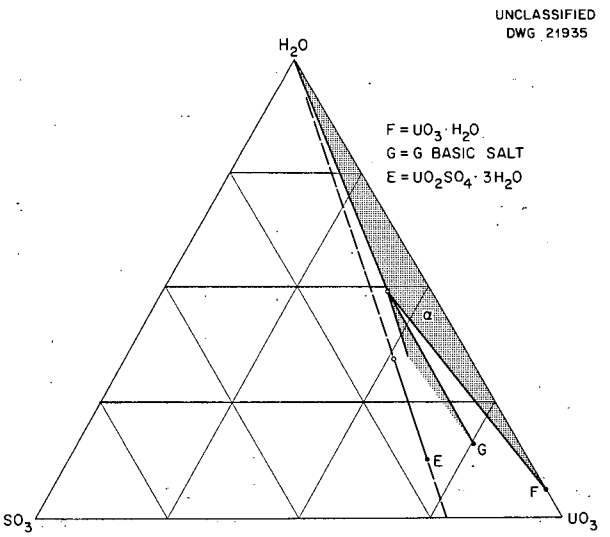

Fig. 64. The System UO_3-SO_3-H_2O at 100°C.

TABLE 36. THE SYSTEM UO_3-SO_3-H_2O AT 250°C

SAMPLE NUMBER	LIQUID PHASE			WET RESIDUE		X-RAY OR MICROSCOPIC IDENTIFICATION OF SOLID
	UO_3 (wt %)	SO_3 (wt %)	Mole Ratio UO_3/SO_3	UO_3 (wt %)	SO_3 (wt %)	
S-1	0.0386	0.0122	0.88			
98-a	0.0413	0.0159	0.73	94.33	<0.1	β-$UO_3 \cdot H_2O$
S-2	0.0678	0.0220	0.86			
97-a	0.1112	0.0382	0.81	94.69	<0.1	β-$UO_3 \cdot H_2O$
93-a	0.114	0.0366	0.87	93.12	<0.1	β-$UO_3 \cdot H_2O$*
S-3	0.130	0.038	0.96			
S-4	0.152	0.040	1.07			
96-a	0.158	0.051	0.86	94.09	<0.1	β-$UO_3 \cdot H_2O$
92-a	0.171	0.054	0.89	90.72	<0.1	β-$UO_3 \cdot H_2O$*
95-a	0.291	0.094	0.87			β-$UO_3 \cdot H_2O$.
S-5	0.458	0.125	1.03			
91-a	0.500	0.143	0.98	93.36	<0.1	β-$UO_3 \cdot H_2O$*
S-7	0.572	0.159	1.01			
101-a	0.736	0.200	1.03	94.65	<0.1	β-$UO_3 \cdot H_2O$
S-8	1.27	0.314	1.14			
103-a	1.68	0.435	1.08	93.00	<0.1	
104-a	3.81	0.999	1.07	93.60	<0.1	
105-a	7.32	1.784	1.15	93.84	<0.1	
106-a	13.71	3.133	1.22	91.08	0.92	**
107-a	20.36	4.63	1.23	82.19	1.00	**
108-a	29.82	6.58	1.27	82.31	0.92	
109-a	44.57	9.52	1.31	87.96	2.08	**
110-a	51.96	11.00	1.32			

*X-ray identification.

**Analytical data indicates anhydrous UO_3.

Further insight into the phase relationships of the UO_3-SO_3-H_2O system can be obtained by reference to Fig. 68. In this figure, temperature is plotted against per cent of UO_3. Lines are drawn through points of constant SO_3 composition. The graph is intended to show two things: first, approximate temperature and composition ranges for the regions in which the different solid phases are stable and, second, the slope of the lines indicate whether the solubility of the stable solid is increasing or decreasing with temperature. Points *B* and *E*, whose exact positions are unknown, represent invariant points at which three solid phases can coexist in equilibrium with saturated solution and vapor.

THE SYSTEM UO_3-SO_3-H_2O ABOVE 300°C

D. W. Sherwood C. H. Secoy

Consideration of the need for further data in the two-liquid-phase region of uranyl sulfate solutions has led to the formulation of a plan of attack

-1674
12/53

TABLE 37. THE SYSTEM UO_2SO_4-$NiSO_4$-H_2O AT 25°C

SAMPLE NUMBER	LIQUID PHASE		WET RESIDUE		X-RAY IDENTIFICATION OF SOLID
	UO_2SO_4 (wt %)	$NiSO_4$ (wt %)	UO_2SO_4 (wt %)	$NiSO_4$ (wt %)	
	61.18	0.00			$UO_2SO_4 \cdot 3H_2O$
21	60.28	2.42	77.0	0.87	
65	57.1	4.96	79.7	1.62	Unknown A
17	56.6	4.85	76.4	1.41	
67	55.2	7.59	78.3	2.51	Unknown A + unknown
53	54.3	8.33	75.8	2.74	$UO_2SO_4 \cdot 3H_2O$ + unknown
15	54.3	8.08	75.2	1.70	
13	54.0	8.31	74.7	2.34	
51	53.1	9.39	73.1	3.56	$UO_2SO_4 \cdot 3H_2O$ + unknown
11	52.3	9.49	75.5	4.08	Unknown
57	50.4	11.45	75.6	3.99	Unknown A
47	50.4	12.20	75.0	4.50	
49	51.5	14.8	27.0	37.1	Unknown
63	54.0	13.4	21.8	41.2	$UO_2SO_4 \cdot 3H_2O$ + unknown
31	42.3	16.56	22.92	38.5	Unknown
59	41.7	16.5	5.49	53.5	$NiSO_4$ hydrate mixture (7-6-1)
61	40.7	17.15	12.3	46.1	Unknown
33	36.8	17.72	19.93	36.82	
35	34.0	17.90	5.98	53.7	
37	33.5	20.06	7.30	50.2	
41	24.0	20.62	2.30	54.7	α-$NiSO_4 \cdot 6H_2O$
39	27.5	20.70	9.61	46.0	
43	11.51	24.20	0.80	56.0	α-$NiSO_4 \cdot 6H_2O$
45	4.07	27.60	0.35	57.8	
	0.00	28.51			$NiSO_4 \cdot 7H_2O$

involving a large pressure vessel with windows that is designed to contain a sealed quartz solution vessel. This quartz vessel is equipped with a spiral quartz capillary gage which is to be used as a null-point instrument by balancing the internal pressure (vapor pressure of the system) with an external inert-gas pressure. By means of the windows, the relative volumes of the three phases present may be determined simultaneously with the vapor pressure determination. Concentrations of each of the components in each of the phases may be calculated from these data.

It is planned to mount the observation windows of the pressure vessel in a way which is new for windows of the proposed size. To this end, experimental work has been under way in testing such a window mounting in type 347 stainless steel. Tests to date at room temperature have been

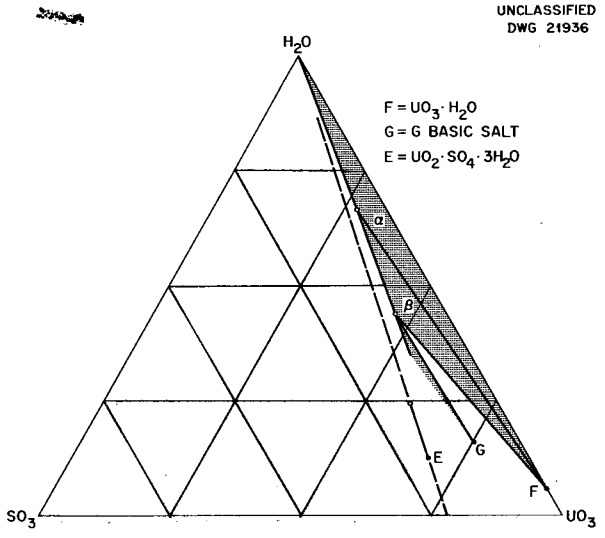

Fig. 65. The System UO_3-SO_3-H_2O at 175°C.

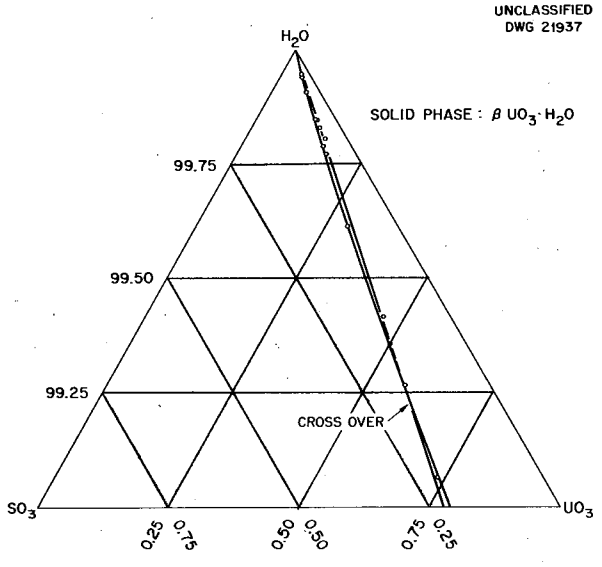

Fig. 66. The System UO_3-SO_3-H_2O at 250°C.

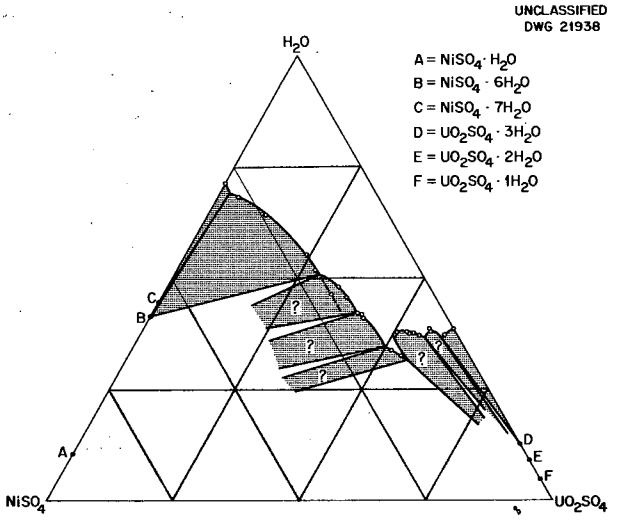

Fig. 67. The System UO_2SO_4-$NiSO_4$-H_2O at 25°C.

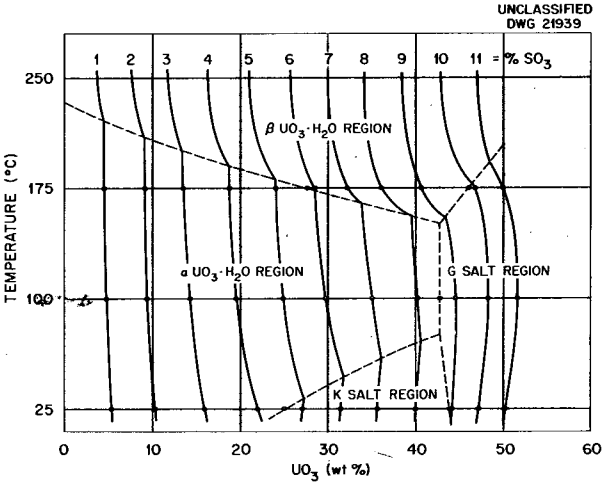

Fig. 68. Schematic Representation of the System UO_3-SO_3-H_2O.

satisfactory, and high-temperature testing is in progress.

PRELIMINARY EXPLORATION OF THE $Th(NO_3)_4$-HNO_3-H_2O SYSTEM AT ELEVATED TEMPERATURE

W. L. Marshall C. H. Secoy

Some experimental data have been obtained previously[2] for the hydrolytic phase stability of $Th(NO_3)_4$ in H_2O at temperatures above 100°C in which the vapor-to-liquid ratio was unity. These data indicated that a maximum temperature before precipitation could be obtained at about 400 g of thorium per liter. The purpose of the present investigation was to estimate the amount of excess HNO_3 necessary to prevent hydrolytic precipitation at higher temperatures than could be obtained with stoichiometric $Th(NO_3)_4$.

Solutions with nitrate-to-thorium ratios of 3.95, 5.47, and 6.65 were prepared in concentrations that varied from 20 to 400 g of thorium per liter. Capillary

[2] W. L. Marshall, J. S. Gill, and C. H. Secoy, *HRP Quar. Prog. Rep. Nov. 30, 1950*, ORNL-925, p. 279.

-1674 12/53

tubes containing these various solutions in a 1:1 vapor-to-liquid ratio were run in the semimicro phase-study apparatus described previously.[3] The temperature was raised rapidly (about 8°C/min) and the point determined at which precipitation occurred. An experiment over a slow period (temperature raised ½°C/min) and also some static runs over three to four days were compared with the rapid experiments in order to decide what correction in temperature should be made to these latter values. The data are given in Table 38, together with some observations on the solid and vapor phases. In Figs. 69 and 70 curves are drawn to represent the best estimate, from these data, of the equilibrium temperatures at which precipitation will occur.

It is significant to note that the first mole of excess nitrate causes the biggest elevation in precipitation temperature, that the vapor-phase coloration is much greater per unit change of nitrate after the initial four moles are added to the thorium, and that in the concentrated regions crystalline solids appear, compositions of which might correspond to acid salts. These latter crystalline compounds are reversible in solubility over the time of the experiments as compared with the apparent irreversibility of the hydrolysis product(s).

It is not to be implied from these data that valid extrapolations or interpolations to other compositions can be made without considering the possibility of additional solid phases not indicated by these data appearing at lower temperatures.

[3] H. W. Wright and W. L. Marshall, *HRP Quar. Prog. Rep. Oct. 1, 1952*, ORNL-1424, p. 108.

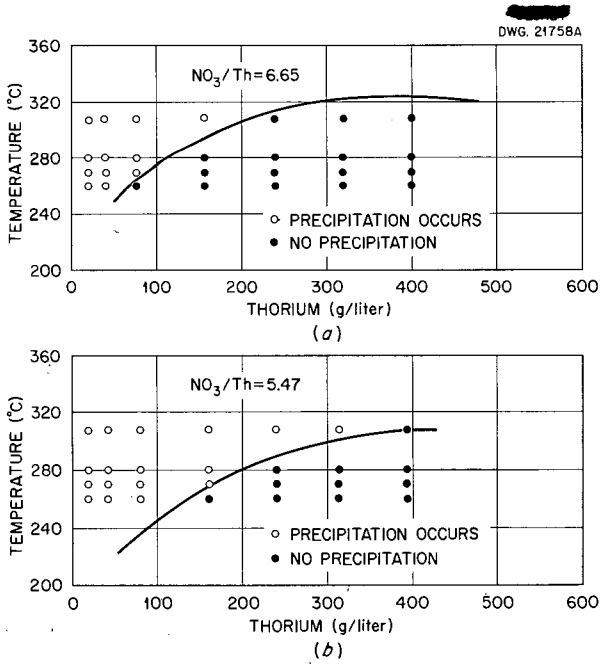

Fig. 69. Estimate of Phase Stability of the System $Th(NO_3)_4$-HNO_3-H_2O.

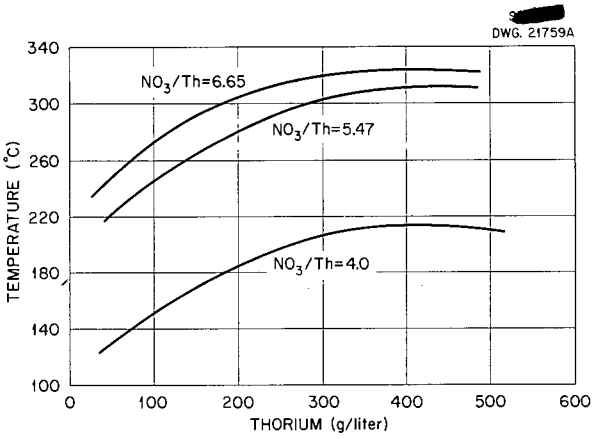

Fig. 70. Estimate of Phase Stability as a Function of Mole Ratio, NO_3/Th, of the System $Th(NO_3)_4$-HNO_3-H_2O.

ESTIMATION OF ACTIVITY COEFFICIENTS OF UO_2SO_4 SOLUTIONS FROM VAPOR-PRESSURE MEASUREMENTS

H. O. Day, Jr. C. H. Secoy

During recent months a considerable amount of data has been obtained on the vapor-pressure depression of water in UO_2SO_4 solutions. Since the vapor pressure of an aqueous solution of a nonvolatile solute is a measure of the activity of the water, the activity of the solute may be computed by means of the Gibbs-Duhem relationship.

The fundamental equation expressing the activity coefficient of a solute as a function of the vapor pressure may be written as

$$d \ln \gamma_{\pm} = -\frac{1}{m} d[m(1-\phi)] ,$$

which on integration gives

$$\ln \gamma_{\pm} = -(1-\phi) - \int_0^m \frac{1-\phi}{m} dm .$$

TABLE 38. EXPLORATION OF HYDROLYTIC PHASE STABILITY FOR THE SYSTEM $Th(NO_3)_4$-HNO_3-H_2O

MOLE RATIO NO_3/Th	THORIUM CONCENTRATION (g/l)	RATE OF TEMPERATURE RISE (°C/min)	PRECIPITATION TEMPERATURE (°C)	SOLID PHASE APPEARANCE*	VAPOR PHASE COLORATION**
		Dynamic Experiments			
3.95	19.9	8	185	Amorphous (?)	None
	39.9	8	200	Amorphous (?)	None
	79.8	8	220	Amorphous (?)	None
	159.5	8	255	Amorphous (?)	None
	239.3	8	268	Amorphous (?)	None
	319.0	8	280	Amorphous (?)	Slight
	398.8	8	272	Crystalline	Yes
5.47	19.7	8	230	Amorphous (?)	None
	39.4	8	274	Amorphous (?)	None
	78.8	8	298	Amorphous (?)	Yes, 285°C
	157.6	8	318	Amorphous (?)	Yes, 285°C
	236.5	8	316	Crystalline	Yes, 285°C
	315.3	8	332	Crystalline	Yes, below 285°C
	394.1	8	300 to 314	Crystalline	Yes, below 250°C
6.65	20.2	8	265	Amorphous (?)	
	40.3	8	302	Amorphous (?)	Yes, 295°C
	80.5	8	308	Crystalline	
	161.1	8	310	Crystalline	Yes, below 280°C
	241.6	8	340	Crystalline	Yes, 260°C
	322.2	8	336	Crystalline	
	402.7	8	332	Crystalline	Yes, 220°C
3.95	398.8	½	225	Crystalline	
		Static Experiments A			
		TIME AT TEMPERATURE			
5.47	394.1	60 hr at 305°C	305	Slight crystalline precipitation	
3.95	398.8	17 hr at 250°C		Crystalline precipitation	
5.47	394.1	17 hr at 250°C		No precipitation	
6.65	402.7	17 hr at 250°C		No precipitation	

*Use of 20X microscope.

**To precipitation temperature.

-1674
12/53

TABLE 38 (continued)

MOLE RATIO NO_3/Th	THORIUM CONCENTRATION (g/l)	PRECIPITATION OF SOLID PHASE			
		At 260°C for 3 hr	At 270°C for 60 hr	At 280°C for 18 hr	At 308°C for 18 hr
Static Experiments B					
5.47	19.7	Yes	Yes	Yes	Yes
	39.4	Yes	Yes	Yes	Yes
	78.8	Yes	Yes	Yes	Yes
	157.6	No	Yes	Yes	Yes
	236.5	No	No	No	Yes
	315.3	No	No	No	Yes
	394.1	No	No	No	No
6.65	20.2	Yes	Yes	Yes	Yes
	40.3	Yes	Yes	Yes	Yes
	80.5	No	Yes	Yes	Yes
	161.1	No	No	No	Yes
	241.6	No	No	No	No
	322.2	No	No	No	No
	402.7	No	No	No	No

In these equations $\gamma_{\pm}$ is the stoichiometric mean ionic molal activity coefficient and is usually called the practical activity coefficient, m is the molality of the UO_2SO_4 solution, and ϕ is the osmotic coefficient; ϕ is a direct function of the vapor pressure of a solution and is defined thusly:

$$\phi = -\frac{1000}{\nu m M_1} \ln \frac{P}{P_0} ,$$

where P is the vapor pressure of the solution at some temperature, P_0 is the vapor pressure of the pure solvent at the same temperature, m is the molality, M_1 is the molecular weight of the solvent, and ν is the stoichiometric number of ions produced when the solute is dissolved in the solvent. For UO_2SO_4, ν is equal to 2.

From this equation, activity coefficients have been calculated from 0.1 to 6.0 m at temperatures from 30 to 100°C. The exact details of the calculation will be described in an ORNL report completing this particular investigation. The calculated activity coefficients have been tabulated in Table 39.

HOMOGENEOUS REACTOR SOLUTIONS UNDER IRRADIATION

C. H. Secoy
H. O. Day, Jr.
B. O. Heston
Q. V. Larson
F. H. Sweeton
W. C. Yee

During the last quarter more studies of the corrosion of metals by homogeneous reactor solutions under pile radiation have been carried out, and, in addition, for comparison purposes, some out-of-pile studies have been made. During this time the instrumentation of the hole HB-6 in the Low-Intensity Test Reactor has been finished, and this new facility has been put into use. The new facility is superior to the older one in HB-5 in that a bomb can be rotated manually while it is in the hole and the reactor is operating. Bombs irradiated in this new hole are normally kept horizontal during the test in order to get quicker equilibrium between the oxygen in the vapor phase and that dissolved in the liquid phase. Tests during the quarter have involved type 347 stainless steel and also titanium.

As before, the change in oxygen partial pressure in a bomb has been used to calculate the corrosion

TABLE 39. VALUES OF THE ACTIVITY COEFFICIENT, $\gamma_{\pm}$

MOLALITY	TEMPERATURE (°C)															
	25	30	35	40	45	50	55	60	65	70	75	80	85	90	95	100
0.1	0.150	0.147_8	0.145_5	0.143_2	0.140_9	0.138_5	0.136_0	0.133_6	0.131_1	0.128_6	0.126_0	0.123_4	0.1207	0.118_0	0.115_2	0.112_4
0.2	0.102	0.100_6	0.0987	0.0969	0.0950	0.0931	0.0911	0.0892	0.0872	0.0852	0.0831	0.0811	0.0791	0.0770	0.0748	0.0727
0.3	0.0807	0.0795	0.0781	0.0766	0.0752	0.0736	0.0720	0.0704	0.0687	0.0670	0.0652	0.0634	0.0614	0.0596	0.0576	0.0557
0.5	0.0611	0.0602	0.0590	0.0579	0.0566	0.0553	0.0538	0.0524	0.0509	0.0494	0.0477	0.0461	0.0444	0.0428	0.0410	0.0393
0.7	0.0515	0.0507	0.0496	0.0484	0.0472	0.0459	0.0446	0.0432	0.0417	0.0403	0.0387	0.0373	0.0357	0.0342	0.0327	0.0312
1.0	0.0439	0.0428	0.0417	0.0404	0.0392	0.0379	0.0366	0.0353	0.0339	0.0325	0.0311	0.0298	0.0284	0.0271	0.0258	0.0245
1.5	0.0385	0.0371	0.0358	0.0344	0.0332	0.0319	0.0305	0.0292	0.0278	0.0266	0.0252	0.0240	0.0227	0.0214	0.0202	0.0190
2.0	0.0367	0.0354	0.0340	0.0326	0.0311	0.0298	0.0283	0.0269	0.0255	0.0242	0.0228	0.0214	0.0201	0.0189	0.0177	0.0165
2.5	0.0370	0.0355	0.0338	0.0323	0.0307	0.02[illegible]	0.0275	0.0260	0.0245	0.0231	0.0217	0.0203	0.0189	0.0176	0.0164	0.0152
3.0	0.0383	0.0366	0.0346	0.0329	0.0310	0.0293	0.0275	0.0259	0.0242	0.0227	0.0212	0.0197	0.0183	0.0170	0.0157	0.0145
3.5	0.0401	0.0383	0.0361	0.0340	0.0319	0.0300	0.0280	0.0262	0.0244	0.0227	0.0211	0.0196	0.0181	0.0167	0.0154	0.0142
4.0	0.0433	0.0405	0.0380	0.0356	0.0332	0.0311	0.0288	0.0268	0.0248	0.0230	0.0213	0.0197	0.0181	0.0167	0.0153	0.0141
4.5	0.0465	0.0434	0.0403	0.0374	0.0348	0.0323	0.0299	0.0277	0.0255	0.0236	0.0217	0.0200	0.0183	0.0168	0.0154	0.0141
5.0	0.0500	0.0464	0.0429	0.0397	0.0367	0.0339	0.0312	0.0287	0.0264	0.0243	0.0222	0.0204	0.0187	0.0171	0.0156	0.0143
5.5	0.0536	0.0497	0.0459	0.0422	0.0389	0.0357	0.0329	0.0300	0.0274	0.0251	0.0229	0.0210	0.0191	0.0175	0.0160	0.0145
6.0	0.0571	0.0531	0.0489	0.0449	0.0412	0.0377	0.0344	0.0314	0.0286	0.0261	0.0238	0.0217	0.0197	0.0179	0.0164	0.0149

-1674
12/53

penetration by assuming that corrosion occurs only on the bomb surface wetted by the test solution, that the corrosion is uniform over that surface, and that there is no selective oxidation of any particular component of the stainless steel.

Stainless Steel

The following out-of-pile tests with stainless steel have been completed during the quarter.

Test H-16A. This test was made by using a special 38-ml bomb that contained an appreciable quantity of stainless steel turnings; therefore the surface-to-volume ratio was larger by a factor of 3 than that of the bombs used in the reactor. Most of the data for the test are included in Fig. 71. As usual, oxygen was added to the bomb in the form of hydrogen peroxide, which later decomposed on heating. The oxygen partial pressure was about 95 psi at the start and decreased gradually during the test to about zero. An analysis of the residual gas in the bomb after the test was stopped showed that actually about 5 psi of oxygen was present and, in addition, about 7 psi of hydrogen. When the bomb was open, all the uranium was found to be precipitated.

The results of the test can be best discussed by breaking the curve of Fig. 71 into three parts. The first part, in which the rate of corrosion is apparently increasing, has not been observed previously

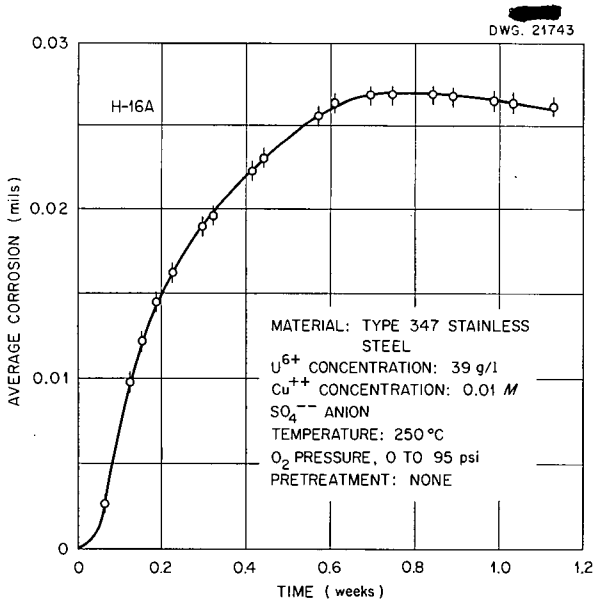

Fig. 71. Out-of-Pile Corrosion of Stainless Steel by Homogeneous Reactor Solution.

in this series of experiments. It may be due to the slowness of oxygen in diffusing from the vapor phase down into the solution where it is being depleted by corrosion. The middle portion of the curve between 0.16 and 0.6 week is quite regular, and it appears to be the more or less normal effect of corrosion on the oxygen pressure. In this region the corrosion appears to progress as the square root of time. The negative slope of the last portion of the curve probably is not real. As usual, the plotted corrosion is that calculated by assuming that all changes in total pressure are due to oxygen being absorbed in the corrosion process and that no other oxidizing agent is acting on the steel. If stainless steel is oxidized by either uranium (with the precipitation of reduced uranium) or water (with the liberation of hydrogen), the calculated corrosion shown in the graph will be erroneously low. This is believed to be true in this case, since both precipitated uranium and hydrogen gas were found when the bomb was opened.

Test H-16B. Another out-of-pile test was later performed with the same bomb. However, the pressure decreased so fast that the bomb appeared to be leaking. Oxygen gas was then added and no further apparent leaking occurred, but the rate of change in pressure was erratic, dropping significantly more during one period of less than 4 hr than either before or after. It is concluded that the data of this test are not reliable because either the surface of the bomb was not equivalent to a new one or the treatment of the bomb when a leak was suspected may have affected its corrosion curve.

Test H-16. The results of another out-of-pile test are shown in Fig. 72. This test was essentially similar to test H-16A except that a bomb of normal size (~9 ml) was used and no turnings were present in the bomb to increase the surface. The corrosion rate decreased throughout the test. The average rate for the last three weeks was 0.1 mpy. The corrosion during the first 0.6 week agreed in general with that of test H-16A within a factor of 2, which is reasonably close when the uncertainty of the microscopic surface area is considered.

Test H-11. This was the first in-pile radiation completed this quarter. As can be seen in Fig. 73, test H-11 was essentially the same as tests H-16 and H-16A except for its fission density and its somewhat higher oxygen partial pressure. This experiment was terminated in order to make room

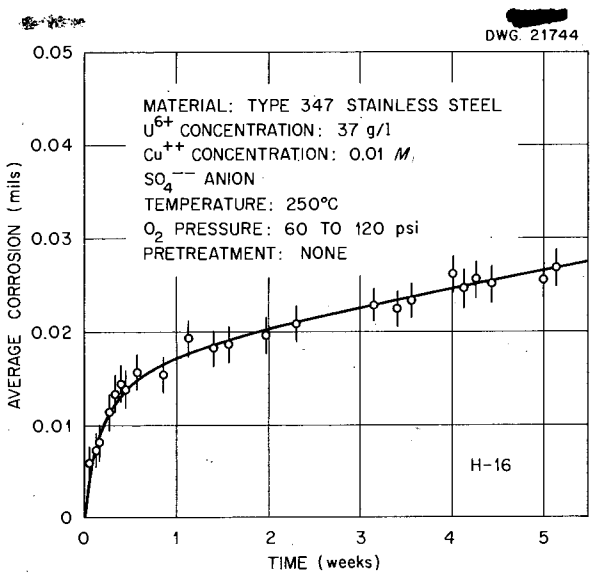

Fig. 72. Out-of-Pile Corrosion of Stainless Steel by Homogeneous Reactor Solution.

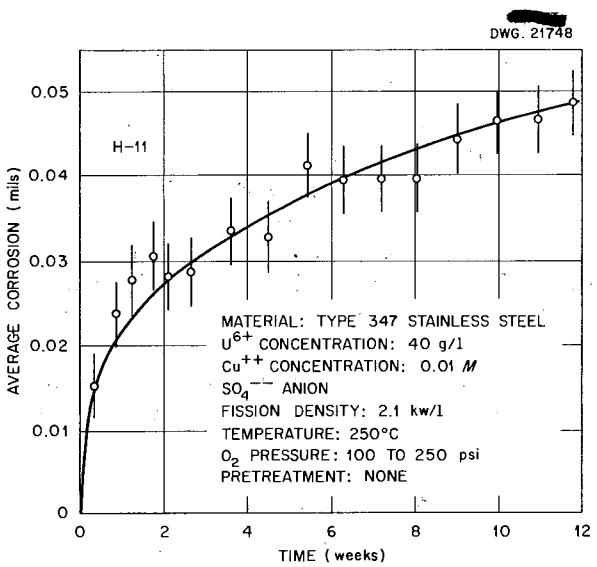

Fig. 73. In-Pile Corrosion of Stainless Steel by Homogeneous Reactor Solution.

for other experiments. As can be seen on the graph, the rate of corrosion continued to decrease. It averaged about 0.1 mpy from the fourth week on to the end. Comparison of the test with tests H-16 and H-16A indicates no appreciable difference in corrosion and suggests that at this fission density (2.1 kw/liter) radiation may not be affecting the corrosion.

Test H-12. This test, described in Fig. 74, was supposedly the same as two tests reported last quarter, H-7 and H-10, except that (1) this bomb had been put through an electropolishing process and (2) the test was made at 290°C instead of 250°C. Only four experimental points were obtained before loss of excess oxygen forced termination of the test in order to avoid precipitation of uranium. These points are in poor agreement. However, they seem to indicate that the corrosion under these conditions is roughly the same as that at 250°C. There is a possibility that geometry may have made electropolishing unsuccessful and may have affected the corrosion rate. Another test at elevated temperature with a mechanically polished bomb will probably be tried.

Test H-13. This test was made at an intermediate power density and, as can be seen in Fig. 75, it showed the high corrosion found at 6 kw/liter. The corrosion was so rapid that the experiment had to be terminated in one week, after only two corrosion points had been obtained. The corrosion appeared to average about 6 mpy during this one week. However, this bomb, like that of H-12, was put through an electropolishing process which may have adversely affected its surface. A repetition of this test with a mechanically polished bomb is desirable.

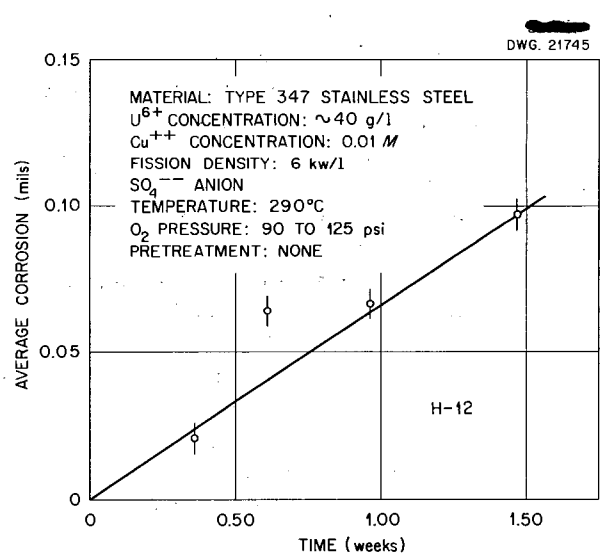

Fig. 74. In-Pile Corrosion of Stainless Steel by Homogeneous Reactor Solution.

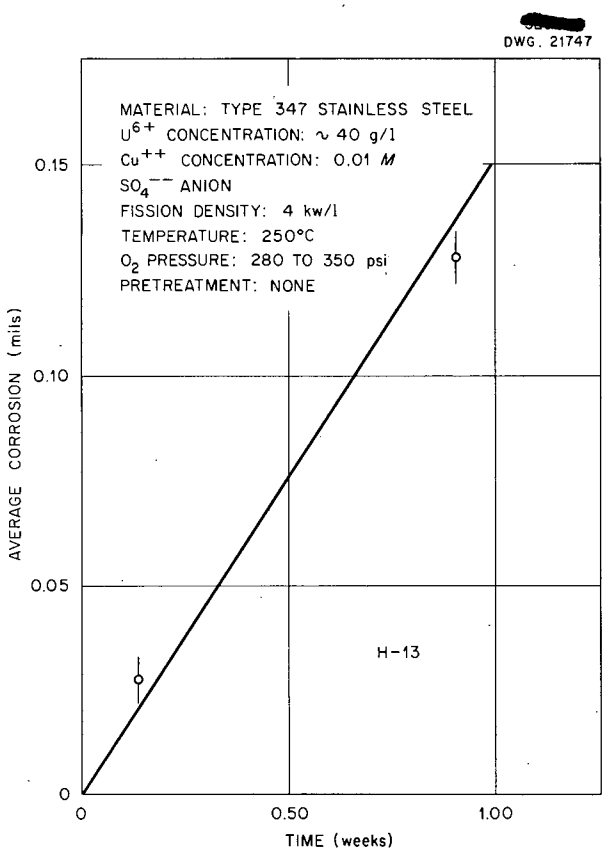

Fig. 75. In-Pile Corrosion of Stainless Steel by Homogeneous Reactor Solution.

Titanium

Tests H-14 and H-15. These tests were made with titanium bombs, and the results are combined in Fig. 76. The two tests were essentially the same except for fission density and a small difference in copper concentration. The corrosion data are strikingly different. The out-of-pile test, H-15, gave high initial corrosion followed by an essentially complete passivation. The in-pile test H-14, however, had a much lower initial rate but never approached a passivated state. The fission density changed during the test as a result of stepping up the reactor operating power. There is a slight indication that the corrosion rate may have been decreasing at the lower fission densities, but at the final power level the corrosion appears to be proceeding at the linear rate of about 1.3 mpy.

[4]H. F. McDuffie, L. F. Woo, and C. H. Secoy, *Chem. Semiann. Prog. Rep. June 20, 1953*, ORNL-1587, p. 98-106.

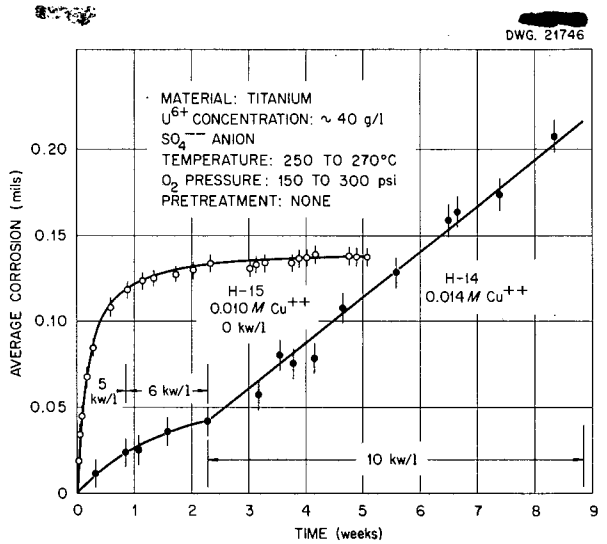

Fig. 76. Corrosion of Titanium by Homogeneous Reactor Solution.

Future Work

Both in-pile and out-of-pile tests will be continued during the next quarter. It is hoped that some of these tests will be with Zircalloy II. The out-of-pile testing equipment is being modified to allow shaking and thus remove diffusion as a possible cause of error in these experiments. T. E. Willmarth of the Analytical Division will make microscopic examination of the surface of out-of-pile bombs and M. J. Feldman of the Solid State Division will similarly examine the in-pile bombs. It is planned to make use of test pins in bombs to provide an independent check on the amount of corrosion and to furnish surface films for microscopic studies.

MECHANISM OF THE HYDROGEN-OXYGEN RECOMBINATION REACTION IN SOLUTIONS

H. F. McDuffie L. F. Woo
C. H. Secoy

An extension of the studies discussed in a previous report[4] has been concentrated on the firmer establishment of the dependence of the reaction rate on copper concentration and temperature, and it has included preliminary studies of the rate of the reaction with deuterium instead of hydrogen.

Dependence on Copper Concentration

The reaction rate at 250°C has been confirmed as first order in copper concentration for solutions of

copper sulfate in uranyl sulfate (0.17 M at room temperature). Table 40 and Fig. 77 show that the first-order behavior has been extended down to solutions which are 10^{-4} M in copper. It will be recalled that in-pile experiments have indicated first-order behavior up to 0.05 M copper; thus a 500-fold range of concentration has been spanned.

The reaction rate at 250°C has likewise been demonstrated to be first order for solutions of copper sulfate in 0.005 M sulfuric acid over the tenfold concentration range of 10^{-4} to 10^{-3} M copper. Table 41 and Fig. 78 illustrate the clean first-order behavior observed.

It was noted that, although first-order behavior was observed in both cases, the actual rates were different. This is believed to be due to the difference in the environment, which affects the copper. One possibility is that the active species changes from Cu^{++} or $Cu(OH)_2$ in perchlorate solutions to the more active $(CuHSO_4)^+$ or $Cu(OH)(HSO_4)$ in dilute sulfuric acid solutions and that it finally is pushed toward the less active $Cu(HSO_4)_2$ in more concentrated sulfuric acid or uranyl sulfate solutions. Changing the anionic constituents would be expected to change the relative catalytic effectiveness, i.e., chloride, bromide, nitrate, acetate, and phosphate might be expected to behave differently from sulfate. Attempts will be made to obtain information through this approach.

TABLE 40. EFFECT OF COPPER SULFATE CONCENTRATION UPON RECOMBINATION RATE AT 250°C IN 0.166 M URANYL SULFATE SOLUTIONS

RUN NUMBER	Cu CONCENTRATION (moles/liter)	k_{sol}
B-202	0.000125	0.75
B-207	0.000125	0.85
B-203	0.00021	1.29
B-205	0.00021	1.23
B-204	0.00042	2.56
B-206	0.00042	2.49
A-216	0.0023	13.0
A-217	0.0022	12.8
A-221	0.0023	12.5
A-277	0.0020	9.3
A-297	0.0021	11.3
A-210	0.0021	11.4
A-213	0.0021	10.5

Temperature Coefficient of the Reaction

Table 42 presents data for the reaction rate at several different temperatures. The starting solutions were the same at room temperature (0.166 M uranyl sulfate, 0.0025 M copper sulfate), and, therefore, the compositions were not precisely the same at the reaction temperature. Corrections for this small difference in composition have been applied to give the observed values for k_{Cu}. The experimentally observed activation energy for the 190 to 250°C values is 24 ± 4 kcal.

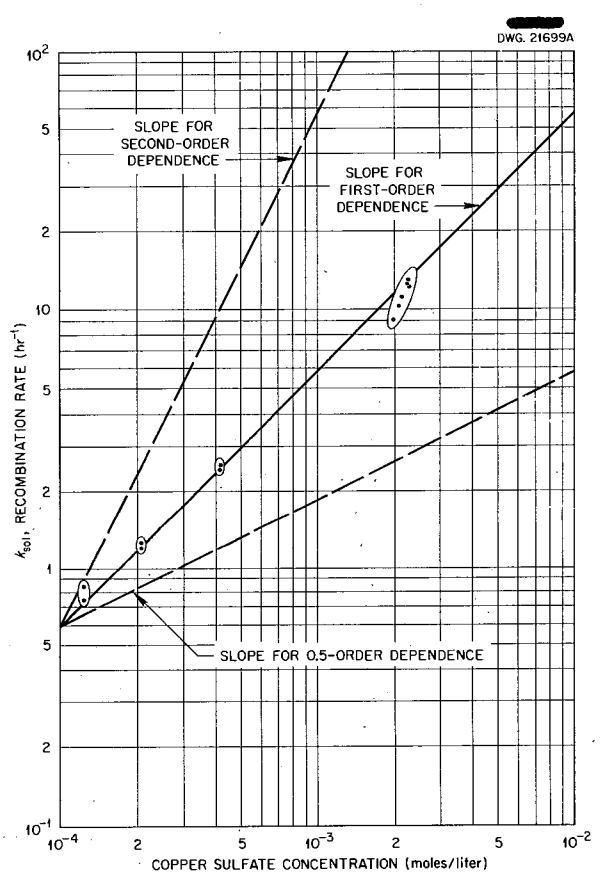

Fig. 77. Effect of Copper Sulfate Concentration Upon Recombination Rate at 250°C in 0.166 M UO_2SO_4 Solutions.

TABLE 41. EFFECT OF COPPER SULFATE CONCENTRATION UPON RECOMBINATION RATE AT 250°C IN 0.005 M SULFURIC ACID SOLUTIONS

RUN NUMBER	Cu CONCENTRATION (moles/liter)	k_{sol}
B-214	0.00010	17.2[a]
B-222	0.00010	1.76
B-223	0.00010	1.38
B-215	0.00025	26.7[a]
B-219	0.00025	8.3[a]
B-221	0.00025	3.97
B-225	0.00025	3.09
B-226	0.00025	2.89
B-216	0.00060	36.3[a]
B-218	0.00060	7.7
B-220	0.00060	7.1
B-224	0.00060	7.6
B-217	0.0010	11.6
B-227	0.00010	1.45[b]
B-228	0.00010	1.39[c]

[a]Data excluded because of contamination from previous runs.
[b]Sulfuric acid concentration 0.0010 M.
[c]Sulfuric acid concentration 0.0030 M.

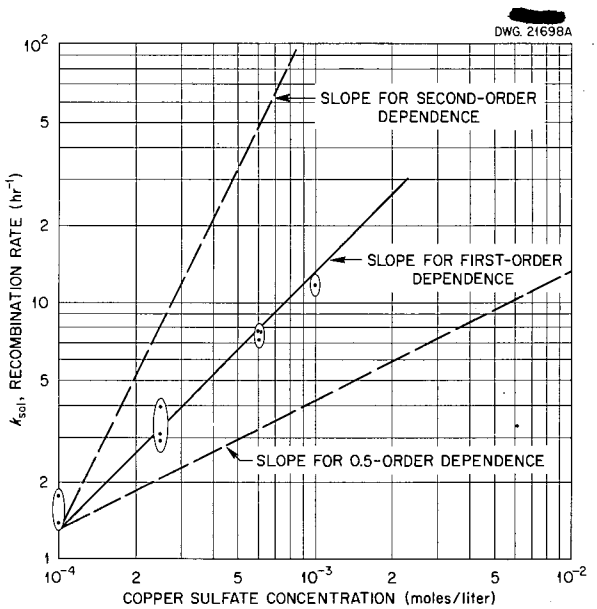

Fig. 78. Effect of Copper Sulfate Concentration Upon Recombination Rate at 250°C in 0.005 M H_2SO_4 Solutions.

Rate of Reaction with Deuterium

Since operating reactors of the homogeneous type may well use heavy-water solutions instead of light water, the decomposition gases would be deuterium and oxygen instead of hydrogen and oxygen. The reaction of deuterium with the catalyst might be expected to be somewhat slower than the reaction of hydrogen. Accordingly, three experiments at different ratios of liquid to gas phase were conducted in which deuterium gas was substituted for hydrogen gas (ultimately the reaction will be checked by using heavy water solutions and deuterium). The solution was one for which considerable data with hydrogen gas were available (0.005 M sulfuric acid and 0.001 M copper sulfate). Results are presented in Table 43. A least-squares line for the relationship[5] between V_g/V_l and $1/k_\pi$ gave the following values:

$$k_{sol} = 2.2$$

$$a = 1.7 \times 10^3 \text{ psi/mole·liter}$$

$$a/k_{sol} = 760$$

Comparison of this value of a/k_{sol} with that for hydrogen, using the same solution (433), indicates that the reaction is about 60% as fast with deuterium as with hydrogen at the same pressure. The solubility of deuterium is indicated as being slightly greater than that of hydrogen in light water, but the number of experiments is too small to permit any strong conclusion. At least the solubilities do not differ substantially.

Plans for Next Quarter

Because of the increasing interest in low concentrations of uranyl sulfate and temperatures higher

[5]C. E. Ronneberg and C. H. Secoy, *Chem. Semiann. Prog. Rep. June 20, 1953*, ORNL-1587, p. 96.

TABLE 42. TEMPERATURE DEPENDENCE OF RECOMBINATION IN 0.166 *M* URANYL SULFATE–0.0025 *M* COPPER SULFATE SOLUTIONS

RUN NUMBER	TEMPERATURE (°C)	k_{sol}	HOT Cu CONCENTRATION (moles/liter)	$k_{Cu} \times 10^{-3}$
A-236	190	0.64	0.0022	0.29
A-237	190	0.58	0.0022	0.26
A-243	190	0.53	0.0022	0.24
				Avg. 0.26
A-233	220	10.3	0.0023	4.55*
A-234	220	3.29	0.0022	1.52
A-240	220	3.01	0.0022	1.40
A-241	220	3.42	0.0022	1.59
				Avg. 1.50
B-208	220	3.69	0.0022	1.71
B-209	220	3.70	0.0022	1.70
B-210	220	3.50	0.0022	1.61
				Avg. 1.67
A-216	250	13.0	0.0023	5.72
A-217	250	12.8	0.0022	5.70
A-221	250	12.5	0.0023	5.51
A-277	250	9.3	0.0020	4.63
A-297	250	11.3	0.0021	5.36
A-210	250	11.4	0.0021	5.43
A-213	250	10.5	0.0021	5.07
				Avg. 5.35

*Discarded – obviously erroneous.

TABLE 43. RECOMBINATION OF DEUTERIUM AND OXYGEN IN LIGHT WATER SOLUTIONS 0.005 *M* SULFURIC ACID AND 0.001 *M* COPPER SULFATE

RUN NUMBER	V_g/V_l	$1/k_{\pi}$
B-233	6.05	7.75
B-234	0.60	1.08
B-235	1.87	2.91

than 250°C, a more intensive study will be made of recombination at 250 to 300°C in uranyl sulfate solutions containing 1 to 10 g of uranium per liter.

The reaction rate will also be checked by using deuterium gas with heavy-water solutions of the catalyst.

As indicated above, variation in the anionic constituent associated with the copper will be attempted in efforts to establish how the anion affects the activity of the copper.